CNO

N

C

Gerald Thiel *Editor*

Designer Receptors Exclusively Activated by Designer Drugs

Humana Press

NEUROMETHODS

For further volumes:
http://www.springer.com/series/7657

Designer Receptors Exclusively Activated by Designer Drugs

Edited by

Gerald Thiel

Department of Medical Biochemistry and Molecular Biology,
University of Saarland Medical Faculty, Homburg, Germany

Humana Press

Editor
Gerald Thiel
Department of Medical Biochemistry
    and Molecular Biology,
University of Saarland Medical Faculty,
Homburg, Germany

Printed on acid-free paper

Series Preface

Experimental life sciences have two basic foundations: concepts and tools. The *Neuromethods* series focuses on the tools and techniques unique to the investigation of the nervous system and excitable cells. It will not, however, shortchange the concept side of things as care has been taken to integrate these tools within the context of the concepts and questions under investigation. In this way, the series is unique in that it not only collects protocols but also includes theoretical background information and critiques which led to the methods and their development. Thus it gives the reader a better understanding of the origin of the techniques and their potential future development. The *Neuromethods* publishing program strikes a balance between recent and exciting developments like those concerning new animal models of disease, imaging, in vivo methods, and more established techniques, including, for example, immunocytochemistry and electrophysiological technologies. New trainees in neurosciences still need a sound footing in these older methods in order to apply a critical approach to their results.

Under the guidance of its founders, Alan Boulton and Glen Baker, the *Neuromethods* series has been a success since its first volume published through Humana Press in 1985. The series continues to flourish through many changes over the years. It is now published under the umbrella of Springer Protocols. While methods involving brain research have changed a lot since the series started, the publishing environment and technology have changed even more radically. Neuromethods has the distinct layout and style of the Springer Protocols program, designed specifically for readability and ease of reference in a laboratory setting.

The careful application of methods is potentially the most important step in the process of scientific inquiry. In the past, new methodologies led the way in developing new disciplines in the biological and medical sciences. For example, Physiology emerged out of Anatomy in the nineteenth century by harnessing new methods based on the newly discovered phenomenon of electricity. Nowadays, the relationships between disciplines and methods are more complex. Methods are now widely shared between disciplines and research areas. New developments in electronic publishing make it possible for scientists that encounter new methods to quickly find sources of information electronically. The design of individual volumes and chapters in this series takes this new access technology into account. Springer Protocols makes it possible to download single protocols separately. In addition, Springer makes its print-on-demand technology available globally. A print copy can therefore be acquired quickly and for a competitive price anywhere in the world.

Wolfgang Walz

Preface

Editorial

The largest group of plasma membrane receptors is the group of G protein-coupled receptors (GPCRs) that can be activated by numerous ligands, including amino acids, ions, peptide neurotransmitters, hormones, fatty acids, and proteins. The receptors share a similar core structure with seven transmembrane α-helices, an extracellular amino terminus, and an intracellular carboxy terminus. The amino termini of GPCRs, together with the extracellular loops, bind the specific ligands, while the intracellular loops provide multiple binding sites for G proteins. According to the current model of GPCR activation, it is assumed that binding of the cognate ligand to the receptor triggers small conformation changes in the arrangement of the transmembrane domains, leading to the dissociation of trimeric G proteins into α and βγ subunits [1]. As a result, effector enzymes are activated, including adenylate cyclase and phospholipase C. The G protein confers specificity to the signaling pathway induced by a particular GPCR.

The Problem: Complexity of GPCR Signaling

Signal transduction via GPCRs is complex, as GPCRs may couple to more than one G protein. Furthermore, a ligand may bind and activate several distinct GPCRs that may differ in their affinities to the type of trimeric G protein, thus leading to the activation of different effector enzymes. The complexity of GPCR signaling is further increased by the involvement of at least 5 Gβ subunits and at least 11 Gγ subunits. In addition to signaling via G proteins, GPCRs have a second signaling mode that is facilitated by the cell-scaffolding β-arrestin proteins, thus providing a distinct G protein-independent intracellular signaling pathway [2]. Together, multiple downstream signaling pathways can be activated as a result of GPCR stimulation. Furthermore, many tissues express several GPCR types that respond to a single ligand. Thus, administration of natural ligands will result in complex responses that are difficult to interpret. Biased drugs have been developed that do not activate equally well both G protein and β-arrestin pathways, but rather preferentially activate either the G protein or the β-arrestin-mediated signaling cascade. However, this approach does not solve the problem that GPCRs are expressed in multiple tissues and are activated by natural ligands as well as by agonists.

The Solution: Designer Receptors Exclusively Activated by Designer Drugs (DREADDs)

To understand the physiological functions of GPCRs, modified receptors are required that couple with only one of the heterologous G proteins or with the arrestin proteins. In addition, these receptors should not respond to their natural ligands but rather to an otherwise pharmacologically inert compound. Finally, tissue or cell type-specific expression of these modified receptors is essential, in order to allow the analysis of GPCR signaling in distinct tissues and cell types. These designer receptors exclusively activated by designer drugs (DREADDs) have been generated via a molecular evolution approach in Bryan Roth's lab, mainly reflecting the work of Blaine Armbruster [3]. "Without him there would be no DREADDs" (Bryan Roth). Furthermore, Bryan Roth is actively promoting the DREADD technology by depositing DREADD expressing transgenic mice to the Jackson laboratory repertoire (STOCK Tg(tetO-CHRM3*)1Blr/J#, http://jaxmice.jax.org/strain/014093.html). The Jackson laboratory now also offers floxed DREADD mice. Viral vectors expressing DREADDs are available from the Gene Therapy Center of the University of North Carolina at Chapel Hill (http://genetherapy.unc.edu/services.htm). New developments of the DREADD technology are found on the DREADD web page (http://www.dreadd.org/) as well as on the DREADD blog (http://chemogenetic.blogspot.com/). The available DREADDs lack constitutive activity, are unresponsive to endogenous ligands, but can be activated by the compound clozapine-N-oxide (CNO). Currently, G protein-coupled designer receptors have been developed that specifically couple to either Gαs, Gαq, or Gαi, following stimulation with a designer drug [3–5]. In addition, an arrestin-biased designer receptor has been designed by introducing a point mutation (R165L) into the Gαq-coupled designer receptor [6].

The development of DREADDs and the functional responses of DREADD activation have been reviewed in recent years [7–11]. Here, we present the first collection of methods that describe how the DREADD technology can successfully be employed to analyze the function of the nervous system.

DREADD Characteristics and Function In Vitro

To employ the designer receptors in research and perhaps in therapeutics, it must be shown that CNO-stimulated designer receptors faithfully mimic acetylcholine-stimulated muscarinic acetylcholine receptors. Thus, the designer receptor should reproduce all biochemical characteristics and biological functions in comparison to the native receptor [12]. In the first chapter, Alvarez-Curto and Milligan present methods for this comparison, including changes in receptor conformation in response to ligand binding, ligand-dependent receptor phosphorylation, downstream signaling events such as β-arrestin-2 recruitment, intracellular Ca^{2+}-mobilization, and phosphorylation of extracellular signal-regulated protein kinase. In addition to ERK, several other signaling molecules, including the protein kinases JNK1/2, p38 and ERK5, and the G proteins Ras, RhoA, Rac1, and Cdc42, are activated downstream of Gαq-coupled designer receptor activation [13]. In Chap. 2, Nakajima et al. provide protocols for the pharmacological and functional characterization of an arrestin-biased DREADD. Rössler and Thiel describe in the third chapter methods to analyze the

activation of transcription factors as a result of designer receptor stimulation. The use of lentiviral gene transfer to implant the reporter genes into the chromatin of the cells ensures that the reporter genes are embedded into a nucleosomal structure and allows the analysis of infected mitotic and postmitotic cells such as neurons.

Regulation of Neuronal Activity by DREADD Stimulation in Transgenic Mice

Several lines of transgenic mice expressing DREADDs have been generated. The analysis of these genetically altered animals underlined the power of this chemical-genetic tool. The first report by the Roth lab showed that stimulation of hM3Dq, a Gαq-coupled designer receptor, in neurons depolarized the cells, enhanced their excitability, and thus triggered a burst-like firing [4]. Therefore, treatment of transgenic mice with CNO enhances neuronal firing of those neurons expressing hM3Dq, thus giving investigators a noninvasive tool at hands to selectively stimulate neuronal populations. In contrast, stimulation of Gαi-coupled designer receptors (hM4Di, derived from M4 muscarinic acetylcholine receptor) in hippocampal neurons induced hyperpolarization and silenced spontaneous and depolarization-evoked firing [3], indicating that this type of designer receptor can be used to interrupt neuronal firing and silence genetically defined neurons. Selective suppression of synaptic transmission is accomplished by expression and activation of hM4D^{NRXN}, a variant of the hM4Di, that is preferentially expressed in axons, due to the axonal C-terminal targeting sequence of neurexin 1a [14].

Four chapters of this book describe the utility of DREADD technology in activating or silencing selected neurons in the brain of transgenic mice. Michael Krashes (Chap. 4) describes the expression of hM3Dq in Agouti-related peptide (AgRP)-expressing neurons in the arcuate nucleus of the hypothalamus. These neurons are activated when the mice are hungry. Stimulation of hM3Dq with CNO activated these neurons and resulted in escalated feeding for several hours, while expression of the Gi/o-coupled inhibitory hM4Di designer receptor hyperpolarized AgRP neurons and reduced food intake [15, 16]. Likewise, expression of hM3Dq receptors in proopiomelanocortin (POMC) neurons was used to investigate the impact of these neurons on feeding behavior. These neurons are part of the neural circuit involved in feeding inhibition. Accordingly, acute or sustained stimulation of hM3Dq receptors in POMC neurons of the nucleus tractus solitarius or arcuate nucleus suppressed feeding behavior [17]. In addition, DREADD technology has been used to identify calcitonin-related peptide-expressing neurons of the parabrachial nucleus that projects to the central nucleus of the amygdala involved in suppressing appetite [18]. The power of DREADD technology to artificially inhibit the activity of selected neuronal populations is further demonstrated by Nunez-Parra et al. (Chap. 5), describing the outcome of an inhibition of GABAergic neurons of the basal forebrain that regulate the activity of granule cells of the olfactory bulb. Expression and stimulation of inhibitory hM4Di receptors in these GABAergic neurons impaired olfactory discrimination, indicating that these inhibitory afferents are important in olfactory processing [19]. Selective expression of excitatory and inhibitory DREADDs in the nucleus accumbens was used to unravel neurons involved in the regulation of ethanol consumption [20], described in Chap. 7. This approach may lead to the dissection of the functional role of particular neuronal populations required for drug-seeking behavior. The DREADD technology also enables an investigation of the neuronal circuits and neuronal types involved in regulating sleep/wakefulness [21], as described in Chap. 6 by Mieda and Sakurai, or underlying drug-seeking behavior,

as outlined in Chap. 8 by Nair et al. In addition, modulation of olfactory response in Drosophila larval sensory neurons and diurnal behavior in adult flies has been obtained by expression of designer receptors [22], indicating that the mammalian DREADDs couple to Drosophila G proteins. The methods for employing DREADD technology in Drosophila are described in Chap. 9 by Charles Nichols and Jaime Becnel.

Behavioral Response to DREADD Activation in Mice

The practical application of the DREADDs allows a precise characterization of complex pathways and connections in the nervous system, as emphasized by the investigation of behavior and memory circuits following stimulation of designer receptors. The most interesting outcome of DREADD stimulation in the brains of transgenic mice is the frequently observed induction of behavioral changes as a result of receptor stimulation. Already the first analysis of hM3Dq expression in the forebrain of transgenic mice reported about increased locomotion of the animals as a result of designer receptor stimulation [4]. In this book, several examples are presented that underline the importance of GPCR stimulation for the regulation of behavioral of transgenic mice. A popular behavioral task to investigate is food intake: the animal eats or it doesn't. Several seminal articles describe the activation or inhibition of food intake as a result of designer receptor activation. Stimulation of hM3Dq in AgRP-expressing neurons in the arcuate nucleus of the hypothalamus resulted in rapid intense food-seeking behavior [15, 16], while stimulation of this receptor in neurons projecting to the central nucleus of the amygdala suppressed appetite [18]. Likewise, stimulation of Gi/o-coupled hM4Di receptors in AgRP neurons or hM3Dq receptors in POMC neurons significantly suppressed food intake [14, 15, 17]. The perception of odors is important for many animals to induce or inhibit behavioral programs, including reproduction, aggression, and food location. Thus, DREADDs expression in selective neuronal populations involved in the sensory perception of odors or the neural processing of this information can be used to unravel the underlying neuronal circuits [19]. Likewise, manipulation of the amount of time spent in wakefulness of transgenic mice has been accomplished by the selective expression and activation of designer receptors [21]. A general description of the use of DREADD technology in behavioral models of transgenic mice is presented in Chap. 7 by Cassataro and Sjulson, who describe several pitfalls in behavior assays and discuss the framework and protocols to avoid them. Analyzing behavioral changes as a result of DREADD activation is not restricted to mice. The regulation of drug-experience-dependent behavior plasticity can be controlled by DREADDs expressed in either striatopallidal or striatonigral neurons of the rat [23], while behavior responses can also be obtained in Drosophila following activation of designer receptors in selective neuronal populations. Most interestingly, the induction or alteration of distinct behavioral programs in mice, rats, or flies is reversible by omitting the DREADD ligand CNO. In summary, the DREADD technology permits experiments to unravel neural circuits controlling natural behavior on the cellular level, allowing the elucidation of causal relationships between selective neuronal populations and a particular type of behavior.

DREADDs: New Tools for the Analysis of Memory Circuits

Neuronal activation can be visualized by the expression of c-Fos, due to the fact that neuronal activity stimulates the c-Fos promoter. By expressing hM3Dq under the control of the c-Fos promoter, the designer receptor is specifically activated in neurons that had been stimulated previously. Administration of CNO stimulates these neurons again, thus allowing the generation of a hybrid memory representation by stimulating an ensemble of previously activated neurons with a designer ligand [24]. Expression and stimulation of hM3Dq in the locus coeruleus enhanced memory in a mouse model of Down syndrome, underlining the importance of the noradrenergic transmitter system for memory function [25].

DREADD Expression in Non-neuronal Tissues: Influencing the Metabolic State of the Organism

DREADDs are chemical-genetic tools that contribute to our understanding about how the brain works. In addition, DREADDs can be used to investigate the function of GPCR in non-neuronal tissues. Pancreatic β-cells, for instance, express numerous Gαs and Gαq-coupled GPCRs that respond to their cognate ligands, including acetylcholine, Ca^{2+}, vasopressin, corticotropin releasing hormone, glucagon-like peptide 1, and others. Expression and activation of Gαq-coupled designer receptors in pancreatic β-cells revealed that insulin release was enhanced and blood glucose levels reduced. Moreover, receptor stimulation improved the glucose tolerance in obese, insulin-resistant mice and increased the β-cell mass [5]. Chronic stimulation of Gαq-coupled designer receptors prevented streptozotocin-induced diabetes as well as the metabolic deficits that occur following consumption of high-fat diet [26]. Overall, Gαq-coupled designer receptor stimulation improved β-cell function. The glucose homeostasis was also changed in transgenic mice expressing activated Gαq-coupled designer receptors in hepatocytes. These mice showed a pronounced upregulation of the blood glucose concentration, similar to the activation of glucagon receptors, due to increased rates of glycogen hydrolysis and gluconeogenesis [27] suggesting that Gαq-coupled receptor of hepatocytes plays a role in the regulation of blood glucose levels. More exciting data from employing the DREADD technology are to expect in the near future, unraveling the biological functions of GPCR in different tissues and cell types.

Conclusion

DREADDs have been shown to be powerful chemical-genetic tools for the investigation of GPCR signaling and function in the brain and in non-neuronal tissues. In particular, the correlation between DREADD activation in the nervous system and changes in animal behavior demonstrates the utility of this technology. The expression of DREADDs in other tissues and cell types will certainly help to understand the signaling pathways of GPCRs in specific tissues. Many new and exciting discoveries are anticipated for the near future employing the DREADD technology. This book provides a snapshot of the current methods used to analyze the properties of DREADDs in vitro and the biological response of

DREADD activation in different cellular systems in vivo. I hope that this compendium will help other investigators to establish the DREADD technology in their laboratories. I would like to thank Wolfgang Walz, the series editor for NEUROMETHODS, for initially suggesting a methods book about DREADDs, and Patrick J. Marton, the Executive Editor of Springer Protocols, for his editorial support.

Homburg, Germany   *Gerald Thiel*

References

1. Venkatakrishnan AJ, Deupi X, Lebon G, Tate CG, Schertler GF, Babu MM (2013) Molecular signatures of G-protein-coupled receptors. Nature 494:185–194.

2. Rajagopal S, Rajagopal K, Lefkowitz RJ (2010) Teaching old receptors new tricks: biased seven-transmembrane receptors. Nat Rev Drug Discov 9:373–386.

3. Armbruster BN, Li X, Pausch MH, Herlitze S, Roth BL (2007) Evolving the lock to fit the key to create a family of G protein-coupled receptors potentially activated by an inert ligand. Proc Natl Acad Sci USA 104:5163–5168.

4. Alexander GM, Rogan SC, Abbas AI, Armbruster BN, Pei Y, Allen JA, Nonneman RJ, H Hartmann J, Moy SS, Nicolelis MA, McNamara JO, Roth BL (2009) Remote control of neuronal activity in transgenic mice expressing evolved G protein-coupled receptors. Neuron 63:27–39.

5. Guettier J-M, Gautam D, Scarselli M, Ruiz de Azua I, Li JH, Rosemond E, Ma X, Gonzalez FJ, Armbruster BN, Lu H, Roth BL, Wess J (2009) A chemical-genetic approach to study G protein regulation of β cell function in vivo. Proc Nat Acad Sci USA 106:19197–19202.

6. Nakajima K-i, Wess J (2012) Design and functional characterization of a novel, arrestin-biased designer G protein-coupled receptor. Mol Pharmacol 82:575–582.

7. Conklin BR, Hsiao E, Claeysen S, Dumuis A, Srinivasan S, Forsayeth JR, Guettier JM, Chang WC, Pei Y, McCarthy KD, Nissenson RA, Wess J, Bockaert J, Roth BL (2008) Engineering GPCR signaling pathways with RASSLs. Nat Meth 5:673–678.

8. Pei Y, Rogan SC, Yan F, Roth BL (2008) Engineering GPCRs as tools to modulate signal transduction. Physiology 23:313–321.

9. Thiel G, Kaufmann A, Rössler OG (2013) G-protein-coupled designer receptors – new chemical-genetic tools for signal transduction research. Biol Chem 394:1615–1622.

10. Wess J, Nakajima K, Jain S (2013) Novel designer receptors to probe GPCR signaling and physiology. Trends Pharmacol Sci 34:385–393.

11. Urban DJ, Roth BL (2015) DREADDs (designer receptors exclusively activated by designer drugs): chemogenetic tools with therapeutic utility. Annu Rev Pharmacol Toxicol 55:399–417.

12. Alvarez-Curto E, Prihandoko R, Tautermann CS, Zwier JM, Pediani JD, Lohse MJ, Hoffmann C, Tobin AB, Milligan G (2011) Developing chemical genetic approaches to explore G-protein coupled receptor function: validation of the use of a receptor activated solely by synthetic ligand (RASSL). Mol Pharmacol 80:1033–1046.

13. Vaqué JP, Dorsam RT, Feng X, Iglesias-Bartolome R, Forsthoefel DJ, Chen Q, Debant A, Seeger MA, Ksander BR, Teramoto H, Gutkind JS (2013) A genome-wide RNAi screen reveals a trio-regulated Rho GTPase circuitry transducing mitogenic signals initiated by G protein-coupled receptors. Mol Cell 49:94–108.

14. Stachniak TJ, Gosh A, Sternson SM (2014) Chemogenetic synaptic silencing of neural circuits localizes a hypothalamus→midbrain pathway for feeding behaviour. Neuron 82:797–808.

15. Krashes MJ, Koda S, Ye C, Rogan SC, Adams AC, Cusher DS, Maratos-Flier E, Roth BL, Lowell BB (2011) Rapid, reversible activation of AgRP neurons drives feeding behavior in mice. J Clin Invest 121:1424–1428.

16. Krashes MJ, Shah BP, Koda S, Lowell BB (2013) Rapid versus delayed stimulation of feeding by the endogenously released AgRP neuron mediators, GABA, NPY and AgRP. Cell Metabol 18:588–595.

17. Zhan C, Zhou J, Feng Q, Zhang J-E, Lin S, Bao J, Wu P, Luo M (2013) Acute and long-term suppression of feeding behaviour by POMC neurons in the brainstem and hypothalamus, respectively. J Neurosci 20:3624–3632.

18. Carter ME, Soden ME, Zweifel LS, Palmiter RD (2013) Genetic identification of a neural

circuit that suppresses appetite. Nature 503:111–114.

19. Nunez-Parra A, Maurer RK, Krahe K, Smith RS, Araneda RC (2013) Disruption of centrifugal inhibition to olfactory bulb granule cells impair olfactory discrimination. Proc. Natl Acad Sci USA 110:14777–14782.

20. Cassataro D, Bergfeldt D, Malekian C, Van Snellenberg JX, Thanos PK, Fishell G, Sjulson L (2013) Reverse pharmacogenetic modulation of the nucleus accumbens reduces ethanol consumption in a limited access paradigm. Neuropsychopharmacology 39:283–290.

21. Sasaki K, Suzuki M, Mieda M, Tsujino N, Roth B, Sakurai T (2011) Pharmacogenetic modulation of orexin neurons alter sleep/wakefulness in mice. PLoS One 6:e20360.

22. Becnel J, Johnson O, Majeed ZR, Tran V, Yu B, Roth BL, Cooper RL, Kerut EK, Nichols CD (2013) DREADDs in Drosophila: a pharmacogenetic approach for controlling behaviour, neuronal signaling, and physiology in the fly. Cell Rep 4:1049–1059.

23. Ferguson SM, Eskenazi D, Ishikawa M, Wanat MJ, Phillips PEM, Dong Y, Roth BL, Neumaier JF (2011) Transient neuronal inhibition reveals opposing roles of indirect and direct pathways in sensitization. Nat Neurosci 14:22–24.

24. Garner AR, Rowland DC, Hwang SY, Baumgaertel K, Roth BL, Kentros C, Mayford M (2012) Generation of synthetic memory trace. Science 335:1513–1516.

25. Fortress AM, Hamlett ED, Vazey EM, Aston-Jones G, Cass WA, Boger HA, Granholm A-CE (2015) Designer receptors enhance memory in a mouse model of down syndrome. J Neurosci 28:1343–1353.

26. Jain S, Ruiz de Azua I., Lu H, White MF, Guettier J-M, Wess J (2013) Chronic activation of a designer G_q-coupled receptor improves β cell function. J Clin Invest 123:1750–1762.

27. Li JH, Jain S, McMillin SM, Cui Y, Gautam D, Sakamoto W, Lu H, Jou W, McGuinness OP, Gavrilova O, Wess J (2013) A novel experimental strategy to assess the metabolic effects of selective activation of a G_q-coupled receptor in hepatocytes in vivo. Endocrinology 154:3539–3551.

Contents

Contributors

ELISA ALVAREZ-CURTO • *Molecular Pharmacology Group, Institute of Molecular, Cell and Systems Biology, College of Medical, Veterinary and Life Sciences, University of Glasgow, Glasgow, UK*

RICARDO C. ARANEDA • *Department of Biology, University of Maryland, College Park, MD, USA*

JAIME BECNEL • *Department of Pharmacology and Experimental Therapeutics, LSU Health Sciences Center, New Orleans, LA, USA*

DANIELA CASSATARO • *Department of Neuroscience and Physiology, NYU School of Medicine, New York, NY, USA*

WILSON CHAN • *Department of Biology, University of Maryland, College Park, MD, USA*

LUIS E. DIAZ GIMENEZ • *Department of Pharmacology, Vanderbilt University Medical Center, Nashville, TN, USA*

VSEVOLOD V. GUREVICH • *Department of Pharmacology, Vanderbilt University Medical Center, Nashville, TN, USA*

KRISTA KRAHE • *Department of Biology, University of Maryland, College Park, MD, USA*

MICHAEL KRASHES • *Diabetes, Endocrinology, and Obesity Branch, Section on Motivational Processes underlying Appetite, NIH, NIDDK, Bethesda, MD, USA*

MICHIHIRO MIEDA • *Department of Molecular Neuroscience and Integrative Physiology, Faculty of Medicine, Kanazawa University, Kanazawa, Japan*

GRAEME MILLIGAN • *Molecular Pharmacology Group, Institute of Molecular, Cell and Systems Biology, College of Medical, Veterinary and Life Sciences, University of Glasgow, Glasgow, UK*

SUNILA G. NAIR • *Department of Psychiatry and Behavioral Sciences, Harborview Medical Center, University of Washington, Seattle, WA, USA*

KEN-ICHIRO NAKAJIMA • *Laboratory of Bioorganic Chemistry, Molecular Signaling Section, NIH-NIDDK, Bethesda, MD, USA*

JOHN F. NEUMAIER • *Department of Psychiatry and Behavioral Sciences, Harborview Medical Center, University of Washington, Seattle, WA, USA*

CHARLES D. NICHOLS • *Department of Pharmacology and Experimental Therapeutics, LSU Health Sciences Center, New Orleans, LA, USA*

ALEXIA NUNEZ-PARRA • *Department of Cell and Developmental Biology, Rocky Mountain Taste and Smell Center and Neuroscience Program, University of Colorado Anschutz Medical Campus, Aurora, CO, USA*

OLIVER G. RÖSSLER • *Department of Medical Biochemistry and Molecular Biology, Medical Faculty, University of Saarland, Homburg, Germany*

TAKESHI SAKURAI • *Department of Molecular Neuroscience and Integrative Physiology, Faculty of Medicine, Kanazawa University, Kanazawa, Japan*

LUCAS SJULSON • *Departments of Psychiatry and Neuroscience and Physiology, NYU School of Medicine, New York, NY, USA*

DENIS SMIRNOV • *Department of Psychiatry and Behavioral Sciences, Harborview Medical Center, University of Washington, Seattle, WA, USA*

GERALD THIEL • *Department of Medical Biochemistry and Molecular Biology, University of Saarland Medical Faculty, Homburg, Germany*

JÜRGEN WESS • *Laboratory of Bioorganic Chemistry, Molecular Signaling Section, NIH-NIDDK, Bethesda, MD, USA*

Chapter 1

Defining the Functional Equivalence of Wild-Type and Chemically Engineered G Protein-Coupled Receptors

Elisa Alvarez-Curto and Graeme Milligan

Abstract

The functional connection between activation of a single G protein-coupled receptor (GPCR) and a specific physiological outcome may be obscured by the presence of other closely related members of the GPCR superfamily that share spatiotemporal patterns of expression and equipotent activation by endogenous ligands. To address this issue, molecular and chemical genetic techniques have been developed to generate mutationally modified GPCRs only susceptible to activation by one or more synthetic ligands that are inactive at the equivalent wild-type receptor. This chapter provides both an overview of strategies used to generate such "receptors activated solely by synthetic ligands" (RASSLs) and, in more detail, approaches that have been used to assess the equivalence or otherwise of function of a wild-type and corresponding RASSL receptor. The human muscarinic M_3 acetylcholine receptor is used as the exemplar but similar preliminary studies should be employed before further use, particularly in vivo, of such RASSLs.

Key words BRET, FRET, G protein-coupled receptor, Muscarinic receptor, Molecular evolution, Clozapine N-oxide

Abbreviations

BAL	2,3-Dimercapto-1-propanol
BRET	Bioluminescence resonance energy transfer
CFP	Cyan fluorescent protein
CNO	Clozapine N-oxide
DREADD	Designer receptor exclusively activated by designer drugs
EDT	2-Ethanedithiol
FRET	Fluorescence resonance energy transfer
Fura-2AM	Fura-2 acetoxymethyl ester
GFP	Green fluorescent protein
GPCR	G protein-coupled receptor
IL3	Third intracellular loop

IP1   Inositol monophosphate
RASSL   Receptor activated solely by synthetic ligands
TMD   Transmembrane domain
YFP   Yellow fluorescent protein

1   Introduction and Background Overview

Segregation of function between many G protein-coupled receptors (GPCRs) belonging to subfamilies in which multiple, genetically distinct members are known and which may often be co-expressed presents many challenges. This is especially so for in vivo studies where the endogenous ligand(s) is shared between the receptors and is produced routinely or continuously. These challenges are amplified if the endogenous ligand(s) shows very limited selectivity between the members of the receptor subfamily and/or if selective synthetic agonists or antagonists are lacking [1, 2]. An obvious example is for the group of muscarinic acetylcholine receptors. Five distinct genes encode the muscarinic acetylcholine M_1–M_5 subtypes and each of these receptors binds acetylcholine with similar affinity [2]. There have been significant advances in the identification and characterization of selective antagonists and, particularly, agonist and positive allosteric modulator ligands in recent years, based on both knowledge of atomic level structures of a number of muscarinic subtypes [3–6] and a drive to develop subtype selective muscarinic M_1 receptor agonists for the treatment of diseases involving impaired cognition, including Alzheimer-type dementia [7]. However, prior to this, and because many of the selective ligands are not widely available then, in large part, understanding of the roles of specific muscarinic subtypes has been predominantly on the use of muscarinic receptor subtype knockout lines of mice [8, 9].

As an alternative, researchers have generated and used mutated variants of the muscarinic receptor subtypes that are unable to be activated by acetylcholine but, instead, respond to the previously inactive ligand clozapine N-oxide (CNO). This general strategy of switching the selectivity of activation of a GPCR from the endogenous ligand(s) to one or more synthetic ligands has been described as producing "receptors activated solely by synthetic ligands" (RASSLs) [10, 11] or "designer receptors exclusively activated by designer drugs" (DREADDs) [12, 13]. In differing examples this has involved either combinations of specific, site-directed mutagenesis taking advantage of an understanding of the basis of ligand binding [14] or, in the case of the muscarinic receptors, directed protein evolution [15].

The first example of a GPCR for which an RASSL variant was created was the β_2-adrenoceptor. With hindsight the approach used is now conceptually obvious but, at the time, was designed initially

to assess the importance of an aspartate residue (Asp113) in transmembrane domain (TMD) III of the receptor in binding the endogenous ligands adrenaline and noradrenaline as well as synthetic agonists containing an amine head group [16, 17]. Inherent in these studies was a drive to identify important positions in receptor structures as a "novel avenue for the design of therapeutic agents" [16]. Mutation of this aspartate to serine resulted in marked loss in potency to catecholamines and related small-molecule ligands and, of equal importance, the development of potency to the synthetic molecule 1-(3′4′-dihydroxyphenyl)-3-methyl-1-butanone (also known as L-158, 870), which has only low affinity and potency at the wild-type β_2-adrenoceptor [16]. This latter point was of key importance in demonstrating that the loss of potency to catecholamines and related ligands was not simply due to poor folding or cell surface expression of the Asp-Ser mutated receptor. Although not employed directly at the time to address other questions, more than 10 years later Sartania et al. [18] took advantage of this mutant to show that when co-expressed along with the wild-type β_2-adrenoceptor, addition of the agonist isoprenaline, which only has significant potency and affinity for the wild-type receptor, caused co-internalization from the cell surface of both wild-type and the Asp-Ser variant forms of the receptor. As addition of L-158, 870, which only has significant potency and affinity for the Asp-Ser variant, also caused co-internalization of both forms of the receptor these results were used to imply that the β_2-adrenoceptor was able to exist and to be internalized as a dimeric or oligomeric complex containing copies of both forms of the receptor.

2   Generation of Muscarinic Receptor RASSL/DREADDs by Molecular Evolution

With a desire to modify muscarinic receptors such that selective activation could be achieved, Armbruster et al. [15] adopted a strategy based on directed protein evolution. This basic approach had been employed much earlier by Campbell and colleagues to "evolve" a gene of *E. coli* that was not involved in lactose utilization to acquire catalytic properties that allowed it to do so [19]. In the studies of Armbruster and colleagues systematic and repeated rounds of random mutagenesis were followed by screening and selection of variants of the wild-type muscarinic M_3 receptor that displayed reduced potency/affinity for acetylcholine and/or enhanced affinity/potency for CNO. Briefly, a library of mutant receptors was generated by error-prone PCR using a yeast expression vector with the template of the rat muscarinic M_3 receptor cloned into it. In such experiments use of a Taq polymerase without proofreading capacity provides a significant error rate and the fidelity of the enzyme can be further reduced by adjusting the buffer

ionic composition and parameters in the thermo cycler program. This, however, must be balanced against the likelihood of generating so many mutations that deconvolution of the molecular basis for any mutants with promising pharmacological properties becomes overwhelmingly difficult. Moreover, integral to the concept is that alteration of the pharmacological specificity of the receptor does not result in alteration in the signalling profile and/or regulation of the receptor.

The inherent use of G protein-mediated signalling by *S. cerevisiae*, and that this organism has been used widely to study the activity of introduced mammalian GPCRs [20, 21], makes it ideally suited for high-throughput and rapid screening for mutants displaying aspects of the final desired pharmacological behavior of the potential RASSL/DREADD. The screening of mutated receptors is carried out in a drug-dependent yeast growth assay using a *S. cerevisiae* strain that has been engineered to couple signalling of the mutated receptor to the yeast pheromone pathway. A series of genetic modifications to the mating signal transduction pathway in the yeast allow agonist-induced growth on selective medium. In native conditions the yeast GPCR Ste2 upon activation by its specific ligand, the alpha-factor, leads to the activation of Gpa1, the yeast Gα subunit, and the dissociation of the Gβγ dimer (Ste4 and Ste18). Agonist-dependent G protein activation results in MAP-kinase activation and subsequent up-regulation of the pheromone response elements FUS1 and FUS2 that are required for yeast mating. Sustained MAP-kinase activation also downregulates this same pathway by activating Far1 and Sst2, leading to cell cycle arrest and reassociation of the Gpa1 and Gβγ complex, respectively. For agonist screening using mutated receptors a genetically modified yeast strain with a simplified version of this pathway is generally used. In this strain the Ste2 and Gpa1 elements are replaced by the mutated receptor of interest and a chimeric yeast Gpa1, respectively, in which the last five carboxyl-terminal amino acids (KIGII) have been replaced by those of receptor species-specific mammalian G_q (EYNLV), G_i (DCGLF), or G_s (QYELL) G protein α subunits. This is generally sufficient to confer specificity for G protein coupling of the introduced receptor but to still retain activation of the yeast pheromone pathway. Moreover, the elements Far1 and Sst2 are knocked out in this strain to avoid cell cycle arrest and to increase the receptor-G protein coupling efficiency and sensitivity for the agonist. Finally, to facilitate detection of growth under restricted conditions, the FUS1 and FUS2 genes are replaced with reporter genes such as FUS1-LacZ and FUS2-CAN and the FUS1-HIS3 gene that allows growth only in the absence of histidine [13, 21].

Despite all this making the process relatively straightforward, expression of the receptor of interest in a yeast system can be problematic with very low receptor expression, lack of function,

or even absence of membrane localization being the most common problems encountered. Membrane targeting can be achieved by inserting a cleavable leader sequence or by fusing the amino terminus of the yeast Ste2 receptor to the receptor of interest [21]. Truncations of certain domains of the receptor, such as the third intracellular loop (IL3), have been shown to resolve the issue of poor level of expression in yeast in several reported studies and to restore function in the G_q-coupled muscarinic receptors hM_1, hM_3, and hM_5 [22].

A truncated form of the rat muscarinic M_3 receptor was at the core of the work carried out by Armbruster and others [15] to evolve the family of RASSL/DREADD receptors. This rat receptor form ($rM_3\Delta3i$) lacks over 190 amino acids of IL3 but shows over 200-fold higher expression (~214 fmol/mg) in yeast systems than the full-length counterpart [22]. By using this receptor as template for random mutagenesis a library of mutants cloned into yeast expression vectors was generated and tested in agonist-dependent growth assays [15]. Yeast expressing mutant receptors were selected for growth in the presence initially of clozapine, a weak partial muscarinic agonist [23, 24]. Positive clones were subsequently tested in liquid medium growth experiments where they were challenged with the native agonist acetylcholine, clozapine, or CNO, a synthetic but inert small molecule related to clozapine. Wild-type expressing strains showed robust responses, i.e., increase in a dose-dependent manner of yeast growth to acetylcholine but not the latter compounds. Additionally, there were a number of mutants that had greatly reduced potency for acetylcholine whilst gaining it for both the other two molecules. All of these positive clones carried a mutation of a tyrosine within TMD III (Y148X$^{3.33}$, where X is any amino acid and 3.33 the relative position of the amino acid in the Ballesteros and Weinstein systematic residue numbering system) [25] known to be important for muscarinic agonist binding [26, 27]. DNA recovered from these clones was subsequently used for a second round of mutagenesis to produce a second-generation pool of mutants. From these two clones that showed potency for CNO of ~10 nM were isolated. The optimal mutation, Y148C$^{3.33}$, was transferred to the equivalent and conserved residue in the human receptor (position 149). This was subsequently tested in conjunction with other mutations within several other TMDs. The human hM_3-RASSL/DREADD with the best response ratio compared to the wild-type receptor contains two point mutations, one in each of two different TMDs: the aforementioned tyrosine in TMDIII (Y$^{3.33}$C), and an alanine in TMDV (A$^{5.46}$G). These changes are sufficient to yield a receptor that has lost substantial potency for the muscarinic agonists acetylcholine and carbachol, but gained it for the synthetic ligand CNO [15].

To validate the use of this modified receptor in mammalian cells accumulation of inositol monophosphates (IP1) as a result of activation of phospholipase C$_\beta$ through G$_q$ signalling was used initially in transiently transfected HEK293 cells. Further tests in human pulmonary artery smooth muscle cells stably expressing the RASSL/DREADD form of hM$_3$ showed functional responses at the levels of hydrolysis of inositol-containing phospholipids, calcium mobilization, and ERK1/2 MAP-kinase phosphorylation that were 40,000-fold more potent in response to CNO than to acetylcholine. These experiments demonstrated that the RASSL/DREADD receptor was functional in a mammalian cellular background. Most notably, introduction of these mutations into the conserved amino acids at the corresponding positions in TMDIII and TMDV in any of the other four members of the muscarinic receptor family resulted in an equivalent switch in pharmacology, resulting in the generation of RASSL/DREADD forms of all five muscarinic receptors.

Following their initial studies Armbruster and co-workers [15] went further to demonstrate the value of the designer receptors as tools, in this case hM$_4$-DREADD, using it to control neuronal signalling. Hippocampal neurons as well as other neuronal populations in the brain show varying levels of expression of muscarinic receptors. Activation of an exogenously expressed hM$_4$-DREADD (also named hM$_4$D$_i$ for its specific coupling to G$_i$) receptor in this system with CNO led to changes in specific GPCR-induced G protein inward-rectifying potassium channel-mediated membrane hyperpolarization that were not present when using the muscarinic agonist carbachol. By contrast no changes in membrane polarization were detected when using CNO on neurones overexpressing the wild-type hM$_4$ receptor, demonstrating the potential of CNO to be used as an exclusive modulator of the mutated receptor in vivo.

A number of independent laboratories have since employed such RASSL/DREADD receptors as discriminating pharmacological tools in vivo by capitalizing on their ability to function on demand upon activation by a synthetic small molecule, and being able to either up-regulate (G$_s$- or G$_{q/11}$-coupled receptors) or downregulate (G$_i$-coupled receptor) cellular functions in very complex structures such as the brain. For example, Ferguson and collaborators have shown that the expression of hM$_4$D$_i$ in the striatum using viral vectors driven by cell-specific neuropeptide promoters (enkephalin or dynorphin) to target receptor expression to either striatopallidal or striatonigral neurons that are physically intermixed and would be otherwise next to impossible to differentiate can contribute to elucidating critical and opposing roles of these cellular populations in the regulation of drug addiction and its molecular basis [28].

An elegant example of how to combine transgenic technology with a tetracycline-repressible system that is tissue specific with a specific and selective pharmacological tool such as a second-generation RASSL/DREADD receptor to obtain in vivo remote control of neuronal behavior is illustrated in the work of Alexander and colleagues [29]. They used in this instance the hM_3-RASSL/DREADD version expressed transgenically under the calcium/calmodulin-dependent kinase α Tet-Off system [30] selectively in hippocampal and cortex neurons. In these studies the authors showed a comprehensive and detailed analysis of the effects of hM_3-RASSL/DREADD expression and activation by CNO in isolated hippocampal slices where they recorded specific CA1 pyramidal neuron responses to the drug, and went further to analyze behavioral changes affected by different doses of CNO in individual mice. These behavioral changes, that in some cases led to seizures in the animals, could be measured and simultaneously correlated to electrophysiological changes [29].

The modified receptor and the synthetic molecule in all of the examples described above may be considered an "orthogonal pair" with two-way selectivity, such as the receptor is not activated by any other ligand, endogenous or otherwise, and the synthetic ligand cannot activate any other receptor. It is pertinent, therefore, to consider how the choice of ligand or series of chemically related molecules is critical for the success of the generation of a RASSL/DREADD. Fewer mutational and functional steps will be necessary to evolve a suitably modified receptor if the molecule chosen as candidate surrogate ligand already has a degree of affinity for the receptor. This was the case for the RASSL/DREADD muscarinic receptor series and CNO pairing [15]. Clozapine binds muscarinic receptor subtypes with similar affinity and can act as a partial agonist [23, 24], so this molecule seemed like a good starting point to develop a new synthetic agonist. In addition to this the seemingly serendipitous loss of potency for acetylcholine in this particular case helped the muscarinic family being ideal for the generation of such RASSL/DREADDs. In other cases, researchers have taken advantage of identified variation in ligand selectivity between species orthologues of a receptor to engineer and develop a RASSL/DREADD pairing and to predict further RASSL/DREADD-specific ligands [14].

The RASSL/DREADD receptor-synthetic ligand pairing ideally should reproduce all the attributes of the wild type-native ligand pair in terms of functional outcomes. However, it is clear that in the context of wild-type receptors, even closely related agonist molecules can favor the stabilization of different receptor conformations and potentially functional outcomes [31–33]. Consequently, unless this question is explored in detail [14, 34] there must be a level of concern that using a nonnative ligand able

to stabilize an "alternative" active conformation of the mutated designer receptor will have a different impact on the receptor's local signalling partner responses with potential bias towards a specific signalling pathway. This would limit the conclusions that might be drawn from work in vivo as they might show novel and difficult-to-interpret pharmacological actions that might have not been anticipated beforehand.

3   A Comprehensive Study to Validate hM$_3$-RASSL/DREADD Receptor Function

Despite the meticulous work presented by Armbruster and others on the function of muscarinic designer receptors [15], the initial studies did not attempt to systematically study if the functionality of the mutant designer receptor matched the wild-type counterpart in steps from receptor activation through to the final signalling outcomes and in terms of ligand pharmacology (Fig. 1). Indeed, an obvious feature of the RASSL/DREADD produced by molecular evolution was the reduced affinity of a
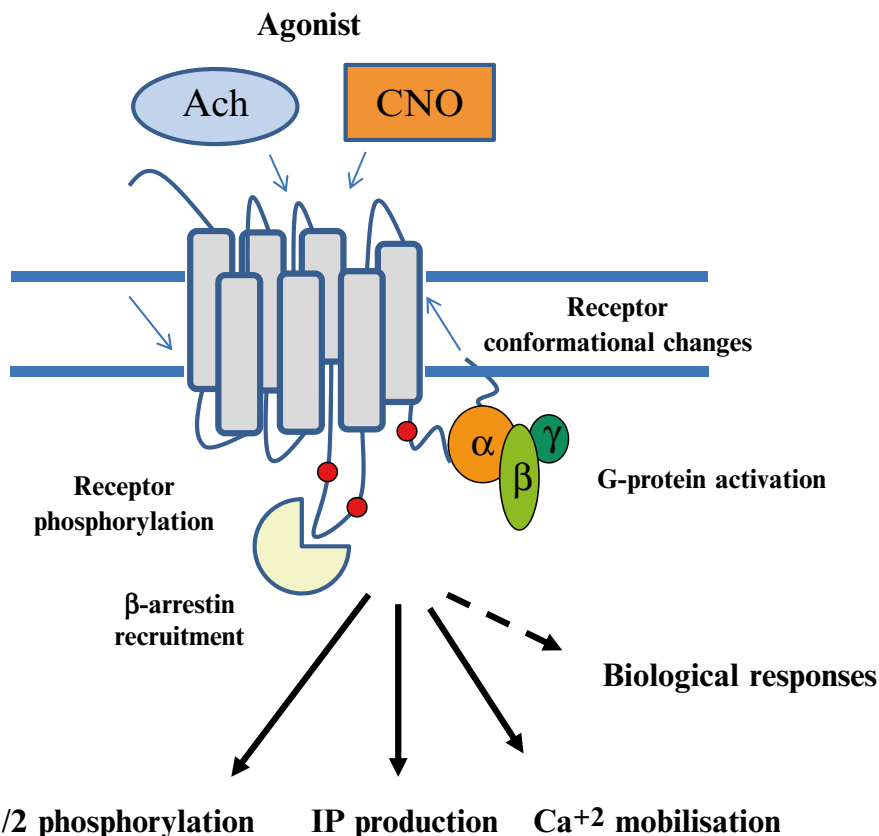
Fig. 1 Cartoon representing the cascade of events after agonist binding to a GPCR and a number of potential signal transduction outcomes

number of standard synthetic muscarinic antagonists [15]. This feature has complicated analysis of expression levels of the RASSL/DREADD variants because of the need to use high concentrations of [³H]muscarinic receptor antagonists which results in poor signal to background [35]. We have used a variety of techniques and different engineered cell lines to assess and compare in vitro the series of steps that follow agonist activation for both wild-type and RASSL/DREADD forms of the hM_3 receptor. Here we describe and discuss these approaches and indicate that such studies should be performed for all new potential RASSL/DREADD receptors prior to their use in transgenic animals if meaningful and relevant physiological information is to be obtained.

4   Changes in Receptor Conformation in Response to Ligands: Intramolecular FRET Sensors

The mechanism of agonist binding and signalling involves alterations in conformation of the ligand-binding pocket that subsequently are transmitted to the intracellular face of the receptor to allow effective interaction with G proteins and/or other effectors. Therefore, the first changes that can be quantitatively measured after ligand binding are those related to changes in receptor conformation, often by means of recording the relative movement of the transmembrane helices at the intracellular membrane face. Specific labelling of restricted domains or regions of the receptor with fluorescent probes can be used to measure changes in the relative orientation of the TMD α-helixes by measuring changes in resonance energy transfer [31, 36, 37]. A number of studies using muscarinic and other receptors [38–40] have introduced small intramolecular probes such as red ReAsH (resorufin arsenical hairpin) or yellow FlAsH (fluorescein arsenical hairpin) tags to generate intramolecular fluorescence resonance energy transfer (FRET) sensors containing the yellow (YFP) or cyan (CFP) fluorescent proteins as partners for the transfer of energy [39, 41–43]. Biarsenical fluorescent probe-binding amino acid sequences such as the fluorescein FlAsH sequence have been employed to allow fluorescent small-molecule labelling of specific locations within a wide range of proteins in live cells with nanomolar or lower affinity for the specific labelling motif [44, 45].

FlAsH plus CFP intramolecular FRET sensors have been engineered by introducing into a GPCR sequence both a CFP protein and a short tetracysteine-containing peptide, CCXXCC (where X denotes any amino acid), although currently, the specific sequence CCPGCC is mostly used as it has been identified as the optimal motif for specific labelling [46, 47]. This motif becomes the target for

labelling with the membrane-permeant fluorogenic biarsenical dye fluorescein arsenical hairpin binder-ethanedithiol (FlAsH-EDT²) (**Note 1**) [45] in intact live cells. The fluorescein dye only becomes fluorescent on binding to the specific amino acid sequence and remains stable for a number of hours after labelling. It is reported that there are negligible levels of binding sites for this molecule in untransfected mammalian cells [45]. This feature is potentially of great advantage in producing low background fluorescence, although in practise this is not as easy to confirm or obtain as suggested by the original reports.

FRET signals are defined and limited by combinations of the distance between and/or the orientation of fluorophores that participate in the transfer of energy [48]. In this regard, there are two main aspects by which using either FlAsH or ReAsH labelling may represent an advantage over a standard autofluorescent protein. The green fluorescent protein (GFP) and its many variants share a β-barrel structure with the fluorophore buried deeply in the middle of an alpha-helix that runs through the cylinder made by 11 antiparallel beta strands. The fluorophore sits in a nearly perfect perpendicular plane to the cylinder and this encapsulation protects it from oxidative quenching and is most likely responsible for the small Stokes shift and high quantum brightness of these types of proteins [49, 50]. However, this also makes the distance between fluorophore and fusion protein greater, sometimes over 15 Å, whereas the fluorescein dye bound to the CCXXCC motif is right at the location within the target protein of interest where the sequence is inserted. The small size of the tetracysteine-containing peptide makes it easier to insert in virtually any domain of a protein of interest without substantial disruption of its structure or function.

Work on the analysis of the hM_3 receptor, in parallel with the hM_3-RASSL/DREADD, was initiated with a hM_3 receptor construct in which this FlAsH recognition sequence was inserted in the IL3 and an enhanced version of CFP placed in frame at the end of the intracellular carboxyl tail [51]. This construct lacks nearly 200 amino acids of the large IL3 found in the hM_3 receptor, with the purpose of optimizing the FRET signal [51], as this is always distance dependent. Detection of FRET to monitor changes upon agonist stimulation was carried out after labelling of cells transfected to express the hM_3-FlAsH/CFP construct with FlAsH-EDT² which rendered the FlAsH-tag fluorescent as described above. Labelled cells were perfused with buffer plus/minus agonists throughout within the imaging chamber at the microscope where changes in wavelength emissions were recorded using a CCD camera. A series of images were recorded and analyzed using the appropriate image software to calculate the final FRET values as emission ratios between the FlAsH and CFP signals (i.e., 535 nm/470 nm).

To establish if the conformational changes taking place in the wild-type hM_3 receptor upon addition of the agonist carbachol were equivalent to those of the hM_3-RASSL/DREADD receptor upon CNO treatment, the $Y^{3.33}C$ and $A^{5.46}G$ mutations were introduced in hM_3 receptor constructs harboring the FlAsH-CFP sensor. In cells transfected transiently to express the wild-type hM_3 receptor intramolecular FRET sensor, carbachol produced a rapid increase in FRET signal which was not replicated by addition of CNO [34]. This increased FRET signal returned to basal with a mono-exponential time decay upon washout of carbachol, presumably reflecting the dissociation rate of the ligand. In equivalent experiments in cells expressing the hM_3-RASSL/DREADD intramolecular FRET sensor (Fig. 2) carbachol was without effect whilst CNO increased the FRET signal in a dose-dependent manner. Interestingly, the rate of increase of the FRET signal of the hM_3-RASSL/DREADD in response to CNO was markedly slower than for the wild-type receptor sensor stimulated by carbachol, whilst the hysteresis back to basal after ligand washout was also much slower. Although these observations presumably relate to association and dissociation rates of the individual ligands, the details of these differences have yet to be explored in detail and reported. To explore the relative contributions of the two sequence alterations to the gain in function for CNO, cells were then transfected with intramolecular FRET sensors incorporating only either the hM_3-$Y^{3.33}C$ or the $A^{5.46}G$ mutation. The hM_3-$Y^{3.33}C$ construct responded to neither carbachol nor CNO, whilst the $A^{5.46}G$ mutant still responded to carbachol (although much more slowly than the wild-type receptor, suggesting loss of potency for carbachol), but also did not respond to CNO. Thus, only when both mutations were present there was a robust response to CNO and of similar magnitude to that of the wild-type receptor to carbachol (Fig. 2). The changes in conformation as measured by intramolecular FRET were concentration dependent with a $pEC_{50} = 4.9 \pm 0.2$ for carbachol at the hM_3 receptor and $pEC_{50} = 5.1 \pm 0.4$ for CNO at the hM_3-RASSL/DREADD receptor form.

To attempt to explain these observations we generated molecular models of the likely binding mode of CNO to the hM_3-RASSL/DREADD receptor. In these the combination of the $Y^{3.33}C$ and $A^{5.46}G$ mutations generated enough space in the binding pocket to allow CNO to interact with a threonine at position 235 ($T^{5.42}$) believed to be critical for muscarinic agonist binding [52]. The model also suggested that tyrosine $Y^{3.33}$ participates together with two further tyrosine residues at positions 507 ($Y^{6.51}$) and 530 ($Y^{7.39}$) to form a "roof" in the wild-type receptor that is not complete in the RASSL/DREADD receptor, allowing more room for the bulkier CNO to fit in the binding pocket. On the other hand, the model indicated that binding of CNO to the wild-type
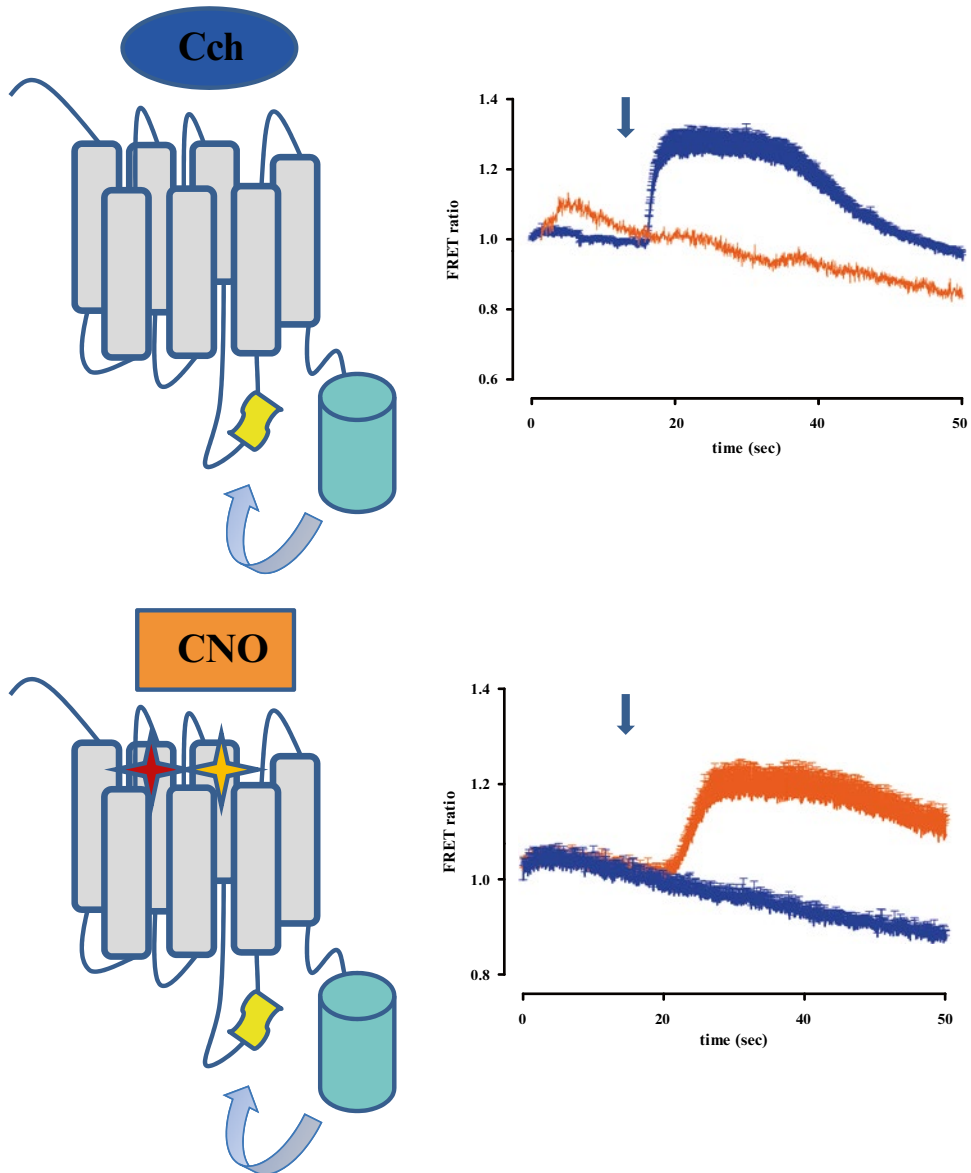
Fig. 2 Time- and agonist-dependent measurements of dynamic FRET between FlAsH (*yellow*) and CFP (*cyan*) are shown from cells expressing either hM$_3$ wild-type (*upper*) or hM$_3$-RASSL/DREADD (*lower*) receptors tagged with the FRET sensors described in the text and in [34]. Cells were exposed to a 15-s pulse (*arrow*) of maximally effective concentrations of the corresponding ligands (1 mM carbachol (Cch), *blue*; 100 μM CNO, *orange*), and subsequently perfused with buffer alone for the time shown

receptor is impaired by the lack of a positively charged head-group able to interact with the aspartate at position 148 (D$^{3.32}$). Therefore, this set of experiments demonstrated that despite CNO displaying different molecular interactions with the RASSL

receptor to acetylcholine and carbachol at the wild-type receptor it is able to elicit similar conformational changes within the seven TMD structure as reflected by the FRET changes that follow ligand addition.

5   Measurements of Agonist-Dependent Receptor Phosphorylation

It has been proposed for some time that differences in agonist-mediated phosphorylation patterns of the same receptor may be produced in different cell types or in response to different agonist ligands, giving rise to the idea of a phosphorylation "bar code" that would direct signalling towards diverse outcomes depending on the specific interactions this might induce with intracellular adaptor proteins [53, 54]. Therefore, we also assessed whether CNO would elicit a similar pattern of phosphorylation in the hM$_3$-RASSL/DREADD as carbachol at the wild-type receptor. In the hM$_3$ receptor agonist-driven activation and changes in conformation lead to the activation of associated G proteins and also phosphorylation on multiple, specific sites, mainly within the IL3 and carboxy-terminal domain [53, 55]. Receptor phosphorylation frequently also results in the recruitment of β-arrestins [56–59]. Therefore, one hypothesis was that differential phosphorylation by CNO at the hM$_3$-RASSL/DREADD receptor compared to that of acetylcholine/carbachol at the wild type might generate a β-arrestin-biased response.

Phosphorylation signatures defined via phospho-peptide maps following limited tryptic digestion are a good way to visualize the extent and potential pattern of receptor phosphorylation after agonist treatment, without the use of detailed mass spectrometric analysis on immunoprecipated receptor protein. They do, however, necessarily rely on the use and incorporation of [^{32}P]-orthophosphate [55] and, therefore, require active alterations in phosphorylation status. Agonist-dependent phosphorylation of both receptor variants expressed as VSV-G and SNAP-tagged forms in Flp-In T-REx 293 cells (*see* next section for details on these cell lines) was assessed after labelling with [^{32}P]-orthophosphate. In these type of metabolic labelling studies cells are exposed to 50–100 μCi/ml [^{32}P]-orthophosphate in phosphate-free Krebs/HEPES buffer for 60–90 min. After this time cells can be treated with the chosen agonist for an empirically determined length of time. In this particular instance cells were treated with either 100 μM CNO or 500 μM acetylcholine for 5 min and subsequently processed for immunoprecipitation using a specific polyclonal hM$_3$ receptor antibody. Size fractionation of the samples on SDS-PAGE gels followed by autoradiography of the blotted membranes revealed distinct agonist-dependent receptor phosphorylation with

the detection of an apparently single species of the size expected for these constructs: 125 kDa. hM_3 receptor showed increased phosphorylation in response to acetylcholine and no change in basal levels upon addition of CNO. This was in clear contrast to the hM_3-RASSL/DREADD where an equivalent increase in the intensity of the band was detected, but only after treatment with CNO. Global patterns of phosphorylation on 2-dimensional maps of peptides generated by limited tryptic digestion were then obtained. These provided insight into the distribution of phosphorylated residues within the receptors, albeit without identification of the specific residues, and indicated that the patterns of phosphorylation produced by the relevant receptor-agonist pairing were highly similar [34]. In such studies, after [^{32}P]-orthophosphate labelling and SDS-PAGE the areas in the nitrocellulose membrane where the phosphorylated receptor was detected (i.e., at 125 kDa) were isolated and digested subsequently with sequencing-grade trypsin (1 μg in 50–100 μl of 50 mM NH_4HCO_3) overnight at 37 °C. Following several rounds of washes and drying steps (*see* [55] for detailed methodology) the samples were separated in two dimensions: electrophoresis in pH 1.9 buffer and ascending thin-layer chromatography using isobutyric acid chromatography buffer [isobutyric acid/n-butanol/pyridine/acetic acid/water, 1250:38:96:58:558 (v/v)]. This resulted in a 2D image of resolved phospho-peptides seen as spots on film or visualized through a phosphor-imager instrument. These patterns can be compared as well as quantified using the appropriate software. The virtually identical patterns generated once more suggested that the behavior of the wild-type receptor activated by acetylcholine and the hM_3-RASSL/DREADD activated by CNO may well result in similar interactions with adaptor proteins and display similar patterns and extents of desensitization. However, as mentioned earlier, this technique does not allow to recognize the specific residues that have been phosphorylated and, of course, these may not be identical. Crucially, to extend these studies, specific individual sites of phosphorylation in the wild-type receptor had been identified in previous studies by Butcher and co-workers, using mass spectrometry [55]. These unveiled two phospho-serines found in the IL3 (Ser412) and in the C-terminal tail (Ser577) to which phospho-specific antibodies were raised [55]. Using these antibodies we were able to show that the hM_3-RASSL/DREADD receptor activated by CNO was specifically phosphorylated at these two residues as was the wild-type receptor after treatment with acetylcholine, further suggesting that the pattern of phosphorylation between the receptor variants is likely to be highly similar or identical [34]. We can conclude, therefore, that the phosphorylation "bar code" elicited by CNO at the hM_3-RASSL receptor is equivalent to that of acetylcholine acting at the wild-type counterpart,

at least in the background of the Flp-In-TRex 293 cell system. Taking into consideration the potential variation in kinases expressed in different cell types, this is something that might vary in diverse cellular backgrounds or tissues and this remains to be established.

6   Downstream Signalling Pathways 1: β-Arrestin-2 Recruitment and Receptor Internalization

Ligand bias and functional selectivity are emerging concepts that are gaining momentum in pharmacology and in the understanding of physiological receptor functions [60]. These terms refer to how ligands may act with different potency and/or efficacy through either G protein-dependent pathways or pathways governed by other adaptor molecules, such as β-arrestins. Since the discovery of β-arrestin-mediated signalling as a set of noncanonical pathways through which signalling may be driven, new technologies have been developed beyond those applied to record G protein activation [61]. It was vital, therefore, to assess if CNO might act as a biased agonist at the hM_3-RASSL/DREADD when compared with the actions of acetylcholine/carbachol at the wild-type receptor. If this was the case then the RASSL/DREADD would not be a comprehensive and effective marker of the functional roles of the hM_3 receptor in vivo. To assess this, the functional responses to both receptor's agonists, acetylcholine and CNO, were assessed in a series of cell-based assays to measure β-arrestin recruitment and receptor internalization.

To do so stable cell lines harboring either hM_3 receptor wild type or the RASSL/DREADD variant containing N-terminal SNAP-tags were generated. The SNAP tag is able to covalently bind specific substrates [35, 62, 63], including a wide variety of fluorophores. Similarly, constructs containing YFP and related autofluorescent proteins fused to the C-terminal tail were also engineered and expressed.

Agonist-mediated β-arrestin-2 (systematically also designated arrestin-3) interactions with GPCRs frequently occur subsequent to agonist-induced receptor phosphorylation and are often monitored using bioluminescence resonance energy transfer (BRET)-based assays [64–66]. This method is inexpensive, is amenable to medium- to high-throughput formats [67], and presents a number of technical advantages to use, not least because as light is generated in a chemiluminescent reaction there is no requirement to use an external light source to excite the molecules involved. This can result in substantial reduction in background fluorescence from plates and cells, as well as eliminating potential concerns with photo-bleaching arising from direct illumination of the sample

under study. The BRET measurements, which reflect β-arrestin-2 receptor interactions, are carried out in live cells, whether adherent or in suspension, and the outputs are calculated in a ratiometric manner (**Note 2**), further increasing the signal-to-noise ratio. hM_3 receptor and hM_3-RASSL/DREADD constructs fused at the C-terminal tail to the YFP mCitrine (acting as energy acceptor) and a β-arrestin-2 protein fused to the bioluminescent enzyme *Renilla* luciferase (acting as energy donor) were generated for these experiments (**Note 3**). There are a number of considerations regarding the level of expression of the fluorescent and luminescent proteins that need to be considered when establishing such assays. When comparing two or more constructs, as in these studies, the level of expression at the cell surface of all receptor constructs should be monitored (e.g., by microscopy or cell surface ELISA) and steps taken to equalize these. Direct measurements of fluorescent protein emission intensity, via a simple plate reader, can also be used to gain information on total levels of receptor expression, although this will not necessarily equate to the amount of receptor at the cell membrane. It is advisable, therefore, to titrate the amount of both acceptor and donor species (in this case the energy acceptor was the receptor construct and the β-arrestin-2 construct the energy donor) to establish the optimal ratio, with an excess of the acceptor protein being the desirable condition in terms of effective energy transfer. Generally in our hands, transient transfections with a plasmid ratio of 1:4 β-arrestin-2 to receptor [68] provides good results. However, this is a parameter that is best defined empirically (**Note 4**).

Upon agonist stimulation, rapid phosphorylation of the receptor leads to recruitment of a β-arrestin to the intracellular face of the receptor and, in so doing, brings the energy donor and energy acceptor into proximity. When the cell-permeable *Renilla* luciferase substrate coelenterazine h is added, this is oxidized by the enzyme and, as part of this process, light with an emission peak of about ~475 nm is produced. This is within the excitation spectrum of the YFP (whether eYFP or mCitrine versions) and when in proximity (<100 Å) energy is transferred, which subsequently is then emitted as light with a peak of ~535 nm. Both of the donor and acceptor emission wavelengths are recorded simultaneously through filters in a compatible microplate reader (such as a PheraStar *FS*, BMG Labtech). Ratiometric values of the fluorescent (long wavelength) over luminescent (short wavelength) signals are calculated and this increases with more effective energy transfer (**Note 2**). The receptor-arrestin interaction can also be monitored kinetically in real time [66]. Such "arrestin" assays are popular both because of the relative ease of measurement and, at least conceptually, the interaction between receptor and arrestin requires receptor occupancy by agonist and, therefore, may provide a

surrogate measure of agonist affinity at the receptor without signal amplification which, therefore, avoids potential effects of receptor reserve.

In our studies comparing the wild-type hM_3 receptor and hM_3-RASSL/DREADD, agonist-driven arrestin recruitment was concentration dependent for both receptors, with potency for carbachol at the wild-type receptor $pEC_{50} = 4.4$ and of CNO at the RASSL/DREADD $pEC_{50} = 6.4$. Treatment of hM_3-RASSL/DREADD-expressing cells with either acetylcholine or carbachol did not elicit any β-arrestin-2 recruitment. Conversely, no CNO effect was recorded when using the wild-type hM_3 receptor. Hence, both variants were equally competent in the recruitment of β-arrestin-2 and displayed the anticipated pharmacological profile.

Subsequent to arrestin recruitment, in many cases receptor internalization occurs in an arrestin-dependent manner. The internalized receptor may then be either recycled to the cell surface or degraded. The ability of CNO to elicit internalization of the hM_3-RASSL/DREADD was monitored and compared to the wild-type hM_3 receptor using stable cell lines expressing either VSV-SNAP-hM_3 receptor or VSV-SNAP-hM_3-RASSL/DREADD constructs in a further FRET-based assay. The cell lines used herein had previously been characterized extensively in regard of GPCR dimerization using time-resolved FRET measurements [35]. The SNAP-tag positioned at the amino terminal end of the receptor is a 20 kDa polypeptide, and is a modified version of O^6-alkylguanine-DNA alkyltransferase. This enzyme recognizes O^6-alkylated benzylguanines and catalyzes the transfer of the alkyl group to a cysteine, forming a covalent bond with the SNAP molecule. For a number of practical applications, including time-resolved FRET, different types of reactive O^6-benzylguanine substrates such as SNAP-Lumi4-Tb have been generated. The VSV-SNAP-hM_3 receptor- or VSV-SNAP-hM_3-RASSL/DREADD-expressing cell lines display the SNAP tag extracellularly, thus allowing labelling only of receptors at the cell surface, on addition of the cell-impermeant SNAP-Lumi4-Tb label. This benzylguanine substrate contains an encaged lanthanide terbium cryptate ion that confers long-lifetime fluorescence emission properties. This was used in an htrFRET-based assay to quantify internalization of the labelled receptor in combination with a fluorescent assay medium, Tag-lite® internalization buffer which, in this context, acts as energy acceptor. This internalization assay is carried out on live cells and can be amenable to medium-throughput format using 96-well plates. Internalization is quantified as a reduction in FRET signal upon agonist treatment. Adherent cells are labelled with saturating concentrations of SNAP-Lumi4-Tb substrate and, after washing off the excess label, treated with agonist for an appropriate time at 37 °C to induce effective receptor internalization. The time of

agonist treatment can be adjusted and optimized for the receptor under study. Changes in dynamic FRET between the SNAP-Lumi4-Tb-labelled receptor and the Tag-lite® internalization buffer are quantified as a reflection of receptor internalization. Maximal FRET will be recorded when all of the receptor is at the cell surface and a decrease in FRET signal is indicative of receptor being removed from the cell surface, taking the covalently linked donor molecule (SNAP-Lumi4-Tb) with it. The results from the experiments carried out with the wild-type hM_3 receptor and hM_3-RASSL/DREADD variant receptors were akin to those noted in the BRET-based β-arrestin-2 recruitment experiments, reinforcing the fact that receptor phosphorylation, β-arrestin-2 recruitment, and internalization are not different between the two receptor variants in response to the corresponding agonist ligand and that they are closely linked phenomena. Moreover, internalization of both hM_3 receptor and the hM_3-RASSL/DREADD displayed concentration dependence with similar potencies for the corresponding agonists as in the BRET assays (carbachol $pEC_{50} = 4.8$; CNO $pEC_{50} = 6.2$). Addition of the muscarinic antagonist atropine to either wild-type or RASSL/DREADD-expressing cells did not elicit dynamic FRET changes, consistent with the antagonist not promoting receptor internalization. In both these assays CNO was more potent at the RASSL/DREADD than acetylcholine/carbachol at the wild-type receptor. This feature is useful for in vivo studies using the RASSL/DREADD because although CNO is described as an "inert ligand," all synthetic small molecules are xenobiotics and, therefore, use at the lowest concentration practical is to be encouraged [15, 69].

7   Downstream Signalling Pathways 2: Intracellular Calcium Mobilization and MAP-Kinase Phosphorylation

Intracellular calcium release and phosphorylation of the mitogen-activated protein kinases ERK1/2 are often used as surrogate measures of G protein or β-arrestin signal amplification, respectively. We were interested in showing that even at these more downstream and amplified signalling endpoints there were no differences between the mutant designer receptor and the wild-type equivalent. There are a considerable number of technologies that can be used to monitor changes in intracellular calcium ions. These changes take place rapidly and can be subtle, therefore making their detection difficult due to differences in cell morphology or subcellular localizations. Consequently standard fluorescent methods are not the best suited for these type of analyses whereas ratiometric imaging on the other hand bypasses some of these

problems by focussing only on the shift of emission wavelengths of fluorophores such as the widely used calcium indicator Fura-2 acetoxymethyl ester (Fura-2AM). Fura-2AM can cross cell membranes due to the lipophilic nature of the conjugated acetoxymethyl ester group (**Note 5**). Once inside the cell the acetoxymethyl ester is cleaved from the molecule by endogenous esterases. In these experiments, cells are loaded with Fura-2 solution and washed subsequently to remove any excess, and subsequently treated with the agonists of interest. Measurements at ~510 nm are recorded after exciting the samples at 340 and 380 nm using a suitable plate reader such as FlexStation or a FLIPR. Calcium-bound Fura-2 is excited at 340 nm whereas the unbound form of Fura-2 is excited at 380 nm. Therefore as calcium is released from the endoplasmic reticulum or enters from the extracellular milieu the fluorescence intensity at 340 nm will increase, with proportional decrease in the 380 nm excitation channel. The 340/380 ratio is therefore used to calculate the extent of alteration of [calcium].

Coupling to $G_{q/11}$ proteins of both wild-type hM_3 receptor and the hM_3-RASSL/DREADD receptor was tested by measuring calcium elevation. We showed that each receptor was able to respond robustly to the appropriate agonists, with very similar potencies for carbachol and acetylcholine in the case of the hM_3 receptor construct and to CNO at the hM_3-RASSL/DREADD within the nanomolar range. This provided confirmation that each variant interacts with the anticipated class of G protein.

To further assess potential for differential signalling of the RASSL/DREADD and that the alteration in ligand pairing might influence signal directionality and produce "ligand bias" [70–75] we explored phosphorylation of the extracellular signal-regulated protein kinases ERK1/2 as a readout for a further amplified response that often incorporates elements of both G protein and β-arrestin-dependent signals. AlphaScreen® SureFire® technology (Perkin Elmer) is a cell-based, homogeneous, and high-throughput format (i.e., 384-well plate compatible) (**Note 6**) that employs donor and acceptor beads consisting of streptavidin-coated beads (donor) or protein A-conjugated beads (acceptor). A mixture of anti-phospho-specific antibodies, targeting the specific phosphorylation epitope in the ERK1/2 proteins and antibodies against structural epitopes within the target, is added to the cell lysates. The phosphorylated ERK1/2 in the cell lysate forms a bridge between donor and acceptor beads that allows for energy transfer to take place. Applying this assay to hM_3 receptor- and hM_3-RASSL/DREADD-expressing cells unveiled no differences in the level of constitutive activity of the receptor variants. ERK1/2 phosphorylation time courses were then performed. Both acetylcholine and CNO at the appropriate variant promoted a peak of ERK1/2 phosphorylation within 5 min of agonist addition that

was largely sustained for as long as 60 min. This was in contrast to the transient nature of ERK1/2 phosphorylation recorded upon addition of foetal bovine serum, used as a positive control, which showed a sharp peak at 5 min of treatment that decayed back rapidly to basal levels. It was noteworthy that a small peak of ERK1/2 phosphorylation was observed in the VSV-SNAP-hM$_3$-RASSL cell line when treated with a high concentration of acetylcholine that followed a similar pattern to that of the FBS-treated cells. It is likely that this reflects the known endogenous expression of muscarinic receptors in HEK293-derived cells [76].

8 Conclusions

Almost all of the studies described in this chapter indicate that the responses of the hM$_3$-RASSL/DREADD receptor to CNO are very similar to that of the hM$_3$ receptor in response to acetylcholine, and that there is no functional selectivity associated with CNO at the hM$_3$-RASSL/DREADD. Although this provides strong validation for the use of this specific RASSL/DREADD receptor in transgenic models and studies of M$_3$ receptor action, marked differences in the apparent ligand association and dissociation rate were noted that may be significant in studies exploring rapid kinetic effects mediated by the M$_3$-RASSL/DREADD.

9 Outlook

The novel use of engineered RASSL/DREADD receptors to interrogate and control signalling pathways is helping to close the gap in understanding the relationship between drug and receptor function (Fig. 3). As discussed through this and other chapters in this book, families of receptors activated selectively and exclusively by a synthetic drug allow exquisite temporal and spatial modulation of their downstream signals in in vitro and, most importantly, in vivo systems. Furthermore, it is becoming evident that RASSL/DREADD receptors can be used efficiently as tools to achieve fine remote spatiotemporal control of specific cellular populations within specific tissues, such as particular brain regions, neuronal populations, or even neuronal subdomains to provide axonal or dendritic targeted expression [13, 29, 77, 78].

Complex cellular processes such as cell migration can be addressed using such chemical genetics approaches. A recent example in the literature reflects the ability of a muscarinic RASSL/DREADD-engineered receptor to redirect cellular migration towards CNO when expressed in HL-60 neutrophils and other mammalian cell lines, such as endothelial cells [79].

Fig. 3 Summary of muscarinic RASSL/DREADD receptor types currently available and some of their practical applications to date. hM_3D_q, human M_3 - G_q coupling; hM_4D_i, human M_4 - G_i coupling; rM_3D_s, rat M_3 - G_s coupling (swapped loops represented in red, see main text for details); $rM_3D_{arr}/R_q(R165L)$, rat M_3 arrestin biased receptor. Stars represent mutations in TMDIII and TMV, whereas the mutation on the DRY motif is represented by a yellow triangle

This orthogonal control of cell chemotaxis can provide a powerful tool for understanding the process that can also be applied to future cell-based therapeutics. In this context cells could be "guided" towards specific locations to exert their effects simply by producing localized concentrations of the synthetic drug, whether compacted in beads, micropumps, or microspheres, to create a gradient of chemoattractant.

The family of muscarinic acetylcholine receptors may be seen as a paradigm in RASSL/DREADD receptors as it has been extensively used due to their tissue distribution and involvement in a wide array of neurological (Parkinson's and Alzheimer's disease, schizophrenia) and metabolic (type 2 diabetes) diseases, which make them a very attractive target for the development of new drugs if the receptor can be validated as a suitable therapeutic target. Hence, there is a clear need for a deeper understanding of their complex pharmacology and, by extension, receptor physiology. Aspects of neural function such as wakefulness, regulation of food intake, and memory [77, 80–82] have been explored using muscarinic RASSL/DREADDs. Human forms of muscarinic RASSL/DREADDs that couple to G_q (hM_3Dq) [29], G_i (hM_4Di) [15], as well as rat/human or rat/turkey (rM_3D$_s$ and rM_3D$_{s/q}$) [83] have been developed to cover three of the major G protein-dependent signalling pathways.

Although in some instances, as described throughout this chapter, biased signalling at the RASSL/DREADD receptor is not desirable, there may be cases in which having a receptor variant biased towards a particular pathway will be advantageous. This has been explored for the M_3 receptor with Nakajima and colleagues recently describing an arrestin-biased receptor that has lost G protein coupling capacity. This engineered receptor form was constructed using the rat M_3 receptor containing the expected RASSL mutations in TMDIII and TMV, plus an arginine-to-leucine mutation within the DRY motif ($R^{3.50}L$) [84]. This substitution rendered the receptor unable to activate the corresponding heterotrimeric G proteins in the presence of the agonist CNO, therefore resulting in it being biased towards the recruitment and initiation of arrestin 2- and 3-dependent signalling in an agonist-dependent manner [84]. Expression of this receptor in a heterologous manner or in animal models under the control of the synthetic ligand makes it a potentially valuable tool to evaluate exclusively β-arrestin-dependent signalling in different tissues or cell types.

Finally, the use of RASSL/DREADD receptors as pharmacological tools has transcended physiological and signalling studies and has also been used to address the molecular mechanisms of receptor dimerization and the potential effects of ligands on its regulation [35]. Based on the increasing literature supporting the idea of GPCRs existing as dimers or higher order oligomers [85, 86], we took advantage of the differential pharmacology of hM_3 receptor and the RASSL/DREADD receptor variant in these studies. Work from Alvarez-Curto [35] and Patowary and colleagues [87] showed that hM_3 receptor wild type and hM_3-RASSL/DREADD forms of the receptors generate complexes that can be dimeric or tetrameric in nature. One of these studies explored agonist-dependent regulation of dimerization and demonstrated, using different biophysical approaches including time-resolved

FRET and single-cell FRET, that when both receptor forms were present treatment only with carbachol but not with CNO had an effect on the dimeric arrangement or at least in the distances between the two protomers [35]. Further insight into receptor dimerization has been gained using the serotonin type 4 receptor, 5-HT$_4$, and a corresponding RASSL/DREADD that also showed how agonist activation of both protomers within a dimer has different effects on G protein activation [88, 89], with better efficiency of G protein activation being produced when both protomers were occupied. Some of the results from these studies, and those carried out by others in relation to ligand regulation of receptor dimerization [35, 89–91], are difficult to interpret, and sometimes limited by the technical approaches used, but they highlight the value of having differential protomer pharmacology to study the molecular basis of dimerization.

Despite all of these advances there are still milestones to reach within the RASSL/DREADD field. There are currently no RASSL/DREADD receptors biased towards G protein signalling only, nor an RASSL/DREADD receptor that selectively activates G$_{12/13}$. Even though there are a number of RASSL/DREADD constructs outwith the muscarinic family, these generally lack a potent and bioavailable synthetic drug selected or identified through molecular evolution techniques. These can be of use in screening novel biased ligands or alternative receptor modulators in vivo [84, 92] as well as to study further aspects of receptor molecular pharmacology such as dimerization in vitro [35, 88].

10   Notes

1. Labelling with biarsenical dyes may be hampered by the presence of BSA in serum-containing medium, so before labelling medium should be carefully washed away using a buffer containing Ca^{2+} and Mg^{2+} ions.

   The biarsenical dye is light sensitive and care should be taken during the preparation of stocks. Both 1,2-ethanedithiol (EDT) and 2,3-dimercapto-1-propanol (BAL) labelling compounds used have an unpleasant odor, so they should always be handled in appropriated fume hoods.

   The labelling procedure should be carried out with particular attention to the several washing steps. All unbound dye should also be carefully removed to avoid undesirable nonspecific background fluorescence by washing cells at least three times for 10 min at 37 °C with wash solution containing either EDT or BAL in standard Hanks' Balanced Salt Solution with 5.6 mM glucose.

2. It is generally accepted when performing this type of assay to include a "luciferase/donor-only" control. This control

allows correction for any background emission that can be detected in the absence of ligand-mediated interaction or in the absence of acceptor. The reading from this set of samples contains signal only from the donor and therefore is subtracted from those containing acceptor and donor constructs to obtain a specific BRET ratio or net BRET. The final calculations will follow the following formula:

$$\text{BRET ratio} = \left[\left(535\,\text{nm reading} \,/\, 475\,\text{nm reading}\right)\right]_{\text{donor+acceptor}}$$
$$- \left[\left(535\,\text{nm reading} \,/\, 475\,\text{nm reading}\right)\right]_{\text{donor only}} \quad .$$

This is sometimes shown as milli BRET units (mBRET) by multiplying the net BRET number by 1000.

3. These constructs are generally generated using the most suitable expression vector, commonly pcDNA3.1 (Life Technologies).

4. To achieve optimal results in resonance energy transfer assays the acceptor molecule should be present in excess of the donor molecule (greater amount of YFP over luciferase in this case). However because in this type of BRET-based arrestin recruitment assay there might be a constraint related to the stoichiometry between arrestin and receptor these two factors should be taken into account when setting up the experiment.

5. Due to the low solubility of AM esters in aqueous solutions low-toxicity dispersing agents such as pluronic acid (Pluronic® F-127) can be used to facilitate cell loading with the calcium dye. Loading times of between 15 min and 1 h are sufficient, and generally this is carried out at the temperature that is optimal for the cells. However, some reports suggest that loading the cells at lower temperatures (room temperature) might result in a reduction of compartmentalization of the dye.

   Also to keep extracellular hydrolysis of the AM and acetate esters to a minimum, it is recommended that a loading buffer free of primary and secondary amines such as PBS be used. Cells should be washed in dye-free buffer after loading.

6. Despite this being an assay that in principle can be used in most cellular backgrounds, from heterologous cells overexpressing constructs of interest to primary cells, not all of these cell lines might express the same level of analyte protein, i.e., ERK1/2. Therefore, not all cell lines will respond the same way and cell line selection is an important consideration when designing an assay.

   This assay is also extremely sensitive to the presence of DMSO in the reaction mixture, so this must be kept to a minimum, with 1 % DMSO as the highest acceptable threshold.

References

1. Digby GJ, Shirey JK, Conn PJ (2010) Allosteric activators of muscarinic receptors as novel approaches for treatment of CNS disorders. Mol Biosyst 6(8):1345–1354

2. Wess J (2004) Muscarinic acetylcholine receptor knockout mice: novel phenotypes and clinical implications. Annu Rev Pharmacol Toxicol 44:423–450

3. Kruse AC, Hu J, Kobilka BK, Wess J (2014) Muscarinic acetylcholine receptor X-ray structures: potential implications for drug development. Curr Opin Pharmacol 16:24–30

4. Haga K et al (2012) Structure of the human M2 muscarinic acetylcholine receptor bound to an antagonist. Nature 482(7386):547–551

5. Kow RL, Nathanson NM (2012) Structural biology: Muscarinic receptors become crystal clear. Nature 482(7386):480–481

6. Kruse AC et al (2012) Structure and dynamics of the M3 muscarinic acetylcholine receptor. Nature 482(7386):552–556

7. McKinney M, Jacksonville MC (2005) Brain cholinergic vulnerability: relevance to behavior and disease. Biochem Pharmacol 70(8): 1115–1124

8. Wess J (2012) Novel muscarinic receptor mutant mouse models. Handb Exp Pharmacol 208:95–117

9. Wess J et al (2003) M1-M5 muscarinic receptor knockout mice as novel tools to study the physiological roles of the muscarinic cholinergic system. Receptors Channels 9(4):279–290

10. Conklin BR et al (2008) Engineering GPCR signaling pathways with RASSLs. Nat Methods 5(8):673–678

11. Coward P et al (1998) Controlling signaling with a specifically designed Gi-coupled receptor. Proc Natl Acad Sci U S A 95(1):352–357

12. Pei Y, Dong S, Roth BL (2010) Generation of designer receptors exclusively activated by designer drugs (DREADDs) using directed molecular evolution. Curr Protoc Neurosc 50: 4.33.1–4.33.25

13. Dong S, Rogan SC, Roth BL (2010) Directed molecular evolution of DREADDs: a generic approach to creating next-generation RASSLs. Nat Protoc 5(3):561–573

14. Hudson BD et al (2012) Chemically engineering ligand selectivity at the free fatty acid receptor 2 based on pharmacological variation between species orthologs. FASEB J 26(12): 4951–4965

15. Armbruster BN, Li X, Pausch MH, Herlitze S, Roth BL (2007) Evolving the lock to fit the key to create a family of G protein-coupled receptors potently activated by an inert ligand. Proc Natl Acad Sci U S A 104(12): 5163–5168

16. Strader CD et al (1991) Allele-specific activation of genetically engineered receptors. J Biol Chem 266(1):5–8

17. Strader CD, Sigal IS, Dixon RA (1989) Genetic approaches to the determination of structure-function relationships of G protein-coupled receptors. Trends Pharmacol Sci Suppl:26–30

18. Sartania N, Appelbe S, Pediani JD, Milligan G (2007) Agonist occupancy of a single monomeric element is sufficient to cause internalization of the dimeric beta2-adrenoceptor. Cell Signal 19(9):1928–1938

19. Campbell JH, Lengyel JA, Langridge J (1973) Evolution of a second gene for beta-galactosidase in Escherichia coli. Proc Natl Acad Sci U S A 70(6):1841–1845

20. Price LA, Kajkowski EM, Hadcock JR, Ozenberger BA, Pausch MH (1995) Functional coupling of a mammalian somatostatin receptor to the yeast pheromone response pathway. Mol Cell Biol 15(11): 6188–6195

21. Pausch MH et al (1998) Heterologous G protein-coupled receptors expressed in Saccharomyces cerevisiae: methods for genetic analysis and ligand Identification and Expression of G protein-coupled Receptors, (196–212) Ed. Wiley-Liss, New York

22. Erlenbach I et al (2001) Functional expression of M-1, M-3, and M-5 muscarinic acetylcholine receptors in yeast. J Neurochem 77(5): 1327–1337

23. Olianas MC, Maullu C, Onali P (1999) Mixed agonist-antagonist properties of clozapine at different human cloned muscarinic receptor subtypes expressed in Chinese hamster ovary cells. Neuropsychopharmacology 20(3): 263–270

24. Davies MA, Compton-Toth BA, Hufeisen SJ, Meltzer HY, Roth BL (2005) The highly efficacious actions of N-desmethylclozapine at muscarinic receptors are unique and not a common property of either typical or atypical antipsychotic drugs: is M1 agonism a prerequisite for mimicking clozapine's actions? Psychopharmacology (Berl) 178(4):451–460

25. Ballesteros JA, Weinstein H (1995) Integrated methods for the construction of three dimensional models and computational probing of structure-function relations in G-protein coupled receptors. Methods Neurosci 25: 366–428

26. Han SJ et al (2005) Identification of an agonist-induced conformational change occurring adjacent to the ligand-binding pocket of the M(3) muscarinic acetylcholine receptor. J Biol Chem 280(41):34849–34858

27. Han SJ et al (2005) Pronounced conformational changes following agonist activation of the M(3) muscarinic acetylcholine receptor. J Biol Chem 280(26):24870–24879

28. Ferguson SM et al (2011) Transient neuronal inhibition reveals opposing roles of indirect and direct pathways in sensitization. Nat Neurosci 14(1):22–24

29. Alexander GM et al (2009) Remote control of neuronal activity in transgenic mice expressing evolved G protein-coupled receptors. Neuron 63(1):27–39

30. Mayford M et al (1996) Control of memory formation through regulated expression of a CaMKII transgene. Science 274(5293):1678–1683

31. Swaminath G et al (2005) Probing the beta2 adrenoceptor binding site with catechol reveals differences in binding and activation by agonists and partial agonists. J Biol Chem 280(23): 22165–22171

32. Kobilka BK, Deupi X (2007) Conformational complexity of G-protein-coupled receptors. Trends Pharmacol Sci 28(8):397–406

33. Bhattacharya S, Hall SE, Li H, Vaidehi N (2008) Ligand-stabilized conformational states of human beta(2) adrenergic receptor: insight into G-protein-coupled receptor activation. Biophys J 94(6):2027–2042

34. Alvarez-Curto E et al (2011) Developing chemical genetic approaches to explore G protein-coupled receptor function: validation of the use of a receptor activated solely by synthetic ligand (RASSL). Mol Pharmacol 80(6): 1033–1046

35. Alvarez-Curto E, Ward RJ, Pediani JD, Milligan G (2010) Ligand regulation of the quaternary organization of cell surface M3 muscarinic acetylcholine receptors analyzed by fluorescence resonance energy transfer (FRET) imaging and homogeneous time-resolved FRET. J Biol Chem 285(30):23318–23330

36. Lohse MJ, Bunemann M, Hoffmann C, Vilardaga JP, Nikolaev VO (2007) Monitoring receptor signaling by intramolecular FRET. Curr Opin Pharmacol 7(5):547–553

37. Lohse MJ et al (2008) Kinetics of G-protein-coupled receptor signals in intact cells. Br J Pharmacol 153(Suppl 1):S125–S132

38. Maier-Peuschel M et al (2010) A fluorescence resonance energy transfer-based M2 muscarinic receptor sensor reveals rapid kinetics of allosteric modulation. J Biol Chem 285(12): 8793–8800

39. Zurn A et al (2009) Fluorescence resonance energy transfer analysis of alpha 2a-adrenergic receptor activation reveals distinct agonist-specific conformational changes. Mol Pharmacol 75(3):534–541

40. Xu TR, Ward RJ, Pediani JD, Milligan G (2011) The orexin OX(1) receptor exists predominantly as a homodimer in the basal state: potential regulation of receptor organization by both agonist and antagonist ligands. Biochem J 439(1):171–183

41. Vilardaga JP (2011) Studying ligand efficacy at G protein-coupled receptors using FRET. Methods Mol Biol 756:133–148

42. Nikolaev VO, Bunemann M, Schmitteckert E, Lohse MJ, Engelhardt S (2006) Cyclic AMP imaging in adult cardiac myocytes reveals far-reaching beta1-adrenergic but locally confined beta2-adrenergic receptor-mediated signaling. Circ Res 99(10):1084–1091

43. Hoffmann C et al (2005) A FlAsH-based FRET approach to determine G protein-coupled receptor activation in living cells. Nat Methods 2(3):171–176

44. Adams SR et al (2002) New biarsenical ligands and tetracysteine motifs for protein labeling in vitro and in vivo: synthesis and biological applications. J Am Chem Soc 124(21): 6063–6076

45. Griffin BA, Adams SR, Tsien RY (1998) Specific covalent labeling of recombinant protein molecules inside live cells. Science 281(5374):269–272

46. Martin BR, Giepmans BN, Adams SR, Tsien RY (2005) Mammalian cell-based optimization of the biarsenical-binding tetracysteine motif for improved fluorescence and affinity. Nat Biotechnol 23(10):1308–1314

47. Hoffmann C et al (2010) Fluorescent labeling of tetracysteine-tagged proteins in intact cells. Nat Protoc 5(10):1666–1677

48. Alvarez-Curto E, Pediani JD, Milligan G (2010) Applications of fluorescence and bioluminescence resonance energy transfer to drug discovery at G protein coupled receptors. Anal Bioanal Chem 398(1):167–180

49. Yang F, Moss LG, Phillips GN Jr (1996) The molecular structure of green fluorescent protein. Nat Biotechnol 14(10):1246–1251

50. Ormo M et al (1996) Crystal structure of the Aequorea victoria green fluorescent protein. Science 273(5280):1392–1395

51. Ziegler N, Batz J, Zabel U, Lohse MJ, Hoffmann C (2011) FRET-based sensors for the human M1-, M3-, and M5-acetylcholine

receptors. Bioorg Med Chem 19(3): 1048–1054

52. Wess J, Maggio R, Palmer JR, Vogel Z (1992) Role of conserved threonine and tyrosine residues in acetylcholine binding and muscarinic receptor activation. A study with m3 muscarinic receptor point mutants. J Biol Chem 267(27): 19313–19319

53. Poulin B et al (2010) The M3-muscarinic receptor regulates learning and memory in a receptor phosphorylation/arrestin-dependent manner. Proc Natl Acad Sci U S A 107(20):9440–9445

54. Tobin AB, Butcher AJ, Kong KC (2008) Location, location, location…site-specific GPCR phosphorylation offers a mechanism for cell-type-specific signalling. Trends Pharmacol Sci 29(8):413–420

55. Butcher AJ, Tobin AB, Kong KC (2011) Examining site-specific GPCR phosphorylation. Methods Mol Biol 746:237–249

56. Gurevich VV, Gurevich EV (2004) The molecular acrobatics of arrestin activation. Trends Pharmacol Sci 25(2):105–111

57. Lefkowitz RJ, Shenoy SK (2005) Transduction of receptor signals by beta-arrestins. Science 308(5721):512–517

58. Lefkowitz RJ, Whalen EJ (2004) beta-arrestins: traffic cops of cell signaling. Curr Opin Cell Biol 16(2):162–168

59. Whalen EJ, Rajagopal S, Lefkowitz RJ (2011) Therapeutic potential of beta-arrestin- and G protein-biased agonists. Trends Mol Med 17(3):126–139

60. Shukla AK (2014) Biasing GPCR signaling from inside. Sci Signal 7(310):pe3

61. Verkaar F et al (2008) G protein-independent cell-based assays for drug discovery on seven-transmembrane receptors. Biotechnol Annu Rev 14:253–274

62. Gautier A et al (2008) An engineered protein tag for multiprotein labeling in living cells. Chem Biol 15(2):128–136

63. Ward RJ, Pediani JD, Milligan G (2011) Heteromultimerization of cannabinoid CB(1) receptor and orexin OX(1) receptor generates a unique complex in which both protomers are regulated by orexin A. J Biol Chem 286(43): 37414–37428

64. Hamdan FF, Audet M, Garneau P, Pelletier J, Bouvier M (2005) High-throughput screening of G protein-coupled receptor antagonists using a bioluminescence resonance energy transfer 1-based beta-arrestin2 recruitment assay. J Biomol Screen 10(5):463–475

65. Kocan M, Pfleger KD (2009) Detection of GPCR/beta-arrestin interactions in live cells using bioluminescence resonance energy transfer technology. Methods Mol Biol 552: 305–317

66. Kocan M, Dalrymple MB, Seeber RM, Feldman BJ, Pfleger KD (2010) Enhanced BRET technology for the monitoring of agonist-induced and agonist-independent interactions between GPCRs and beta-arrestins. Front Endocrinol 1:12

67. Kocan M, See HB, Seeber RM, Eidne KA, Pfleger KD (2008) Demonstration of improvements to the bioluminescence resonance energy transfer (BRET) technology for the monitoring of G protein-coupled receptors in live cells. J Biomol Screen 13(9):888–898

68. Jenkins L et al (2012) Antagonists of GPR35 display high species ortholog selectivity and varying modes of action. J Pharmacol Exp Ther 343(3):683–695

69. Rogan SC, Roth BL (2011) Remote control of neuronal signaling. Pharmacol Rev 63(2): 291–315

70. Mailman RB (2007) GPCR functional selectivity has therapeutic impact. Trends Pharmacol Sci 28(8):390–396

71. Violin JD, Lefkowitz RJ (2007) Beta-arrestin-biased ligands at seven-transmembrane receptors. Trends Pharmacol Sci 28(8):416–422

72. Vaidehi N, Kenakin T (2010) The role of conformational ensembles of seven transmembrane receptors in functional selectivity. Curr Opin Pharmacol 10(6):775–781

73. Rajagopal S, Rajagopal K, Lefkowitz RJ (2010) Teaching old receptors new tricks: biasing seven-transmembrane receptors. Nat Rev Drug Discov 9(5):373–386

74. Kenakin T (2011) Functional selectivity and biased receptor signaling. J Pharmacol Exp Ther 336(2):296–302

75. Smith NJ, Bennett KA, Milligan G (2011) When simple agonism is not enough: emerging modalities of GPCR ligands. Mol Cell Endocrinol 331(2):241–247

76. Shaw G, Morse S, Ararat M, Graham FL (2002) Preferential transformation of human neuronal cells by human adenoviruses and the origin of HEK 293 cells. FASEB J 16(8): 869–871

77. Garner AR et al (2012) Generation of a synthetic memory trace. Science 335(6075): 1513–1516

78. Zhu H et al (2014) Chemogenetic inactivation of ventral hippocampal glutamatergic neurons disrupts consolidation of contextual fear memory. Neuropsychopharmacology 39(8): 1880–1892

79. Park JS et al (2014) Synthetic control of mammalian-cell motility by engineering chemotaxis to an orthogonal bioinert chemical signal. Proc Natl Acad Sci U S A 111(16): 5896–5901

80. Sasaki K et al (2011) Pharmacogenetic modulation of orexin neurons alters sleep/wakefulness states in mice. PLoS One 6(5), e20360

81. Krashes MJ et al (2011) Rapid, reversible activation of AgRP neurons drives feeding behavior in mice. J Clin Invest 121(4):1424–1428

82. Wess J, Nakajima K, Jain S (2013) Novel designer receptors to probe GPCR signaling and physiology. Trends Pharmacol Sci 34(7):385–392

83. Guettier JM et al (2009) A chemical-genetic approach to study G protein regulation of beta cell function in vivo. Proc Natl Acad Sci U S A 106(45):19197–19202

84. Nakajima K, Wess J (2012) Design and functional characterization of a novel, arrestin-biased designer G protein-coupled receptor. Mol Pharmacol 82(4):575–582

85. Milligan G, Canals M, Pediani JD, Ellis J, Lopez-Gimenez JF (2006) The role of GPCR dimerisation/oligomerisation in receptor signalling. Ernst Schering Found Symp Proc 2: 145–161

86. Ferre S et al (2014) G protein-coupled receptor oligomerization revisited: functional and pharmacological perspectives. Pharmacol Rev 66(2):413–434

87. Patowary S et al (2013) The muscarinic M3 acetylcholine receptor exists as two differently sized complexes at the plasma membrane. Biochem J 452(2):303–312

88. Pellissier LP et al (2011) G protein activation by serotonin type 4 receptor dimers: evidence that turning on two protomers is more efficient. J Biol Chem 286(12):9985–9997

89. Claeysen S, Donneger R, Giannoni P, Gaven F, Pellissier LP (2013) Serotonin type 4 receptor dimers. Methods Cell Biol 117:123–139

90. Herrick-Davis K, Grinde E, Harrigan TJ, Mazurkiewicz JE (2005) Inhibition of serotonin 5-hydroxytryptamine2c receptor function through heterodimerization: receptor dimers bind two molecules of ligand and one G-protein. J Biol Chem 280(48):40144–40151

91. Herrick-Davis K (2013) Functional significance of serotonin receptor dimerization. Exp Brain Res 230(4):375–386

92. Gaven F et al (2013) Pharmacological profile of engineered 5-HT(4) receptors and identification of 5-HT(4) receptor-biased ligands. Brain Res 1511:65–72

Design and Analysis of an Arrestin-Biased DREADD

Ken-ichiro Nakajima, Luis E. Diaz Gimenez, Vsevolod V. Gurevich, and Jürgen Wess

Abstract

Muscarinic receptor-based designer G protein-coupled receptors (GPCRs) have emerged as novel pharmacological tools to address key questions regarding GPCR function and biology. These mutant muscarinic receptors are unable to bind acetylcholine (ACh), the endogenous muscarinic receptor ligand, but can be efficiently activated by clozapine-N-oxide (CNO), an otherwise pharmacologically inert compound. These CNO-sensitive designer GPCRs (alternative name: designer receptors exclusively activated by designer drug/DREADDs) have proven highly useful to explore the in vivo roles of distinct G protein signaling pathways in specific cell types or tissues. Like native GPCRs, CNO-activated DREADDs do not only couple to heterotrimeric G proteins but can also recruit proteins of the arrestin family (arrestin-2 and -3). Many studies have shown that arrestins can act as scaffolding proteins to promote signaling through G protein-independent pathways. To develop a novel tool useful for studying the physiological relevance of these arrestin-dependent signaling pathways, we recently described the development of an M_3 muscarinic receptor-based DREADD that is no longer able to couple to G proteins but can recruit arrestins and initiate arrestin-mediated signaling in a CNO-dependent fashion. In this chapter, we provide protocols useful for the pharmacological and functional characterization of this newly developed DREADD. These protocols can be applied more generally to all other members of the DREADD receptor family.

Key words GPCR, Arrestin, DREADD, Transfection, Radioligand binding, FLIPR, BRET recruitment, Signal transduction

1 Introduction

G protein-coupled receptors (GPCRs) represent a superfamily of cell surface receptors that regulate the activity of virtually every cell type. GPCRs are activated following the binding of extracellular ligands (neurotransmitters, hormones, neuromodulators, sensory stimuli, etc.), allowing the receptors to interact with and activate specific classes of heterotrimeric G proteins, which in turn modulate the activity of numerous effector enzymes and ion channels. The activated GPCRs are rapidly phosphorylated by G protein-coupled receptor kinases (GRKs; [1, 2]). In most cases, the phosphorylated receptors bind to members of the arrestin protein

family (arrestin-2 and -3; also known as β-arrestin-1 and -2), a process which interferes with receptor/G protein coupling [3] and promotes GPCR internalization by targeting the receptors to clathrin-coated pits [4].

1.1 Arrestin-Dependent Signaling Pathways

During the past 10–15 years, it has become increasingly clear that arrestin-2 and -3 can also serve as adaptor proteins that transduce signals to multiple effector pathways including different MAP kinase cascades [5–7]. A better understanding of the physiological roles of such pathways should prove beneficial for developing novel classes of clinically useful drugs, including arrestin-biased agonists [5, 6, 8]. However, research in this area is complicated by the fact that activated GPCRs trigger G protein- and arrestin-dependent signaling in an overlapping fashion.

1.2 Development of an Arrestin-Biased DREADD

During the past few years, CNO-sensitive designer muscarinic receptors (DREADDs) endowed with different coupling properties have emerged as novel experimental tools to probe the physiological relevance of activating different functional classes of heterotrimeric G proteins in a particular cell type in vivo (for recent reviews, refs. [9] and [10]). Like endogenous GPCRs, CNO-activated DREADDs can also recruit proteins of the arrestin family (arrestin-2 and -3) to the activated designer receptors [11, 12]. In order to facilitate studies of the physiological relevance of arrestin-dependent signaling pathways, we recently developed a novel DREADD that can recruit arrestins in a CNO-dependent fashion but is no longer able to activate heterotrimeric G proteins [12]. Structurally, this DREADD is identical to a previously described M_3 receptor-based G_q DREADD (rM3Dq according to the nomenclature proposed in ref. [10]), except for a $R165L^{3.50}$ point mutation at the bottom of transmembrane domain 3 (TM3) (Fig. 1). In the following, we simply refer to the rM3Dq construct and the arrestin-biased version of this designer receptor simply as Rq and Rq(R165L), respectively. The mutated arginine residue ($R^{3.50}$) is part of the DRY motif that is highly conserved among class A GPCRs. Numerous studies have shown that this residue plays a key role in productive receptor/G protein coupling (for an important structural study, *see* ref. [13]). Several years ago, we demonstrated that introduction of this point mutation into the wild-type (WT) rat M_3 receptor abolished the ability of the receptor to activate G proteins of the G_q family [14]. We therefore speculated that introduction of this point mutation into Rq would cause a similar functional deficit. Consistent with this notion, we demonstrated that CNO treatment of cells expressing the Rq(R165L) DREADD did not lead to an increase in intracellular calcium levels, a response that is typically observed after the activation of G_q-type G proteins. Additional biophysical and biochemical studies showed that the Rq(R165L) receptor retained the ability to interact with arrestins and to initiate arrestin-dependent signaling in
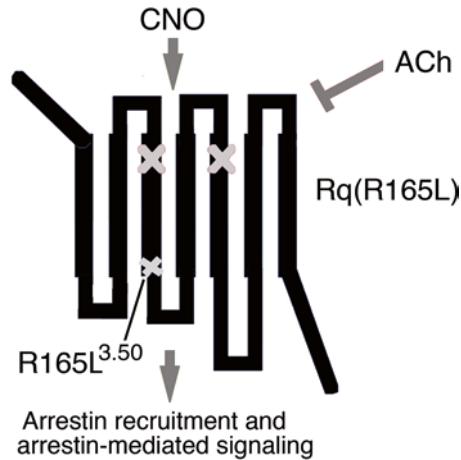
Fig. 1 Structure of an arrestin-biased DREADD. This designer receptor, referred to as Rq(R165L) in this chapter, is derived from the Gq DREADD (Rq) described in ref. [15]. Besides the two point mutations (large "x" marks) that alter the ligand binding properties of this modified M_3 receptor, the Rq(R165L) construct contains the additional R165L[3.50] point mutation at the bottom of transmembrane helix 3 (TM3) which abolishes productive receptor/G protein coupling [12]. However, the Rq(R165L) DREADD retains the ability to recruit arrestin-2 and -3 in a CNO-dependent fashion [12]

a CNO-dependent fashion [12]. Thus, this newly developed arrestin-biased DREADD represents a powerful new tool to study the physiological relevance of arrestin-dependent signaling cascades.

In this chapter, we describe several methods useful for the pharmacological characterization of the Rq(R165L) designer receptor as well as DREADDs in general. These methods include radioligand binding and calcium mobilization assays as well as BRET techniques to study DREADD/arrestin interactions.

2   Transient Expression of DREADDs in Cultured Cells

For pharmacological studies, DREADDs can be expressed at high levels in transiently transfected COS-7 cells. The ligand binding and functional properties of the designer receptors can then be determined in radioligand binding and functional assays.

2.1   Materials   COS-7 cells (ATCC, Manassas, VA); DMEM, lipofectamine, PLUS reagent, and penicillin/streptomycin (Life Technologies). The coding sequence of Rq (ref. [15]), including an N-terminal hemagglutinin (HA) epitope tag, was inserted into the pcDNA3.1 (−) vector (Life Technologies) using the *EcoR*I and *BamH*I sites. The Rq(R165L) plasmid is identical to Rq-pcDNA3.1 (−) except for the R165L point mutation which was introduced by using the QuikChange site-directed mutagenesis kit (Agilent) [12].

2.2 Methods   One day prior to transfection, COS-7 cells are seeded into 100 mm dishes at 1×10^6 cells/dish and cultured in DMEM including 10 % FBS and penicillin (100 units/ml)/streptomycin (100 μg/ml) in a humidified atmosphere of 5 % CO_2/95 % O_2 at 37 °C. On the day of transfection, cells should be ~60–80 % confluent. Four μg DNA of DREADD plasmid DNA (coding for Rq or Rq(R165L)) and 20 μl of PLUS reagent are added to a 1.5 ml Eppendorf tube containing 1 ml of serum-free DMEM, followed by a 15-min incubation at room temperature (RT). In a second 1.5 ml tube, 30 μl of lipofectamine is added to 1 ml of serum-free DMEM. The two mixtures are then combined, gently mixed, and incubated for another 15 min at RT. In the meantime, the cells are washed with 1× PBS and 3 ml of fresh, serum-free DMEM is added. After the 15-min incubation period, the transfection mixture is added to the culture dish. The cells are then incubated for 3–6 h at 37 °C, followed by the addition of 5 ml DMEM containing 20 % FBS. After this step, the cells are cultured for ~48 h and then used for various assays (*see* below).

2.3 Notes   Cell density can greatly affect transfection efficiency. Cells that are 100 % confluent or less than 50 % confluent are usually not suitable for transfection. For control purposes, cells transfected with vector DNA alone (e.g., pcDNA) should always be included in the experimental setup.

3 Receptor Binding Assays

Radioligand binding experiments can be used to determine the presence, density, and pharmacological characteristics of DREADDs (or GPCRs in general) expressed in transfected cells. As mentioned in Sect. 1, DREADDs are unable to interact with the endogenous agonist, acetylcholine (ACh), but can bind CNO with high affinity. Following the modification of an existing DREADD by site-directed mutagenesis, it is important to demonstrate that the resulting construct retains DREADD-like binding properties. Several studies have shown that DREADDs retain the ability to bind radio-labeled muscarinic antagonists such as [³H]-N-methylscopolamine ([³H]-NMS) or [³H]-quinuclidinyl benzilate ([³H]-QNB) (*see*, for example, refs. [15, 16]). However, NMS and QNB bind to DREADDs with considerably reduced affinity, as compared to the WT muscarinic receptors from which they are derived. For example, while [³H]-NMS binds to the WT mouse M_3 receptor with very high affinity (K_D ~70 pM), it binds to the Rq DREADD with ~40-fold lower affinity (K_D ~3 nM; ref. [15]).

In the following, we describe standard protocols for determining DREADD (Rq or Rq(R165L)) binding affinities for [³H]-NMS, ACh, and CNO. These protocols can be used for essentially all muscarinic receptor-based DREADDs.

3.1 Preparation of Receptor-Containing Membranes

Radioligand binding assays can be carried out with crude cell membranes prepared from transfected COS-7 cells.

3.1.1 Materials

For this procedure, only standard reagents are needed. We usually use an ultrasonic homogenizer from BioLogics Inc. (Manassas, VA). The BCA Protein Assay Kit is from Thermo Scientific/Pierce (Rockford, IL).

3.1.2 Methods

All buffers are kept cold (4 °C). Crude membranes are prepared from receptor-expressing COS-7 cells ~48 h after transfection. DMEM is removed via aspiration from the 100 mm plates containing the transfected cells. Each dish is then washed with 10 ml of PBS. One milliliter of binding buffer (25 mM phosphate buffer containing 5 mM $MgCl_2$, pH 7.4) is added to each dish, followed by a 15-min incubation on ice. The cells are then removed from the plates using a cell scraper and transferred to a chilled 1.5 ml Eppendorf tube. This procedure is repeated once with 350 µl of binding buffer in order to collect the remaining cells. The cells are then homogenized by using an ultrasonic tissue homogenizer (keep the tubes on ice). Subsequently, cell homogenates are centrifuged at $18,000 \times g$ for 15 min at 4 °C. The supernatants are discarded, and the membrane pellets are resuspended in binding buffer (1 ml/plate), and then re-sonicated until the samples are fully homogenized. Protein concentrations are determined by using the BCA Protein Assay Kit. Finally, samples are directly used for radioligand binding studies or snap-frozen on dry ice for 5–10 min and then stored at –80 °C until use.

3.1.3 Notes

One 100 mm dish of transfected cells should yield enough material (crude membranes) to generate multiple saturation and competition binding curves (*see* below).

3.2 Saturation Binding Studies

For [3H]-NMS saturation binding studies, increasing concentrations of [3H]-NMS are incubated with crude membrane preparations of receptor (DREADD)-expressing COS-7 cells. From the resulting saturation binding curves, B_{max} (receptor density) and K_D (a measure of affinity) values for [3H]-NMS can be calculated for a given receptor/DREADD.

3.2.1 Materials

[3H]-NMS (79–83 Ci/mmol; PerkinElmer Life Sciences, Downers Grove, IL); atropine sulfate and polyethyleneimine (PEE; Sigma-Aldrich, St. Louis, MO); glass test tubes (12×75 mm; Kimble Chase, Vineland, NJ); Biosafe II scintillation cocktail and 20 ml glass scintillation vials (Fisher Scientific, Hampton, NH); Brandel cell harvester and Whatman GF/C glass filters (Brandel, Gaithersburg, MD). GraphPad Prism® v4.0b software (GraphPad Software, Inc., San Diego, CA) is used for analyzing radioligand binding data.

3.2.2   Methods

To measure [³H]-NMS binding to DREADD-containing crude cell membranes, six different concentrations of [³H]-NMS (0.5–50 nM; serial 1:2.5 dilutions) are used. For each [³H]-NMS concentration, four glass test tubes (12 × 75 mm) are needed. Two tubes are used to determine total [³H]-NMS binding (specific plus nonspecific binding), and the other two to measure nonspecific binding in the presence of an excess amount of atropine (10 μM), a high-affinity muscarinic receptor antagonist. In total, 24 tubes are needed for a single experiment.

Add:

50 μl of binding buffer to all 24 tubes.

50 μl of binding buffer to the 12 tubes used to determine total binding.

50 μl of atropine solution (100 μM; in binding buffer) to the 12 tubes used to determine nonspecific binding.

350 μl of crude cell membranes (~25 μg protein/ml) to all 24 tubes.

50 μl of the appropriate 10× [³H]-NMS dilution (all tubes).

Total volume: 500 μl.

The tubes are covered with plastic wrap and incubated at RT for 3 h to achieve equilibrium binding. During this time, GF/C filters are soaked in 0.3 % PEE to reduce nonspecific binding. After the 3-h incubation period, the PEE-soaked filters are placed on the Brandel cell harvester, and the samples are transferred onto the filters via the use of a vacuum pump. The filters are then washed twice with ~3 ml of ice-cold water to wash out unbound [³H]-NMS and then removed from the harvester. Between sample sets, the harvester is washed (without filter) twice with ~3 ml of chilled water. The individual filter circles are transferred into 20 ml glass scintillation vials. After the addition of 7 ml of Biosafe II scintillation cocktail to each vial, vials are incubated overnight at RT. On the next day, the vials are briefly vortexed and then transferred to a scintillation counter (count each vial for several minutes). Binding data are fitted to a one-site binding hyperbola via nonlinear regression analysis by using GraphPad Prism software. The amount of specific binding (total minus nonspecific binding) is plotted on the *y*-axis as a function of the [³H]-NMS concentration plotted on the *x*-axis. Specific binding is usually expressed as picomoles or femtomoles per mg protein. The extrapolated amount of [³H]-NMS bound by the receptor/DREADD when binding is saturated is defined as the number of receptor sites (B_{max}). In addition, the concentration of [³H]-NMS required to occupy 50 % of the available specific binding sites is defined as the [³H]-NMS binding affinity (K_D).

3.2.3   Expected Results

Typical [³H]-NMS saturation binding curves using crude membranes prepared from COS-7 cells expressing the Rq or Rq(R165L) DREADDs are shown in Fig. 2a.
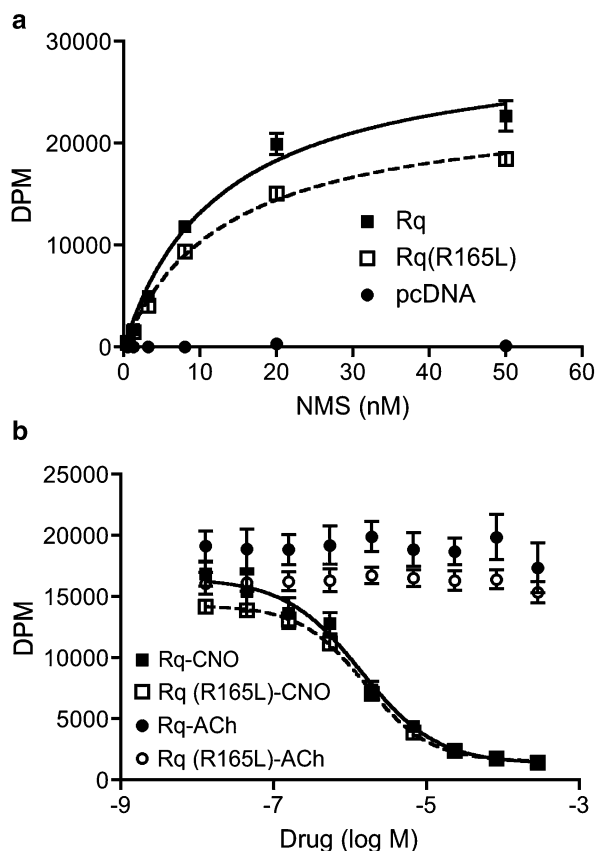
Fig. 2 Typical [³H]-NMS saturation (**a**) and competition (**b**) binding curves obtained with the Rq and Rq(R165L) DREADDs. Membranes prepared from COS-7 cells transfected with either the Rq or Rq(R165L) DREADDs (or vector DNA) were subjected to [³H]-NMS saturation and [³H]-NMS/CNO (or ACh) competition binding studies. The data shown are from representative experiments carried out in duplicate

3.2.4   Notes

Since [³H]-NMS binds to DREADDs with reduced affinity as compared to WT muscarinic receptors, relatively high [³H]-NMS concentrations need to by employed in DREADD saturation binding assays. As a result, nonspecific binding may sometimes interfere with the quality of the obtained binding data. In this case, the amount of nonspecific binding can be reduced by decreasing the volume of the binding mixture (e.g., 250 µl instead of 500 µl) or by additional washes of the [³H]-NMS-containing samples during the filtration process.

3.3   Competition Binding Studies

For [³H]-NMS competition binding studies, a fixed concentration of [³H]-NMS is incubated with increasing concentrations of nonradioactive (cold) ligands (ACh or CNO) and crude membranes prepared from receptor/DREADD-expressing COS-7 cells.

The half-maximal inhibitory concentration (IC_{50}) of the cold ligand derived from such experiments is converted to a measure of its affinity (K_i) for the particular receptor under investigation.

3.3.1 *Materials*

The materials and equipment required for competition binding studies are identical to those listed above for saturation binding assays, except for β-methyl cyclodextrin, CNO, and ACh chloride (Sigma-Aldrich, St. Louis, MO).

3.3.2 *Methods*

For competition binding studies, ten different concentrations of CNO and ACh are prepared in binding buffer (final concentrations: ACh, 0.127 μM to 10 mM; CNO, 0.0127 μM to 1 mM; serial 1:3.5 dilutions). We recommend the use of 10× stock solutions. CNO (10 mM) is dissolved in 50 mg/ml β-methyl cyclodextrin solution. It takes ~30 min and shaking at 37 °C to dissolve CNO completely. For each competition binding curve (Rq or Rq(R165L)), 24 tubes (12 sets of duplicate tubes) are used.

Add:

50 μl of binding buffer to all 24 tubes.

50 μl of binding buffer to set 1 tube (2 tubes).

50 μl of atropine (final concentration: 10 μM) to set 2 tubes (2 tubes).

50 μl of increasing ACh or CNO dilutions to set 3–12 tubes (20 tubes total, 2 tubes per ligand concentration).

350 μl of crude membranes (~8–10 μg total protein) to all 24 tubes.

50 μl of [³H]-NMS solution (final concentration: 20 nM) to all 24 tubes.

Total volume: 500 μl.

Binding mixtures are then incubated and processed in the same fashion as described under Sect. 3.2. Competition binding data are analyzed via nonlinear regression analysis by using GraphPad Prism software ("best fit"). The resulting IC_{50} values (concentration of the cold inhibitor that reduces specific [³H]-NMS binding by 50 %) are converted to actual ligand affinities (K_i values) by using the Cheng-Prusoff equation: $K_i = IC_{50} / \left(1 + [L]/K_D\right)$. [L] is the concentration of [³H]-NMS used in the assay, and K_D is the affinity of [³H]-NMS for the receptor/DREADD under investigation.

3.3.3 *Expected Results*

Typical [³H]-NMS/CNO competition binding curves obtained with COS-7 cells transfected with the Rq or Rq(R165L) DREADDs are shown in Fig. 2b. Please note that ACh has no effect on [³H]-NMS binding to these two designer receptors in the concentration range studied (Fig. 2b).

3.3.4 *Notes*	The caveats raised under Sect. 3.2.4 also apply for competition binding assays. Instead of ACh, other muscarinic agonists, such as carbachol, methacholine, or oxotremorine-M, are frequently used for pharmacological studies. However, when DREADDs are used for in vivo studies, it is essential to demonstrate that the designer receptors lack ACh binding activity.

4   Fluorometric Imaging Plate Reader Assay

CNO treatment of cells expressing the Rq designer receptor leads to the selective activation of G proteins of the G_q family [11, 15, 16]. The stimulation of G_q-type G proteins leads to the generation of inositol 1,4,5,-trisphosphate (IP_3), which triggers the release of Ca^{2+} from intracellular stores. In the following, we provide a simple protocol that uses fluorometric imaging plate reader (FLIPR) technology to monitor changes in $[Ca^{2+}]_i$. This fluorescence-based method allows for the rapid measurement of receptor/DREADD-mediated increases in $[Ca^{2+}]_i$ in live cells.

4.1 *Materials*	For transfections, the same reagents are used as described under Sect. 2. Probenecid (Sigma); FLIPR Tetra High Throughput Cellular Screening System, FLIPR Tetra Pipette tips, and FLIPR calcium 4 assay kit (Molecular Devices, Sunnyvale, CA); 96-well assay plates (black-wall and clear bottom for cell culture) and 96-well assay plates (clear-wall for ligands) (Corning, NY).

4.2 *Methods*	For FLIPR assays, COS-7 cells are grown in 6-well plates. When the cells are 60–80 % confluent, a mixture of 0.8 µg DNA (Rq plasmid, Rq(R165L) plasmid, or pcDNA vector DNA) and lipofectamine and PLUS reagent (6 µl lipofectamine and 4 µl PLUS, respectively) is added to each well. The cells are then incubated overnight at 37 °C. On the following day, the cells are detached by incubation with 100 µl of 0.05 % trypsin (for ~5 min at 37 °C). Trypsin is then inactivated by adding 900 µl of DMEM containing 10 % FBS to each well, and cell clusters are disrupted by gently pipetting up and down. Subsequently, cells from each well are transferred to 15 ml conical tubes, and cell densities are determined by using a standard hemocytometer. Cell suspensions are diluted with DMEM to a concentration of $3–6 \times 10^5$ cells/ml. Subsequently, 100 µl aliquots of the cell suspension are added to the individual wells of a 96-well black clear-bottom plate by using a multi-pipettor. For each receptor construct to be tested, at least 16 wells are needed to test seven different concentrations of CNO (DREADD agonist) in duplicate. The cells are incubated overnight at 37 °C. About 48 h after transfection, a 10 mM CNO stock solution is prepared using FLIPR buffer (contained in the explorer kit) supplemented with 50 mg/ml

β-methyl cyclodextrin. Using this stock solution, seven different concentrations of CNO are prepared by performing 1:10 serial dilutions in FLIPR buffer from 2 mM to 2 nM (seven tubes total). The different CNO solutions are then added to a clear 96 well plate (two wells per CNO concentration; 200 μl/well). Moreover, CNO-free FLIPR buffer is added to two of the wells (200 μl/well). This plate is referred to as "CNO plate."

Next, the calcium indicator dye solution is prepared as follows: a vial of Component A from the kit is equilibrated to RT. The dye is then completely dissolved in 10 ml of FLIPR buffer by vortexing. A sufficient amount of the dye solution (30 μl is needed per well) is added to a 1.5 ml tube. To increase dye retention in cells, a 250 mM probenecid acid stock solution in 500 mM NaOH is added to the dye solution (final probenecid concentration: 5 mM). The dye solution without probenecid can be stored at −20 °C until needed. In the next step, the media is removed from the transfected cells grown in the cell plates and 30 μl of the dye solution containing 5 mM probenecid acid is added to each well. The plates are then covered with aluminum foil in the dark and incubated for 1 h at 37 °C in the cell culture incubator. During this incubation period, the CNO plate and the FLIPR TETRA pipette tips are gathered, and the FLIPR Tetra is turned on. After the 1-h incubation at 37 °C, the cell plate is placed in the "read" slot, the CNO plate in the "source 1" slot, and the tips in the "tips" slot. Changes in cell fluorescence are then measured at RT (excitation wavelength: 470–495 nm; emission wavelength: 515–575 nm). Increases in intracellular calcium levels are expressed as the difference between maximum fluorescence values after CNO exposure and the corresponding basal fluorescence values prior to the addition of CNO. Assays are carried out in duplicate.

The resulting fluorescence data are analyzed with GraphPad Prism software. After selection of "XY with 2 replicates," the CNO concentrations are entered as X values and the fluorescence readings as Y values. Data are analyzed via nonlinear regression analysis (select "sigmoidal dose–response with variable slope"), yielding CNO EC_{50} and E_{max} values.

4.3   Expected Results

Figure 3 shows that CNO treatment of Rq(R165L)-expressing COS-7 cells has no significant effect on intracellular calcium levels ($[Ca^{2+}]_i$). In contrast, CNO induced robust, concentration-dependent increases in $[Ca^{2+}]_i$ in Rq-expressing COS-7 cells (Fig. 3), indicating that the Rq(R165L) designer receptor lacks the ability to activate G proteins of the G_q family.

4.4   Notes

Solutions containing CNO at concentrations greater than 0.1 mM exhibit a yellow color which may interfere with FLIPR measurements. Consequently, CNO concentrations >0.1 mM should be avoided in this particular assay.
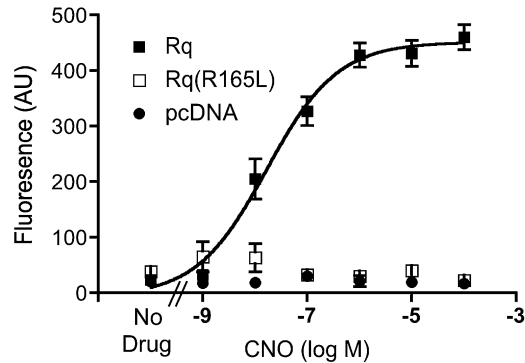
Fig. 3 CNO stimulation of the Rq(R165L) DREADD has no effect on intracellular calcium levels ([Ca^{2+}]$_i$). COS-7 cells were transfected with the indicated DREADD constructs (Rq or Rq(R165L)) or vector DNA. CNO-induced changes in [Ca^{2+}]$_i$ were measured by using FLIPR technology, as described in the text. The figure shows data from a representative experiment, carried out in duplicate. Note that CNO treatment of Rq(R165L)-expressing COS cells has no effect on [Ca^{2+}]$_i$. Data were taken from ref. [12]

Removal of culture media via suction from cells grown in 96-well plates can easily cause the dislodgement of cells. This can be avoided by turning the plate upside down and "flicking" the liquid out into a bucket or sink, followed by dabbing of the plate on a paper towel to remove residual liquid.

5   Receptor/DREADD-Mediated Recruitment of Arrestins Studied via BRET

BRET-based assays offer a compelling option for the assessment of GPCR-arrestin interactions in live cells, amenable for high-throughput screening settings [17, 18]. In the following, we describe a BRET[1] protocol that we routinely use to monitor receptor-dependent arrestin recruitment in cultured cells [19, 20].

5.1   Materials   COS-7 cells (ATCC, Manassas, VA); Lipofectamine® 2000 transfection reagent, Opti-MEM I, DMEM high glucose without phenol red, and 5 % trypsin 5.3 mM EDTA without phenol red (10× concentrated solution that must be diluted in Hanks' balanced salts solution without Ca^{2+} and Mg^{2+}): all from Life Technologies (Carlsbad, CA); Nunc™ F96 MicroWell™ black and white polystyrene plates (Thermo Scientific, Waltham, MA); Coelenterazine-*h* (NanoLight Technology, Pinetop, AZ).

5.2   General Principles   BREt allows for the monitoring of the physical interactions between two proteins, one of which is fused to a bioluminescent donor moiety and the other one to a fluorescent acceptor moiety,

allowing for measurements of resonance energy transfer (RET) between these two moieties (Fig. 4). The intensity of the signal is dependent on orientation, distance, and spectral overlap between BRET donor and acceptor [21]. In BRET, the donor moiety is a version of the bioluminescent enzyme luciferase from *Renilla reniformis* (*R*luc). *R*luc is an oxidoreductase that catalyzes the oxidation of the imidazolopyrazine coelenterazine (clz) to coelenteramide with the emission of a photon in the blue spectrum (peak emission of *R*luc-clz: 475 nm). Peak emission is dependent on the type of luciferase and substrate used, as chemical modifications of native (i.e., naturally occurring) clz can shift peak emission or change quantum yield (e.g., synthetic coelenterazine-*h* has a quantum yield ten times higher than native clz) [22]. Part of the energy released from this reaction can be transferred, in a non-radiative fashion, to an acceptor that has an overlapping excitation spectrum.

In *R. reniformis* and other bioluminescent marine organisms, the acceptor of resonance energy is some form of green fluorescent protein (GFP) that emits at a longer wavelength (509 nm) than *R*luc-clz, producing green instead of blue light. In an effort to improve the signal-to-noise ratio that results from significant spectral overlap between *R*luc-clz and GFP, red-shifted GFP derivatives including yellow fluorescent protein (YFP) or enhanced versions of YFP such as YFP-Venus (or just Venus) are now commonly used. Venus has an excitation peak of 515 nm and an emission peak of 528 nm and its use offers several other advantages over that of GFP [23]. The use of different substrates and modified versions of luciferase and acceptor fluorophores has led to minimization in the spectral overlap between BRET donor and acceptor [17, 21].

5.3 Methods

5.3.1 Generation of Receptor and Arrestin Constructs Used for BRET Assays

To analyze GPCR-arrestin interactions via BRET (Fig. 4), the *R*luc8 coding sequence is fused to the cytoplasmic C-terminus of the receptor (note that *R*luc8 is a variant of *R*luc with enhanced stability and enzymatic activity). Since arrestins contain a relatively unstructured C-terminal domain, many studies have used arrestin constructs where Venus was fused to the arrestin C-terminus. However, we observed, consistent with data reported in the literature, that only N-terminal Venus-arrestin fusion proteins yielded agonist-specific net BRET [12, 19, 20, 24]. To prevent Venus from disrupting the structure of the N-terminal arrestin domain, we typically insert a ten-amino acid linker sequence (SGLKSRRALDS) between the two proteins.

5.3.2 Experimental Setup

Initially, it is recommended to characterize a specific receptor-arrestin pair in a BRET saturation assay where receptor-*R*luc8 expression is kept constant while Venus-arrestin expression levels are increased so that the agonist-dependent BRET signal reaches a plateau. BRET assays examining GPCR-arrestin interactions can be performed in 2–3 days and include three distinct steps: cell
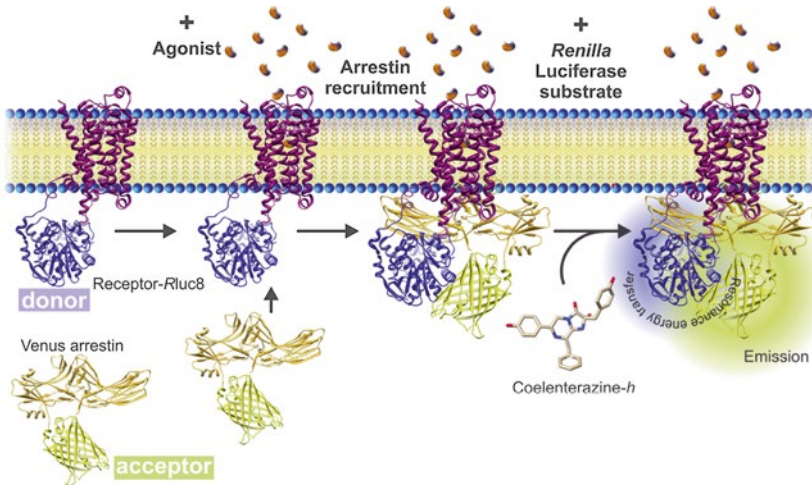
Fig. 4 BRET assay for the detection of arrestin recruitment by GPCRs. Upon agonist stimulation and phosphorylation of GPCRs by GRKs, GPCRs are able to interact with arrestins. To study this process by BRET, receptors are fused to *Renilla* luciferase variant 8 (*R*luc8), which serves as the donor of resonance energy. The acceptor Venus, an enhanced variant of YFP, is fused to the N-terminus of arrestin. Luciferase oxidases the membrane-permeable coelenterazine-*h* substrate, producing luminescence and resonance energy transfer (RET) to the nearby acceptor, Venus-arrestin. After RET, the Venus acceptor emits fluorescence that can be readily detected. The ratio between the acceptor peak emission and the donor peak emission constitutes the BRET ratio. The agonist-dependent net BRET ratio is the difference between BRET ratios measured in the presence and absence of agonist

transfection, passaging of cells to multi-well plates, and agonist stimulation and reading of dual-channel filtered luminescence from cells seeded into white multi-well plates and of fluorescence from cells seeded into black multi-well plates, respectively. Dual-channel luminescence readings are used to estimate BRET ratios as explained below. The readings are also used to determine the relative expression of Rluc8-fused receptors, as luminescence is proportional to luciferase expression and activity (Fig. 5b). Likewise, fluorescence readings are used to estimate the expression levels of the Venus-tagged arrestin proteins (Fig. 5a). The ratio between Venus-arrestin fluorescence (F) and receptor-Rluc8 luminescence (L) represents the relative arrestin/receptor expression ratio and allows for the direct comparison of data obtained in different experiments carried out under the same experimental conditions.

Below we describe the steps of an arrestin titration assay where the expression of the receptor-Rluc8 construct is kept constant. In the case described below, the M_3 muscarinic receptor (M3R) fused to Rluc8 represents the BRET donor (M3R-Rluc8), while Venus-arrestin-3 (-arrestin-2) serves as the BRET acceptor. Agonist-dependent arrestin recruitment is initiated with a saturating concentration of the muscarinic agonist, carbachol (100 μM). Note that DREADDs are no longer able to bind ACh, carbachol,
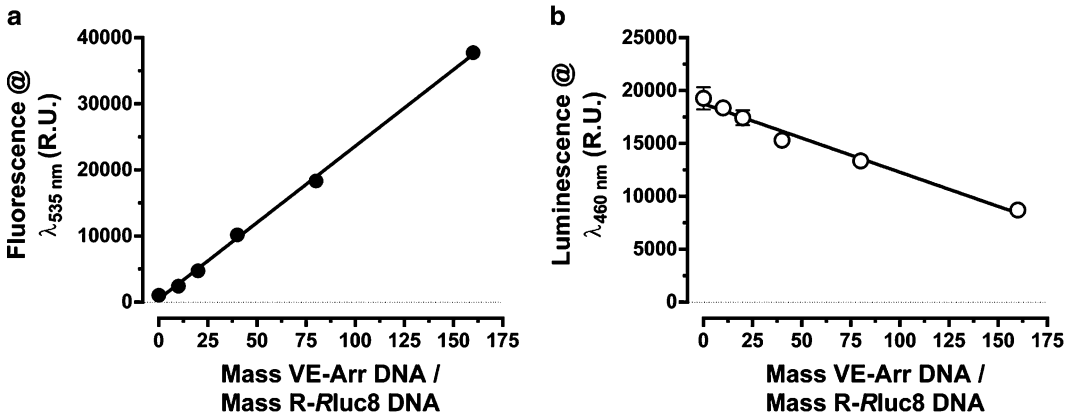
Fig. 5 Peak fluorescence and luminescence are proportional to Venus-arrestin and receptor-*R*luc8 expression, respectively, and are used to determine the F/L ratio. The M_3 muscarinic receptor-*R*luc8 fusion protein (M3R-*R*luc8) served as the BRET donor and Venus-arrestin-3 as the BRET acceptor. Studies were carried out with transfected COS-7 cells. (**a**) Fluorescence at 535 nm is directly proportional to the amount of transfected Venus-arrestin-3 DNA. An excitation filter with transmittance centered at 485 nm (bandwidth of 20 nm), 535 nm emission filter (bandwidth of 25 nm), and 510 nm dichroic mirror were used to monitor relative fluorescence values. (**b**) Filtered luminescence at 460 nm from the same cells shown in panel (**a**). Note the usual decrease in M3R-*R*luc8 expression levels as the Venus-arrestin-3 plasmid amount increases. A representative experiment is shown

or other orthosteric muscarinic agonists, but can be efficiently activated by CNO. Thus, CNO must be used as an agonist in BRET studies examining DREADD-arrestin interactions.

5.3.3 Transfection of COS-7 Cells

We use one 60 mm cell culture dish per condition (i.e., Venus-arrestin plasmid amount) and seed 4×10^5 low-passage (<20 passages) COS-7 cells in exponential growth phase (the number of cells needs to be optimized for each cell line). On the following day, the cells are usually ~90 % confluent and are ready to be transfected. We use Lipofectamine® 2000 transfection reagent from Life Technologies (Carlsbad, CA) at a ratio of 2.2 μl of transfection reagent per μg of total plasmid DNA per condition. Typical amounts of plasmid DNAs used are shown in Table 1. Plasmid DNAs and transfection reagent are mixed in minimal essential medium (such as Opti-MEM® from Life Technologies) in the absence of fetal bovine serum following the manufacturer's instructions. After transfection, cells are incubated for 10–16 h inside a cell culture incubator (95 % humidity, 5 % CO_2, 37 °C) with the DNA-lipid complexes.

5.3.4 Passaging of Cells to Multi-well Plates

After incubation of cells for 10–16 h with the DNA-lipid complexes, cells are passaged to multi-well plates using standard cell culture procedures. Note that all cell culture reagents (culture media, trypsin-EDTA solution, etc.) should be devoid of phenol red to prevent interference with the BRET measurements. We use

Table 1
Venus-arrestin and M3R-Rluc8 plasmid amounts used for an arrestin titration BRET assay

Venus-Arr-3 plasmid[a] (µg)	M3R-Rluc8 plasmid[b] (µg)	pcDNA3.1(+)[c] (µg)
–	0.2	12
0.75	0.2	11.25
1.5	0.2	10.5
3	0.2	9
6	0.2	6
12	0.2	–

[a]Venus-Arr-3 plasmid: Venus-arrestin-3 (bovine) fusion construct in pcDNA3 (Life Technologies)
[b]M_3 muscarinic receptor fused to *Renilla* luciferase variant 8 in pcDNA3
[c]pcDNA3.1(+) empty vector used to ensure that the amount of transfected plasmid DNA is equal in all assays

96-well white opaque cell culture plates for measurement of filtered luminescence and 96-well black opaque plates for fluorescence measurements, respectively (*see* Sect. 5.1). Typically, we seed 20,000–40,000 cells per well. To obtain a sufficient amount of cells, we resuspend the cells harvested from one 60 mm dish in a sufficient volume of media to yield 20 wells of a 96-well plate (100 l of cell suspension per well). This makes it possible to set up an experiment with eight replicates of agonist-treated and vehicle-treated cells in addition to four replicates for the determination of

fluorescence from a black opaque 96-well plate. We then allow cells to recover for 24 h from the stress of passaging prior to agonist stimulation and BRET measurements.

5.3.5 *Agonist Stimulation and BRET Measurements*

On the assay day, transfected cells are stimulated in 96-well plates with a saturating concentration (100 μM) of carbachol (or 10 μM of CNO in the case of DREADDs) in the presence of 5 μM clz-*h*, and BRET measurements are taken. Agonist and luciferase stock solutions (4×) are diluted in DPBS supplemented with 1 g/l D-glucose, 36 mg/l sodium pyruvate, and 25 mM HEPES (pH 7.2). Naïve (untreated) cells receive vehicle. In the first step, the cell culture media in the white multi-well plates to be used for luminescence measurements is replaced with 100 μl of HEPES-DPBS. Carbachol (100 μM final) (or 10 μM of CNO in the case of DREADDs) or vehicle is then added to stimulated or naïve cells, respectively, and clz-*h* (5 μM final) is added to all wells of the multi-well plate. These reagents can be added by hand with the aid of a multichannel pipette or by using the injectors that are part of many plate readers. The optimum agonist incubation time varies depending on the receptor being studied and should be determined in each case experimentally. For M_3 receptor-based DREADDs, we found that BRET signals were most robust after treatment of cells for 45 min with CNO. Longer incubation times result in a reduced luminescence signal due to oxidation of clz-*h*.

The ideal instrument for BRET measurements is capable of dual-luminescence measurements: one channel for the donor (475 nm) and the other for the acceptor (528 nm) for each microplate well. Donor and acceptor light output must be taken consecutively (by rapidly switching filters) or simultaneously (if two channels are available) before moving to the next well. The best filter set for BRET[1] avoids any spectral overlap to circumvent or minimize bleed through light and consists of a 60–80 nm bandpass, 460 nm centered (or below) filter for the measurement of *R*luc8-clz-*h* peak emission and a 40–60 nm band-pass, 540 nm centered filter for measuring peak emission of Venus. Read integration time should be set to 0.5–1 s. We have used instruments from PerkinElmer (Victor2 or Envision), BioTek (Synergy series of microplate readers), Tecan (Infinite F500), and BMG Labtech (POLARStar Optima dual-channel emission detection).

Data from arrestin titration experiments are plotted as BRET ratio versus the acceptor fluorescence over donor luminescence ratio (F/L). To determine acceptor fluorescence, measurements are taken from cells growing in the black multi-well plates. Plate reader settings should match Venus excitation and emission spectra. Table 2 summarizes instrument settings for the measurement of Venus fluorescence.

BRET ratios are calculated by dividing the long-wavelength (i.e., 528 nm) luminescence values from the short-wavelength

Table 2
Instrument settings for estimating relative Venus-arrestin expression levels by fluorescence measurements

| Parameter[a] |
| --- |
| Setting |
| Excitation wavelength |
| 485 nm |
| Excitation bandwidth |
| 20 nm |
| Emission wavelength |
| 535 nm |
| Emission bandwidth |
| 25 nm |
| Dichroic mirror |
| 510 nm |

[a]Some instruments allow for the control of output of the excitation light source while others provide different aperture settings for a diaphragm interposed in the light path to regulate output. The number of flashes, integration time, and photomultiplier (detector) amplifier gain are additional parameters that need to be adjusted to achieve a maximum dynamic range and optimal signal-to-noise ratio

(i.e., 475 nm) values. To determine specific BRET ratios resulting from agonist-dependent arrestin recruitment, the difference between the BRET ratios in the presence and absence of agonist needs to be determined. This difference is also referred to as "net BRET" [25]. Saturation plots are constructed by graphing F/L on the x-axis against net BRET ratios on the y-axis (Fig. 6a). Data points are fitted to a one-site binding hyperbola by computer-aided nonlinear regression using GraphPad Prism software. Net $BRET_{MAX}$ can be inferred from the resulting curves, as long as the arrestin-receptor interaction reaches saturation.

BRET experiments can also be performed to obtain agonist concentration-response curves for receptor/DREADD-mediated arrestin recruitment [12]. In this case, the receptor/DREADD-Rluc8 and the Venus-arrestin fusion proteins are expressed at a constant level (Fig. 6b, c).

5.4 Notes

1. Arrestins preferentially recognize GPCR in their active state following their phosphorylation by GRKs [26]. Many cell lines express sufficient endogenous amounts of GRKs to phosphorylate overexpressed receptor-Rluc8 fusion proteins [24].
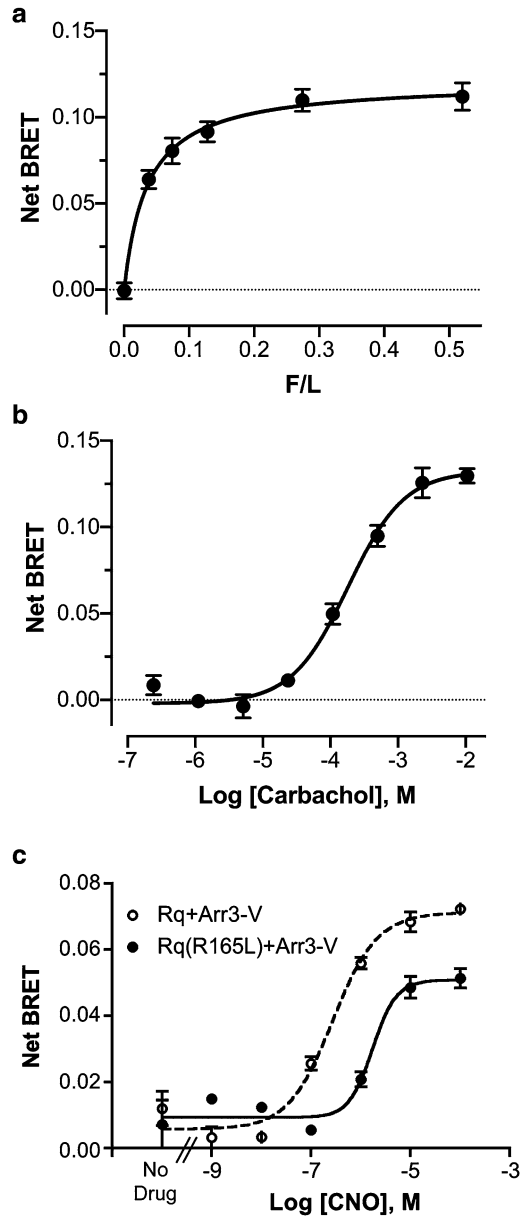
Fig. 6 BRET analysis of receptor/DREADD-arrestin interactions in transfected COS-7 cells. (**a**) Titration of arrestin-3 recruitment by the M_3 muscarinic receptor (M3R). M3R-*R*luc8 served as the BRET donor and Venus-arrestin-3 as the BRET acceptor. Net BRET resulting from the difference between the BRET ratios measured in the presence or absence of 100 μM carbachol (M3R agonist) is plotted against F/L ratios. (**b**) Agonist (carbachol) concentration-response curve for the recruitment of arrestin-3 by the M3R. Carbachol (0.2 μM–10 mM) was used to stimulate cells co-transfected with M3R-*R*luc8 DNA (same plasmid amount as in panel (**a**) and Venus-arrestin-3 plasmid DNA (the amount used yields saturating expression levels as determined in (**a**)). (**c**) CNO concentration-response curves for the recruitment of arrestin-3 by the Rq and Rq(R165L) DREADDs. CNO was used to stimulate cells co-transfected with DREADD-*R*luc8 and Venus-arrestin-3 plasmid DNAs. Representative experiments are shown in all panels

However, if the observed BRET signal is low, signal strength can often be improved by adding a GRK-expression plasmid (e.g., a plasmid coding for GRK2) to the transfection mixture.

2. An issue that is critical for any kind of BRET experiment is to distinguish "true" protein–protein interactions from bystander BRET [25]. In a system where receptor and arrestin proteins are overexpressed, it is possible that receptors interact with arrestins in a "kiss-and-run" fashion. Such interactions have no physiological significance but can readily yield RET. To account for these nonspecific interactions, basal bystander BRET should be determined by using a non-interacting protein of similar size and structure. Recently, we described several arrestin mutants which can be used to determine background BRET ratios [19, 24]. These arrestin mutants are unable to bind GPCRs.

3. The fusion of large (~25–28 kDa) BRET acceptor and donor moieties to arrestins and receptors may interfere with the function of these proteins. It is therefore essential to confirm that the fusion proteins have similar functional properties as the unmodified receptors and arrestins. Ideally, in the case of Venus-tagged arrestins, receptor recruitment, internalization, and in vitro binding studies should be performed and arrestin-dependent downstream signaling should be monitored [24, 27]. Luciferase-fused GPCRs/DREADDs should be tested in ligand binding assays and functional studies to confirm that the modified receptors are folded properly and are able to interact with G proteins and/or arrestins. Ideally, receptor localization studies should also be carried out.

Acknowledgements

References

1. Pierce KL, Premont RT, Lefkowitz RJ (2002) Seven-transmembrane receptors. Nat Rev Mol Cell Biol 3:639–650

2. Gurevich EV, Tesmer JJG, Mushegian A, Gurevich VV (2012) G protein-coupled receptor kinases: more than just kinases and not only for GPCRs. Pharmacol Ther 133:40–69

3. Krupnick JG, Gurevich VV, Benovic JL (1997) Mechanism of quenching of phototransduction. Binding competition between arrestin and transducin for phosphorhodopsin. J Biol Chem 272:18125–18131

4. Goodman OB, Krupnick JG, Santini F, Gurevich VV, Penn RB, Gagnon AW, Keen JH, Benovic JL (1996) β-Arrestin functions as a clathrin adaptor to promote β2-adrenergic receptor endocytosis. Nature 383:447–450

5. Rajagopal S, Rajagopal K, Lefkowitz RJ (2010) Teaching old receptors new tricks: biasing seven-transmembrane receptors. Nat Rev Drug Discov 9:373–386

6. Shukla AK, Xiao K, Lefkowitz RJ (2011) Emerging paradigms of β-arrestin-dependent seven transmembrane receptor signaling. Trends Biochem Sci 36:457–469

7. Luttrell LM, Miller WE (2013) Arrestins as regulators of kinases and phosphatases. Prog Mol Biol Transl Sci 118:115–147

8. Luttrell LM (2013) Arrestin pathways as drug targets. Prog Mol Biol Transl Sci 118: 469–497

9. Rogan SC, Roth BL (2011) Remote control of neuronal signaling. Pharmacol Rev 63: 291–315

10. Wess J, Nakajima K, Jain S (2013) Novel designer receptors to probe GPCR signaling and physiology. Trends Pharmacol Sci 34: 385–392

11. Alvarez-Curto E, Prihandoko R, Tautermann CS, Zwier JM, Pediani JD, Lohse MJ, Hoffmann C, Tobin AB, Milligan G (2011) Developing chemical genetic approaches to explore G protein-coupled receptor function: validation of the use of a receptor activated solely by synthetic ligand (RASSL). Mol Pharmacol 80:1033–1046

12. Nakajima KI, Wess J (2012) Design and functional characterization of a novel, arrestin-biased designer G protein-coupled receptor. Mol Pharmacol 82:575–582

13. Rasmussen SG, DeVree BT, Zou Y, Kruse AC, Chung KY, Kobilka TS, Thian FS, Chae PS, Pardon E et al (2011) Crystal structure of the β2 adrenergic receptor-Gs protein complex. Nature 477:549–555

14. Li B, Nowak NM, Kim SK, Jacobson KA, Bagheri A, Schmidt C, Wess J (2005) Random mutagenesis of the M3 muscarinic acetylcholine receptor expressed in yeast: identification of second-site mutations that restore function to a coupling-deficient mutant M3 receptor. J Biol Chem 280:5664–5675

15. Guettier JM, Gautam D, Scarselli M, Ruiz de Azua I, Li JH, Rosemond E, Ma X, Gonzalez FJ, Armbruster BN, Lu H, Roth BL, Wess J (2009) A chemical-genetic approach to study G protein regulation of β cell function in vivo. Proc Natl Acad Sci U S A 106:19197–19202

16. Armbruster BN, Li X, Pausch MH, Herlitze S, Roth BL (2007) Evolving the lock to fit the key to create a family of G protein-coupled receptors potently activated by an inert ligand. Proc Natl Acad Sci U S A 104:5163–5168

17. Pfleger KD, Eidne KA (2006) Illuminating insights into protein-protein interactions using bioluminescence resonance energy transfer (BRET). Nat Methods 3:165–174

18. Kocan M, Pfleger KD (2009) Detection of GPCR/beta-arrestin interactions in live cells using bioluminescence resonance energy transfer technology. Methods Mol Biol 552: 305–317

19. Vishnivetskiy SA, Gimenez LE, Francis DJ, Hanson SM, Hubbell WL, Klug CS, Gurevich VV (2011) Few residues within an extensive binding interface drive receptor interaction and determine the specificity of arrestin proteins. J Biol Chem 286:24288–24299

20. Gimenez LE, Vishnivetskiy SA, Baameur F, Gurevich VV (2012) Manipulation of very few receptor discriminator residues greatly enhances receptor specificity of non-visual arrestins. J Biol Chem 287:29495–29505

21. Dacres H, Michie M, Wang J, Pfleger KD, Trowell SC (2012) Effect of enhanced Renilla luciferase and fluorescent protein variants on the Forster distance of Bioluminescence resonance energy transfer (BRET). Biochem Biophys Res Commun 425:625–629

22. Loening AM, Fenn TD, Wu AM, Gambhir SS (2006) Consensus guided mutagenesis of Renilla luciferase yields enhanced stability and light output. Protein Eng Des Sel 19:391–400

23. Nagai T, Ibata K, Park ES, Kubota M, Mikoshiba K, Miyawaki A (2002) A variant of yellow fluorescent protein with fast and efficient maturation for cell-biological applications. Nat Biotechnol 20:87–90

24. Gimenez LE, Kook S, Vishnivetskiy SA, Ahmed MR, Gurevich EV, Gurevich VV (2012) Role of receptor-attached phosphates in binding of visual and non-visual arrestins to G protein-coupled receptors. J Biol Chem 287:9028–9040

25. Drinovec L, Kubale V, Nøhr Larsen J, Vrecl M (2012) Mathematical models for quantitative assessment of bioluminescence resonance energy transfer: application to seven transmembrane receptors oligomerization. Front Endocrinol (Lausanne) 3:104

26. Gurevich VV, Gurevich EV (2006) The structural basis of arrestin-mediated regulation of G protein-coupled receptors. Pharmacol Ther 110:465–502

27. Breitman M, Kook S, Gimenez LE, Lizama BN, Palazzo MC, Gurevich EV, Gurevich VV (2012) Silent scaffolds: inhibition OF c-Jun N-terminal kinase 3 activity in cell by dominant-negative arrestin-3 mutant. J Biol Chem 287: 19653–19664

Regulation of Gene Transcription Following Stimulation of Gαq-Coupled Designer Receptors

Oliver G. Rössler and Gerald Thiel

Abstract

Stimulation of G protein-coupled receptors induces an intracellular signaling cascade that activates transcription factors in the nucleus and thus ultimately leads to transcriptional changes. We have designed reporter genes that specifically measure the activities of the stimulus-responsive transcription factors AP-1, CREB, Egr-1, and serum response factor/ternary complex factor. The transcriptional activation potential of CREB and Elk-1 is measured using fusion proteins consisting of the phosphorylation-dependent activation domain of these transcription factors joined with the DNA-binding domain of the yeast transcription factor GAL4. Lentiviral gene transfer is used to implant the reporter genes into the chromatin of the cells, to ensure that the reporter genes are embedded into a nucleosomal structure. Recombinant lentiviruses infect mitotic and postmitotic cells such as neurons, thus allowing the analysis of transcriptional changes following the activation of G protein-coupled designer receptors.

Key words Designer receptor, Lentivirus, Reporter gene, Egr-1, Elk-1, CREB, AP-1, Transcription

1 Background/Introduction

Stimulation of Gαq-coupled receptors leads to the activation of phospholipase C. As a result, the intracellular Ca^{2+} concentration increases via IP$_3$ generation/IP$_3$ receptor stimulation. Ca^{2+} ions then trigger an activation of protein kinase C and the subsequent phosphorylation and activation of MAP kinases, including extracellular signal-regulated protein kinase (ERK), c-Jun N-terminal protein kinase (JNK), and p38 protein kinase [1]. The phosphorylated and activated protein kinases translocate into the nucleus and phosphorylate gene regulatory proteins. Thus, Gαq-coupled receptor stimulation triggers a change of the genetic program of the cells. Recently, we showed that stimulation of Gαq-coupled AT$_1$ angiotensin II receptors, calcium-sensing receptors, muscarinic acetylcholine receptors, protease-activated receptors, or gonadotropin-releasing hormone receptors has a profound effect on transcriptional regulation [2–6]. Likewise, stimulation of Gαq-coupled designer receptors

activates stimulus-responsive transcription factors [7, 8], indicating that the regulation of gene transcription is an integral part of Gαq-coupled receptor signaling.

There are several methods to detect the activation of transcription factors resulting from cellular stimulation. The biosynthesis of the transcription factors Egr-1 and c-Fos is upregulated as a result of cellular stimulation. Thus, immunohistochemistry is often used to detect expression of these proteins in tissues and cells. In particular, c-Fos expression is used as an indirect marker of neuronal activity [9, 10]. In fact, c-Fos immunoreactivity was used to detect the activation of designer receptors in neurons [11, 12]. Transcription factors such as CREB and c-Jun are phosphorylated following stimulation of the cells with appropriate ligands. Thus, phospho-specific antibodies can be used to detect the activated form of these transcription factors. However, phosphorylation of CREB at the critical serine residue 133 is not a reliable predictor of CREB target gene transcription [13], as underlined by the fact that depolarization of neurons triggers phosphorylation of Ser-133 of CREB within minutes, while the activation of CREB-regulated gene transcription needs much longer [14]. Moreover, a rise in intracellular Ca^{2+} fails to activate CREB-dependent transcription in astrocytes, although phosphorylation of Ser-133 of CREB occurs [15]. Immunocytochemistry is also difficult to employ for the detection of activated AP-1 transcription factor, which can be found as a homodimers, or heterodimer composed of various members of the Fos, Jun, and ATF basic region leucine zipper subfamilies [16]. In vitro protein-DNA binding assays are often used as a measure for an activated transcription factor. However, for AP-1 it has been shown that DNA binding activity does not mirror the transcriptional activity of the AP-1 transcriptional complex [17].

To analyze the activity of a particular transcription factor, it is essential to measure its ability to stimulate transcription of a transcription factor-responsive reporter gene. Here, we describe methods to analyze the activities of stimulus-regulated transcription factors following stimulation of Gαq-coupled designer receptors using chromatin-embedded reporter genes. Figure 1 depicts reporter genes designed to measure the activity of the transcription factors Egr-1, AP-1, CREB, and SRF. The EBS1[4].luc reporter gene contains the luciferase reporter gene (**Note # 1**), controlled by a minimal promoter consisting of four binding sites for Egr-1 (termed EBS), a TATA box, and an initiator element [18] (Fig. 1a). To monitor AP-1 activity, a collagenase promoter/luciferase reporter gene is frequently used (Fig. 1b), as this promoter contains an AP-1-binding site termed 12-*O*-tetradecanoylphorbol-13-acetate (TPA)-responsive element (TRE) in its proximal promoter region [19]. Activation of CREB-regulated transcription is detected with the reporter gene c-FosCRE[4].luc [20] (Fig. 1c). This reporter gene contains, upstream of the luciferase open reading frame, four copies of the cyclic AMP-responsive element (CRE) derived from the
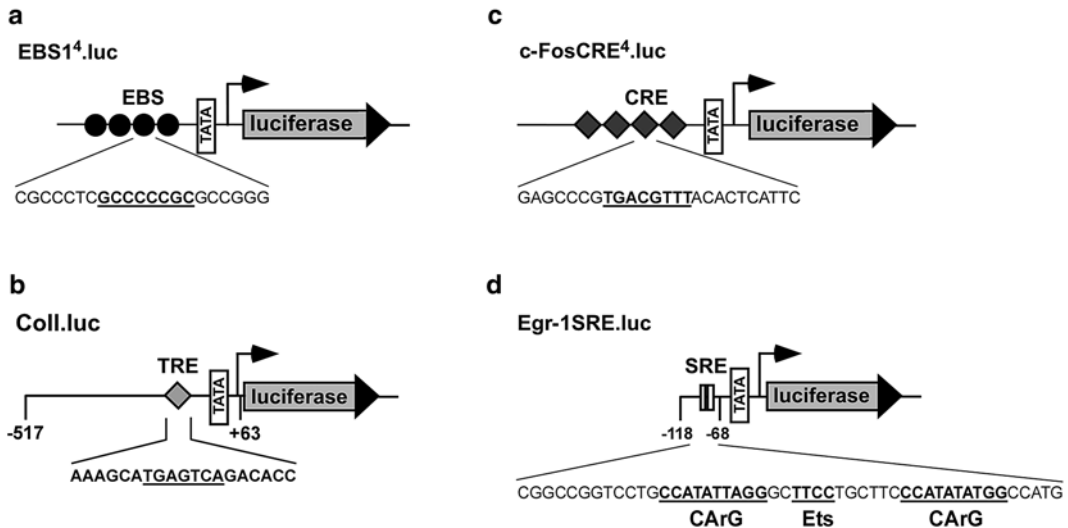
Fig. 1 Reporter genes. (**a**) EBS2⁴.luc. (**b**) Coll.luc. (**c**) c-FosCRE⁴.luc. (**d**) Egr-1SRE.luc. The sequences of the transcription factor-binding sites for Egr-1 (EBS), AP-1 (TRE), CREB (CRE), and SRF/TCF (CArG and Ets) are underlined

human c-Fos promoter that is responsive to elevated intracellular cAMP and Ca^{2+} concentrations [21]. The transcription unit Egr-1SRE.luc has been designed to measure the activity of a gene that is regulated by a serum-responsive element (SRE) [4] (Fig. 1d). The SRE encompasses the consensus sequence $CC[A/T]_6GG$, also termed the CArG box. Many genes contain adjacent to this CArG box a binding site for ternary complex factors (Ets) having the Ets consensus core sequence A/TTCC.

To measure the transcriptional activation potential of stimulus-responsive transcription factors, fusion proteins are expressed consisting of the DNA-binding domain of the yeast transcription factor GAL4 and the activation domain of transcription factors that are regulated by phosphorylation. Figure 2a, b shows the modular structure of the fusion proteins GAL4-Elk (a) and GAL4-CREB (b). Elk-1 and CREB are activated via phosphorylation by various protein kinases. CREB is a substrate for the cAMP-dependent protein kinase PKA, the Ca^{2+}/calmodulin-regulated protein kinase CaMKIV, and the mitogen-induced protein kinase MSK [22]. Elk-1, a member of the Ets family of transcription factors that is an essential component of the serum response ternary complex that binds to DNA and to the serum response factor SRF, is phosphorylated by various MAP kinases [23, 24]. As a control, a fusion protein of the DNA-binding domain of GAL4 and the transcriptional activation domain of Sp1 (GAL4-Sp1) is analyzed (Fig. 2c). A GAL4-sensitive reporter gene is used to measure the transcriptional activity of the GAL4 fusion proteins. Figure 2d shows the schematic representation of the transcription unit encoding a luciferase reporter gene under the control of the minimal
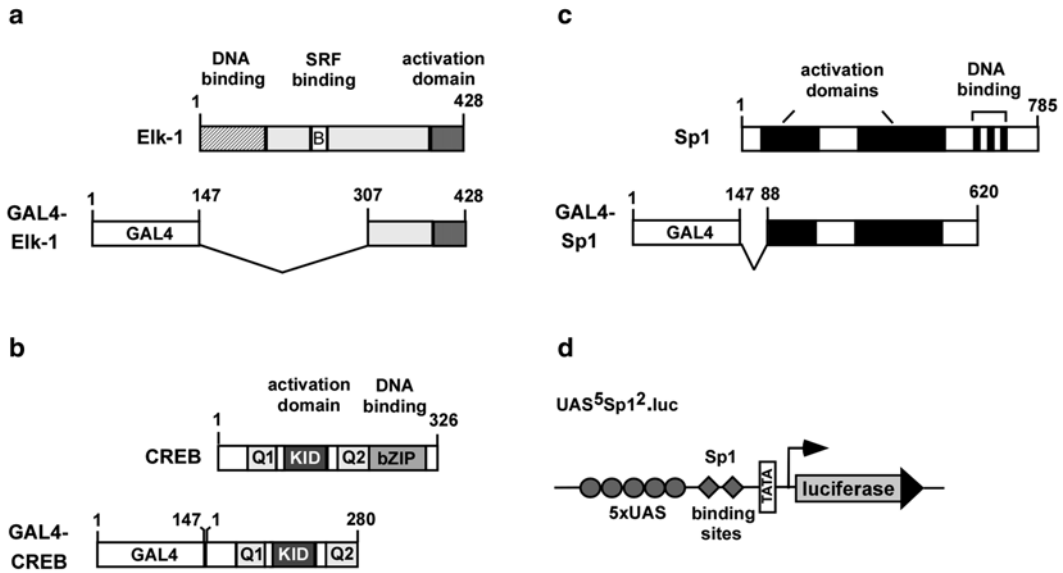
Fig. 2 Modular structure of GAL4 fusion proteins. Schematic representation of the modular structure of Elk-1 and GAL4-Elk-1 (**a**), CREB and GAL4-CREB (**b**), and Sp1 and GAL4-Sp1 (**c**). The GAL4-responsive transcription unit is shown in (**d**). The reporter contains a luciferase reporter gene under the control of the minimal promoter, consisting of two Sp1-binding sites, a TATA box, and five GAL4-binding sites termed UAS (UAS, upstream activating sequence)

promoter. Upstream of the minimal promoter, five GAL4-binding sites (UAS, upstream activating sequence) are present. Since GAL4 does not bind to any known mammalian gene promoter element, interference by other transcriptional regulatory proteins is avoided.

Frequently, transient transfections are used to introduce promoter/reporter gene transcription units into cultured cells. This approach has the disadvantage that the structure of the transfected plasmids may be incompletely organized in comparison to cellular chromatin, and may thus resemble a prokaryotic gene organization including a nonrestrictive transcriptional ground state. In contrast, the chromatin structure in eukaryotes causes a restrictive ground state, occluding proteins such as RNA polymerases and transcriptional regulators from binding to DNA. Thus, promoter/reporter genes need to be integrated into the chromatin to ensure that they packed into an ordered nucleosomal structure. This goal can be accomplished by using lentiviral gene transfer that leads to the integration of the reporter gene into the genome of the infected cell. Recombinant lentiviruses have the main advantage of infecting proliferating and nonproliferating cells. Virus production is accomplished by transfecting an envelope protein encoding plasmid (pCMV-VSV-G), a packaging vector, containing the HIV genes gag, pol, and rev, and a transfer vector into HEK 293T/17 cells. The transfer vector provides the genome for the virus (Fig. 3).
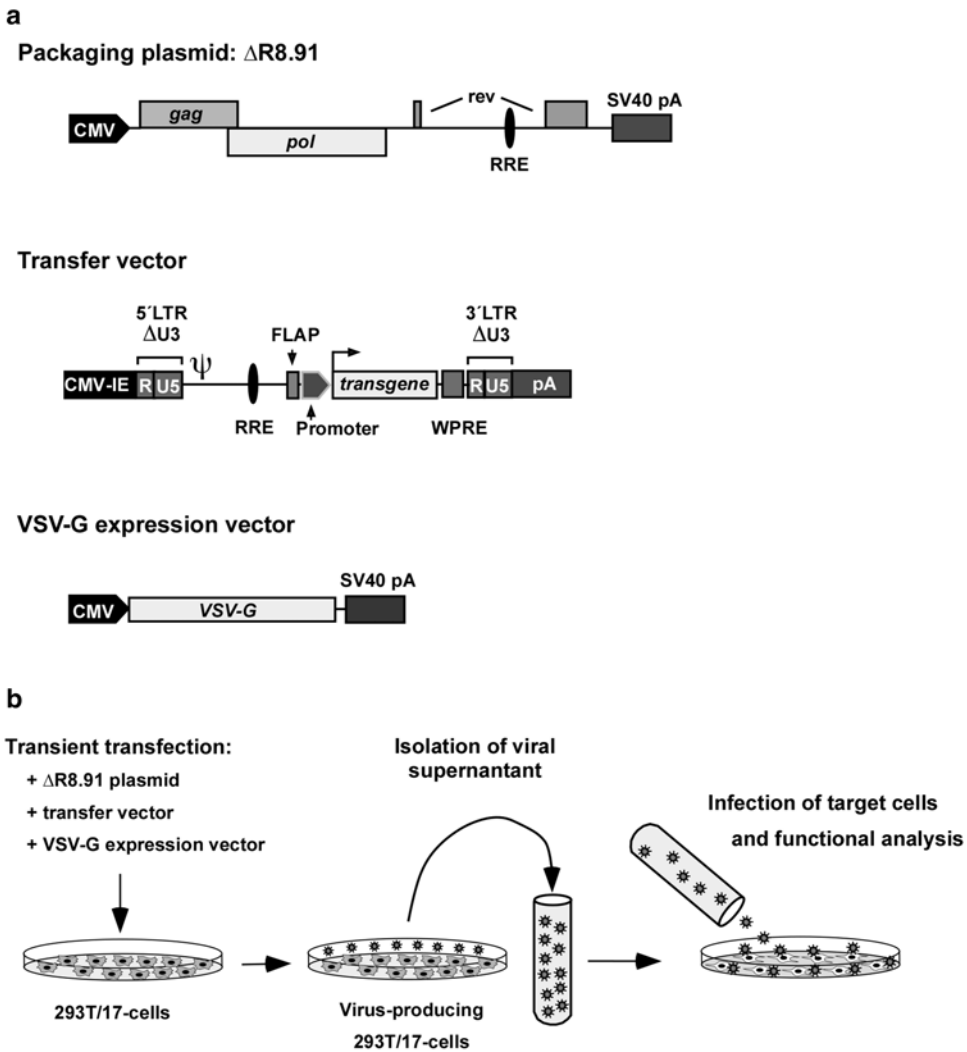
Fig. 3 Generation and infection with recombinant lentiviruses. HEK 293T/17 cells are transfected with three plasmids: The packaging plasmid contains the gag, pol, and rev genes of HIV. The envelope glycoprotein of the vesicular stomatitis virus is expressed from the pCMV-VSV-G plasmid. The lentiviral transfer vector provides the genome for the recombinant viruses. Virus stock is harvested 3 days after transfection, filtered, supplemented with polybrene, and used to infect target cells

2   Equipment, Materials, and Setup

2.1   Materials for Transfection of HEK 293T/17 Cells

1. HEK 293T/17 cells.

2. Cell culture equipment, media.

3. Lentiviral packaging vector Δ8.91 [25].

4. VSVG envelope protein expression vector pCMV-VSV-G (Addgene, plasmid # 8454).

5. Lentiviral transfer vector pFUW-Rαq: This lentiviral transfer plasmid encodes for a Gαq-coupled designer receptor under the control of the human UbC promoter [7, 8].

6. pFW-c-FosCRE[4].luc (reporter measuring CREB activity; [5]).

7. pFW-EBS1[4].luc (reporter measuring Egr-1 activity, [5]).

8. pFW-Egr1-SRE.luc (reporter measuring SRF/TCF activity, [4]).

9. pFW-Coll.luc (reporter measuring AP-1 activity, [3]).

10. pFW-UAS[5]Sp1[2].luc (reporter measuring the activity of GAL4 fusion proteins, [26]).

11. pFUW-GAL4-CREB, pFUW-GAL4-Elk-1, pFUW-GAL4-Sp1 (lentiviral transfer vectors for expressing GAL4 fusion proteins, [5]).

12. Chemicals for transfection: $CaCl_2$ (Sigma), chloroquine diphosphate salt (Sigma # C6628).

2.2 Materials for Infection with Recombinant Lentivirus, Stimulation, and Reporter Gene Analysis

1. Chemical for infection: Hexadimethrine bromide (Polybrene, Sigma # H9268), 8 mg/ml in H_2O, filter sterilized through a 0.22 μM filter.

2. 0.45 μm filter units (Sarstedt, Nürmbrecht, Germany, # 83.1826).

3. Antiviral agent (Bacillol).

4. Reporter lysis buffer (Promega, Mannheim, Germany).

3 Procedures

3.1 Virus Production: Transfection of HEK 293T/17 Cells with Calcium Phosphate

The viral particles are produced by transient transfection of HEK 293T/17 cells using the calcium phosphate coprecipitation technique.

1. Seed 2×10^6 HEK293T/17 cells in a 60-mm plate. Incubate the cells overnight in complete DMEM medium (containing 10 % fetal bovine serum, penicillin (100 U/ml), and streptomycin (100 μg/ml)) at 37 °C in 5 % CO_2.

2. Remove the medium, and add complete DMEM containing chloroquine (25 μM).

3. Transfect the cells with the calcium phosphate coprecipitation methods:

   Three plasmids are transfected into the cells: 6.6 μg of the transfer vector, 5 μg of the pCMVΔR8.91 packaging vector, and 2.3 μg of plasmid pCMV-VSV-G, encoding the vesicular stomatitis virus glycoprotein. Transfections are performed in the presence of chloroquine (25 μM). The cells are incubated for 8–16 h with the calcium phosphate-DNA precipitate.

4. The cells are washed twice with PBS and incubated in complete DMEM at 37 °C for 2–3 days.

3.2 Virus Collection and Infection of Neuronal Cells/ Neurons with Recombinant Lentivirus

The production and handling of lentiviral vectors should be carried out using the proper biosafety containment. *See* Biosafety for Research with Lentiviral Vectors (http://www4.od.nih.gov/ova/RAC/ Guidance/LentiVirus_Caintainment/pdf/Lenti_Containment_ Guidance.pdf).

1. Transfer viral supernatant from 60 mm dishes to 50 ml tubes.

2. Centrifuge for 5 min at 1000 rpm to pellet unattached HEK 293T/17 cells.

3. Pass viral supernatant through 0.45 μM filter.

4. Add polybrene to viral supernatant (final concentration: 8 μg/ml).

5. Seed the target cells together with the virus stock and incubate overnight (**Note # 2**).

To analyze Rαq-regulated gene transcription, the target cells are infected with two virus stocks encoding the designer receptor Rαq and the reporter gene, respectively.

3.3 Stimulation and Reporter Gene Analysis

1. The virus is removed and the cells are maintained for 24 h in complete DMEM medium.

2. The medium is changed and the cells are incubated in DMEM medium containing 0.05 % fetal bovine serum (**Note # 3**).

3. Stimulate the cells in serum-reduced medium with clozapine-*N*-oxide (CNO, Enzo Life sciences, # NS-105-0005) (1 μM) for 24 h.

4. Cell extracts of stimulated cells are prepared using reporter lysis buffer (Promega, Mannheim, Germany) and analyzed for luciferase activities as described [5, 6]. Luciferase activity is normalized to the protein concentration.

4   Typical/Anticipated Results

HEK 293T/17 cells expressing stimulated Gαq-coupled designer receptors were stimulated with CNO. To measure Egr-1 activity, an Egr-1-responsive luciferase reporter gene EBS1^{4}luc was integrated into the chromatin of the cells. Stimulation of the cells with CNO significantly increased the transcription of the Egr-1-responsive reporter gene (Fig. 4a), indicating that stimulation of Gαq-coupled designer receptors increases the concentration of biologically active Egr-1 protein. These data were corroborated by a Western blot analysis, showing that stimulation of the designer receptor induced the biosynthesis of Egr-1 (Fig. 4b). Stimulation of the Gαq-coupled designer receptor with CNO additionally enhanced transcription of the AP-1-responsive reporter gene Coll.

a

EBS1^4.luc

relative luciferase activity (fold induction)

5
4
3
2
1

−   +   CNO [1 μM]

b

← Egr-1

← HDAC1

−   1   3   5   [h] CNO [1 μM]

c

Coll.luc

6
5
4
3
2
1

−   +   [h] CNO [1 μM]

d

← c-Fos

← HDAC1

−   1   3   5   [h] CNO [1 μM]

← c-Jun

← HDAC1

−   1   3   5   [h] CNO [1 μM]

e

c-FosCRE^4.luc

relative luciferase activity (fold induction)

6
5
4
3
2
1

−   +   CNO [1 μM]

f

Egr-1SRE.luc

relative luciferase activity (fold induction)

3
2
1

−   +   CNO [1 μM]
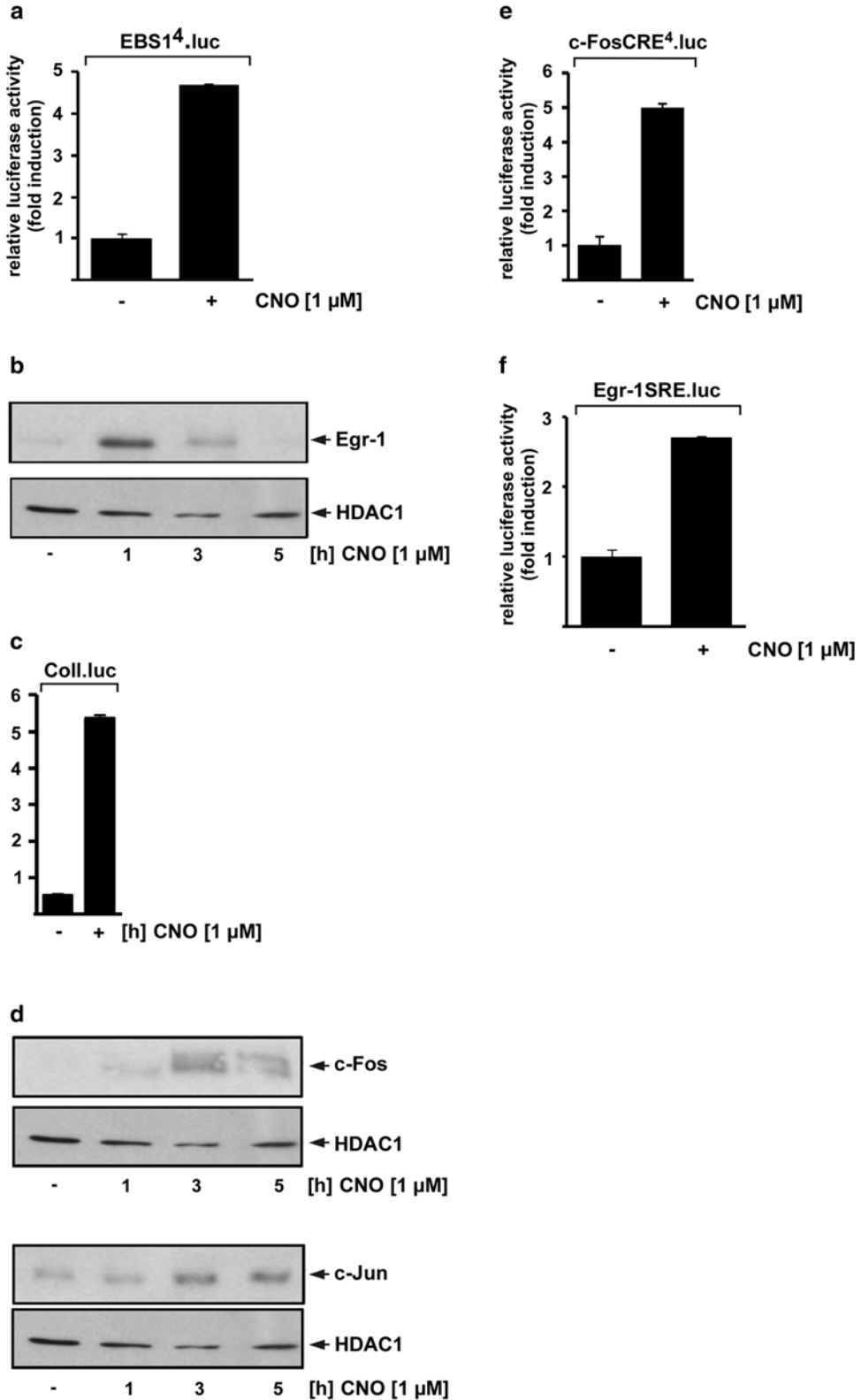
luc (Fig. 4c). Western blot experiments supported these findings, showing that expression of c-Fos and c-Jun was upregulated following designer receptor stimulation (Fig. 4d). c-Fos and c-Jun are frequently included into functional AP-1 complexes. Finally, transcription of reporter genes controlled by either CRE or SRE motifs was stimulated as a result of designer receptor activation (Fig. 4e, f).

Furthermore, stimulation of Gαq-coupled designer receptors increased the transcriptional activation potential of the transcription factors Elk-1 and CREB, as depicted in Fig. 5a, b, while the transcriptional activity of GAL4-Sp1 fusion protein, consisting of the DNA-binding domain of GAL4, fused to the activation domain of the transcription factor Sp1, was not altered as a result of designer receptor activation (Fig. 5c).

5 Conclusion

As the regulation of gene transcription is an integral part of the Gαq-coupled receptor signaling pathways, tools are required to measure genetic changes in cells and tissues. The combination of reporter genes, together with lentiviral gene transfer, allows the incorporation of transcription units into the genome of dividing and nondividing cells. Viral infection of particular neuronal populations can be combined with the use of transgenic mice expressing G protein-coupled designer receptors in selected areas of the brain.

Fig. 4 Transcription activation of Egr-1, AP-1, SRF, and CREB-controlled reporter genes in cells expressing a stimulated Gαq-coupled designer receptor. HEK293T/17 cells were infected with a recombinant lentivirus encoding one of the reporter genes EBS1^4.luc (**a**), Coll.luc (**c**), c-FosCRE^4.luc (**e**), or Egr-1SRE.luc (**f**). In addition, cells were infected with a lentivirus encoding a Gαq-coupled designer receptor. The cells were serum-starved for 24 h and then stimulated with CNO (1 μM) for 24 h. Cell extracts were prepared and analyzed for luciferase activities. (**b**, **d**) Induction of transcription factor biosynthesis in CNO-stimulated HEK 293T/17 cells expressing a Gαq-coupled designer receptor. Cells were cultured for 24 h in medium containing 0.05 % serum. Stimulation with CNO (1 μM) was performed with medium containing 0.05 % serum. Nuclear extracts were prepared and subjected to Western blot analysis using antibodies directed against either Egr-1 (**b**), c-Fos (**d**), or c-Jun (**d**). The antibody directed against histone deacetylase-1 (HDAC1) was used as a loading control (reproduced with modifications from [7] with permission of John Wiley & Sons Ltd.)
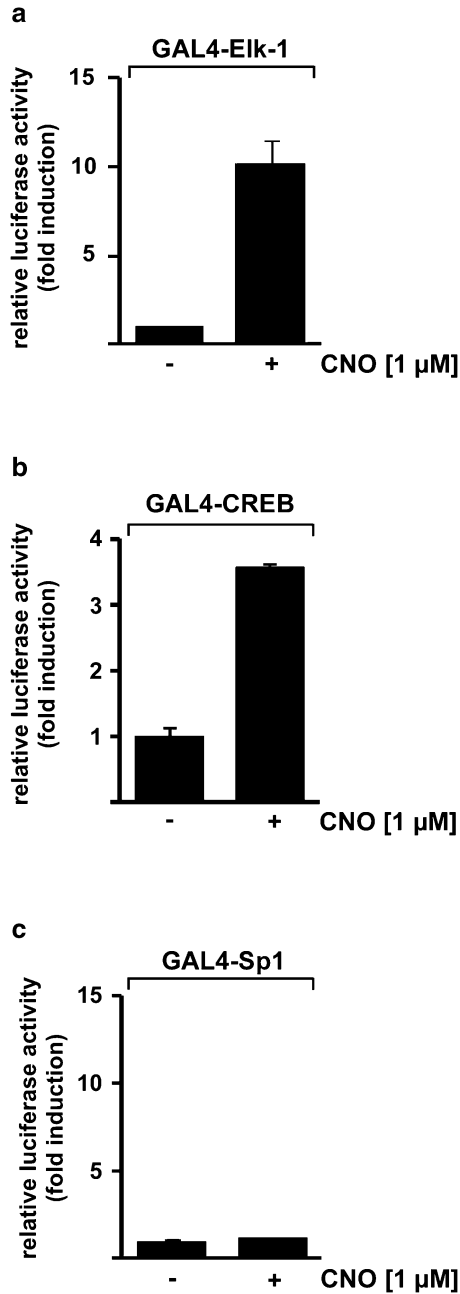
Fig. 5 Upregulation of the transcriptional activation potential of Elk-1 and CREB following stimulation of Gαq-coupled designer receptors with CNO. HEK293T/17 cells were double-infected with a lentivirus encoding the GAL4-responsive luciferase reporter gene UAS⁵Sp1².luc and a lentivirus encoding either GAL4-Elk-1 (**a**), GAL4-CREB (**b**), or GAL4-Sp1 (**c**). In addition, the cells were infected with a lentivirus encoding the Gαq-coupled designer receptor. The infected cells were stimulated with CNO (1 μM) for 24 h. Cell extracts were prepared and analyzed for luciferase activities. Luciferase activity was normalized to the protein concentration (reproduced with modifications from [7] with permission of John Wiley & Sons Ltd.)

6   Notes

1. Luciferase is the reporter gene of choice for in vitro experiments, due to the absence of luciferase activity inside the cells, the ease of detecting luciferase activity via luminometric analysis, and its high sensitivity. For in vivo experiments, fluorescent reporter genes, e.g., variants of green fluorescent protein, may be better suited.

2. We harvest the target cells and seed them together with the virus. Thus, adherence and infection are taking place at the same time. This approach is not feasible for sensitive cells such as neural stem cells [26]. Here, cells have to be seeded 12–24 h before infection.

3. Stimulation of cells expressing Gαq-coupled designer receptors with CNO activates signaling pathways in the cells that are also activated by ligands of receptor tyrosine kinases, which are present in fetal bovine serum. Thus, performing the experiments in the presence of 10 % serum will mask the effect of designer receptor stimulation, due to the stimulation of gene transcription by serum ingredients [27]. In contrast, maintaining cells in medium containing 0.05 % serum may not support survival for neuronal cells. In this case, serum concentration has to be increased to 0.5 or 1 %.

References

1. Vaqué JP, Dorsam RT, Feng X, Iglesias-Bartolome R, Forsthoefel DJ, Chen Q, Debant A, Seeger MA, Bsander BR, Teramoto H, Gutkind JS (2013) A genome-wide RNAi screen reveals a tri-regulated Rho GTPase circuitry transducing mitogenic signals initiated by G protein-coupled receptors. Mol Cell 49:94–108

2. Mayer SI, Dexheimer V, Nishida E, Kitajima S, Thiel G (2008) Expression of the transcriptional repressor ATF3 in gonadotrophs is regulated by Egr-1, CREB, and ATF2 after gonadotropin-releasing hormone receptor stimulation. Endocrinology 149:6311–6325

3. Rössler OG, Henß I, Thiel G (2008) Transcriptional response to muscarinic acetylcholine receptor stimulation: regulation of Egr-1 biosynthesis by ERK, Elk-1, MKP-1, and calcineurin in carbachol-stimulated human neuroblastoma cells. Arch Biochem Biophys 470:93–102

4. Rössler OG, Thiel G (2009) Thrombin induces Egr-1 expression in fibroblasts involving elevation of the intracellular Ca^{2+} concentration, phosphorylation of ERK and activation of ternary complex factor. BMC Mol Biol 10:40

5. Thiel G, Rössler OG (2011) Immediate-early transcriptional response to angiotensin II in human adrenocortical cells. Endocrinology 152:4211–4223

6. Thiel G, Lesch A, Keim A (2012) Transcriptional response to calcium-sensing receptor stimulation. Endocrinology 153:4716–4728

7. Kaufmann A, Keim A, Thiel G (2013) Regulation of immediate-early gene transcription following activation of Gαq-coupled designer receptors. J Cell Biochem 114:681–696

8. Kaufmann A, Rössler OG, Thiel G (2014) Expression of the transcription factor Egr-1 in pancreatic acinar cells following stimulation of cholecystokinin or Gαq-coupled designer receptors. Cell Physiol Biochem 33:1411–1425

9. Reijmers LG, Perkins BL, Matsuo N, Mayford M (2007) Localization of a stable neural correlate of associative memory. Science 317:1230–1233

10. Carter ME, Soden ME, Zweifel LS, Palmiter RD (2013) Genetic identification of a neural circuit that suppresses appetite. Nature 503:111–114

11. Zhan C, Zhou J, Feng Q, Zhang J-E, Lin S, Bao J, Wu P, Luo M (2013) Acute and long-term suppression of feeding behavior by POMC neurons in the brainstem and hypothalamus, respectively. J Neurosci 33: 3624–3632

12. Krashes MJ, Shah BP, Madara JC, Olson DP, Strochlic DE, Garfield AS, Vong L, Pei H, Watabe-Uchida M, Uchida N, Liberles SD, Lowell BB (2014) An excitatory paraventricular nucleus to AgRP neuron circuit that drives hunger. Nature 507:238–242

13. Zhang X, Odom DT, Koo S-H, Conkright MD, Canettieri G, Best J, Chen H, Jenner R, Herbolsheimer E, Jabobsen E, Kadam S, Ecker JR, Emerson B, Hogenesch JB, Unterman T, Young RA, Montminy M (2005) Genome-wide analysis of cAMP-response element binding protein occupancy, phosphorylation, and target gene activation in human tissues. Proc Natl Acad Sci U S A 102:4459–4464

14. West AE, Chen WG, Dalva MB, Dolmetsch RE, Kornhauser JM, Shaywitz AJ, Takasu MA, Tao X, Greenberg ME (2001) Calcium regulation of neuronal gene expression. Proc Natl Acad Sci U S A 98:11024–11031

15. Murray PD, Kingsbury TJ, Krueger BK (2009) Failure of Ca^{2+}-activated, CREB-dependent transcription in astrocytes. Glia 57:828–834

16. Vinson C, Myakishev M, Acharya A, Mir AA, Moll JR, Bonovich M (2002) Classification of human B-ZIP proteins based on dimerization properties. Mol Cell Biol 22:6321–6335

17. Karin M (1995) The regulation of AP-1 activity by mitogen-activated protein kinases. J Biol Chem 270:16483–16486

18. Al-Sarraj A, Day RM, Thiel G (2005) Specificity of transcriptional regulation by the zinc finger transcription factors Sp1, Sp3, and Egr-1. J Cell Biochem 94:153–167

19. Angel P, Baumann I, Stein B, Delius H, Rahmsdorf HJ, Herrlich P (1987) 12-O-tetradecanoyl-phorbol-13-acetate induction of the human collagenase gene is mediated by an inducible enhancer located in the 5′ flanking region. Mol Cell Biol 7:2256–2266

20. Thiel G, Al Sarraj J, Vinson C, Stefano L, Bach K (2005) Role of basic region leucine zipper transcription factors cyclic AMP response element binding protein (CREB), CREB2, activating transcription factor 2 and CAAT/enhancer binding protein alpha in cyclic AMP response element-mediated transcription. J Neurochem 92:321–336

21. Sheng M, McFadden G, Greenberg ME (1990) Membrane depolarization and calcium induce c-Fos transcription via phosphorylation of transcription factor CREB. Neuron 4:571–582

22. Mayr B, Montminy M (2001) Transcriptional regulation by the phosphorylation-dependent factor CREB. Nat Rev Mol Cell Biol 2: 599–609

23. Cavigelli M, Dolfi F, Claret FX, Karin M (1995) Induction of c-fos expression through JNK-mediated TCF/Elk-1 phosphorylation. EMBO J 14:5957–5964

24. Cruzalegui FH, Cano E, Treisman R (1999) ERK activation induces phosphorylation of Elk-1 at multiple S/T-P motifs to high stoichiometry. Oncogene 18:7948–7957

25. Zufferey R, Nagy D, Mandel RJ, Naldini L, Trono D (1997) Multiply attenuated lentiviral vector achieves efficient gene delivery in vivo. Nat Biotechnol 15:871–875

26. Ekici M, Hohl M, Schuit F, Martínez-Serrano A, Thiel G (2008) Transcription of genes encoding synaptic vesicle proteins in human neural stem cells: chromatin accessibility, histone methylation pattern, and the essential role of REST. J Biol Chem 283:9257–9268

27. Müller I, Rössler OG, Thiel G (2011) Pregnenolone sulfate activates basic region leucine zipper transcription factors in insulinoma cells: role of voltage-gated Ca^{2+} channels and transient receptor potential melastatin 3 channels. Mol Pharmacol 80:1179–1189

Chapter 4

Chemogenetic Deconstruction of Feeding Circuits

Michael Krashes

Abstract

The sensation of hunger and subsequent act of eating for nourishment are the most basic behaviors across all animals. One can trace its rampage through human history by examining how it has shaped our genes, cultures, and landscapes. Yet, despite the shared familiarity of eating, the neural circuits underlying the motivational processes underlying shifts in appetite have remained elusive due to a lack of methods sensitive enough to probe defined subpopulations of brain cells with temporal and spatial precision. Chemogenetics is an innovative neuroscience approach that has recently been applied in order to dissect feeding circuits by allowing for remote, reversible control of specific neural networks. The technique involves the use of exogenously expressed, molecularly evolved G-protein-coupled receptors (GPCRs) in discrete neural populations followed by their unique ligand-dependent activation. These receptors are modified to couple through cellular machinery resulting in either stimulation or inhibition of neural activity. This allows researchers to acutely and explicitly "turn on" and "turn off" a cell type of choice and assess the resulting behavioral output. Here, I describe how these tools have developed over the years and how they have been applied to the deconstruction of central circuits governing feeding. A thorough comprehension of these critical signals and neural pathways will aid in our fight against obesity and the multitude of eating-related disorders.

> A major first step, then, is to identify the many different types of neuron existing in the cerebral cortex and other parts of the brain. One of the next requirements is to be able to turn the firing of one or more types of neuron on and off in the alert animal in a rapid manner.
>
> Francis Crick, Proc Royal Soc London 1999

1   Background and Historical Overview

Feeding is necessary for growth, self-maintenance, and reproduction rendering this directed action obligatory for survival. Selective pressure to locate, obtain, and consume nutrients makes feeding activity the most powerful agent in the evolution of species. Feeding can be thought of as the decisive behavioral component of a common physiological process, that of nutrition. Metabolic demand drives food selection and magnitude of consumption to provide the body with metabolizable energy used to cover energy

expenditure (such as carbohydrates, fats, and proteins) as well as essential amino acids, minerals, and vitamins required for growth and sustenance.

However, hunger is not simply a homeostatic process; it is a dynamic transaction that commands profound influence on emotion, cognition, and behavior [1]. It sits at the center of various public health concerns that span multiple disciplines of modern medicine. These include ailments such as malnutrition, obesity, and type II diabetes that negatively impact physical as well as emotional [2–5] and cognitive [6–8] well-being. The pervasiveness of hunger in public health crises compounds the importance for experimental research. A fundamental understanding of the biological manifestation of hunger in the brain could provide potentially unifying information about these disease states and lead to groundbreaking new frameworks in which to approach these problems.

Clearly, the fundamental power of appetite has always captured our attention and has been the subject of countless studies throughout human history. Only recently, however, rather than merely evaluating the intensity of hunger in man have investigators turned to employing animal models to answer complicated questions within this discipline. Such animal studies address the questions of how a combination of internal and external signals governs the selection and intake of foods, and how feeding behavior is integrated into the overall process of nutritional homeostasis.

The overarching complexity and multiple layers of eating behavior, in addition to its increased interest to the general public at large, make understanding the molecular, cellular, and neural machinery controlling feeding imperative to both our health and curiosity. To this end, the last century has made significant progress toward this goal using a variety of approaches. For the purposes of this chapter, emphasis will be placed on rodent models.

Classic work demonstrated a key role of the hypothalamus in hunger by using lesions [9–17], intracranial drug delivery [18–24], and electric brain stimulation in animal models [25, 26]. This work culminated into a theory that attributed the balance between hunger and satiety to distinct nuclei of the hypothalamus, including the lateral hypothalamus (LH), paraventricular hypothalamus (PVH), ventral medial hypothalamus (VMH), dorsal medial hypothalamus (DMH), and arcuate nucleus (ARC).

Although this work clearly demonstrated a role for the LH, PVH, VMH, DMH, and ARC in appetite and reward, the techniques used in these studies carry serious limitations. While these methods were very powerful, they lacked specificity. For example, electric brain stimulation activates all neurons within the radius of the electrode as well as all axons passing through the region, which has grave implications on downstream targets. Conversely, lesions destroy all cell types in the affected area, including both afferent

and efferent processes outside the intended lesion zone. Moreover, these past approaches often lacked anatomical precision resulting in off-target effects, as discrete nuclei of the hypothalamus border one another and are roughly defined.

The paucity of specificity in these techniques has likely led to the diversity of effects found among different behavioral paradigms (from feeding to aggression to drinking to mating), which has given us a broad and disjointed understanding of the role of the hypothalamus in regulating appetite. Fortunately, recent breakthroughs in neuroscience allow for more targeted approaches to empirical questions.

Studying the mechanisms of homeostatic food intake is challenging due to slow temporal kinetics of the parameters mediating the switch between hunger and satiety. Hormones need to be released from peripheral tissues, travel to the brain, and signal nutrient-sensing neurons to direct food-seeking and consumption behavior. These prolonged changes in energy deficit considerably hamper the examination of the contributing relationships between deprivation-sensitive sensory systems and the downstream brain circuits they engage. To sidestep this difficulty, manipulations of molecularly circumscribed nutrient-sensing neurons can be used to prove the central control of feeding. Once identified, the afferent and efferent pathways modulating both hunger and satiety can be further analyzed in detail [27].

This need to obtain discrete access to defined neurons is essential given the diversity and complexity of the neural circuits underlying feeding behaviors. For example, the Agouti-related peptide (ARC^{AgRP}) and proopiomelanocortin (ARC^{POMC}) neuronal populations are not only adjacent, but are also anatomically intermingled with each other in the arcuate nucleus. Given that these separate cell types are thought to evoke opposing functions on appetite, gaining command over each unique population is essential to unraveling their behavioral contributions.

A common way to achieve such specificity is through a two-pronged approach using genetically engineered mice that express Cre-recombinase, a tyrosine recombinase enzyme derived from bacteriophage, in defined neurons, often driven off the endogenous gene promoter, in combination with Cre-dependent viral vectors expressing activity modulators to stimulate or silence neuronal activity [28]. These adeno-associated viruses (AAV) are designed in such a way that the open reading frame of the coding sequence is inverted, in the antisense orientation, flanked by two pairs of heterotypic, antiparallel loxP-type recombination sites. In the presence of Cre-recombinase, the recombination sites first undergo an inversion of the coding sequence followed by excision of two sites, leading to one of each orthogonal recombination site oppositely oriented and incapable of further recombination [29, 30]. This Cre-dependent viral approach is commonly referred to as a FLEX

switch or double-floxed inverse open reading frame (DIO) [29, 31], and is used to target specific cell types with spatial precision via intracranial surgeries in distinct Cre driver mouse lines.

Two methods, optogenetics and chemogenetics, devised for manipulating neural activity in vivo have benefited tremendously from this viral approach. Optogenetics (which will not be described in detail in this chapter) involves the use of microbial and chimeric-vertebrate opsin genes that have been developed to control highly defined electrical activity with cell-type selectivity, high temporal precision and rapid reversibility. As most neurons in the brain are not naturally light sensitive, selective expression of opsin genes in targeted neural populations makes it possible to specifically control the activity in these populations through optical light delivery, and the resulting fast on–off kinetics make it possible to evoke or inhibit neural activity within milliseconds, on a time scale relevant to the physiological brain functions [32, 33].

Chemogenetics is a system to control neuronal activity *non-invasively* in the mammalian brain by regulating signaling through a G protein-coupled receptor (GPCR) [28, 34] or recently using ligand-activated ion channels [35–37]. These pharmacological approaches to manipulate neuronal activity through GPCR signaling pathways in neurons both in vitro and in vivo include ectopic expression of either GPCRs with engineered binding sites such as *r*eceptors *a*ctivated *s*olely by *s*ynthetic *l*igands (RASSLs) [38, 39] or nonnative GPCRs such as the Drosophila allatostatin receptor (AlstR) [40, 41].

Despite the vast contributions utilizing these methods, continued improvements were needed to facilitate regulation of activity of discrete populations of CNS neurons selectively and noninvasively in vivo. RASSLs, for example, are activated by nonselective, pharmacologically active small molecules and in some tissues exhibit high levels of signaling in the absence of exogenous small-molecule agonists, which can result in pathologic phenotypes [42–45]. Although AlstR displays no evidence of basal signaling, it does not allow for remote manipulations of neuronal activity, as its ligand is unlikely to cross the blood–brain barrier and must be directly infused into brain tissue [41]. Furthermore, AlstR is coupled only to neuronal silencing, so it cannot be used for neuronal activation.

Advancing on these methods, *d*esigner *r*eceptors *e*xclusively *a*ctivated by *d*esigner *d*rug (DREADDs) were developed to provided researchers with a system for neuronal regulation in which (1) the exogenous ligand would be pharmacologically inert, (2) the exogenous ligand could be administered in the periphery and cross the blood–brain barrier to access receptors in deep brain structures and/or widely distributed neuronal populations, (3) receptor expression alone would not induce pathology, (4) neuronal activity could be both increased and decreased, and (5) both spatial and temporal resolution would be sufficient to facilitate the study of brain function in health and disease [46].

DREADDs are molecularly evolved GPCRs derived from human muscarinic receptors that have lost the ability to bind the endogenous ligand, acetylcholine, and instead have been mutated, so they are only activated by the pharmacologically inert compound, clozapine-N-oxide (CNO) [34, 47]. Importantly, distinct DREADD receptors have been generated to stimulate neural activity, through the canonical G_q [34, 46] or G_s signaling pathways [48], or inhibit neural activity, via $G_{i/o}$ molecular signaling [34, 49].

Merging viral-assisted, Cre-dependent strategies to deliver optogenetic and chemogenetic tools with various Cre-recombinase-expressing mouse lines grant researchers with unprecedented, demarcated control of neuronal subtypes allowing for the probing of causal relationships of defined, cellular manipulation with a myriad of behaviors. Since the introduction of these novel techniques, the feeding field has made significant progression into the understanding of the neural circuits underlying the homeostatic and hedonic processes of appetite regulation. Given the immense heterogeneity that exists in the brain, particularly elaborate structures such as the hypothalamus, it is absolutely essential to have tools to ensure specific manipulation of delineated cell types. The key to dissecting a complex anatomical neural circuit is to find a key node in which to start. Once identified, additional strategies can be used to deconstruct these multifaceted networks and unravel functional connectivity, ultimately helping us comprehend just how these circuits guide behavior. The natural question is where do we begin.

AgRP neurons, located in the arcuate nucleus (henceforth referred to as ARCA^{gRP} neurons), are unique in that they are state dependent, meaning that their neural activity differs depending on the hunger-satiety state of the animal. These neurons are relatively quiescent when mice are sated and fire at a much higher frequency when the animals are physiologically hungry or fasted [50, 51], which is related to increased excitatory transmission onto ARCA^{gRP} neurons [52, 53]. Additionally, pharmacological administration of the peptides released by these neurons [54–56] or GABA receptor agonists [57] into downstream ARCA^{gRP} target regions induces a robust hyperphagic response. Finally, given the severe reduction in body weight and food intake observed following acute ARCA^{gRP} cell ablation in adults [58, 59], ARCA^{gRP} neurons were the ideal testing ground for these innovative, remote, and reversible tools.

Although chemogenetic and optogenetic strategies have been applied to assign behavioral function to a number of feeding circuits [35–37, 51, 60–68], for the purpose of this Methods Chapter, focus will be concentrated specifically on the role of ARCA^{gRP} neurons on appetite regulation. Chemogenetic DREADD-mediated ARCA^{gRP} stimulation resulted in escalated feeding over several hours as a single injection of CNO (0.3 mg/kg) continues to activate the targeted receptor (predicted half-life ~8 h) [46, 64]. Importantly, this induction of feeding occurs in calorically replete mice with no homeostatic motive to consume food, as assessed

near the beginning of the light cycle period when mice are coming off dark cycle feeding bouts. This evoked rapid feeding behavior in naïve animals was phenocopied utilizing optogenetics to photactivate ARCA[gRP] neurons [60]. Interestingly, after the acute activation of ARCA[gRP] neurons with DREADD technology, both GABA and NPY were found to be required for the rapid stimulation of feeding, and the neuropeptide AgRP, through action on MC4Rs, was sufficient to induce feeding over a delayed yet prolonged period [51].

Chronic activation of ARCA[gRP] neurons over 5 days caused marked weight gain, accompanied with increased fat stores, due to hyperphagia and most likely decreased energy expenditure, as acute ARCA[gRP] activation drastically reduces energy expenditure [64]. Remarkably, following drug withdrawal, the CNO-induced obesity and increased fat mass were normalized, and this reversal was associated with compensatory hypophagia, strongly supporting the existence of a "set point" for these parameters [64].

It has been suggested that the hypothalamic neurocircuitry responsible for integrating metabolic signals is embedded within a complex network that permits both the adaptation and synchronization of nutrient needs to conditions in the animal's local environment [69]. It is likely that these same neurons invoke neural mechanisms of reward, motivation, and decision making, all of which are integrated to serve the ultimate goal of obtaining and ingesting food.

Of note, ARCA[gRP] neurons not only drive homeostatic feeding when food is freely available but also engage a behavioral program to work for and seek out food. Chemogenetic ARCA[gRP] activation significantly increases a sated animal's willingness to work for food as determined through a classic nosepoke assay, in a similar magnitude to that induced by the calorically deficient, fasted state [64]. This finding was replicated employing optogenetics to photostimulate ARCA[gRP] neurons in sated animals during lever-press task [35].

To further investigate goal-directed behavior aimed at food acquisition, physical activity was measured during the light cycle when mice are relatively inactive. Stimulating ARCA[gRP] neurons in the absence of food led to intense, unrelenting activity, a behavioral state that continued unabated for hours. This was interpreted as food-seeking behavior for two major reasons. Firstly, the mice were often seen visiting areas of the cage where food was normally located or accumulated and engaged in vigorous digging-type behaviors. Secondly, when the same mice were again given CNO on a different day, this time in the presence of food, this sharp increase in activity was completely absent, indicating that the marked activity was directed toward the acquisition and consumption of food [64].

The following protocol will provide the reader with the equipment, materials, and setup necessary to carry out virally

mediated chemogenetic studies as well as the procedures for assessing feeding behavior. Moreover, experimental variables and typical/anticipated results will be discussed. Finally, troubleshooting common problems with this technique will be examined.

2 Equipment, Materials, and Setup

As alluded to in Sect. 1, the chemogenetic method described here requires two essential cogs: (1) a genetically modified mouse line expressing Cre-recombinase in moleculary restricted neurons, commonly driven off the endogenous promoter of your gene of interest (in this case ARCA^{gRP} neurons expressed via an *Agrp-Ires-cre* knock-in mouse), and (2) a Cre-dependent viral vector expressing the chemogenetic receptor, often accompanied with a fluorescent marker, used to selectively target these Cre + neurons via intracranial, stereotaxic surgery (in this case either AAV-hsyn-DIO-hM3Dq-mCherry or AAV-hysn-DIO-hM4Di-mCherry used to activate or inhibit neural activity, respectively).

Information on how to engineer mice to express Cre-recombinase in discrete cell types can be found elsewhere. However, several sources are available to purchase transgenic and/or knock-in mice expressing Cre-recombinase under specific promoters conferring expression of Cre in restricted neural populations:

(http://cre.jax.org/index.html).
(http://www.gensat.org/cre.jsp).

For example, *Agrp-Ires-cre* knock-in mice can be ordered directly from The Jackson Laboratory (Strain Name: STOCK *Agrp$^{tm1(cre)Lowl}$/J*; Stock Number: 012899.

Similarly, protocols for the design and construction of novel viral vectors are beyond the scope of this book chapter. Nevertheless, multiple sources are available to purchase packaged Cre-dependent (DIO or FLEX) viral vectors in different AAV serotypes:

(http://genetherapy.unc.edu/services.htm).
(http://www.med.upenn.edu/gtp/vectorcore/).

For example, AAV-hsyn-DIO-hM3Dq-mCherry and AAV-hysn-DIO-hM4Di-mCherry virus can be ordered directly from the Gene Therapy Center at University of North Carolina (In-Stock AAV Vectors—Dr. Bryan Roth; no MTA is required). Additionally, many viral vectors are made readily available for purchase by investigators through companies such as Addgene:

https://www.addgene.org/.

Once a Cre-expressing mouse line and a Cre-dependent virus are procured, a stereotaxic surgery setup is essential for precise targeting of the virus into the mouse brain. Several options for a

stereotaxic frame are available, many of which come with a digital readout of X-, Y-, and Z-plane coordinates. These allow for meticulous control of dorsal-ventral, medial-lateral, and rostral-caudal delivery of the viral payload using the attached stereotaxic arm. Various strategies to inject the virus into the mouse brain exist ranging from syringe pumps to micro-injectors to compressed air systems. This protocol uses the latter, so the required components consist of a micromanipulator or stimulator, a tank of compressed air, tubing and accompanying valves, glass micropipettes for the physical delivery of the viral payload into the brain of the animal, as well as a large syringe used to load the glass micropipette with virus. In addition, a drill is commonly employed to puncture the skull surface so that the glass micropipette containing the viral payload can be successfully lowered into the targeted, anatomical brain site. This drill can be attached directly to the stereotaxic arm to facilitate precision, or alternatively can be manually held and controlled by the experimenter. An electric trimmer is used to shave the fur from the dorsal surface of the mouse head to clearly visualize and properly clean the site of incision with iodine and alcohol. Pre-cleaned and autoclaved surgical tools such as tweezers may be useful during the procedure to fit the mouse in the apparatus and/or peel back the skin during the incision, which requires a sterilized scalpel. Also, proper anesthetic and analgesic agents are vital for anesthetizing the animal before surgery (isoflurane or xylanine: 5 mg/kg and ketamine: 75 mg/kg diluted in saline 350 mg/kg) and pain management post-surgery (such as Metacam), respectively. A heated pad is generally used post-surgery to allow for quicker recovery. Finally, appropriate items for reclosing the incision made along the dorsal skin surface of the animal head are required; either sutures or specialized tissue adhesive glue can be used.

Food intake can either be assessed using home cages provided by the animal facility or specialized cages specifically designed to more accurately measure the amount of food ingested by the animal. For simplification, this protocol will describe quantitative analysis of food consumption utilizing facility-issued home cages as these are normally provided for the researcher at no additional cost. These cages should comprise a food hopper where pre-weighed food pellets can be stored for easy access by both the animals during eating and the experimenter during food measurements. However, it should be noted that automated systems dedicated to calculating food intake levels are available, most of which rely on infrared beam break mechanisms to trigger the delivery of pre-weighed, caloric food pellets (Coulbourn Instruments; http://www.coulbourn.com/category_s/288.htm).

Clozapine-N-oxide (CNO), the activating ligand of DREADD receptors, can be obtained via the NIH RAID program (http://grants.nih.gov/grants/guide/notice-files/NOT-RM-10-012.html) or purchased from chemical companies such as Sigma-Aldrich:

http://www.sigmaaldrich.com/catalog/product/sigma/c0832?lang=en&region=US.

DMSO and 0.9 % saline are required for making the final CNO solution to be injected. Additionally, a vortex mixer is helpful in ensuring that the CNO goes into solution. Insulin injection syringe needles are used to load and i.p. deliver the CNO solution to the animals.

Finally, a calibrated balance scale (preferably one that reads to the hundredth place) is used to measure the weight of the food used in the experiment.

2.1 Equipment, Materials List

1. Cre-expressing mouse line.
2. Cre-dependent viral vector, packaged into AAV.
   Stereotaxic Surgery
3. Stereotaxic frame (KOPF Model 963) with drill.
4. Micromanipulator (Grass Technologies, Model S48 Stimulator).
5. Compressed air (95 % CO_2/5 % O_2).
6. Tygon material tubing and large syringe for loading pipette.
7. Pulled-glass pipette with 20–40 mm tip diameter (pulled by Narishige pipette puller) and scale bar.
8. Surgical tools such as fine tweezers.
9. Electric shaver.
10. Iodine.
11. Alcohol.
12. Scalpel.
13. Cotton swabs.
14. Ketamine and xylazine.
15. Metacam meloxicam.
16. T-pump circulating water animal-warming system.
17. Sutures (either absorbable or non-absorbable depending on the animal protocol) or Vetbond tissue adhesive.
18. "The Mouse Brain in Stereotaxic Coordinates" by George Paxinos.

2.2 DREADD-Mediated Food Intake Assessment

19. Animal facility-issued home cage outfitted with a food hopper.
20. CNO (Sigma-Aldrich, catalog #CO832).
21. DMSO.
22. 0.9 % Saline.
23. Vortex mixer.

24. Insulin-injection syringe needles.

25. Calibrated balance scale.

26. Mouse chow pellets (typically ~4 g in weight).

2.3 Verification of Injection Site, Number of Neurons Transduced, and CNO-Induced Neural Activity

27. PFA for perfusion and accompanying tools to extract brain tissue.

28. 20 % Sucrose solution.

29. Microtome.

30. Paintbrushes.

31. PBS.

32. 6- or 12-well plates.

33. Microscope slides.

34. Epi-fluorescent microscope.

35. Antibody raised against Fos.

3 Procedures

3.1 Stereotaxic Surgery

3.1.1 Virus Preparation

Cre-dependent viral vectors are stored at −80° (in this case AAV8-hsyn-DIO-hM3Dq-mCherry). During the day of surgery a small aliquot of the virus (typically 5 μL) in a centrifuge tube is thawed and stored on ice. This is transported to the surgery suite along with the animals scheduled for the procedure. A pre-pulled glass micropipette is firmly attached to the block of a stereotaxic arm and the large syringe is connected to the top of the micropipette via tubing. Next, the micropipette is carefully lowered into the aliquoted tube containing the liquid virus and the latter is pulled up into the micropipette using the large syringe. Once a sufficient amount is taken up, the micropipette is slowly raised out of the aliquoted tube and a scale bar is taped to the pipette. Thus, when the virus is being administered into the brain of the animal, the amount of virus can be measured based on the dip in the meniscus of the liquid virus in the glass micropipette. Finally, the tubing connecting the large syringe is replaced by the tubing connected to the micromanipulator (stimulator) controlling the delivery of the compressed air.

3.1.2 Animal Preparation

Surgery is usually performed in adult mice aged 6–8 weeks (in this case *Agrp-Ires-cre* knock-in mice and wild-type littermate controls). Animals are anesthetized with xylazine (5 mg/kg) and ketamine (75 mg/kg) diluted in saline (350 mg/kg), shaved with an electric hair trimmer, and placed into a stereotaxic apparatus (KOPF Model 963) after their failure to respond to a toe-pinch (this typically takes between 5 and 10 min). Mice are firmly inserted into the ear bars and mouthpiece of the stereotaxic frame so that

the head is stable. This is essential given that the accuracy of the viral delivery depends on stereotaxic coordinates, which can be altered and detrimental to the experiment if the mouse is improperly secured. Once stabilized in the frame, the dorsal surface of the head is cleaned with iodine and alcohol and a small vertical incision is made along the dorsal axis of the skin with a scalpel. Cotton swabs can be used to peel back the skin and expose the dorsal surface of the skull. Repeatedly rubbing the skull with the cotton swabs will help reveal the lambda and bregma landmarks on the skull surface. These will be used to both level the brain and determine your coordinates for injection of virus.

3.1.3 Verification of Stereotaxic Coordinates

Once the lambda and bregma positions are clearly exposed, the brain is leveled on the vertical plane (rostral-caudal axis). To achieve this, the glass micropipette is first cautiously lowered to the lambda skull surface, where the Z-axis is zeroed, and then moved and lowered to the bregma skull surface. When the glass micropipette is just touching bregma, the reading on the Z-axis should be within 0.10 mm of when it was just touching lambda. This will ensure that the brain is level on the rostral-caudal axis. Next, to level the brain on the horizontal plane (medial-lateral axis), the tip of the glass micropipette is moved approximately 1 mm from the midline and slowly lowered so that it just touches the skull surface on one side of the brain. The Z-axis is then zeroed again. Next, the glass micropipette is moved approximately 1 mm from the midline and slowly lowered so that it just touches the skull surface on the opposite side of the brain. Again, the reading on the Z-axis should be within 0.10 mm to certify that the brain is level on the medial-lateral axis.

Once the brain is properly leveled, the glass micropipette can be raised and the stereotaxic arm containing the glass micropipette detached and replaced with the secured drill arm. The drill is slowly lowered so that the drill bit is just touching the bregma skull surface. From here, the X- and Y-axes are zeroed. Next, the drill is slightly raised and positioned over the anatomical brain region intended for injection. This can be determined using a stereotaxic mouse brain atlas such as "The Mouse Brain in Stereotaxic Coordinates" by George Paxinos. In this example, the targeted site is the arcuate nucleus (ARC), which is located –1.40 mm anterior-posterior from bregma (Y-axis) and ±0.30 mm medial-lateral from bregma (X-axis). Once the drill is positioned using these coordinates, it is slowly lowered to puncture a clean hole in the skull surface at this specified spot. The drill should just be lowered to penetrate the skull and it should be avoided lowering it into the brain itself. Nonetheless, based on the position of the drill hole on the skull surface, bleeding may occur which can be cleaned with 0.9 % saline and cotton swabs. Once the hole has been made the drill arm can be detached and replaced back with the stereotaxic arm containing the glass micropipette filled with virus.

3.1.4 Delivery of the Viral Payload	The glass micropipette is again carefully lowered to the bregma skull surface. From here, the *X*-, *Y*-, and *Z*-axes are zeroed. The stereotaxic arm is then slightly raised and moved to the designated coordinates (in this example over the ARC; coordinates from bregma: anterior-posterior, –1.40 mm; lateral, ±0.30 mm). The glass micropipette is then lowered down into the brain through the drill hole to the designated coordinates (in this example over the ARC; coordinates from bregma: dorsal-ventral, –5.80 mm). Once correctly positioned, the air tank is opened and the micromanipulator (Grass Technologies, Model S48 Stimulator) is switched on to slowly force the viral contents of the glass micropipette into the designated brain region. The micromanipulator is used to control injection speed at 25 nL/min. The volume of virus injected depends on a number of parameters including (1) the size of the intended target, (2) the expression of the genetically engineered Cre-expressing mouse, and (3) the serotype and diffusion properties of the virus. In this example, although the ARC is a small structure and the AAV8 serotype has enhanced diffusion properties, a large volume (200–400 nL) is injected per hemisphere due to the restricted expression of Cre-recombinase in ARCA^{gRP} cells conferred by the *Agrp-Ires-cre* knock-in mouse line. The pipette is withdrawn 5 min after the termination of viral injection. Next the glass micropipette is lowered to the contralateral side to bilaterally transduce ARCA^{gRP} neurons on both sides of the brain. Again, the pipette is withdrawn 5 min after the termination of viral injection to avoid spillage of the virus as it is retracted from the brain. Lastly, wild-type littermate controls should undergo the identical surgical procedure.
3.1.5 Mouse Recovery	Immediately following the removal of the glass micropipette, sutures or Vetbond tissue adhesive can be used to sew up or glue shut, respectively, the incision made to the dorsal skin surface of the head. At this point, analgesic can be administered to the animal (Metacam meloxicam or alternative, approved pain medication according to the animal protocol). Finally, mice are allowed to recover using a T-pump circulating water animal-warming system, until consciousness is regained and the animals are transferred to sterile animal facility-appointed mouse cages.
3.2 DREADD-Mediated Food Intake Assessment *3.2.1 Acclimation Period*	Typically, AAVs are allowed 3 weeks to aptly recombine and transduce the Cre-expressing neurons. During this time the researcher should begin an acclimation period, whereby group-housed, surgerized *Agrp-Ires-cre* knock-in and wild-type littermate animals are separated into individual cages to adapt to solitary environmental conditions, which act as a natural stress on social rodents such as mice. The conditions during the acclimation period should mimic those of the experiment. Therefore, mice should be handled

("scruffed") by the investigator and poked intraperitoneally (i.p.) with an insulin-injection needle syringe to reduce stress levels. Additionally, cages should be changed for new, clean ones and food measured to familiarize the animals to novel home cages and researcher intervention during food intake quantification. This adjustment period acts to minimize anxiety and stress that results in lower experimental noise and variability.

3.2.2 Food Intake Measurements

Three weeks after intracranial surgery and a 10–14-day acclimation period, food intake studies are initiated. Typically, multiple mice are run simultaneously and injected with either CNO or saline as a control. CNO is administered at 0.3–1.0 mg/kg of body weight (see below on how to make CNO). Saline is delivered at the same volume to maintain consistency in the studies. Crossover studies are suggested to diminish inconsistencies beyond the investigator control, such as external noises or unanticipated fluctuations in temperature or humidity. Cages are switched immediately following the injection and pre-measured food pellets, via a calibrated balance scale, are presented to the animals ad libitum, typically using a food hopper or bowl where animals have easy access to the food. This cage change is important when food intake is being assessed as older food can crumble and mix into the old bedding making accurate measurements difficult to ascertain. This same pre-weighed food is then quantified at desired time points post-i.p. injection and presented back to the animal until the next reading. In this example, food intake is measured at 30 min and 1, 2, and 4 h after saline or CNO injection. The opposite treatment is then administered the following day. Thus, if an *Agrp-Ires-cre* mouse received a saline injection on "day 1," it would get a CNO injection on "day 2." These studies are often replicated multiple times over the course of a couple of weeks to ensure consistency and reproducibility.

Food intake can be assessed either near the beginning of the light cycle when feeding baselines are low or at the onset of the dark cycle when feeding baselines are high. It is the decision of the investigator to determine the quintessential time where potential DREADD-mediated alterations in food intake would be apparent. For example, if one predicts that an acute activation or inhibition of the neural circuit in question would lead to an orexigenic response resulting in hyperphagic behavior, it may be beneficial to evaluate feeding behavior during the light cycle when mice normally refrain from high levels of food consumption. If however one predicts that an acute activation or inhibition of the neural circuit in question would lead to an anorexigenic response resulting in hypophagic behavior, it may be beneficial to evaluate feeding behavior during the dark cycle when mice normally engage in high levels of food consumption.

In this instance, since we predict that acute stimulation of ARCA^{gRP} neurons would intensify hunger drive, food intake would be analyzed during the light cycle when consumption is low and differences in DREADD-mediated ARCA^{gRP} neural activation are more easily detectable. Specifically, food intake (2–3 pre-weighed ~4 g chow pellets) for *Agrp-Ires-cre* and wild-type controls injected with AAV8-hsyn-DIO-hM3Dq-mCherry is measured near the beginning of the light cycle at 9:00 a.m. and food intake was monitored 30 min and 1, 2, and 4 h after i.p. injection between 9:00 a.m. and 1:00 p.m. It is imperative that the data from each mouse is collected separately, as it is possible that some animals will not have correct targeting of the virus.

3.2.3 Making CNO Solution (Directions to Create 0.1 mg/mL CNO Solution in 0.9 % Saline for Injection into Animals)

The CNO used in this example is from the NIH RAID program (other batches have also been used with this method). (a) Approximately 0.5 mg is weighed into a 15 mL conical. (b) An appropriate amount of DMSO is added that will make a final DMSO concentration of 0.5 % (for 0.1 mg/mL, divide the mg of CNO in half, and that number = μL of DMSO to add to conical). The DMSO is flick-mixed or gently vortexed (1–2-s bursts to prevent matter from traveling up tube-goal is to keep matter in the bottom of the conical) to ensure that all dry CNO is in suspension in the DMSO. (c) With time and more gently vortexing, the solution turns translucent indicating that the CNO has gone into solution.

3.3 Verification of Injection Site, Number of Neurons Transduced, and CNO-Induced Neural Activity

Before euthanizing the experimental animals, CNO should be administered ~90–120 min prior. This will allow for the opportunity to perform an immunohistochemical analysis of Fos activity (a marker of neural activity). Note that, for this approach, the experimenter should expect an induction of Fos protein in the desired cell type using the stimulatory hM3Dq DREADD and a reduction of Fos protein in the desired cell type using the inhibitory hM4Di DREADD. In this example, one would expect to detect an induction of Fos protein specifically in ARCA^{gRP} neurons since these cells alone express the stimulatory hM3Dq DREADD receptor. Furthermore, due to the fused fluorophore in the DREADD viruses, one can detect native fluorescence after brain sectioning. In this case, one would expect to observe a high-intensity mCherry fluorophore specifically in ARCA^{gRP} neurons. It is very important to confirm the proper anatomical targeting of the virus to your cells of interest. The fluorophore also allows one to count the number of neurons transduced.

3.3.1 Euthanizing Animals and Brain Extraction

Approximately 90–120 min after a final CNO injection, experimental animals can be anesthetized with xylazine (5 mg/kg) and ketamine (75 mg/kg) diluted in saline (350 mg/kg) and perfused with PFA. After the blood has been replaced with PFA and the animals become stiff, sterile tools can be used to carefully extract

the brain tissue. Each brain can be placed in a labeled canonical 15 mL tube filled with PFA to continue fixing the tissue. After 1–2 days, the brain can be transferred to a newly labeled canonical 15 mL tube filled with a 20 % sucrose solution to minimize any ice crystals that may form during brain slicing.

3.3.2 Brain Sectioning, Mounting, and Fluorophore Detection

After the brains in the 20 % sucrose solution sink to the bottom of the tube (typically within 24–48 h), the brains are then mounted on a freeze-stage microtome, sectioned in multiple series at a specified thickness (typically 30–60 μm), collected with a paintbrush, and stored in well plates filled with PBS. Next, brain sections floating in PBS are mounted onto microscope slides using a paintbrush. The sections and slide are allowed to dry and then are coverslipped. Finally, an epi-fluorescent microscope is used to visualize the fluorophore confirming the specificity of the viral transduction and number of neurons infected. Finally, immunohistochemistry can be used to evaluate Fos protein as a readout for increases or decreases in neural activity.

3.4 Analysis of Food Intake Data

The food intake data from all days following saline/CNO injections are then averaged and combined for analysis based on genotype. This takes into account any "missed" or "incomplete" hits as verified by histology above.

4   Experimental Variables and Troubleshooting

As with any experimental procedures, evaluating DREADD-mediated changes in food consumption can be variable. This section highlights and addresses some common causes for the observed inconsistencies. As this viral approach is dependent on Cre expression to successfully recombine and express the DREADD receptor, it is vital that the genotypes of the mice are confirmed before surgery. Moreover, for one reason or another, different batches of virus may ectopically express or display "leakiness," reducing the accuracy of your results. It is recommended that on procurement of a new virus test it in a Cre-expressing mouse line that can then be verified with an antibody against those particular neurons to ensure the specificity of the virus.

A very common explanation for variability among experiments is the efficiency and accuracy of the viral payload delivery. As mentioned above, although these viruses are engineered to only infect neurons expressing Cre-recombinase, it is extremely common to have a genetically modified mouse line that expresses Cre in multiple, proximal brain sites. Thus, to discretely transduce your neurons of interest without accidental infection of adjacent Cre-expressing population requires repeated practice and optimization of the stereotaxic coordinates. Injecting smaller volumes of virus or using

serotypes known for reduced diffusion rates can additionally control for this transduction of off-target neural populations. Furthermore, different levels of DREADDs will be expressed in distinct mice and thus these stoichiometric disparities may lead to variable results.

Unfortunately, the pattern of the DREADD-expressing neurons is not revealed until the conclusion of the experiment after the animal is euthanized and the brain tissue is analyzed. This is why it is so important to record feeding numbers on individual animals before grouping them together as it is not uncommon to discover mice with little, no or off-target expression of the DREADD receptor. These are typically excluded from the final statistical analyses depending on the experimental standards selected at the start of the studies.

Another cause for variability is the exclusion of an acclimation period whereby the animals become adjusted to being individually housed, handled by the investigator, cage switches, and food intake measurements. As all of these situations are stressful to the animals, an adaptation phase is necessary to accustom the animals to conditions that will be replicated during the actual experiment. Failure to familiarize animals with these circumstances can certainly lead to erraticism in the studies and should be consistent across all animals.

Another common mistake, especially when large cohorts are being gauged for food consumption, is simply mixing up the cage order, the amount of food measured, or the experimental treatment administered (CNO versus saline). To avoid these errors, it is recommended to create an Excel worksheet or handwritten account of the animal numbers or designation, food weight by exact measurement time, and type of treatment by date. Additionally, although fixed variables are thought to remain consistent throughout the experiments, it is often possible that these will differ. These factors could range from audible noise emanating throughout the animal facility to slight oscillations in room temperature or humidity. Thus, it is recommended that crossover studies are carried out where one group is administered saline and the other group is administered CNO on "day 1" and then this is switched on "day 2." Therefore, all of the animals are not receiving the identical treatment on the same day, which controls for external inconsistencies that are more difficult to identify and have direct influence over.

Additional variability can develop during food measurement. Depending on the method of assessing food consumption, the precision can vary. For example, by quantifying the amount of chow pellets in the food hopper, the experimenter cannot account for the crumbs inevitably created as the mouse breaks off chunks to consume. Although this seems like a large concern, the amount lost is minimal and is consistent from animal to animal. However, an alternative method is using a food dish or bowl where the food is stored. During these measurements, it is possible to include the

crumbs in the quantification as they typically remain in the food dish. However, it is not uncommon for an animal to take the food pellet out of the food dish making the accuracy of this technique less reliable. Finally, as mentioned above, specialized feeding systems are available although many of them are expensive and not optimized to fit in the animal's home cage.

A major concern when investigating neural subpopulations that may impinge on feeding behavior is the loss-of-function phenotype, that is, a reduction in food intake. If an animal fails to eat, one must consider alternative explanations for this observation. For example, did the acute manipulation of the neurons in question lead to a motor deficit, anxiety, hyperarousal, sickness, pain, or fear, all of which can lead to a decline in food intake. Therefore, it is valuable to have bidirectional control over your neurons of interest to physiologically confirm that acute activation leads to increases in food consumption and acute inhibition results in decreases of feeding behavior. Gain-of-function phenotype, that is, induction of food intake, is more apparent as this drives a discrete, motivational behavior, that of selectively seeking out and consuming food.

Lastly, proper organization is key during euthanization, brain sectioning, mounting, and verification of DREADD expression as the information gained at the conclusion of the experiment for each individual mouse needs to be matched to the behavioral output of that mouse. Any potential mix-up can be detrimental to the overall interpretation of the results. Once again, it is suggested that each animal is treated as a separate entity throughout the duration of the experiment and mice and the tubes, well plates, and microscope slides containing the brain tissue are clearly marked and systematically labeled to avoid error and correctly match the respective individual mouse with both its DREADD expression pattern and food intake data.

5   Typical/Anticipated Results

If the investigator has successfully identified a neural circuit that mediates feeding changes, the anticipated results should be statistically significant from controls (both within the same animal, CNO versus saline and against wild-type controls, CNO versus saline). If the newly identified neurons are orexigenic in nature, as are the ARCA^{gRP} cells in this example, then acute activation should propel feeding behavior in calorically replete mice and acute inhibition should halt food intake in calorically deficient mice. Conversely, if the subgroup of neurons is anorexigenic in nature, acute activation should direct lower levels of feeding in energy deficient mice and acute inhibition should evoke feeding episodes in mice with an energy surfeit.

In the example illustrated here, we stereotaxically targeted stimulatory DREADDs (AAV-hsyn-DIO-hM3Dq-mCherry) bilaterally to the arcuate nucleus of *Agrp-Ires-Cre* and wild-type mice, whereby the DREADDs are selectively expressed in ARCA[gRP] neurons in the former but are lacking in the latter due to the presence and absence of Cre-recombinase, respectively. After an acclimation phase lasting approximately 2 weeks to familiarize the mice to solitary living conditions, experimenter handling, intraperitoneal injections, cage changes, and steady food measurements, the study was initiated. To assess the effects of ARCA[gRP] activation on acute feeding behavior near the beginning of the light cycle when animals were in a calorically replete condition, post-DREADD surgery *Agrp-Ires-Cre* and wild-type mice were injected i.p. with saline or CNO, the latter of which crossed the blood–brain barrier, bound to, and activated the hM3Dq DREADD receptors expressed on ARCA[gRP] neurons. This acute ARCA[gRP] stimulation rapidly drove food intake over the 4-h time window of the light cycle, as preweighed food pellets were measured 30 min and 1, 2, and 4 h after i.p. injection. This upsurge in eating activity was significantly higher than baseline feeding during this time in the same animals following a saline injection. Additionally, this increase in food consumption was significantly greater than wild-type mice injected with CNO. The experiments were repeated to ensure consistency and reproducibility.

Following completion of the feeding studies, the animals were all injected with CNO and euthanized 90–120 min later, which permitted Fos analysis to verify CNO-mediated increases of neural activity in ARCA[gRP] neurons expressing hM3Dq DREADD receptors. We also confirmed that ARCA[gRP] neurons were transduced with hM3Dq DREADD receptors by quantifying mCherry fluorescence signal. Lastly, the food intake data from all days following saline/CNO injections were then averaged and combined for analysis based on genotype. This finalized data took into account any "missed" or "incomplete" hits as verified by histology.

6   Conclusion and Future Directions

Contemporary efforts to elucidate the functioning of the brain focus heavily on neural circuits, the level at which the brain really operates. Neural circuits are comprised of distinct populations or ensembles of interconnected neurons that work in concert to perform specific sensory, motor, or cognitive functions. A central goal in understanding the neural circuit basis of brain function is to identify and manipulate subpopulations of cells and link these "circuit signatures" or "neural codes" to behavioral output. Feeding is required in all living species but the neural mechanisms underlying the homeostatic and hedonic underpinnings of eating behavior

remain to be fully realized. Through the use of techniques, such as chemogenetics and optogenetics, novel circuit nodes heavily connected to appetite control are being uncovered at an unprecedented rate. Through the use of newly engineered mice and molecular tools used to both manipulate and monitor neural activity in freely moving mice, the ambitious goal of mapping and deconstructing the complex neural networks fundamental to feeding becomes one of reality.

References

1. Rolls ET (2000) Precis of the brain and emotion. Behav Brain Sci 23:177–191, discussion 192–233

2. Galler JR et al (2010) Early childhood malnutrition predicts depressive symptoms at ages 11-17. J Child Psychol Psychiatry 51:789–798. doi:10.1111/j.1469-7610.2010.02208.x

3. Luppino FS et al (2010) Overweight, obesity, and depression: a systematic review and meta-analysis of longitudinal studies. Arch Gen Psychiatry 67:220–229. doi:10.1001/archgenpsychiatry.2010.2

4. Pouwer F et al (2010) Prevalence of comorbid depression is high in out-patients with Type 1 or Type 2 diabetes mellitus. Results from three out-patient clinics in the Netherlands. Diabet Med 27:217–224. doi:10.1111/j.1464-5491.2009.02903.x

5. Strine TW et al (2008) The association of depression and anxiety with obesity and unhealthy behaviors among community-dwelling US adults. Gen Hosp Psychiatry 30:127–137. doi:10.1016/j.genhosppsych.2007.12.008

6. Elias MF, Elias PK, Sullivan LM, Wolf PA, D'Agostino RB (2005) Obesity, diabetes and cognitive deficit: The Framingham Heart Study. Neurobiol Aging 26(Suppl 1):11–16. doi:10.1016/j.neurobiolaging.2005.08.019

7. van den Berg E, Kloppenborg RP, Kessels RP, Kappelle LJ, Biessels GJ (2009) Type 2 diabetes mellitus, hypertension, dyslipidemia and obesity: a systematic comparison of their impact on cognition. Biochim Biophys Acta 1792: 470–481. doi:10.1016/j.bbadis.2008.09.004

8. Waber DP et al (2011) Cognitive impairment as a mediator in the developmental pathway from infant malnutrition to adolescent depressive symptoms in Barbadian youth. J Dev Behav Pediatr 32:225–232. doi:10.1097/DBP.0b013e31820b7707

9. Anand BK, Dua S, Shoenberg K (1955) Hypothalamic control of food intake in cats and monkeys. J Physiol 127:143–152

10. Aravich PF, Sclafani A (1983) Paraventricular hypothalamic lesions and medial hypothalamic knife cuts produce similar hyperphagia syndromes. Behav Neurosci 97:970–983

11. Bergen HT, Mizuno TM, Taylor J, Mobbs CV (1998) Hyperphagia and weight gain after gold-thioglucose: relation to hypothalamic neuropeptide Y and proopiomelanocortin. Endocrinology 139:4483–4488. doi:10.1210/endo.139.11.6324

12. Gold RM, Jones AP, Sawchenko PE (1977) Paraventricular area: critical focus of a longitudinal neurocircuitry mediating food intake. Physiol Behav 18:1111–1119

13. Gold RM, Quackenbush PM, Kapatos G (1972) Obesity following combination of rostrolateral to VMH cut and contralateral mammillary area lesion. J Comp Physiol Psychol 79:210–218

14. Holzwarth-McBride MA, Hurst EM, Knigge KM (1976) Monosodium glutamate induced lesions of the arcuate nucleus. I. Endocrine deficiency and ultrastructure of the median eminence. Anat Rec 186:185–205. doi:10.1002/ar.1091860205

15. Holzwarth-McBride MA, Sladek JR Jr, Knigge KM (1976) Monosodium glutamate induced lesions of the arcurate nucleus. II. Fluorescence histochemistry of catecholamines. Anat Rec 186:197–205. doi:10.1002/ar.1091860206

16. Leibowitz SF, Hammer NJ, Chang K (1981) Hypothalamic paraventricular nucleus lesions produce overeating and obesity in the rat. Physiol Behav 27:1031–1040

17. Teitelbaum P, Epstein AN (1962) The lateral hypothalamic syndrome: recovery of feeding and drinking after lateral hypothalamic lesions. Psychol Rev 69:74–90

18. Boghossian S, Park M, York DA (2010) Melanocortin activity in the amygdala controls appetite for dietary fat. Am J Physiol Regul Integr Comp Physiol 298:R385–R393. doi:10.1152/ajpregu.00591.2009

19. Booth DA (1968) Mechanism of action of norepinephrine in eliciting an eating response on injection into the rat hypothalamus. J Pharmacol Exp Ther 160:336–348

20. de Backer MW et al (2011) Melanocortin receptor-mediated effects on obesity are distributed over specific hypothalamic regions. Int J Obes 35:629–641. doi:10.1038/ijo.2010.169

21. Grill HJ, Ginsberg AB, Seeley RJ, Kaplan JM (1998) Brainstem application of melanocortin receptor ligands produces long-lasting effects on feeding and body weight. J Neurosci 18:10128–10135

22. Grossman SP (1960) Eating or drinking elicited by direct adrenergic or cholinergic stimulation of hypothalamus. Science 132:301–302

23. Leibowitz SF (1970) Reciprocal hunger-regulating circuits involving alpha- and beta-adrenergic receptors located, respectively, in the ventromedial and lateral hypothalamus. Proc Natl Acad Sci U S A 67:1063–1070

24. Williams DL, Kaplan JM, Grill HJ (2000) The role of the dorsal vagal complex and the vagus nerve in feeding effects of melanocortin-3/4 receptor stimulation. Endocrinology 141:1332–1337. doi:10.1210/endo.141.4.7410

25. Hoebel BG, Teitelbaum P (1962) Hypothalamic control of feeding and self-stimulation. Science 135:375–377

26. Tenen SS, Miller NE (1964) Strength of electrical stimulation of lateral hypothalamus, food deprivation, and tolerance for quinine in food. J Comp Physiol Psychol 58:55–62

27. Sternson SM (2013) Hypothalamic survival circuits: blueprints for purposive behaviors. Neuron 77:810–824. doi:10.1016/j.neuron.2013.02.018

28. Luo L, Callaway EM, Svoboda K (2008) Genetic dissection of neural circuits. Neuron 57:634–660. doi:10.1016/j.neuron.2008.01.002

29. Atasoy D, Aponte Y, Su HH, Sternson SM (2008) A FLEX switch targets Channelrhodopsin-2 to multiple cell types for imaging and long-range circuit mapping. J Neurosci 28:7025–7030. doi:10.1523/JNEUROSCI.1954-08.2008

30. Schnutgen F et al (2003) A directional strategy for monitoring Cre-mediated recombination at the cellular level in the mouse. Nat Biotechnol 21:562–565. doi:10.1038/nbt811

31. Witten IB et al (2010) Cholinergic interneurons control local circuit activity and cocaine conditioning. Science 330:1677–1681. doi:10.1126/science.1193771

32. Tye KM, Deisseroth K (2012) Optogenetic investigation of neural circuits underlying brain disease in animal models. Nat Rev Neurosci 13:251–266. doi:10.1038/nrn3171

33. Yizhar O, Fenno LE, Davidson TJ, Mogri M, Deisseroth K (2011) Optogenetics in neural systems. Neuron 71:9–34. doi:10.1016/j.neuron.2011.06.004

34. Armbruster BN, Li X, Pausch MH, Herlitze S, Roth BL (2007) Evolving the lock to fit the key to create a family of G protein-coupled receptors potently activated by an inert ligand. Proc Natl Acad Sci U S A 104:5163–5168. doi:10.1073/pnas.0700293104

35. Atasoy D, Betley JN, Su HH, Sternson SM (2012) Deconstruction of a neural circuit for hunger. Nature 488:172–177. doi:10.1038/nature11270

36. Magnus CJ et al (2011) Chemical and genetic engineering of selective ion channel-ligand interactions. Science 333:1292–1296. doi:10.1126/science.1206606

37. Stachniak TJ, Ghosh A, Sternson SM (2014) Chemogenetic synaptic silencing of neural circuits localizes a hypothalamus→midbrain pathway for feeding behavior. Neuron 82:797–808. doi:10.1016/j.neuron.2014.04.008

38. Redfern CH et al (1999) Conditional expression and signaling of a specifically designed Gi-coupled receptor in transgenic mice. Nat Biotechnol 17:165–169. doi:10.1038/6165

39. Zhao GQ et al (2003) The receptors for mammalian sweet and umami taste. Cell 115:255–266

40. Lechner HA, Lein ES, Callaway EM (2002) A genetic method for selective and quickly reversible silencing of Mammalian neurons. J Neurosci 22:5287–5290

41. Tan EM et al (2006) Selective and quickly reversible inactivation of mammalian neurons in vivo using the Drosophila allatostatin receptor. Neuron 51:157–170. doi:10.1016/j.neuron.2006.06.018

42. Hsiao EC et al (2008) Osteoblast expression of an engineered Gs-coupled receptor dramatically increases bone mass. Proc Natl Acad Sci U S A 105:1209–1214. doi:10.1073/pnas.0707457105

43. Peng J et al (2008) Conditional expression of a Gi-coupled receptor in osteoblasts results in trabecular osteopenia. Endocrinology 149:1329–1337. doi:10.1210/en.2007-0235

44. Redfern CH et al (2000) Conditional expression of a Gi-coupled receptor causes ventricular conduction delay and a lethal cardiomyopathy. Proc Natl Acad Sci U S A 97:4826–4831

45. Sweger EJ, Casper KB, Scearce-Levie K, Conklin BR, McCarthy KD (2007) Development of hydrocephalus in mice expressing the G(i)-coupled GPCR Ro1 RASSL receptor in astrocytes. J Neurosci 27:2309–2317. doi:10.1523/JNEUROSCI.4565-06.2007

46. Alexander GM et al (2009) Remote control of neuronal activity in transgenic mice expressing evolved G protein-coupled receptors. Neuron 63:27–39. doi:10.1016/j.neuron.2009.06.014

47. Conklin BR et al (2008) Engineering GPCR signaling pathways with RASSLs. Nat Methods 5:673–678. doi:10.1038/nmeth.1232

48. Farrell MS et al (2013) A Galphas DREADD mouse for selective modulation of cAMP production in striatopallidal neurons. Neuropsychopharmacology 38:854–862. doi:10.1038/npp.2012.251

49. Ferguson SM, Phillips PE, Roth BL, Wess J, Neumaier JF (2013) Direct-pathway striatal neurons regulate the retention of decision-making strategies. J Neurosci 33:11668–11676. doi:10.1523/JNEUROSCI.4783-12.2013

50. Takahashi KA, Cone RD (2005) Fasting induces a large, leptin-dependent increase in the intrinsic action potential frequency of orexigenic arcuate nucleus neuropeptide Y/Agouti-related protein neurons. Endocrinology 146:1043–1047. doi:10.1210/en.2004-1397

51. Krashes MJ, Shah BP, Koda S, Lowell BB (2013) Rapid versus delayed stimulation of feeding by the endogenously released AgRP neuron mediators GABA, NPY, and AgRP. Cell Metab 18:588–595. doi:10.1016/j.cmet.2013.09.009

52. Yang Y, Atasoy D, Su HH, Sternson SM (2011) Hunger states switch a flip-flop memory circuit via a synaptic AMPK-dependent positive feedback loop. Cell 146:992–1003. doi:10.1016/j.cell.2011.07.039

53. Liu T et al (2012) Fasting activation of AgRP neurons requires NMDA receptors and involves spinogenesis and increased excitatory tone. Neuron 73:511–522. doi:10.1016/j.neuron.2011.11.027

54. Clark JT, Kalra PS, Crowley WR, Kalra SP (1984) Neuropeptide Y and human pancreatic polypeptide stimulate feeding behavior in rats. Endocrinology 115:427–429. doi:10.1210/endo-115-1-427

55. Rossi M et al (1998) A C-terminal fragment of Agouti-related protein increases feeding and antagonizes the effect of alpha-melanocyte stimulating hormone in vivo. Endocrinology 139:4428–4431. doi:10.1210/endo.139.10.6332

56. Semjonous NM et al (2009) Coordinated changes in energy intake and expenditure following hypothalamic administration of neuropeptides involved in energy balance. Int J Obes 33:775–785. doi:10.1038/ijo.2009.96

57. Stratford TR, Kelley AE (1997) GABA in the nucleus accumbens shell participates in the central regulation of feeding behavior. J Neurosci 17:4434–4440

58. Gropp E et al (2005) Agouti-related peptide-expressing neurons are mandatory for feeding. Nat Neurosci 8:1289–1291. doi:10.1038/nn1548

59. Luquet S, Perez FA, Hnasko TS, Palmiter RD (2005) NPY/AgRP neurons are essential for feeding in adult mice but can be ablated in neonates. Science 310:683–685. doi:10.1126/science.1115524

60. Aponte Y, Atasoy D, Sternson SM (2011) AGRP neurons are sufficient to orchestrate feeding behavior rapidly and without training. Nat Neurosci 14:351–355. doi:10.1038/nn.2739

61. Betley JN, Cao ZF, Ritola KD, Sternson SM (2013) Parallel, redundant circuit organization for homeostatic control of feeding behavior. Cell 155:1337–1350. doi:10.1016/j.cell.2013.11.002

62. Carter ME, Soden ME, Zweifel LS, Palmiter RD (2013) Genetic identification of a neural circuit that suppresses appetite. Nature 503:111–114. doi:10.1038/nature12596

63. Jennings JH, Rizzi G, Stamatakis AM, Ung RL, Stuber GD (2013) The inhibitory circuit architecture of the lateral hypothalamus orchestrates feeding. Science 341:1517–1521. doi:10.1126/science.1241812

64. Krashes MJ et al (2011) Rapid, reversible activation of AgRP neurons drives feeding behavior in mice. J Clin Invest 121:1424–1428. doi:10.1172/JCI46229

65. Krashes MJ, Kravitz AV (2014) Optogenetic and chemogenetic insights into the food addiction hypothesis. Front Behav Neurosci 8:57. doi:10.3389/fnbeh.2014.00057

66. Krashes MJ et al (2014) An excitatory paraventricular nucleus to AgRP neuron circuit that drives hunger. Nature 507:238–242. doi:10.1038/nature12956

67. Land BB et al (2014) Medial prefrontal D1 dopamine neurons control food intake. Nat Neurosci 17:248–253. doi:10.1038/nn.3625

68. Zhan C et al (2013) Acute and long-term suppression of feeding behavior by POMC neurons in the brainstem and hypothalamus, respectively. J Neurosci 33:3624–3632. doi:10.1523/JNEUROSCI.2742-12.2013

69. Shin AC, Zheng H, Berthoud HR (2009) An expanded view of energy homeostasis: neural integration of metabolic, cognitive, and emotional drives to eat. Physiol Behav 97:572–580. doi:10.1016/j.physbeh.2009.02.010

Chapter 5

Dissecting Neuronal Circuits Involved in Olfactory-Mediated Behaviors

Alexia Nunez-Parra, Krista Krahe, Wilson Chan, and Ricardo C. Araneda

Abstract

Feedback projections from upstream targets and neuromodulatory systems provide real time regulation of information processing. In the olfactory pathway, sensory neurons establish synapses with principal neurons of the olfactory bulb (OB), where the earliest stages of odor processing occur. Unlike other sensory systems, output neurons in the OB project to the olfactory cortex bypassing the thalamus. Therefore, neural circuits in the OB, and odor processing, are tightly regulated by several top-down mechanisms. A large source of modulatory signals to the OB arises from neurons of the basal forebrain, most importantly from clusters of cholinergic and GABAergic neurons. While cholinergic modulation of the OB circuit is thought to be critical in olfactory processing, including odor discrimination and perceptual learning, the role of the inhibitory GABAergic input from the basal forebrain is poorly understood. Here we describe an experimental approach that uses virus-mediated expression of Designer Receptor Exclusively Activated by Designer Drugs (DREADDs) in basal forebrain GABAergic neurons, and behavioral tests, to examine how this inhibitory modulation contributes to olfactory processing.

Key words Basal forebrain, GABA, Inhibition, Chemogenetics, Olfactory bulb, Odor discrimination, Learning

1 Overview

One of the greatest challenges in neuroscience is to understand the relationship between neuronal activity and behavior. This task is extremely difficult since the behavioral output of an individual is not always stereotypical, but rather, behavior is influenced by constantly varying environmental cues. Thus, to accurately respond to environmental changes, and to create an adequate representation of the external world, sensory information is highly modified at each relay stage in the sensory pathway. An important regulation of networks involved in sensory processing is achieved by feedback projections from upstream targets and by the action of neuromodulatory systems of the brain. Therefore, one approach used to

understand the relation between network activity and behavior is to modify the activity of these neural networks using several approaches that target feedback projections and neuromodulation.

2 Designer Receptor Exclusively Activated by Designer Drugs (DREADDs)

Recently, several laboratories have developed a large number of molecular tools to selectively regulate neuronal activity with a precise spatiotemporal control [1]. Nowadays, opto- and chemogenetics are the most widely used techniques to genetically manipulate neural circuits. In optogenetics, proteins derived from algae light-activated opsins, such as channelrhodopsin and halorhodopsin, are expressed in mammalian neurons. Stimulation with light of the appropriate wavelength activates these proteins and produce neuronal depolarization or hyperpolarization, respectively [2–4]. Optogenetics is currently widely used due to its high temporal resolution; it affords control of neuronal activity within a few ms [2]. Also, selective opsin expression in a subset of neurochemically identical neurons can be achieved using the Cre-lox system [5, 6]. It has been shown, however, that opsins rapidly desensitize to light stimuli, which can be a serious limitation in behavioral studies in which trials last from seconds to minutes and even hours. Similarly, rapid desensitization of the opsins limits their use in experiments that test the effect of pharmacological agents during prolonged and constant application. Another drawback in animal behavior studies is that light stimulation is achieved through optic fibers that are surgically attached via a cannula to the targeted brain region. These surgical procedures are often time consuming and they can damage other brain circuits. Lastly, the high-powered light source required to produce behavioral changes, usually consists of expensive lasers. As a result, an alternate emerging approach is the use of chemogenetics, in particular, the use of Designer Receptor Exclusively Activated by Designer Drugs (DREADDs) [1, 7–16]. One class of DREADDs consists of modified G-protein coupled muscarinic acetylcholine receptors that are specifically activated by clozapine-N-oxide (CNO), an exogenous ligand, which is inert at other endogenous targets [17]. Expression of specific genetically modified muscarinic receptors produces neuronal excitation (hM3Dq) or inhibition (hM4Di) [1, 7, 17]. DREADDs DNA can be delivered into a desired brain region using stereotactical viral injections, offering great spatial resolution. Moreover, Cre-dependent DREADD adeno-associated viruses (AAV) can be injected into transgenic mice lines to restrict the DREADD expression to a subset of neurons in the region of interest [1]. The virus injection procedure is fast, taking only 20–30 min per mouse. In addition, a variety of DREADD viral constructs, with reporter

proteins that at emit at different wavelengths (e.g., red or green fluorescent proteins, RFP or GFP, respectively) are readily available (and affordable) from several vector cores, making these techniques extremely easy to implement. Finally, reporter proteins of different colors facilitate confocal imaging analysis to estimate the number of neurons in a particular region that were activated by the CNO injection. All of these features make the DREADD technology an excellent candidate to selectively manipulate neuronal circuits while the animal is actively engaging in behavioral tasks.

3 Regulation of Neural Circuits That Process Olfactory Information

Most mammals strongly rely on the sense of smell to engage in behaviors that lead to survival and reproductive success. These behaviors, which include food location, predator identification, mating and aggression, among others, are initiated by the interaction of odor molecules with olfactory sensory neurons (OSN) located in the nasal epithelium [18]. OSNs project their axons to the surface of the olfactory bulb (OB), to an anatomical specialization known as the glomerulus, where the sensory axons synapse with apical dendrites of mitral and tufted cells (herein, MCs), which are the bulbar output neurons. Activity of MCs, and hence the neural output of the bulb, is regulated by inhibition from the largest population of local neurons in the OB, the granule cells (GCs) [19–21]. GCs are axonless GABAergic neurons that form dendrodendritic synapses (DDS) with the lateral dendrites of MCs. At these DDS an active MC releases glutamate onto GCs dendrites and the ensuing depolarization, in turn, releases GABA onto MCs [22–24]. Importantly, GCs synapse with the lateral dendrite of several other MCs and therefore the activation of a given MC can result in inhibition of other MCs, in a process called lateral inhibition [25, 26]. MCs form local excitatory synapses onto GC and therefore, GABA release from DDS can affect MCs via recurrent, lateral and feedback inhibition. Not surprisingly GC-mediated inhibition of MCs is also under precise control by feedback projections from upstream MC's targets and from neuromodulatory systems (see below), which regulate excitability of GCs. Neurons in the OB, particularly GCs, receive feedback projections from the piriform cortex (PCx) and accessory olfactory nucleus (AON) [27]. Recently, in vitro electrophysiological recordings using optogenetic techniques showed that feedback projections from the PCx excite GCs, inhibiting the activity of MCs [28]. On the other hand, glutamatergic feedback projections from the AON also terminate in bulbar interneurons that inhibit MCs, but these fibers in addition synapse onto MCs and depolarize them [29]. In vivo neuronal recordings in mice have suggested that feedback fibers

are necessary to amplify odor evoked inhibition, increase the precision of MC firing and to decrease background interference in MCs [28, 29].

Several neuromodulatory systems innervate different layers of the bulb, affecting neuronal excitability of both intrinsic and output neurons [27, 30]. Neurons in the basal forebrain, specifically in the horizontal limb of the diagonal band of Broca (HDB) send extensive cholinergic and GABAergic projections to the OB [31, 32]. Several lines of evidence indicate that modulation of OB circuits by these systems can affect odor discrimination, and at a cellular level, a predominant effect of cholinergic modulation is to increase GC excitability [30, 33–35]. Recent in vivo recordings of MCs in anesthetized animals have shown that acetylcholine released by optogenetic activation of HDB neurons sharpens MC's tuning curves [36], in agreement with studies showing that cholinergic modulation is required in the OB to facilitate olfactory discrimination of perceptually similar odors [30, 37–40]. Recently, it has also been suggested that local cholinergic release increases the excitability of MCs, regulating its sensitivity to odors during active sensing [41]. In stark contrast, the contribution of HDB GABAergic modulation in OB neurons is poorly understood. We successfully used Cre-dependent expression of DREADDs in GABAergic neurons in the HDB and showed that silencing these cells disrupted discrimination of closely related odors [11]. Below we describe how olfactory-mediated behaviors can be assessed using the DREADD technology, which is used to directly modify the activity of a specific group of neurons.

4   Equipment and Materials

Note: All the experiments are conducted following the guidelines of the Institutional Animal Care and Use Committee at the respective institution. Extra care must be taken to ensure the depth of anesthesia during the procedures (i.e., testing for pinching reflexes).

Mice of postnatal age 30 days (P30) or older, expressing Cre-recombinase under a promoter of interest are stereotactically injected with an adeno-associated virus (AAV) encoding a gene of interest flanked by loxP sites. Currently available AAV viruses use the Double-floxed Inverted Orientation (DIO) system (http://genetherapy.unc.edu/services.htm). Under these conditions, only neurons expressing the Cre- protein and infected with the virus will transcribe the DREADD of choice. For these procedures a stereotaxic apparatus and a virus delivery method, a microsyringe, is needed; this syringe can be controlled manually or automated with a micropump controller.

For our experiments we used an AAV virus encoding for DREADDs and a reporter gene, which we use to verify the injection site. Some DREADD virus express a hemagglutinin tag (HA tag) while others encode for a fluorescent protein such as mCherry. These proteins are detected through standard immunofluorescence techniques and confocal imaging, after the animal has been intracardially perfused with paraformaldehyde 4 % and the brain sliced using a vibratome. Antibodies, a shaker and other basic laboratory supplies (such as culture plates) are needed to perform the immunohistochemistry.

Once the injection volume and timing of optimal DREADD expression is determined, mice receive an i.p. injection of CNO or PBS (control) and are then exposed to the behavioral tasks (Fig. 1a). We assess olfactory function by testing the ability of animals to naturally discriminate odors using the habituation/dishabituation paradigm, and their ability to recognize odors using associative learning, with a food reward. In addition, odor detection threshold can be determined using a modified version of the habituation/dishabituation paradigm. We use a behavioral arena (i.e., a mouse cage) and record the behavior using a Camcorder for post ad hoc analysis. Pure odors are presented, at standardized concentrations, using wooden blocks and the food reward is a small piece of cookie hidden under the bedding (cookie test).
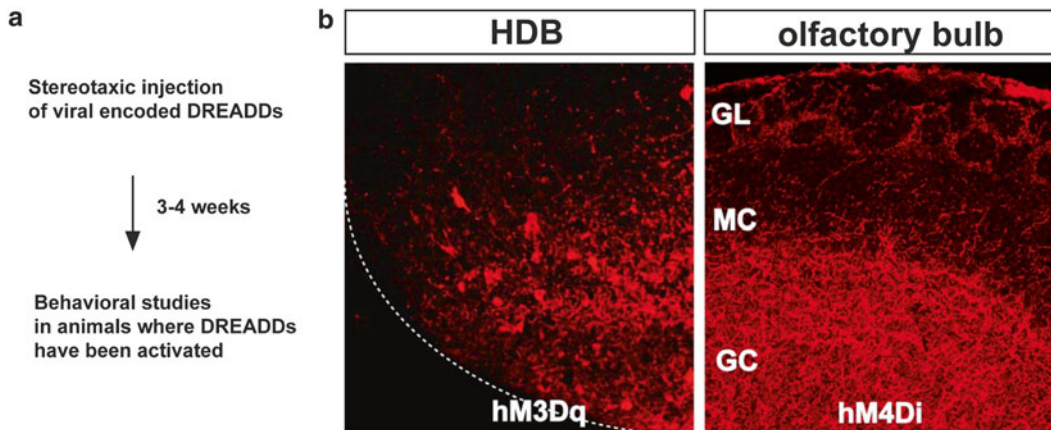
Fig. 1 DREADD expression in GABAergic neurons of the HDB. (**a**) General strategy used to dissect neuronal circuits underlying olfactory-mediated behaviors. DREADD expression is detected between 3 and 4 weeks post-injection. (**b**) Confocal image of a brain slice from a mouse injected with rAAV8/hSyn-DIO-hm3D (Gq) mCherry (*left*) and rAAV8/hSyn-DIO-hm4D (Gi) mCherry (*right*). Adeno-associated viral injections were performed at P30 into the HDB using the following coordinates, with respect to Bregma: medial–lateral, −1.63 mm; anterior–posterior, +0.14 mm; dorsoventral: −5.40 mm. At P60 mCherry was detected by immunohistochemistry using the primary antibody mouse anti-RFP (1:1000, Abcam AB65856) and the secondary donkey anti mouse Alexa 594 (1:750, Life Technologies A21203)

5   Procedures

5.1   Viral Delivery of DREADD Proteins

Prior to surgery autoclave all surgical tools. On the day of the surgery place a warming blanket under the stereotaxic apparatus and allow the virus stock to thaw on ice.

Place the syringe (5 μL, 33 gauge, Hamilton) into the holder. Withdraw the proper amount of the virus using an automated Pump Controller (MicroSyringe Pump Controller Micro4, World Precision Instruments). The amount of virus to inject will depend on the size of the region of interest, the titer and infective capacity of the virus (50 nL–1 μL).

Deeply anesthetize the mouse using isoflurane and place its teeth in the teeth bar of the stereotaxic apparatus. Position stereotaxic bars in ear canals and gently tighten the bars enough so that the head is firmly locked, taking care that the head is leveled in all three axes.

Apply enough optical ointment to cover and hydrate the eyes and apply a local anesthetic subcutaneously to the scalp (S.Q., i.e., lidocaine 1–2 %, dosage 2–4 mg/kg). Clean the incision area with ethanol and betadine. With a scalpel, make a small incision in the skin above the center of the skull. Secure the skin flaps out of the way using hooks made of bent needles.

Position the tip of the needle directly over the center of Bregma, this will serve as the (0,0) coordinate. Record the location of the needle, or reset all positions to 0, if a digital measurement reader is available (Kopf). Move the needle to the desired coordinates with respect to Bregma and mark that position using a fine-point marker or tattoo ink.

Drill a hole through the skull using a Dentist's drill (Cordless MicroDrill, Stoelting), using a 0.6 mm drill bit (Ideal Micro-Drill Burr Set, Cell Point Scientific). Use cotton swabs to stop any bleeding, while keeping the brain moistened (see below).

Slowly, lower the needle until reaching the brain surface. Record the location of the needle (or reset all positions to 0). The needle needs to slide easily into the brain, if not re-drill a larger diameter hole. Lower the needle gently until the desired position in the z-axis is reached.

Infuse the virus at a rate of 0.1 μL/min and once finished wait 5 min to allow virus diffusion into the tissue before retrieving the needle. During the whole procedure keep the skull moistened with saline or PBS.

Suture the skin, take the animal out of the stereotaxic apparatus and allow the mouse to recover. For post-operative care inject carprofen (4 mg/kg), or similar analgesic, for 72 h and monitor the animal daily.

6   DREADD Expression Verification

Preparation of brain for immunohistochemistry: For intracardial perfusions we use standard protocols [42]. Briefly, previously injected mice (3–4 weeks post injection) are anesthetized with isoflurane (2 %) and transcardially perfused with ice-cold PBS and then 4 % PFA (diluted from 10 mL of 16 % stock, Electron Microscopy Sciences) in PBS. We usually perfuse 10–20 mL of PBS, or until the liver is sufficiently lightened in color and then approximately 20 mL 4 % PFA until the tail and neck become extremely stiff. Dissected brains are postfixed in 4 % PFA overnight at 4 °C.

Immunofluorescence: Fixed brains are sliced (50–100 µm) using a Vibratome (Series 1000) and the sections collected directly in PBS. Free-floating sections are washed 1× for 5 min in PBS and 1× for 5 min in PBS with Triton X-100 (PBS-T) 0.1 %. Slices are then incubated for 1 h in 10 % donkey serum (Sigma-Aldrich) in PBS-T (0.1 %). Afterward, slices are incubated overnight with the primary antibody, prepared in PBS-T with 2.5 % of serum, followed by 7× washes for 5 min with PBS-T. Incubate the slices with the secondary antibody for 2 h and then wash them 3× for 5 min each in PBS-T and 3× for 5 min each in PBS alone. Mount with VECTASHIELD (Vector Laboratories). Image detection and analysis is performed using a confocal microscope (Leica SP5 ×) and associated software (Fig. 1b).

7   Olfactory-Mediated Behaviors

Habituation/Dishabituation Test: Inject mice with the desired virus into the target brain region 4–5 weeks previous to the behavioral assay. The day of the experiment inject the animals with a single i.p. injection of either PBS (control group) or 0.5–2 mg/kg clozapine-N-oxide (CNO) (treated group). Previous studies have shown that the maximal effect occurs between 30 min and 4 h after the injection of CNO [8, 9, 12, 16]. Under our experimental conditions we tested the animals at 1, 2, 3, and 4 h. after injection and achieved statistically significant results as early as 2 h post injection (Fig. 2). A clean standard mouse cage (15 cm × 30 cm × 15 cm) without bedding is used for the test. Mice are placed in the cage and allowed to become familiar with the test environment for 30 min. During this time a wooden cube (2 cm³) is placed in the cage and at the conclusion of the familiarization phase, the wooden block is removed for 1 min. Thereafter, the mouse is exposed to a wooden block painted with pure water (3×, 2 min exposures). These exposures allow the mouse to familiarize to the habituation procedure. The second phase consists of three consecutive exposures to a wooden block scented with 100 µL of an odor pair
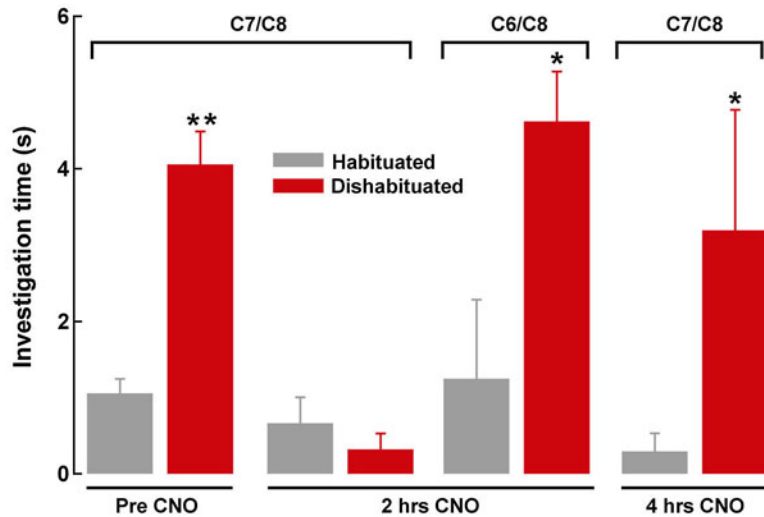
Fig. 2 Disruption of inhibition from the HDB/MCPO affects odor discrimination. A virus encoding for hM4Di was injected into the HDB/MCPO of GAD65-Cre mice. Four weeks later, animals received an i.p. injection of either PBS (control condition) or CNO (treated condition) and were tested for odor discrimination using the habituation/dishabituation paradigm. Before the CNO injection, mice habituated to C7 (*grey bar*) and showed a significant increase in investigation time in the presence of the dishabituated odor, C8 (*red bar*). Two hours after the CNO injection, mice habituated to C7 failed to show an increase in investigation time for C8. However, the investigation time was increased significantly for a pair of odors differing by two carbons (C6/C8). The inability to discriminate between C7 and C8 was recovered completely 4 h after CNO administration. *$P < 0.05$; **$P < 0.02$

(habituated odor), followed by the presentation of the test odor (dishabituated odor; 2 min with at 1-min intervals). Each trial is videotaped, and the time the mouse spent investigating the block is quantified offline. Investigation is defined as the time during which the mouse's nose is within a 2-cm radius from the block. To determine the exact odor dilution, an odor threshold paradigm needs to be performed (see below). The following structurally similar odors are presented to test for fine olfactory discrimination: water, 3×; ethyl heptanoate (C7), 3× and ethyl octanoate (C8), 1×. Using more dissimilar odors can decrease the difficulty of the task (ethyl hexanoate, C6, vs. ethyl octanoate, C8) (Fig. 2).

Odor-Detection Threshold: Control (PBS-injected) and treated (CNO-injected) mice are exposed to a modified version of the habituation/dishabituation paradigm explained above. Animals are kept under the same conditions, but instead of being presented with a particular odor pair, they are tested for the same odor at different dilutions. In general, after three presentations of wooden blocks containing only water, animals are presented with blocks scented with odor dilutions (1:60,000, 1:40,000, 1:30,000, 1:20,000, 1:10,000, and 1:1,000, v/v, in water). Under these
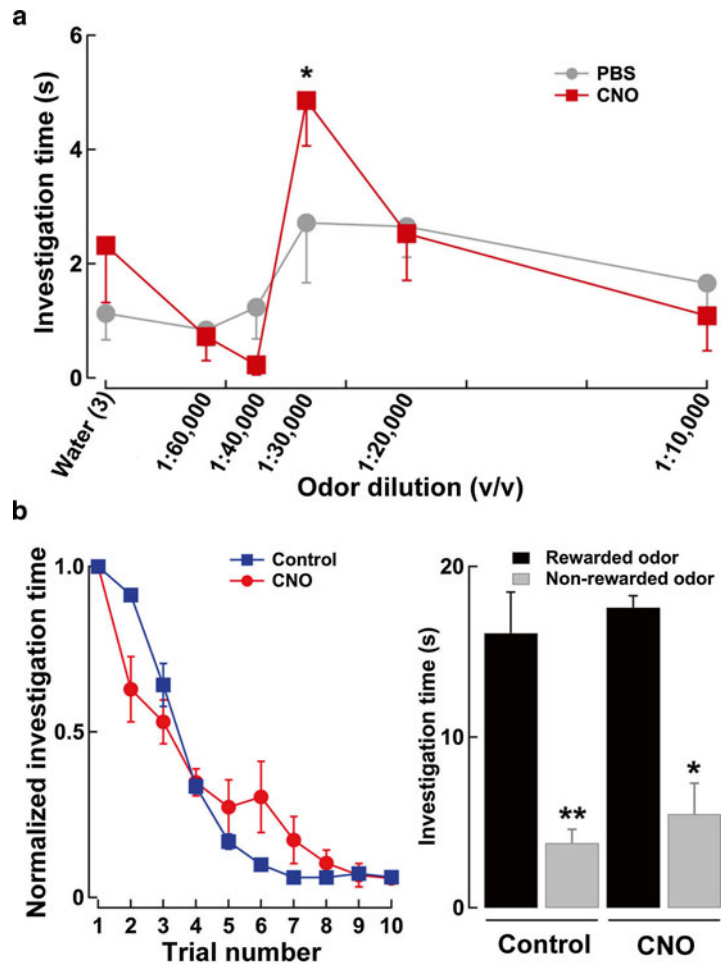
Fig. 3 (**a**) Odor detection threshold and associative odor learning is not affected in the DREADD injected mice. In both groups (control and CNO injected), the investigation time increased significantly when mice were presented with an odor at a dilution of 1:30,000 (*, $P < 0.03$, compared with 1:60,000). Notice that in this paradigm, the investigation time declines at higher concentrations as the odor novelty decreases due to the consecutive odor presentations. (**b**) Control and hM4Di injected mice learn to associate an odor with food reward. *Left*, normalized investigation time during the associative learning trials. During the first trial the investigation time was 123 ± 6 s (control, $n=4$, *blue squares*) and 170 ± 20 s (CNO injected, $n=3$, *red circles*). *Right*, at the end of 4 days (control) or 5 days (CNO-injected hM4Di mice) of associative training, mice spend significantly more time investigating the rewarded odor, in the absence of the food reward (control, 16.1 ± 2.4 vs. 3.8 ± 0.8 s; CNO, 17.6 ± 0.7 vs. 5.5 ± 1.8; *$P < 0.03$; **$P < 0.002$)

conditions, for simple esters, odor detection threshold are usually above 1:30,000 in wild type mice ([11] Fig. 3a).

Associative Odor Learning: Injected mice are housed individually and placed on food restriction, with ad libitum access to water.

For the duration of the associative learning trials, the weight of each animal is monitored daily and maintained at 85 % of its original body weight. Two hours before each training day mice receive a single injection of CNO (0.5 mg/kg, treated group) or PBS (control group). During the trials mice are trained to associate an odor (L-carvone) with a piece of cookie hidden under a 2-cm² filter paper soaked with 75 μL of L-carvone (1:100), both buried under the bedding. A filter paper soaked with the untrained odor (D-Carvone; 1:100) was buried in the opposite side of the cage. Each day of training consisted of five trials in which the time the mouse took to retrieve the food reward was recorded. Under our experimental conditions, both control and hM4Di-injected mice equally learned to retrieve the cookie buried under the trained odor within 2 days [11]. At the end of the day 2 of training, mice are presented with both odors simultaneously for 2 min, in the absence of the food reward. A mouse is deemed able to discriminate between the pair of odors when it spent a significantly longer time investigating the rewarded odor than the non-rewarded odor. The associative training is continued until the mouse is able to discriminate between odors presented simultaneously (Fig. 3b).

8   Notes

Virus delivery: The brain region and the delivery method chosen can dramatically affect the ability of the virus to infect neurons and the yield of cells expressing the desired protein. To troubleshoot this particular issue we suggest varying the speed of injection, the speed of needle retrieval and the angle of the needle tip. Custom made needles can be obtained from specialized companies. In addition, different AAV serotypes containing the gene of interest are available and some serotypes might be better at infecting a particular neuronal class.

Immunofluorescence: For free floating immunofluorescence it is recommended to use section holders to change the slices from one solution to the other (for example, tissue processing wells, Netwells from EMS). These containers easily fit into 12 or 24 culture plates. Additionally, to mount the slices, fill a large Petri dish to the rim with PBS. Place the slide in the Petri dish and use a brush to drag the slice towards the slide and up the surface. After carefully drying the PBS off the slide, pipette 5 μL of mounting media (VECTASHIELD) over the slice and seal the coverslip borders with nail polish and store until confocal imaging.

Acknowledgements

References

1. Rogan SC, Roth BL (2011) Remote control of neuronal signaling. Pharmacol Rev 63: 291–315

2. Boyden ES, Zhang F, Bamberg E, Nagel G, Deisseroth K (2005) Millisecond-timescale, genetically targeted optical control of neural activity. Nat Neurosci 8:1263–1268

3. Fenno L, Yizhar O, Deisseroth K (2011) The development and application of optogenetics. Annu Rev Neurosci 34:389–412

4. Zhang F, Wang LP, Brauner M, Liewald JF, Kay K, Watzke N, Wood PG, Bamberg E, Nagel G, Gottschalk A, Deisseroth K (2007) Multimodal fast optical interrogation of neural circuitry. Nature 446:633–639

5. Atasoy D, Aponte Y, Su HH, Sternson SM (2008) A FLEX switch targets Channel-rhodopsin-2 to multiple cell types for imaging and long-range circuit mapping. J Neurosci 28:7025–7030

6. Zhang F, Gradinaru V, Adamantidis AR, Durand R, Airan RD, de Lecea L, Deisseroth K (2010) Optogenetic interrogation of neural circuits: technology for probing mammalian brain structures. Nat Protoc 5:439–456

7. Dong S, Rogan SC, Roth BL (2010) Directed molecular evolution of DREADDs: a generic approach to creating next-generation RASSLs. Nat Protoc 5:561–573

8. Krashes MJ, Koda S, Ye C, Rogan SC, Adams AC, Cusher DS, Maratos-Flier E, Roth BL, Lowell BB (2011) Rapid, reversible activation of AgRP neurons drives feeding behavior in mice. J Clin Invest 121:1424–1428

9. Sasaki K, Suzuki M, Mieda M, Tsujino N, Roth B, Sakurai T (2011) Pharmacogenetic modulation of orexin neurons alters sleep/wakefulness states in mice. PLoS One 6, e20360

10. Garner AR, Rowland DC, Hwang SY, Baumgaertel K, Roth BL, Kentros C, Mayford M (2012) Generation of a synthetic memory trace. Science 335:1513–1516

11. Nunez-Parra A, Maurer RK, Krahe K, Smith RS, Araneda RC (2013) Disruption of centrifugal inhibition to olfactory bulb granule cells impairs olfactory discrimination. Proc Natl Acad Sci U S A 110:14777–14782

12. Soumier A, Sibille E (2014) Opposing effects of acute versus chronic blockade of frontal cortex somatostatin-positive inhibitory neurons on behavioral emotionality in mice. Neuropsychopharmacology 39:2252–2262

13. Vazey EM, Aston-Jones G (2014) Designer receptor manipulations reveal a role of the locus coeruleus noradrenergic system in isoflurane general anesthesia. Proc Natl Acad Sci U S A 111:3859–3864

14. Zhu H, Pleil KE, Urban DJ, Moy SS, Kash TL, Roth BL (2014) Chemogenetic inactivation of ventral hippocampal glutamatergic neurons disrupts consolidation of contextual fear memory. Neuropsychopharmacology 39(8): 1880–1892

15. Urban DJ, Roth BL (2015) DREADDs (designer receptors exclusively activated by designer drugs): chemogenetic tools with therapeutic utility. Annu Rev Pharmacol Toxicol 55:399–417

16. Yau JO, McNally GP (2015) Pharmacogenetic excitation of dorsomedial prefrontal cortex restores fear prediction error. J Neurosci 35:74–83

17. Armbruster BN, Li X, Pausch MH, Herlitze S, Roth BL (2007) Evolving the lock to fit the key to create a family of G protein-coupled receptors potently activated by an inert ligand. Proc Natl Acad Sci U S A 104: 5163–5168

18. Su CY, Menuz K, Carlson JR (2009) Olfactory perception: receptors, cells, and circuits. Cell 139:45–59

19. Farbman AI (1992) Cell biology of olfaction. Cambridge University Press, New York, NY, USA

20. Levine C, Marcillo A (2008) Origin and endpoint of the olfactory nerve fibers: as described by Santiago Ramon y Cajal. Anat Rec (Hoboken) 291:741–750

21. Shepherd GM (1972) Synaptic organization of the mammalian olfactory bulb. Physiol Rev 52:864–917

22. Isaacson JS, Strowbridge BW (1998) Olfactory reciprocal synapses: dendritic signaling in the CNS. Neuron 20:749–761

23. Jahr CE, Nicoll RA (1982) An intracellular analysis of dendrodendritic inhibition in the turtle in vitro olfactory bulb. J Physiol 326: 213–234

24. Schoppa NE, Kinzie JM, Sahara Y, Segerson TP, Westbrook GL (1998) Dendrodendritic inhibition in the olfactory bulb is driven by NMDA receptors. J Neurosci 18:6790–6802

25. Imamura K, Mataga N, Mori K (1992) Coding of odor molecules by mitral/tufted cells in rabbit olfactory bulb. I. Aliphatic compounds. J Neurophysiol 68:1986–2002

26. Shepherd GM, Chen WR, Willhite D, Migliore M, Greer CA (2007) The olfactory granule cell: from classical enigma to central role in olfactory processing. Brain Res Rev 55:373–382

27. Matsutani S, Yamamoto N (2008) Centrifugal innervation of the mammalian olfactory bulb. Anat Sci Int 83:218–227

28. Boyd AM, Sturgill JF, Poo C, Isaacson JS (2012) Cortical feedback control of olfactory bulb circuits. Neuron 76:1161–1174

29. Markopoulos F, Rokni D, Gire DH, Murthy VN (2012) Functional properties of cortical feedback projections to the olfactory bulb. Neuron 76:1175–1188

30. Devore S, Linster C (2012) Noradrenergic and cholinergic modulation of olfactory bulb sensory processing. Front Behav Neurosci 6:52

31. Gracia-Llanes FJ, Crespo C, Blasco-Ibanez JM, Nacher J, Varea E, Rovira-Esteban L, Martinez-Guijarro FJ (2010) GABAergic basal forebrain afferents innervate selectively GABAergic targets in the main olfactory bulb. Neuroscience 170:913–922

32. Zaborszky L, Carlsen J, Brashear HR, Heimer L (1986) Cholinergic and GABAergic afferents to the olfactory bulb in the rat with special emphasis on the projection neurons in the nucleus of the horizontal limb of the diagonal band. J Comp Neurol 243:488–509

33. Smith RS, Araneda RC (2010) Cholinergic modulation of neuronal excitability in the accessory olfactory bulb. J Neurophysiol 104: 2963–2974

34. Smith RS, Weitz CJ, Araneda RC (2009) Excitatory actions of noradrenaline and metabotropic glutamate receptor activation in granule cells of the accessory olfactory bulb. J Neurophysiol 102:1103–1114

35. Zimnik NC, Treadway T, Smith RS, Araneda RC (2013) 1A-Adrenergic regulation of inhibition in the olfactory bulb. J Physiol 591: 1631–1643

36. Ma M, Luo M (2012) Optogenetic activation of basal forebrain cholinergic neurons modulates neuronal excitability and sensory responses in the main olfactory bulb. J Neurosci 32: 10105–10116

37. Devore S, de Almeida L, Linster C (2014) Distinct roles of bulbar muscarinic and nicotinic receptors in olfactory discrimination learning. J Neurosci 34:11244–11260

38. Chaudhury D, Escanilla O, Linster C (2009) Bulbar acetylcholine enhances neural and perceptual odor discrimination. J Neurosci 29:52–60

39. Hellier JL, Arevalo NL, Blatner MJ, Dang AK, Clevenger AC, Adams CE, Restrepo D (2010) Olfactory discrimination varies in mice with different levels of alpha7-nicotinic acetylcholine receptor expression. Brain Res 1358:140–150

40. Smith RS, Hu R, DeSouza A, Eberly CL, Krahe K, Chan C, Araneda RC (2015) Differential muscarinic modulation in the olfactory Bulb J Neurosci (in press)

41. Rothermel M, Carey RM, Puche A, Shipley MT, Wachowiak M (2014) Cholinergic inputs from Basal forebrain add an excitatory bias to odor coding in the olfactory bulb. J Neurosci 34:4654–4664

42. Nunez-Parra A, Pugh V, Araneda RC (2011) Regulation of adult neurogenesis by behavior and age in the accessory olfactory bulb. Mol Cell Neurosci 47:274–285

Chapter 6

The Use of DREADDs (Designer Receptors Exclusively Activated by Designer Receptors) in Transgenic Mouse Behavioral Models

Daniela Cassataro and Lucas Sjulson

Abstract

Designer Receptors Exclusively Activated by Designer Drugs (DREADDs) are increasingly used to manipulate activity in specific neuronal populations in the brains of awake, behaving mice. Here we review the pros and cons of DREADDs relative to other genetically encoded neuromodulation technologies and describe in detail methods for using DREADDs with transgenic mouse behavioral models. This approach can not only provide insight into the role of specific neural circuits in behavior but also identify potential neuromodulation targets for the treatment of neuropsychiatric disorders.

Key words DREADDs, CNO, Reverse pharmacogenetics, Addiction, Mouse behavior, Transgenic mice

1 Background and Introduction

Since the development of the Designer Receptors Exclusively Activated by Designer Drugs (DREADDs) [1] and their first use in awake behaving mice [2], there have been an increasing number of studies using this technology to examine the behavioral relevance of specific neural circuits in mice. A number of these studies have focused on the circuitry of the striatum, examining the differential roles of the direct and indirect pathways in amphetamine sensitization [3, 4] or the effect of modulating ventral striatum in a preclinical model of alcohol abuse [5]. Others have taken advantage of the cell-type specificity of DREADDs to determine the differential roles of AgRP-expressing [6] and POMC-expressing [7] neurons of the hypothalamus in feeding behavior as well as orexin-expressing hypothalamic cells in sleep-related behavior [8].

Given the increasing availability of Cre recombinase mouse driver lines selective for different neuronal populations [9] and the growing relevance of mouse behavior in neuroscience in general,

this trend will only continue. While DREADDs are a robust technology, there are nevertheless a number of potential pitfalls to be avoided when using them in mouse behavioral assays. In this chapter, we describe several of these pitfalls as well as the framework and protocols that we have found to be effective in avoiding them. We hope that this will facilitate the successful application of this technology to dissecting the functional roles of specific neural circuits as well as to identifying novel targets and strategies for the treatment of neuropsychiatric disorders.

2　Experiment Planning

2.1　DREADDs Versus the Alternatives

The first issue to address in the planning stage is to determine whether or not DREADDs are the optimal tool for the particular experimental question at hand. The primary features of DREADDs are that they enable (1) genetic targeting of specific neuronal subtypes, (2) reversibility on a timescale of hours, (3) focal neuromodulation without chronically implanted hardware, and (4) modulation of large brain structures that are difficult to illuminate. If any of these are not required for the experiment at hand, other techniques should also be considered. For example, if genetic encodability is not required, techniques such as lesioning, electrical stimulation, or focal drug infusion strategies may be preferable (Table 1). Similarly, if genetic targeting is required but reversibility is unnecessary or even undesirable, alternatives include genetically encoded tetanus toxin [10] or ion channels such as NaChBac [11] or Kir2.1 [12, 13], which depolarize or hyperpolarize the membrane, respectively.

If both genetic targeting and reversibility are required, then alternative genetically encoded neuromodulation technologies should still be considered. Two of the most widely used options include optogenetics [14, 15] and the PSAM/PSEM system [16]. The primary advantage of optogenetics is its fast reversibility, which can be advantageous in certain behavioral paradigms in which modulation and control trials can be interleaved on timescales of seconds. However, optogenetics requires indwelling optical fibers and lasers for illumination, severely restricting the throughput of behavioral assays. In contrast, DREADDs enable a large number of animals to be tested in parallel without the need for extensive equipment. Additionally, DREADDs can target multiple sites simultaneously, which is often necessary for large brain structures and can be difficult using optogenetics because it requires complex implantations of multiple optical fibers.

The PSAM/PSEM system is another reverse pharmacogenetic system in which engineered receptors are expressed ectopically in the neurons of interest and activated by administration of an otherwise-inert ligand. A key difference between PSAMs and

Table 1

Comparison of several common methods for modulating neural activity in behaving mice

Method	Reversible?	Cell-type specificity	Effect on membrane potential	Onset of effect	Duration of effect
DREADDs	Yes	Yes	Depolarize or hyperpolarize	~30 min with IP administration	2–3 h with IP administration
Microbial opsins (e.g., channelrhodopsin-2)	Yes	Yes	Depolarize or hyperpolarize	Milliseconds	Milliseconds to hours
PSAM/PSEMs	Yes	Yes	Depolarize or hyperpolarize	Minutes	~10 min with IP injection
Kir2.1	No	Yes	Hyperpolarize	Days	Permanent
NaChBac	No	Yes	Depolarize	Days	Permanent
AAV-Tetanus toxin	No	Yes	Blocks synaptic vesicle release	Days	Permanent
Lesioning	No	Variable	Cell death	Days	Permanent
Electrical stimulation	Yes	No	Depolarize	Milliseconds	Milliseconds to hours
Local drug infusion	Yes	No	Depolarize or hyperpolarize	Seconds	Minutes to hours

DREADDs is that PSAM ligands (PSEMs) have significantly shorter half-lives than the DREADD ligand CNO and are also not available commercially. Another important difference is that PSAMs are ion channels that alter membrane potential directly, but DREADDs are G protein-coupled receptors that influence membrane potential indirectly by modulating endogenous ion channels. This means that the efficacy of DREADDs will differ between different cell types and developmental time points. For example, one important limitation of DREADD-hM4Di is that it is unlikely to be effective at early postnatal time points (e.g., before P10) because of insufficient expression of endogenous GIRK channels [17, 18]. Even in adult mice, DREADD-hM4Di may only be sufficient to partially silence some cell types. Additionally, DREADDs alter G-protein dependent cellular processes beyond membrane potential, which may complicate interpretation of results in some experiments. Nevertheless, DREADDs have proven to be a robust technology that works in a variety of cell types and brain regions.

2.2 Targeting the Cells of Interest

Having decided on the DREADD/CNO system, the next step is to determine how to express the chosen DREADD in the cells of interest. The two main methods are transgenic DREADD-expressing mouse

lines and viral vector approaches. Several DREADD mouse lines developed by the Dymecki and Roth laboratories are now available from the Jackson Laboratory [4, 19, 20]. The primary advantage of transgenic mouse lines over viral vectors is that with viral vectors only a subset of the cells are infected, while with transgenic animals virtually 100 % of the cells of interest will express the DREADD given an efficient driver line. This also leads to greater uniformity of expression levels across the cell population. However, this approach is frequently problematic if DREADDs are expressed in undesired brain regions or outside the brain, leading to nonspecific effects if CNO is administered systemically.

For this reason, we generally use adeno-associated viral (AAV) vectors to express DREADDs in the brain, which enables us to restrict expression to specific anatomical regions. In addition, AAV provides high transduction efficiencies (up to 80 %) and expression levels with low toxicity, and it is commercially available at relatively low cost. There are several possible methods for targeting AAV expression to particular cells of interest, but we will focus on three: using cell-type specific promoters, using Cre-dependent AAV to target specific anatomical projections, and using Cre-dependent AAV in Cre-expressing transgenic mice.

Cell type-specific promoters are of limited utility in AAV for several reasons. Most promoters are too large for the ~5 kb packaging limit, drive transgene expression too weakly, and/or exhibit leaky expression in undesired cell types, possibly due to the high number of viral genomes introduced to each cell. To date, the only well-validated cell-type specific promoter for use in AAV is a minimal CaMKIIa promoter that in cortex and hippocampus drives expression selectively in excitatory pyramidal cells. This promoter was first validated in lentiviral vectors and then in AAV [21, 22]. Other viral vectors with larger capacity can carry longer promoter sequences that in theory could provide higher specificity than AAV; nevertheless, this approach frequently leads to leaky nonspecific expression.

As a result, the more common approach is to use AAV containing Cre-dependent "FLEX" [23] or "DIO" [24] cassettes, in which the transgene of interest (e.g., a DREADD) is initially in the reverse orientation and hence inactive. The presence of Cre recombinase irreversibly inverts the orientation of the transgene, activating transcription (Fig. 1). Using this approach, it is possible to target cells based on projection pattern by injecting Cre-dependent AAV near the somata of the cells of interest and a retrograde Cre vector near the axon terminals [25–28]. However, a more common method is to use transgenic/knock-in mouse lines that express Cre in a subset of cells based on the expression profile of a given gene. A growing number of Cre driver lines are commercially available from vendors such as Jackson Laboratories, as well as from publicly funded projects such as the GENSAT project [9].
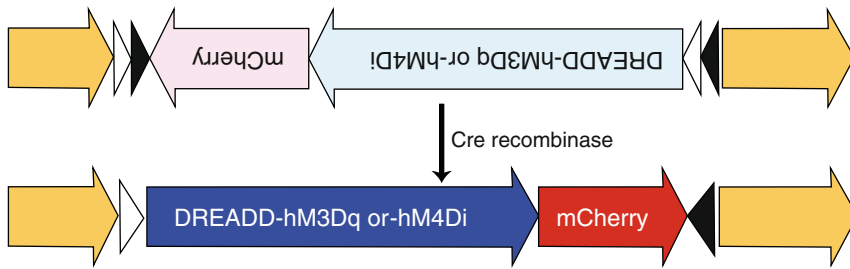
Fig. 1 The flip-excision ("FLEX")/double-inverted open reading frame ("DIO") method restricts expression of DREADDs to Cre-positive cells

2.3 Mouse Breeding

Another important consideration that should be planned as far in advance as possible is the breeding scheme for the experiments. Power calculations should be performed to estimate the number of animals needed, and the breeding scheme should be based on this estimate. Relevant considerations also include whether males, females, or both will be used; the proportion of mice expected to carry the required allele/alleles; and the number of mice required for control groups including Cre-negative littermates and Cre-positive littermates injected with a control AAV not encoding a DREADD. The background strain of the mice is also important, and transgenic mouse lines should generally be backcrossed onto an inbred background such as C57BL/6 in order to minimize variability in anatomical targeting and behavioral performance. While C57BL/6 is the most common inbred strain used for behavior assays, we generally prefer to use C57BL/6×FVB/NJ F1 hybrids because FVB females generate larger litter sizes, and hybrid mice are larger, healthier, and, at least in our hands, more reliable overall.

2.4 Incorporating DREADDs into the Behavioral Paradigm of Interest

One of the key features of DREADDs is that the modulatory effect is reversible, which enables partial within-subjects experimental designs in which the behavioral effects of DREADDs are ascertained by comparing the difference between the CNO and CNO-negative control condition within a single animal. Although this may slightly complicate analysis, we strive to use within-subjects designs whenever possible because using each animal as its own control helps to minimize variability and reduce the number of animals required. Nevertheless, a number of control conditions are usually necessary. Because a number of Cre lines exhibit abnormal behavior, it is important to perform control experiments in which Cre-positive animals are injected with an AAV that does not encode a DREADD. An equally important but lesser-recognized control involves injecting Cre-dependent AAV into Cre-negative littermates, which we have found for some AAVs can have a surprisingly large effect on behavior. Depending on the behavior being tested,

it is frequently necessary to perform experiments controlling for nonspecific effects such as impaired locomotion or motor coordination. Although the need for this type of control experiment applies to any intervention, DREADDs offer the advantage of a within-subjects design for these experiments as well (e.g., comparing open field locomotion in saline vs. CNO conditions).

Finally, the CNO delivery method, delivery time, and dose must also be determined. The most common delivery methods are oral administration and IP injection, though focal infusions directly into the brain are also effective [29]. For long-term administration (e.g., overnight), we generally use CNO in drinking water at 0.1 mg/mL. Since a 30 g mouse generally drinks about 3 mL/day, this amounts to an approximate dose of 10 mg/mL of CNO daily. For shorter-term administration, we dissolve CNO in sterile PBS and inject intraperitoneally at a dose of 1–5 mg/kg. Under these conditions, DREADD activation generally takes ~30 min and lasts about 2–4 h. However, Alexander et al. [2] have reported a longer duration of effects.

3 Preexperiment Optimization

The single most important factor in the success of behavioral experiments using DREADDs is obtaining high levels of DREADD expression selectively in the cells and target region of interest. Careful preexperiment optimization is crucial.

3.1 Optimizing Anatomical Targeting

Before starting experiments, it is important to test viral injection conditions and optimize targeting of the brain structure of interest. Stereotactic coordinates from atlases are a good starting point, but in our experience these coordinates typically require refinement. When targeting a new brain structure, especially structures that are small and/or ventral, we first start by injecting small volumes (e.g., 50 nL) of Evans Blue followed immediately by sectioning the brain to verify targeting accuracy. Alternatively, one can also place a small electrolytic lesion (100 μA cathodal current for two seconds from a 50 μm tungsten electrode) and section the brain 24–48 h later. The use of dye or lesions rather than AAV-EGFP in pilot injections provides rapid feedback and a more precise estimate of the true location than EGFP expression, which fills the processes of the cells and thus extends to a larger spatial area. It is important to use mice of the same background strain, age, and sex that will be used for the experiments. If possible, we use inbred mice or F1 hybrids so that all mice are genetically identical, minimizing anatomical variability. After refining and validating coordinates, we inject commercially available AAV-EGFP to verify the amount of spread and optimal volume of virus to inject. The degree of spread is dependent on serotypes and titer, so it is best to use the same serotype that will be used for experiments.

<table>
<tr><td>

3.2 Optimizing Cellular Targeting

</td><td>

To target a molecularly defined cell population with Cre driver lines and Cre-dependent AAV, both the mouse line and the viral vector must be validated and optimized if this has not been done in the past. An underappreciated aspect of using AAV is that even among serotypes with known tropism for neurons, different serotypes infect various neuronal subtypes with different degrees of efficiency. When targeting a novel cell type, we first test a panel of several AAV serotypes (e.g., AAV1, AAV5, and AAV9) to see which is the most efficient for the cell type of interest. For our studies in striatum, we generally use AAV5, which infects most striatal neurons efficiently with relatively low levels of retrograde infection. AAV-DREADDs are now commercially available in AAV2, 5, and 8 from the University of North Carolina Vector Core, providing several options.

When using an untested Cre driver line, it is important to verify that expression is actually restricted to the cells of interest. This is particularly true for transgenic Cre lines, in which the expression pattern is less likely to mimic the endogenous expression pattern than with knock-in lines. The simplest technique is to inject a Cre-dependent AAV encoding a fluorescent protein such as GFP, then use immunohistochemistry to verify that all of the green cells also express the marker gene of interest (Fig. 2). For marker genes where no suitable antibody is available, a logical approach would be to cross the Cre driver with a Cre-dependent fluorescent protein reporter line, then inject the Cre-dependent AAV and quantify colocalization of the two fluorescent proteins. However, we and others [30] have found that this approach is not reliable because most Cre-dependent AAVs will suppress expression of Cre-dependent genomic reporters. Additionally, expression patterns in reporter lines may be broader than with Cre-dependent AAV due to recombination at early developmental time points. As a result, the best approach in this case is to find alternative markers for immunohistochemistry or to perform in situ hybridizations.

</td></tr>
</table>

4 Performing the Experiment

<table>
<tr><td>

4.1 Stereotactic Injection Protocol

</td><td>

A protocol for stereotactic injections will vary depending on the specific hardware and has been covered in detail elsewhere [31]. Nevertheless, given the importance of proper injection technique, we will review the factors that we consider to be critical.

</td></tr>
</table>

- Fill the injector pipet/syringe with AAV before anesthetizing the first animal. We typically fill the pipet with enough AAV to inject several animals in a row. Upon receiving a new AAV stock, we make 8 μL aliquots in PCR tubes and store at –80 °C. Only thaw each aliquot once—after thawing, an aliquot is stable
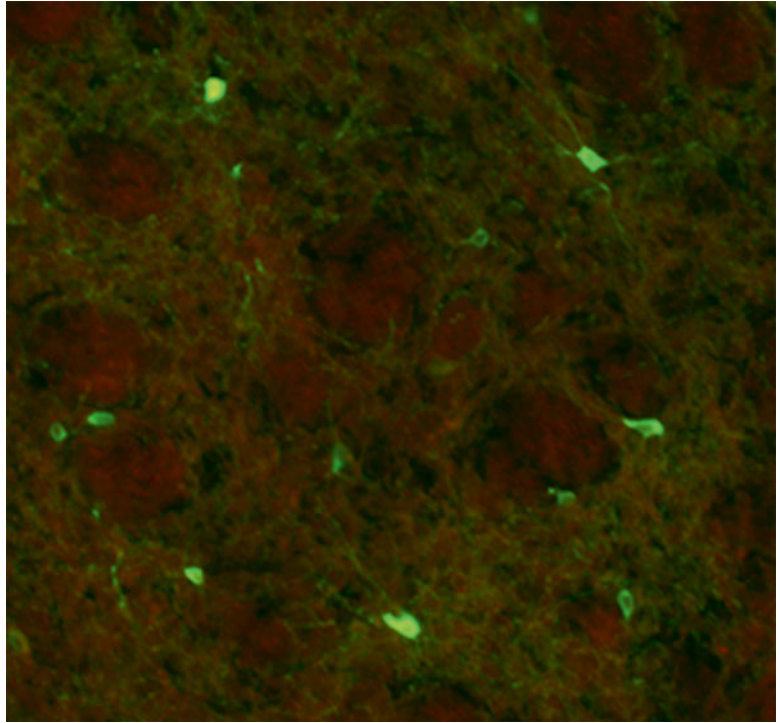
Fig. 2 Validation of cre driver line by immunohistochemical colocalization of a cellular marker (*green*) and DREADD-mCherry (*red*). Since the AAV does not infect all neurons, some green neurons do not express mCherry, but all mCherry-expressing neurons are positive for the immunohistochemical marker, consistent with the cre driver line restricting DREADD-mCherry expression to the cells of interest

at 4 °C for up to a month. Prepare all other instruments and supplies prior to starting anesthesia to minimize the duration of anesthesia.

- Anesthetize the animal. We prefer the use of isoflurane to injectable anesthetics such as ketamine/xylazine because the animals recover much more rapidly after surgery. When using isoflurane, be sure to use a heating pad and monitor the animal's body temperature and respiratory rate every 15 min. If the rate drops below 20 respirations in 15 s, lower the isoflurane concentration. For complex surgeries requiring more than three hours of anesthesia, we administer atropine 1 mg/kg intraperitoneally at the start of the procedure to reduce secretions that can lead to respiratory compromise.

- Fix the animal's head in the stereotactic frame securely. This may sound trivial, but doing this properly is the most technically difficult aspect of the procedure and is a key step in achieving accurate, reproducible results. First, coat the tips of the ear

bars with topical lidocaine cream, which decreases anesthesia requirements. When using isoflurane anesthesia, place the animal in the nosepiece first and stabilize the level of anesthesia at a higher isoflurane concentration than used for maintenance anesthesia (e.g., 2 %). Next, loosen the nosepiece so the skull can tilt up and down freely, and lift the animal by the tail until the skull is level before securing the ear bars. Note that ear bars should not be placed in the ear canals but on the skull anterior to the ear opening, which provides greater stability. After tightening the ear bars and nosepiece, push on the head to verify that the skull does not move. Next, cover the eyes with eye ointment or a mix of petroleum jelly and mineral oil, and reduce the isoflurane concentration to a maintenance level (e.g., 0.8–1 %).

- After removing the hair and prepping the skin with betadine, inject bupivacaine subcutaneously, and open the scalp with sharp scissors cutting from posterior to anterior along the midline. Bupivacaine decreases anesthesia requirements, but it may still be necessary to increase the isoflurane concentration for this step. Clear away the connective tissue covering the skull, and hold the incision open with small retractors or hooks fashioned from bent needles. Push the skull with blunt forceps to verify that the head is fixed securely, and if necessary, reposition or tighten.

- Under maximum magnification, mark the calibration points bregma and lambda on the skull with a scalpel or sterile razor blade. Mark these locations with an "X" by interpolating along the skull sutures—do not use the actual intersections of the skull sutures, which vary considerably from animal to animal. Touch the corners of the "X" with a new fine-tip permanent marker—the ink will flow into the "X," marking it for easy visualization.

- Ensure that the skull is level, first by visual inspection and next by measuring the Z-axis (vertical) position of points 2.5 mm to the left and right of bregma. For small and/or ventral targets, our rule is that the difference in Z-axis measurements must be 80 µm or less. Next, ensure that the difference in Z-axis positions of lambda and bregma is also 80 µm or less. For this step, it is highly advantageous to have a stereotactic frame that allows adjustment of head angle without loosening the ear bars, such as the Kopf Instruments 1900.

- Mark the desired injection sites and drill craniotomies. Stop drilling before puncturing the dura and clear skull fragments from the craniotomy using a small (~28–30 gauge) needle with the tip bent away from the opening to form a hook. The dura is difficult to visualize in mice, so the best way to determine

if it is intact is to poke the brain surface lightly with a sharp needle. If the dura is intact, the brain surface will indent visibly around the needle. After cutting craniotomies, keep them from drying out using sterile saline and saline-soaked gel foam.

- Fit the injector onto the frame and re-calibrate coordinates to bregma and lambda. Lower the pipet slowly, punching through the dura, to reach the target coordinates.

- Infuse AAV at a rate of 50–100 nL/min, then wait 5 min after the injection to remove the needle/pipet. Withdraw the pipet slowly to minimize backflow of virus along the injection tract.

- Close the incision, stop anesthesia, and monitor the animal until it has recovered.

4.2 Post-surgery Recovery

For the first 3–4 days after injection, house animals individually to prevent other mice from opening the wound. After this period, we recommend group housing animals if possible to minimize the behavioral effects of social isolation. Although fluorescent protein expression is detectable as early as 3 days after AAV injection, we recommend waiting at least 2 weeks before starting experiments. Expression typically peaks around 3–4 weeks after injection and generally persists for months.

4.3 Preexperiment Conditioning and Behavioral Data Collection

Perform any necessary preexperiment conditioning (e.g., habituation to a test chamber and IP injections), and collect the behavioral data. The actual procedure will vary depending on the assay, but the procedural aspects of CNO administration are the same as any other drug delivered through the same route. As with any behavioral assay, uniform handling is critical to minimize variability.

5 Post-experiment Verification and Data Analysis

After the experiment, harvest and process brains for histology according to any standard protocol. We sacrifice animals with an overdose of sodium pentobarbital, followed immediately by transcardial perfusion with a fresh solution of 4 % paraformaldehyde in ice-cold PBS. After perfusion, we harvest the brain and postfix in 4 % PFA for 1 h, then cryoprotect the tissue with 30 % sucrose in PBS overnight. For sensitive detection of fluorescent proteins, we cut 20 μm cryosections and perform immunohistochemistry against the fluorescent reporter (in our case, usually mCherry). However, in cases where the density of mCherry-positive cells is high, it is possible to save time by cutting thick (100–150 μm) sections, mounting them, and visualizing native mCherry fluorescence (Fig. 3). When rating the accuracy of anatomical targeting, it is crucial that the person rating the brains is blinded to the experimental group of each sample to prevent bias.
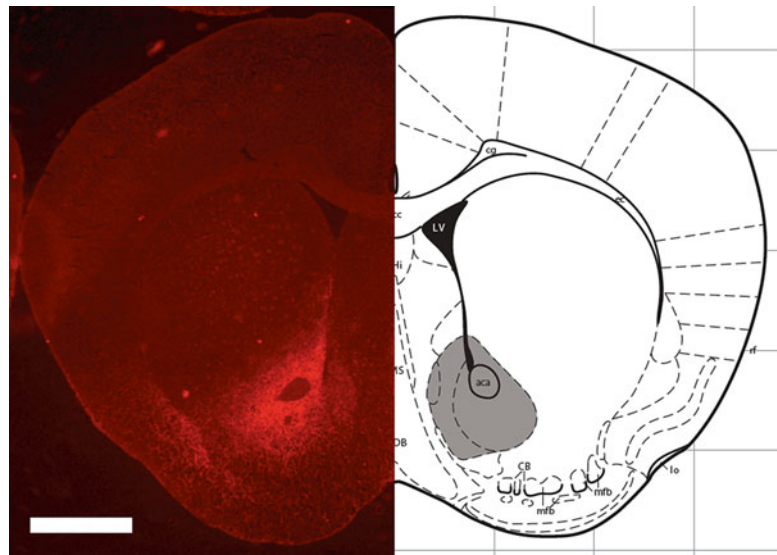
Fig. 3 Visualization of DREADD-mCherry expression after stereotactic AAV injection in the nucleus accumbens

6   Conclusion

The DREADD-CNO system enables targeted modulation of specific neuronal populations in vivo and possesses numerous features making it well suited for behavioral assays in transgenic mice. DREADDs provide genetic specificity and reversibility, allowing partial within-subjects study designs. Additionally, unlike optogenetics, DREADDs enable large numbers of animals to be tested in parallel without the need for lasers or indwelling implants and tethers that can restrict free movement of the animal. DREADDs can also affect cells over large anatomical regions that would be difficult to illuminate.

In this chapter, we focus on expression of DREADDs using Cre-dependent AAV with Cre driver lines that restrict expression to subsets of cells that normally express a given gene. This powerful approach provides two layers of specificity: cell-type specificity from restricted Cre expression and anatomical specificity due to precisely localized injections. For most applications, both of these are essential for minimizing off-target effects. Nevertheless, the genetic specificity of the DREADDs provides flexibility that extends well beyond this approach to include expression of DREADDs from genomic loci [4, 19], based on projection patterns [25–28], or even based on recent activity patterns [20, 32].

Using DREADDs to manipulate a specific cell population in a specific area of the brain not only adds to our understanding of the

roles of those cells in their circuit—it also clears a path toward potential clinical applications. A primary limitation of current treatments for neuropsychiatric disorders is insufficient specificity for affecting specific components of dysfunctional circuits. Information gained using DREADDs in transgenic mouse models may thereby help identify targets and methods for the eventual treatment of neuropsychiatric disorders in humans.

Acknowledgments

References

1. Armbruster BN, Li X, Pausch MH, Herlitze S, Roth BL (2007) Evolving the lock to fit the key to create a family of G protein-coupled receptors potently activated by an inert ligand. Proc Natl Acad Sci U S A 104:5163–5168, published online EpubMar (10.1073/pnas.0700293104)

2. Alexander GM, Rogan SC, Abbas AI, Armbruster BN, Pei Y, Allen JA, Nonneman RJ, Hartmann J, Moy SS, Nicolelis MA, McNamara JO, Roth BL (2009) Remote control of neuronal activity in transgenic mice expressing evolved G protein-coupled receptors. Neuron 63:27–39, published online EpubJul (10.1016/j.neuron.2009.06.014)

3. Ferguson SM, Eskenazi D, Ishikawa M, Wanat MJ, Phillips PE, Dong Y, Roth BL, Neumaier JF (2011) Transient neuronal inhibition reveals opposing roles of indirect and direct pathways in sensitization. Nat Neurosci 14:22–24, published online EpubJan (10.1038/nn.2703)

4. Farrell MS, Pei Y, Wan Y, Yadav PN, Daigle TL, Urban DJ, Lee HM, Sciaky N, Simmons A, Nonneman RJ, Huang XP, Hufeisen SJ, Guettier JM, Moy SS, Wess J, Caron MG, Calakos N, Roth BL (2013) A Gαs DREADD mouse for selective modulation of cAMP production in striatopallidal neurons. Neuropsychopharmacology 38:854–862, published online EpubApr (10.1038/npp.2012.251)

5. Cassataro D, Bergfeldt D, Malekian C, Van Snellenberg JX, Thanos PK, Fishell G, Sjulson L (2014) Reverse pharmacogenetic modulation of the nucleus accumbens reduces ethanol consumption in a limited access paradigm. Neuropsychopharmacology 39:283–290, pub-

lished online EpubJan (10.1038/npp.2013.184)

6. Krashes MJ, Koda S, Ye C, Rogan SC, Adams AC, Cusher DS, Maratos-Flier E, Roth BL, Lowell BB (2011) Rapid, reversible activation of AgRP neurons drives feeding behavior in mice. J Clin Invest 121:1424–1428, published online EpubApr (10.1172/JCI46229)

7. Zhan C, Zhou J, Feng Q, Zhang JE, Lin S, Bao J, Wu P, Luo M (2013) Acute and long-term suppression of feeding behavior by POMC neurons in the brainstem and hypothalamus, respectively. J Neurosci 33:3624–3632, published online EpubFeb (10.1523/JNEUROSCI.2742-12.2013)

8. Sasaki K, Suzuki M, Mieda M, Tsujino N, Roth B, Sakurai T (2011) Pharmacogenetic modulation of orexin neurons alters sleep/wakefulness states in mice. PLoS One 6:e20360, 10.1371/journal.pone.0020360)

9. Gerfen CR, Paletzki R, Heintz N (2013) GENSAT BAC cre-recombinase driver lines to study the functional organization of cerebral cortical and basal ganglia circuits. Neuron 80:1368–1383, published online EpubDec (10.1016/j.neuron.2013.10.016)

10. Murray AJ, Sauer JF, Riedel G, McClure C, Ansel L, Cheyne L, Bartos M, Wisden W, Wulff P (2011) Parvalbumin-positive CA1 interneurons are required for spatial working but not for reference memory. Nat Neurosci 14:297–299, published online EpubMar (10.1038/nn.2751)

11. Sim S, Antolin S, Lin CW, Lin Y, Lin YX, Lois C (2013) Increased cell-intrinsic excitability induces synaptic changes in new

neurons in the adult dentate gyrus that require Npas4. J Neurosci 33:7928–7940, published online EpubMay (10.1523/JNEUROSCI.1571-12.2013)

12. De Marco García NV, Karayannis T, Fishell G (2011) Neuronal activity is required for the development of specific cortical interneuron subtypes. Nature 472:351–355, published online EpubApr (10.1038/nature09865)

13. Yu CR, Power J, Barnea G, O'Donnell S, Brown HE, Osborne J, Axel R, Gogos JA (2004) Spontaneous neural activity is required for the establishment and maintenance of the olfactory sensory map. Neuron 42:553–566

14. Sjulson L, Miesenböck G (2008) Photocontrol of neural activity: biophysical mechanisms and performance in vivo. Chem Rev 108:1588–1602, published online EpubMay (10.1021/cr078221b)

15. Fenno L, Yizhar O, Deisseroth K (2011) The development and application of optogenetics. Annu Rev Neurosci 34:389–412, 10.1146/annurev-neuro-061010-113817)

16. Magnus CJ, Lee PH, Atasoy D, Su HH, Looger LL, Sternson SM (2011) Chemical and genetic engineering of selective ion channel-ligand interactions. Science 333:1292–1296, published online EpubSep (10.1126/science.1206606)

17. Tan EM, Yamaguchi Y, Horwitz GD, Gosgnach S, Lein ES, Goulding M, Albright TD, Callaway EM (2006) Selective and quickly reversible inactivation of mammalian neurons in vivo using the Drosophila allatostatin receptor. Neuron 51:157–170, published online EpubJul (10.1016/j.neuron.2006.06.018)

18. Chen SC, Ehrhard P, Goldowitz D, Smeyne RJ (1997) Developmental expression of the GIRK family of inward rectifying potassium channels: implications for abnormalities in the weaver mutant mouse. Brain Res 778:251–264

19. Ray RS, Corcoran AE, Brust RD, Kim JC, Richerson GB, Nattie E, Dymecki SM (2011) Impaired respiratory and body temperature control upon acute serotonergic neuron inhibition. Science 333:637–642, published online EpubJul (10.1126/science.1205295)

20. Garner AR, Rowland DC, Hwang SY, Baumgaertel K, Roth BL, Kentros C, Mayford M (2012) Generation of a synthetic memory trace. Science 335:1513–1516, published online EpubMar (10.1126/science.1214985)

21. Dittgen T, Nimmerjahn A, Komai S, Licznerski P, Waters J, Margrie TW, Helmchen F, Denk W, Brecht M, Osten P (2004) Lentivirus-based genetic manipulations of cortical neurons and their optical and electrophysio- logical monitoring in vivo. Proc Natl Acad Sci U S A 101:18206–18211, published online EpubDec (10.1073/pnas.0407976101)

22. Nathanson JL, Yanagawa Y, Obata K, Callaway EM (2009) Preferential labeling of inhibitory and excitatory cortical neurons by endogenous tropism of adeno-associated virus and lenti- virus vectors. Neuroscience 161:441–450, published online EpubJun (10.1016/j.neuroscience.2009.03.032)

23. Atasoy D, Aponte Y, Su HH, Sternson SM (2008) A FLEX switch targets Channelrhodopsin-2 to multiple cell types for imaging and long-range circuit mapping. J Neurosci 28:7025–7030, published online EpubJul (10.1523/JNEUROSCI.1954-08.2008)

24. Cardin JA, Carlén M, Meletis K, Knoblich U, Zhang F, Deisseroth K, Tsai LH, Moore CI (2009) Driving fast-spiking cells induces gamma rhythm and controls sensory responses. Nature 459:663–667, published online EpubJun (10.1038/nature08002)

25. Gradinaru V, Zhang F, Ramakrishnan C, Mattis J, Prakash R, Diester I, Goshen I, Thompson KR, Deisseroth K (2010) Molecular and cellular approaches for diversifying and extending optogenetics. Cell 141:154–165, published online EpubApr (10.1016/j.cell.2010.02.037)

26. Kremer EJ, Boutin S, Chillon M, Danos O (2000) Canine adenovirus vectors: an alterna- tive for adenovirus-mediated gene transfer. J Virol 74:505–512

27. Hnasko TS, Perez FA, Scouras AD, Stoll EA, Gale SD, Luquet S, Phillips PE, Kremer EJ, Palmiter RD (2006) Cre recombinase-mediated restoration of nigrostriatal dopamine in dopamine-deficient mice reverses hypopha- gia and bradykinesia. Proc Natl Acad Sci U S A 103:8858–8863, published online EpubJun (10.1073/pnas.0603081103)

28. Znamenskiy P, Zador AM (2013) Corti- costriatal neurons in auditory cortex drive deci- sions during auditory discrimination. Nature 497:482–485, published online EpubMay (10.1038/nature12077)

29. Mahler SV, Vazey EM, Beckley JT, Keistler CR, McGlinchey EM, Kaufling J, Wilson SP, Deisseroth K, Woodward JJ, Aston-Jones G (2014) Designer receptors show role for ven- tral pallidum input to ventral tegmental area in cocaine seeking. Nat Neurosci, published online EpubMar (10.1038/nn.3664)

30. Saunders A, Johnson CA, Sabatini BL (2012) Novel recombinant adeno-associated viruses for Cre activated and inactivated transgene

expression in neurons. Front Neural Circuits 6:47. doi:10.3389/fncir.2012.00047

31. Cetin A, Komai S, Eliava M, Seeburg PH, Osten P (2006) Stereotaxic gene delivery in the rodent brain. Nat Protoc 1:3166–3173. doi:10.1038/nprot.2006.450

32. Guenthner CJ, Miyamichi K, Yang HH, Heller HC, Luo L (2013) Permanent genetic access to transiently active neurons via TRAP: targeted recombination in active populations. Neuron 78:773–784, published online EpubJun (10.1016/j.neuron.2013.03.025)

Chapter 7

Pharmacogenetic Dissection of Neural Mechanisms Underlying the Regulation of Sleep–Wakefulness Using DREADDs

Michihiro Mieda and Takeshi Sakurai

Abstract

Sleep and wakefulness are controlled by a complex network of neurons harboring diverse neurochemical characteristics, including glutamatergic, GABAergic, monoaminergic, cholinergic, and peptidergic neurons. To understand the precise role of each type of neuron in this circuit, it is useful to artificially manipulate the activity of a particular type of neuron to see its effect on behavior. The DREADD system has made such a strategy possible. Here, we review our recent work using DREADD to pharmacogenetically dissect neural mechanisms regulating sleep–wakefulness, describe the protocol we used, and discuss the technical aspects of our studies.

Key words Sleep–wakefulness, Orexin, Narcolepsy, Neuropeptide, Preoptic area, Hypothalamus, Transgenic mice

1 Introduction

Designer receptors exclusively activated by designer drugs (DREADD) are artificially generated mutants of human muscarinic receptors that lose the ability to bind natural ligands, acetylcholine, while they gain the ability to be activated by the otherwise pharmacologically inert ligand clozapine-N-oxide (CNO) with nanomolar potency [1, 2]. The stimulatory DREADD, designated "hM3Dq," couples with the G_q pathway to depolarize neurons, while the inhibitory DREADD, "hM4Di," couples with the $G_{i/o}$ pathway to hyperpolarize neurons. Therefore, in combination with genetic techniques to target expression of exogenous genes, DREADDs function as powerful tools of neuroscience research to artificially manipulate the activity of a certain population of neurons to reveal its physiological and pathological roles.

Compared to optogenetics [3], which utilizes photoactivatable cation channels, ion pumps, or GPCRs to manipulate neural activities, the time resolution of DREADD technology is limited. On the other hand, it is less invasive and its effects last for longer periods, which may be suitable for studying events occurring on a time scale of minutes to hours, such as sleep–wakefulness cycles. In addition, since CNO is a stable substance that can cross the blood brain barrier, it can be readily administered intraperitoneally (i.p.) or orally while only minimally interfering with the behavioral state in freely moving animals.

We have been studying the neural mechanisms underlying the regulation of sleep–wakefulness since our discovery of the neuropeptide orexin [4, 5] (further explained later). Proper wakefulness and vigilance are essential for us to behave in an appropriate manner, while sleep is vital for the normal function and homeostasis of our brains, as well as for efficient memory formation. Thus, understanding the regulation of the sleep–wakefulness cycle is of tremendous importance. Since the development of DREADD technology by Dr. Bryan Roth's group at the University of North Carolina [1, 2], we have utilized DREADD technology to dissect neural circuits regulating the vigilance states. We so far have demonstrated (1) that changes in the activity of orexin neurons can alter the behavioral state of animals [6], (2) that activation of dorsal raphe (DR) serotonergic neurons and locus coeruleus (LC) noradrenergic neurons suppress cataplexy and fragmentation of wakefulness, respectively, in narcoleptic mice [7], and (3) that stimulation of GABAergic neurons in the preoptic area (POA) leads to an increase in the amount of non-rapid eye movement (NREM) sleep [8]. These findings will be described below in more detail.

2 Pharmacogenetic Modulation of Orexin Neurons Alters Sleep–Wakefulness States in Mice [6]

The neuropeptides orexin A and orexin B, also called hypocretin 1 and hypocretin 2, are produced by cleavage of a single precursor polypeptide, prepro-orexin, in neurons located in the lateral hypothalamic area (LHA) [5, 9]. These neuropeptides act on G protein-coupled receptors, termed orexin receptors type 1 and type 2 (OX1R and OX2R). Intracerebroventricular administration of orexin in animals increases the amount of wakefulness, accompanied by decreases in the amount of both NREM and REM sleep [10–12]. Neurons expressing orexins (orexin neurons) send projections throughout the brain and spinal cord, with particularly dense innervations to nuclei containing monoaminergic and cholinergic neurons in the hypothalamus and brainstem, which are implicated in the promotion of wakefulness and constitute the ascending reticular activating system [4, 5, 9, 13–15]. In vitro slice

electrophysiology studies have further shown that orexin increases the firing rates of monoaminergic neurons in the LC [16, 17], DR [18, 19], and tuberomammillary nucleus (TMN) [20–22], as well as the cholinergic neurons in the basal forebrain and laterodorsal tegmental nucleus (LDT) [23]. The critical roles of orexins and orexin neurons in the consolidation of wakefulness are further highlighted by the fact that the disruption of orexin signaling results in narcolepsy in mice, rats, dogs, and humans [4, 24–29]. Narcolepsy is a sleep disorder characterized by difficulties in maintaining prolonged episodes of wakefulness [30] (described in detail later).

Consistent with wake-promoting roles of orexin neurons, their activity increases during wakefulness and decreases during sleep [31–33]. However, it remains unclear whether changes in the activity of orexin neurons result in changes of sleep–wakefulness states. Since orexin neurons receive input from various brain regions, including those involved in sleep–wakefulness regulation [34, 35], changes in their activity may occur secondarily to changes in sleep–wakefulness states. Alternatively, the alterations in activity of orexin neurons may actively affect the vigilance states of animals.

To address this question, we utilized DREADD technology to artificially manipulate the activity of orexin neurons to see its consequence on sleep–wakefulness [6]. To target the expression of DREADDs specifically in orexin neurons, we injected recombinant adeno-associated virus (AAV) vectors, utilizing the flip-excision (FLEX) switch [36] that restores the open reading frame in a Cre-dependent manner, into the LHA of *Orexin-Cre* transgenic mice, in which Cre-recombinase is expressed exclusively in orexin neurons [37]. The successful targeting of the expression of DREADDs in orexin neurons was confirmed by double-immunostaining, demonstrating that hM3Dq and hM4Di were expressed in 78.3 and 73.3 % of orexin neurons, respectively, without any ectopic expression in non-orexin neurons.

Stimulation by i.p. CNO administration of excitatory hM3Dq expressed in orexin neurons significantly increased Fos expression, a marker of neuronal activity, while stimulation of inhibitory hM4Di in orexin neurons significantly decreased Fos expression in these neurons during light and dark periods, respectively. This demonstrates that the DREADD system can be used to manipulate the activity of orexin neurons. Electroencephalogram/electromyogram (EEG/EMG) recordings demonstrated that excitation of orexin neurons significantly increased the amount of time spent in wakefulness and decreased both NREM and REM sleep times, while inhibition of orexin neurons decreased wakefulness time and increased NREM sleep time (Fig. 1). These findings clearly show that changes in the activity of orexin neurons can alter the behavioral state of animals and also validate this novel approach for manipulating neuronal activity in awake, freely moving animals.
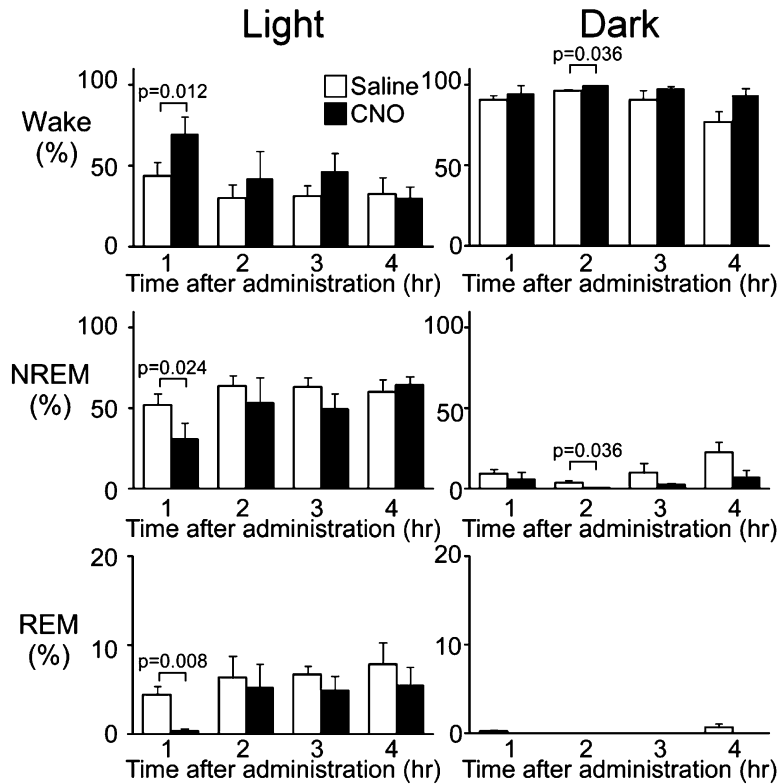
Fig. 1 Effect of stimulation of orexinergic tone by hM3Dq on vigilance states of mice during light and dark periods (*left* and *right panels*, respectively) [6]. Hourly analysis of sleep–wake states in transgenic and wild-type mice, both injected with rAAV-DIO-HAhM3Dq, after administration of CNO at ZT4 or ZT12. Amounts of wakefulness (Wake, *upper panels*), NREM sleep (*middle panels*), and REM sleep (*lower panels*) are shown

Artificial manipulation of the activity of orexin neurons was initially achieved by optogenetics: the photostimulation of orexin neurons expressing channelrhodopsin 2 increased the probability of transition to wakefulness from either NREM or REM sleep [38]. However, chronic photo-stimulation (15 ms pulses at 20 Hz for 10 s every minute for 1 h) of orexin neurons did not increase total wake time, although the number of NREM sleep-to-wake transitions was increased [39]. This fact suggests that DREADD-mediated pharmacogenetic stimulation has an advantage, evoking a greater potent and chronic stimulation of orexin neurons than ChR2-mediated photo-stimulation does, although the time resolution was less for the former than for the latter.

3 Pharmacogenetic Activation of DR Serotonergic and LC Noradrenergic Neurons Differentially Ameliorate Narcolepsy in a Mouse Model [7]

As mentioned previously, the degenerative loss of orexin neurons in humans is associated with narcolepsy (type I narcolepsy: narcolepsy with cataplexy), a debilitating neurological disorder that provides a unique perspective on the mechanisms of sleep–wakefulness control [26–28]. The narcolepsy syndrome consists of excessive daytime sleepiness that often results in sleep attacks (sudden onset of NREM sleep), cataplexy (sudden bilateral skeletal muscle weakening triggered by emotions without impairment of consciousness), hypnagogic hallucinations, and sleep paralysis. These symptoms can be divided into two independent pathological phenomena [30]. One is the inability to maintain a consolidated waking period, characterized by abrupt transitions from wakefulness to NREM sleep (i.e., dysregulation of NREM sleep onset). This phenomenon manifests clinically as excessive daytime sleepiness or sleep attacks. The other key phenomenon is the pathological intrusion of REM sleep or REM atonia into wakefulness or at sleep onset (i.e., dysregulation of REM sleep onset; normal sleep is characterized by an orderly progression from wakefulness to NREM sleep and then to REM sleep) [30]. It is during these periods that patients may experience cataplexy, hypnagogic hallucinations, and sleep paralysis.

Similarly, mice deficient in orexin signaling, such as mice lacking the *prepro-orexin* gene (*Orexin$^{-/-}$* mice), orexin neurons (*orexin/ataxin-3* mice), or orexin receptors (*OX1R$^{-/-}$; OX2R$^{-/-}$* mice), display a phenotype strikingly similar to human narcolepsy: markedly decreased duration of wakefulness episodes during the dark phase (i.e., inability to maintain a long waking period, or sleepiness) and abrupt behavioral arrests with muscle atonia (i.e., potentially cataplexy) that manifest as direct transitions from wakefulness to REM sleep in EEG/EMG recordings [4, 29, 40].

However, the precise neural mechanisms downstream of orexin neurons, which play important roles in consolidating wakefulness and inhibiting inappropriate transitions from wakefulness to NREM or REM sleep, have remained largely unknown. In vitro studies have shown that orexin activates wake-active monoaminergic and cholinergic neurons in the hypothalamus and brainstem [16–23]. However, neurons activated by the pharmacological application of exogenous orexin are not necessarily essential for the endogenous mechanisms by which orexin neurons regulate sleep–wakefulness in a physiological condition. In order to identify neurons that are directly activated by endogenous orexins and mediate their wake-stabilizing effect in a particular natural context, we searched for monoaminergic and cholinergic nuclei in which the focal rescue of orexin receptor expressions in *OX1R$^{-/-}$; OX2R$^{-/-}$* mice ameliorates

their narcoleptic phenotype. As a result, we found that the targeted restoration of orexin receptor expression in the DR and in the LC of *OX1R*$^{-/-}$*; OX2R*$^{-/-}$ mice differentially inhibited their cataplexy-like episodes and pathological fragmentation of wakefulness (i.e., sleepiness), respectively [7]. The suppression of cataplexy-like episodes was correlated with the number of serotonergic neurons restored with orexin receptor expression in the DR, while the consolidation of fragmented wakefulness was correlated with the number of noradrenergic neurons restored in the LC.

To further confirm that our conclusion originated from the receptor-restoration experiments, we used the DREADD system to examine whether the artificial activation of DR serotonergic and LC noradrenergic neurons using orexin neuron-ablated narcoleptic mice (*orexin/ataxin-3* mice) [7]. In these mice, orexin neurons degenerate postnatally due to the transgenic expression of a truncated Machado-Joseph disease gene product, mimicking the pathophysiological condition of human narcolepsy [29]. For this purpose, we generated AAV vectors encoding hM3Dq under the control of either a serotonergic neuron-selective promoter (*Pet1* promoter) [41] or a noradrenergic neurons-selective promoter (*PRSx8* promoter) [42]. Although the specificity of these neuron type-selective promoters was not perfect, causing some leaked expression, most of the neurons expressing hM3Dq were cells of interest. This suggests that these promoters were acceptable for demonstrating serotonergic or noradrenergic neuron-specific effects of neuronal activation mediated by hM3Dq when careful control experiments were combined. As described in the previous section, we could ideally target the hM3Dq expression in DR serotonergic and LC noradrenergic neurons by microinjecting AAV vectors utilizing the FLEX switch in the DR and LC of mice expressing Cre specifically in serotonergic neurons and noradrenergic neurons, respectively. However, for the purpose of this study, we needed *orexin/ataxin-3* mice that had a Cre-expressing allele, which were laborious to obtain for our experiments. Thus, we considered our approach using neuron type-selective promoters in recombinant AAV vectors to be practical.

When AAV-Pet1/hM3Dq was microinjected into the DR, *hM3Dq* mRNA expression was detected in 78.4 ± 1.5 % of serotonergic neurons in the DR, and 83.1 ± 1.0 % of *hM3Dq*(+) cells were serotonergic [7]. No *hM3Dq* mRNA expression was detected in the area surrounding the DR. I.p. administration of CNO into *orexin/ataxin-3* mice injected with AAV-Pet1/hM3Dq in the DR immediately before the start of the dark period substantially reduced the frequency of and time spent in cataplexy-like episodes during the subsequent 6 h in the dark period (Fig. 2a). In contrast, fragmentation of wakefulness was not improved by CNO administration (Fig. 2b).
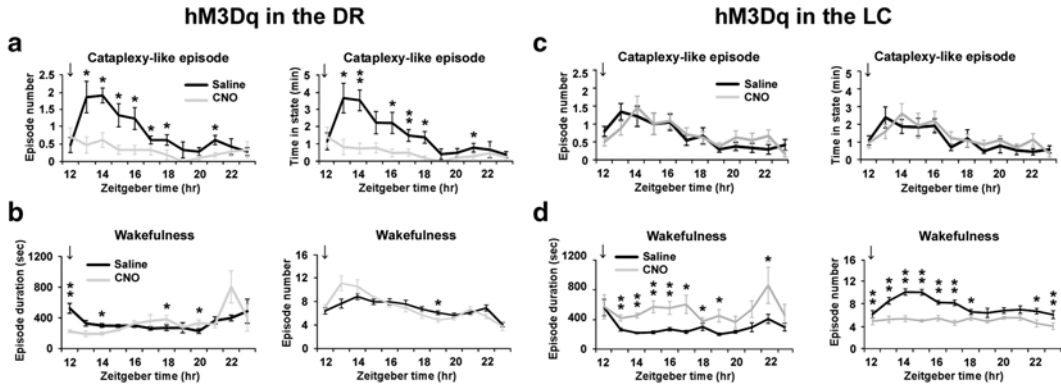
Fig. 2 Pharmacogenetic activation of DR serotonergic and LC noradrenergic neurons suppresses cataplexy-like episodes and consolidates wakefulness, respectively [7]. *Orexin/ataxin-3* mice with DR serotonergic neuron-selective (**a**, **b**) or LC noradrenergic neuron-selective (**c**, **d**) expression of hM3Dq were injected with saline or CNO. Hourly plots of number and total time of cataplexy-like episodes (**a**, **c**) or hourly plots of wakefulness duration and number (**b**, **d**) within 12 h after administration at ZT 12 (*arrows*). *$P < 0.05$, #$P < 0.01$, 2-tailed Student's paired *t* test. Values are mean ± SEM

Similarly, when AAV-PRSx8/hM3Dq was microinjected into the LC, *hM3Dq* mRNA expression was detected in 68.1 ± 3.9 % of noradrenergic neurons in the LC, and 81.1 ± 1.5 % of *hM3Dq*(+) cells were noradrenergic [7]. In these mice, the duration of wakefulness episodes during the subsequent 6 h of the dark period was significantly increased in the CNO-treated condition as compared to the saline-injected control condition (Fig. 2d). The total time spent in wakefulness during the same period was not significantly increased when CNO was administered. In contrast, the administration of CNO did not significantly affect the frequency of cataplexy-like episodes in these mice (Fig. 2c). Importantly, the wake-stabilizing effect of CNO was not observed in *orexin/ataxin-3* mice with off-target hM3Dq expression, which have similar numbers of hM3Dq-expressing cells in the regions surrounding the LC but have almost no such cells in the LC. In addition, the wake-stabilizing effect of CNO was strongly correlated with the number of *hM3Dq*(+) noradrenergic neurons in the LC noradrenergic neurons, but not with the number of *hM3Dq*(+) non-noradrenergic neurons in any of surrounding areas.

These data suggest that the pharmacogenetic activation of DR serotonergic and LC noradrenergic neurons in narcoleptic mice is sufficient to significantly suppress cataplexy-like episodes and consolidate wakefulness, respectively [7]. In addition, our success in improving narcoleptic symptoms by DREADD may lead to a novel type of gene therapy: the delivery of an artificial receptor into neurons using a viral vector—together with the subsequent administration of an artificial ligand for the receptor with the appropriate timing, in which the effectiveness, specificity, and safety of that

artificial receptor-ligand system have been well established—can be used to ameliorate symptoms of interest.

4   Pharmacogenetic Stimulation of POA GABAergic Neurons Increases NREM Sleep in Mice [8]

The POA of the hypothalamus is thought to play an important role in the initiation and maintenance of sleep. Electrical or chemical stimulation of the lateral POA in animals promotes EEG slow-wave activity and sleep onset [43–46]. Consistently, lesions in the POA have been shown to result in profound and persistent sleep loss [47, 48]. The extracellular recording studies in vivo have identified sleep-active neurons in a region extending from the medial through the lateral POA [49, 50]. In addition, neurons in the rat ventrolateral preoptic area (VLPO) and median preoptic nucleus (MPO) have been reported to drastically increase Fos expression following consolidated sleep [51, 52].

The POA sends GABAergic inhibitory projections to wake-active monoaminergic regions, including the LC, DR, and the TMN [52–55]. The VLPO receives projections from wake-active monoaminergic neurons, such as TMN histaminergic, DR serotonergic, and LC noradrenergic neurons, and electrophysiological studies have demonstrated that VLPO neurons are inhibited by noradrenaline and serotonin [56]. These facts suggest mutually inhibitory interactions between VLPO and the monoaminergic arousal systems [57].

Thus, we aimed to specifically activate GABAergic neurons in the POA using excitatory DREADD hM3Dq and examine its effects on sleep–wakefulness and on the activity of wake-promoting orexin neurons [8]. For this purpose, we injected an AAV vector containing the inverse hM3Dq cDNA in combination with the FLEX switch into the POA of Gad67-Cre mice, in which GABAergic neurons specifically express Cre recombinase. Specific stimulations of hM3Dq-expressing GABAergic neurons in the POA by i.p. CNO administrations significantly increased the amount of NREM sleep, regardless of whether CNO was administered during the light or dark phase (Fig. 3). We further confirmed direct connectivity between POA GABAergic neurons and orexin neurons, in addition to their widespread projections to wakefulness-related areas in the hypothalamus and brainstem, using channelrhodopsin 2 (ChR2) as an anterograde tracer. Optogenetic stimulation of the nerve terminals of POA GABAergic neurons on orexin neurons rapidly inhibited the activity of orexin neurons and evoked fast IPSC in slice preparations, and pharmacogenetic stimulation of POA GABAergic neurons in vivo mediated by hM3Dq significantly reduced Fos expression in orexin neurons. These
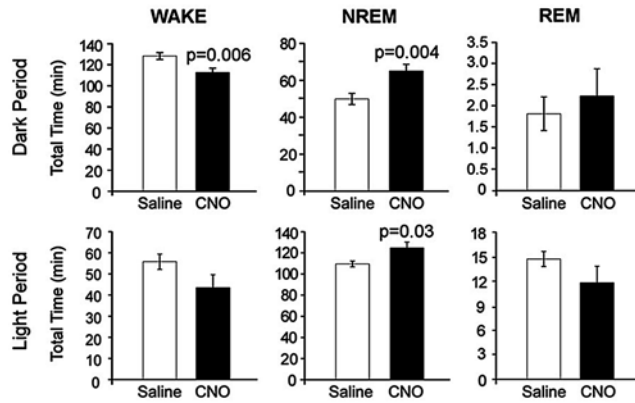
Fig. 3 Specific pharmacogenetic stimulation of GABAergic neurons in the POA increased NREM sleep amount [8]. Total time of wakefulness (WAKE), NREM sleep, and REM sleep for 3 h after CNO (or saline) administration at ZT12 (*upper panels*) and at ZT4 (*lower panels*)

observations suggest that activation of POA GABAergic neurons is sufficient to increase NREM sleep, which might be at least partly through the inhibition of orexin neurons [8].

5   Technical Considerations on the Strategy of DREADD Expression

As in the previous sections, we used recombinant AAV vectors to express DREADDs in the neurons of interest in the brain. Even with ubiquitous, powerful promoters, such as EF1α and CAG promoters, stereotaxic microinjections of AAV vectors can target the expression of transgenes in the areas of interest. Practically, however, it is difficult to perfectly restrict expression in only the small areas of interest in mice, often resulting in additional expression in the adjacent areas. Additionally, multiple types of neurons are usually intermixed within a particular brain area. Thus, Cre-dependent AAV expression vectors, utilizing the FLEX switch [36], are an excellent strategy for targeting DREADD expression, specifically in a neurochemically defined neuronal population located in a particular brain area of interest when suitable transgenic mice expressing Cre recombinase are available. Note that specificity of Cre expression is required only in the brain area of interest and its surrounding regions. Undesired Cre expression in the brain regions located apart from the area of interest (>~1 mm) is of no matter, since stereotaxic injection of AAV vectors can avoid the infection and expression in such areas. On the other, the expression of DREADDs should be confirmed in every mouse that receive AAV injections because the location and spread of AAV infection inevitably varies among individual injected mice.

Alternatively, DREADDs can, of course, be expressed by generating transgenic mice with cell-specific promoters. It is worth noting that two useful transgenic mouse lines have been developed. One expresses hM3Dq specifically in tTA (tetracycline-controlled transactivator)-expressing cells [1], while the other expresses hM4Di in Cre and/or Flp recombinase-dependent manner [58]. We also generated transgenic mice in which hM3Dq or hM4Di fused with the loxP-flanked transcriptional blocker are knocked-in in the Rosa26 allele so that DREAD receptors are expressed in a Cre-dependent manner. By using these transgenic mice in combination with other transgenic mice expressing tTA, Cre or Flp specifically in the neuronal population of interest, we can target the DREADD expression in the cells of interest with minimal variation of expression among individual mice. However, in these cases, systemic administration of CNO would result in the activation or inhibition of not only the cells of interest but also of other neurons expressing Cre or Flp in the regions of no interest. Thus, the outcomes of DREADD activation should be carefully interpreted. This problem may be resolved by focal administration of CNO in the brain area of interest [59, 60].

6   Protocols

6.1   AAV Production and Purification

First of all, it should be noted that multiple AAV vectors of DREADDs, which are purified and have high titer, are currently available from the Gene Therapy Center of the University of North Carolina at Chapel Hill (http://genetherapy.unc.edu/services.htm).

Viruses are produced using a triple-transfection, helper-free method in which the recombinant expression plasmid, containing the AAV-2 (serotype 2) inverted terminal repeat (ITR) sequences and an expression cassette of gene of interest, is co-transfected into the HEK293 cells with a helper plasmid carrying adenovirus-derived genes and a plasmid carrying AAV replication (rep) and capsid (cap) genes.

6.2   AAV Serotypes

There are many AAV serotypes available, each incorporating a different viral capsid protein and each mediating different transduction characteristics within the brain and peripheral tissues [61]. The AAV2 serotype has been most studied and utilized as a recombinant vector. However, when the expression cassette flanked by AAV2 ITRs is cross-packaged into capsid proteins of other serotypes, the hybrid AAV vectors have been reported to infect neurons more efficiently as compared to AAV2 vectors. On the other hand, AAV2 can be relatively easily purified using a heparin-agarose column [62]: purification of viral particles of other serotypes needs ultracentrifugation over either a CsCl or iodixanol gradient, which is cumbersome and expensive. Thus, we decided to utilize AAV2 vectors containing a mutant form of AAV2 capsid protein to

increase the efficiency of transgene expression (kindly provided by Dr. Arun Srivastava of the University of Florida) [63], which retains the ability to bind to heparin for purification, and this was used for the three studies described above. We will describe the protocol of viral production and purification in detail later.

Recently, it was discovered that microinjection of unpurified AAV viral solutions in the brain may not cause significant pathological damage to the tissue [64]. Therefore, we are currently using unpurified AAV vectors with capsid proteins of rh10 serotype [65], which seem to infect neurons more efficiently than mutant AAV2.

6.3 Plasmids

We initially constructed ITR-containing plasmids with DREADD cDNAs in combination with the FLEX switch by replacing ChR2::EYFP genes of pAAV-double floxed-hChR2(H134R)-EYFP-WPRE-pA [66], provided by Dr. Karl Deisseroth of Stanford University (http://www.stanford.edu/group/dlab/optogenetics/), with HA-hM3Dq or HA-hM4Di cDNAs derived from the plasmids pcDNA5/FRT-HA-hM3Dq and pcDNA5/FRT-HA-hM4Di [2], provided by Dr. Bryan Roth of University of North Carolina. Currently, mCherry-fusioned DREADDs have been developed and are available from Dr. Roth's laboratory or addgene, which are easier than using HA-tagged DREADDs to detect protein expression. Therefore, we are currently using Cre-dependent AAV vectors expressing mCherry-fusioned DREADDs.

For producing AAV-2 vectors used in the studies described previously, we used pACG-2-Y730F [63], which contains a mutant form of AAV2 capsid protein, as the rep/cap plasmid. To produce AAV-rh10 vectors, we replaced pACG-2-Y730F with pAAV2/rh10, which contains AAV2 rep gene and AAVrh10 cap gene (available from the Vector Core of the University of Pennsylvania, http://www.med.upenn.edu/gtp/vectorcore/index.shtml). For the helper plasmid carrying adenoviral genes, we used pHelper (Stratagene), but a similar helper plasmid pAd-DeltaF6 is also available from the Vector Core of the University of Pennsylvania.

6.4 HEK293 Cells

We used 293A cells (Invitrogen), which are a subclone of the HEK293 cell line and were originally established for the production of recombinant adenoviral vectors. They grow efficiently and adhere to the culture dishes better. The commonly used HEK293 cell line should work for AAV production, and another subclone AAV-293, which had been screened for AAV production, is available from Stratagene. We have no information about which 293 cells are the best for the production of recombinant AAV vectors. Note that the following protocol is on the 293A cells.

6.5 Packaging

1. Plate ~4.5×10^6 cells per 100-mm tissue culture dish in 10 ml of DMEM medium 24–28 h prior to transfection. We usually

prepare ten dishes for producing one AAV-2 vector with a purification step (the following protocol describes the amount of reagents for 10 dishes). When producing AAV-rh10 vectors without purification, we downscale to four culture dishes per vector.

2. Inspect the host cells that were split 1 day before; they should be approximately 90–100 % confluent.

3. Add 100 μg of each of the three plasmid DNA solutions: pHelper, pACG-2-Y730F, and the ITR-containing expression plasmid) to 10 ml of 0.3 M $CaCl_2$ in a 50-ml conical tube and mix gently.

4. Pipet 10 ml of 2× HBS (NaCl 8.182 g, Na_2HPO_4 0.106 g, HEPES 5.958 g/500 ml, pH 7.10, filter-sterilized; adjust pH to 7.06–7.07 because filtration slightly increases pH) into a second 50-ml conical tube. Add the 10-ml DNA/$CaCl_2$ mixture (step 3) dropwise with gentle rocking of the conical tube. Mix gently by inversion or by repeated pipetting.

5. Leave the DNA/$CaCl_2$/HBS suspension for 20 min at room temperature.

6. Apply the DNA/$CaCl_2$/HBS suspension to the dish of cells (2 ml/dish) in a dropwise fashion, swirling gently to distribute the DNA suspension evenly in the medium.

7. Return the tissue culture dishes to the 37 °C CO_2 incubator overnight.

8. At the end of the incubation period, remove the medium from the dishes and replace it with 10 ml/dish of fresh DMEM growth medium.

9. Return the dishes to the 37 °C incubator for an additional 2 days.

10. At the end of incubation, the density of cells is much higher than at transfection, with each cell appearing compressed. Most cells remain attached to the dishes.

11. Scrape and transfer the transfected cells plus DMEM growth medium to two 50-ml conical tubes.

12. Collect cells by centrifugation at ~150 g for 10 min at room temperature.

13. Discard the supernatant and resuspend the cells in binding buffer (10 ml of 0.15 M NaCl, 50 mM Tris–HCl, pH 8.0). The cells can be stored frozen in the –80 °C deep freezer for a long period before purification.

For production of AAV-rh10 vectors, wash cells once with PBS, pellet the cells, and resuspend in 400 μl (for 4 dishes) of PBS containing 1 mM of $MgCl_2$. The following steps (step 14~) are essentially same, except that we use benzonase nuclease instead of DNaseI and RNaseA, pellet cellular debris by

microcentrifuge at the maximal speed, and omit the purification step (step 19~).

6.6 Purification

14. Subject the cell suspension to two rounds of freeze–thaw by alternating the tubes between the –80 °C deep freezer and the 37 °C water bath.

15. Pellet cellular debris by centrifugation at ~2000 × g for 15 min.

16. Transfer the supernatant (~10 ml) to a fresh tube and add 40 μl of DNaseI (10 mg/ml) and 80 μl of RNaseA (5 mg/ml).

17. Incubate for 30 min in the 37 °C water bath.

18. Centrifuge the viral solution at ~2000 × g for 15 min and transfer the supernatant to a fresh tube.

19. Add 500 μl (1/20 volume) of 10 % Sodium deoxycholate to the viral solution, and then incubate it for 30 min in the 37 °C water bath.

20. Centrifuge the viral solution at ~2000 × g for 15 min and recover the supernatant.

21. Pass the viral solution through a 5 μm-syringe filter, then through a 0.4 μm-syringe filter.

22. (In parallel to the treatment of the viral solution, prepare heparin-agarose resin) Transfer 1.5 ml of Heparin-agarose suspension (Sigma) into a 15-ml conical tube with 5 ml of binding buffer.

23. Centrifuge the Heparin-agarose suspension for a minute, discard the supernatant, and wash the Heparin-agarose with another 5 ml of biding buffer.

24. Centrifuge the Heparin-agarose suspension for a minute and discard the supernatant. Add the viral solution prepared in step 21 to the Heparin-agarose.

25. Suspend the viral solution/Heparin-agarose by rocking at 4 °C for 1 h.

26. Transfer the viral solution/Heparin-agarose into a bio-spin column (Bio-Rad) and allow the column to empty by gravity flow.

27. Wash the Heparin-agarose resin three times with 2 ml of binding buffer.

28. Add 1 ml of elution buffer (0.5 M NaCl, 50 mM Tris, pH 8.0) to the resin and collect the eluate in a fresh tube.

29. Cap the tip of column, add another 1 ml of elution buffer, and leave the column for 5 min.

30. Remove the cap at the tip of column and collect the eluate in the tube.

31. Add another 1 ml of elution buffer to the column and collect the eluate (total ~3 ml of eluate).

6.7 Dialysis and Concentration

32. Transfer the eluate containing AAV particles into a Slide-A-Lyzer Dialysis Cassette (Pierce, Slide-A-Lyzer Gamma Irradiated Dialysis Cassete Extra-strength, 0.5–3 ml, 10,000 MWCO) and dyalize it against 1 l of PBS (KH_2PO_4 0.144 g, NaCl 9.0 g, $Na_2HPO_4 \cdot 12H_2O$ 1.062 g, $MgCl_2 \cdot 6H_2O$ 0.10 g, $CaCl_2 \cdot 2H_2O$ 0.133 g/1 l, pH 7.4, filter-sterilized; adjust pH to 7.36–7.37 because filtration slightly increases pH) overnight at 4 °C. Change the dialysate once.

33. Concentrate the dialyzed viral solution by placing the Dialysis Cassette into the Slide-A-Lyzer Concentration Solution (Pierce) inside the resealable plastic bag and rock the bag for 60–90 min at 4 °C.

34. Recover the concentrated viral solution from the cassette, make aliquots, freeze rapidly, and store at –80 °C. Typically, we can obtain 400–800 µl of concentrated viral solution.

35. Measure the titer of the viral stocks by real-time PCR. Prior to PCR, 2 µl of viral solution is pretreated in 100 µl of 50 mM NaOH for 30 min at 95 °C to liberate AAV genome DNA from viral particles, followed by neutralization by adding 8.4 µl of 1 M Tris–HCl pH 8.0. Further dilute the DNA solution 20-fold and use 2.5 µl of diluted solution per PCR reaction in 10 µl. Use serial dilution of ITR-containing plasmid as the reference to write standard curves for calculating viral titers. We amplify the WPRE sequence, which is contained in most of the recombinant AAV vectors we generated, by Roche LightCycler 480 using two primers 5′-actgtgtttgctgacgcaac-3′ and 5′-agcgaaagtcccggaaag-3′ in combination with an universal probe #77. When using other types of real-time PCR reagents and cyclers, primer sequences may need to be optimized. Typically, we obtain final viral stocks with the titer of 2×10^{12}–2×10^{13} genome copies/ml.

6.8 Surgery of Mice

Male mice (10–20 weeks old) were anesthetized with sodium pentobarbital (0.5 mg/kg, i.p.) and positioned in a stereotaxic frame (David Kopf Instruments). For microinjection of viral solutions, we used the Hamilton syringe (10 µl, 701RN) in combination with a 33-gage needle (1 in. long).

The coordinates for injection sites depend on the location and size of the area of interest. The following are the coordinates we used, with reference to the bregma; anteroposterior, AP ("–" means posterior to the bregma); mediolateral, ML ("±" means bilateral injections); dorsoventral, DV ("–" means ventral to the skull surface):

LHA (targeting orexin neurons) [6]: AP, –1.4 mm; ML, ±0.9 mm; DV, –5.5 mm; and AP, –1.8 mm; ML, ±0.9 mm; DV, –5.7 mm. Since orexin neurons are scattered in the LHA and perifornical area, we microinjected viruses in four sites. LC: AP, –5.4 mm; ML, ±0.9 mm; DV, –3.7 mm. DR: AP, –4.4 mm; ML, ±0 mm; DV, –3.0 and

–3.5 mm. TMN: AP, –2.5 mm; ML, ±1.0 mm; DV, –5.6 mm. PPT: AP, –4.5 mm; ML, ±1.0 mm; DV, –3.7 mm. PB: AP, –5.4 mm; ML, ±1.0 mm bilaterally; DV, –3.5 mm [7]. POA: AP, +0.3 mm; ML, ±0.65 mm; DV, –5.72 mm [8]. Note that the coordinates of injection may need to be optimized for each experimenter and mouse age and strain.

Small holes were drilled into the skull at the position corresponding to the injection sites, and the needle was inserted slowly and progressively to minimize tissue damage until the tip of needle reaches to the injection site. Then, 0.2–1 μl of viral solution was delivered to each site over a 10-min period using KDS310 Nano Pump Syringe Pumps (KD Scientific). After 5 min of rest, the needles were slowly removed. Injection using 33-gage stainless needles caused minimal tissue damage in most cases. However, when relatively small nuclei are targeted, the thickness of the needle and the volume of viral solution injected may cause broader infection than expected. Microinjection of smaller volume using fine glass micropipettes would be more suitable for finer expression, although targeting small volume to very restricted areas might make the targeting technically more difficult. From this perspective, the Cre-dependent expression system utilizing the FLEX switch is a useful strategy to target the expression into the cells of interest in spite of the broader infection of AAV vectors in the surrounding cells/areas.

Following virus administration, electrodes for EEG and EMG recording were implanted in the skull of each mouse [4, 6–8]. The EEG/EMG implant was based on a six-pin double inline microcomputer connector, modified to form four EEG electrodes and two EMG wire electrodes soldered to the pins. Four holes were drilled on the skull, and the four arms of the EEG electrode were placed anterior and posterior to the bregma (AP, +1.2 mm; ML, ±1.2 mm and AP, –1.2 mm; ML, ±1.2 mm). Stainless steel wires for EMG recording were bilaterally sutured to the neck muscles of each mouse, and each electrode was glued solidly to the skull.

Silicon tubes (Shinetsu Polymer, CP-N, outside diameter: 1 mm, inside diameter: 0.5 mm) were implanted for remote CNO injection [6, 8]. The tube was implanted subcutaneously from the abdominal to the neck. The tip of a 30 cm-long silicon tube was inserted 1 cm into the peritoneal cavity and sutured to the abdominal wall. The other end of the silicon tube was placed outside the body through an incision in the neck, and all incisions were sutured. Implanting silicon tubes minimizes the disturbance due to the CNO administrations. Alternatively, the CNO can be administered i.p. by conventional injections using syringes and needles with proper acclimations to the injection before the experiments, reducing the invasiveness of surgery [7].

All animals were then housed individually for a recovery period of at least 7 days. Generally, transgene expression by AAV vectors plateaued about 2 weeks after injection.

6.9 Sleep Recordings

After the recovery period, animals were moved to a recording cage placed in an electrically shielded and sound-attenuated room. A cable for signal output was connected to the implanted electrode and animals were allowed to move freely. Signals were amplified through an amplifier (AB-611J, Nihon Koden, Tokyo) and digitally recorded on a PC using EEG/EMG recording software (Vital recorder, Kissei Comtec). Animals were allowed at least 7 days to adapt to the recording conditions prior to any EEG/EMG recording session. Following the adaptation period, each animal was injected with both CNO and saline on separate experimental days with at least a 2-days interval. The order of injection (i.e., either CNO first or saline first) should be randomized. EEG/EMG data were evaluated and staged for 24 h on the day of CNO or saline administration. Data acquired on the day of saline administration were used as controls [6–8].

6.10 Histological Confirmation of DREADD Expression

After EEG/EMG recordings, efficiency and specificity of DREADD expression should be determined histologically. Mouse brains were fixed by transcardial perfusion with 4 % paraformaldehyde and serial coronal brain sections were prepared by standard procedures. Immunostaining with a mouse anti-HA antibody (Covance, 1:1000) detects HA-tagged DREADDs expressed at relatively high level [1, 6, 8]. However, the sensitivity of detection is not good enough to detect low-level expression. Thus, as an alternative method, DREADD mRNA can be detected by nonradioisotope in situ hybridization using digoxigenin-labeled antisense riboprobes for DREADDs [7]. Using mCherry-fusioned DREADDs makes it much easier to check their expression, by the fluorescence of mCherry or immunostaining with rabbit anti-DsRed antibody (Clontech 632496, 1:2000).

7 Conclusion

Overall, there are clear benefits to using DREADD technology in the analysis of neural circuits underlying sleep–wakefulness regulation. We successfully manipulated the activity of neurons involved in sleep–wake regulation and detected the effects of manipulation. The same strategy can be applicable to other types of neurons, which may lead to the understanding of the whole picture of how our vigilance states are controlled, and further to a novel therapeutical approach to multiple sleep disorders, such as insomnia and narcolepsy.

References

1. Alexander GM, Rogan SC, Abbas AI et al (2009) Remote control of neuronal activity in transgenic mice expressing evolved G protein-coupled receptors. Neuron 63:27–39

2. Armbruster BN, Li X, Pausch MH et al (2007) Evolving the lock to fit the key to create a family of G protein-coupled receptors potently activated by an inert ligand. Proc Natl Acad Sci U S A 104:5163–5168

3. Yizhar O, Fenno LE, Davidson TJ et al (2011) Optogenetics in neural systems. Neuron 71: 9–34

4. Chemelli RM, Willie JT, Sinton CM et al (1999) Narcolepsy in orexin knockout mice: molecular genetics of sleep regulation. Cell 98:437–451

5. Sakurai T, Amemiya A, Ishii M et al (1998) Orexins and orexin receptors: a family of hypothalamic neuropeptides and G protein-coupled receptors that regulate feeding behavior. Cell 92:573–585

6. Sasaki K, Suzuki M, Mieda M et al (2011) Pharmacogenetic modulation of orexin neurons alters sleep/wakefulness states in mice. PLoS One 6, e20360

7. Hasegawa E, Yanagisawa M, Sakurai T, Mieda M (2014) Orexin neurons suppress narcolepsy via 2 distinct efferent pathways. J Clin Investig 124:604–616

8. Saito YC, Tsujino N, Hasegawa E et al (2013) GABAergic neurons in the preoptic area send direct inhibitory projections to orexin neurons. Front Neural Circ 7:192

9. de Lecea L, Kilduff TS, Peyron C et al (1998) The hypocretins: hypothalamus-specific peptides with neuroexcitatory activity. Proc Natl Acad Sci U S A 95:322–327

10. Hagan JJ, Leslie RA, Patel S et al (1999) Orexin A activates locus coeruleus cell firing and increases arousal in the rat. Proc Natl Acad Sci U S A 96:10911–10916

11. Piper DC, Upton N, Smith MI, Hunter AJ (2000) The novel brain neuropeptide, orexin-A, modulates the sleep-wake cycle of rats. Eur J Neurosci 12:726–730

12. Mieda M, Hasegawa E, Kisanuki YY et al (2011) Differential roles of orexin receptor-1 and -2 in the regulation of non-REM and REM sleep. J Neurosci 31:6518–6526

13. Peyron C, Tighe DK, van den Pol AN et al (1998) Neurons containing hypocretin (orexin) project to multiple neuronal systems. J Neurosci 18:9996–10015

14. Nambu T, Sakurai T, Mizukami K et al (1999) Distribution of orexin neurons in the adult rat brain. Brain Res 827:243–260

15. Date Y, Ueta Y, Yamashita H et al (1999) Orexins, orexigenic hypothalamic peptides, interact with autonomic, neuroendocrine and neuroregulatory systems. Proc Natl Acad Sci U S A 96:748–753

16. Horvath TL, Peyron C, Diano S et al (1999) Hypocretin (orexin) activation and synaptic innervation of the locus coeruleus noradrenergic system. J Comp Neurol 415:145–159

17. van den Pol AN, Ghosh PK, Liu RJ et al (2002) Hypocretin (orexin) enhances neuron activity and cell synchrony in developing mouse GFP-expressing locus coeruleus. J Physiol 541: 169–185

18. Liu RJ, van den Pol AN, Aghajanian GK (2002) Hypocretins (orexins) regulate serotonin neurons in the dorsal raphe nucleus by excitatory direct and inhibitory indirect actions. J Neurosci 22:9453–9464

19. Brown RE, Sergeeva O, Eriksson KS, Haas HL (2001) Orexin A excites serotonergic neurons in the dorsal raphe nucleus of the rat. Neuropharmacology 40:457–459

20. Bayer L, Eggermann E, Serafin M et al (2001) Orexins (hypocretins) directly excite tuberomammillary neurons. Eur J Neurosci 14:1571–1575

21. Eriksson KS, Sergeeva O, Brown RE, Haas HL (2001) Orexin/hypocretin excites the histaminergic neurons of the tuberomammillary nucleus. J Neurosci 21:9273–9279

22. Yamanaka A, Tsujino N, Funahashi H et al (2002) Orexins activate histaminergic neurons via the orexin 2 receptor. Biochem Biophys Res Commun 290:1237–1245

23. Burlet S, Tyler CJ, Leonard CS (2002) Direct and indirect excitation of laterodorsal tegmental neurons by Hypocretin/Orexin peptides: implications for wakefulness and narcolepsy. J Neurosci 22:2862–2872

24. Lin L, Faraco J, Li R et al (1999) The sleep disorder canine narcolepsy is caused by a mutation in the hypocretin (orexin) receptor 2 gene. Cell 98:365–376

25. Beuckmann CT, Sinton CM, Williams SC et al (2004) Expression of a poly-glutamine-ataxin-3 transgene in orexin neurons induces narcolepsy-cataplexy in the rat. J Neurosci 24:4469–4477

26. Nishino S, Ripley B, Overeem S et al (2000) Hypocretin (orexin) deficiency in human narcolepsy. Lancet 355:39–40

27. Peyron C, Faraco J, Rogers W et al (2000) A mutation in a case of early onset narcolepsy and a generalized absence of hypocretin peptides in human narcoleptic brains. Nat Med 6:991–997

28. Thannickal TC, Moore RY, Nienhuis R et al (2000) Reduced number of hypocretin neurons in human narcolepsy. Neuron 27:469–474

29. Hara J, Beuckmann CT, Nambu T et al (2001) Genetic ablation of orexin neurons in mice results in narcolepsy, hypophagia, and obesity. Neuron 30:345–354

30. Sakurai T (2007) The neural circuit of orexin (hypocretin): maintaining sleep and wakefulness. Nat Rev Neurosci 8:171–181

31. Lee MG, Hassani OK, Jones BE (2005) Discharge of identified orexin/hypocretin neurons across the sleep-waking cycle. J Neurosci 25:6716–6720

32. Mileykovskiy BY, Kiyashchenko LI, Siegel JM (2005) Behavioral correlates of activity in identified hypocretin/orexin neurons. Neuron 46:787–798

33. Takahashi K, Lin JS, Sakai K (2008) Neuronal activity of orexin and non-orexin waking-active neurons during wake-sleep states in the mouse. Neuroscience 153:860–870

34. Sakurai T, Nagata R, Yamanaka A et al (2005) Input of orexin/hypocretin neurons revealed by a genetically encoded tracer in mice. Neuron 46:297–308

35. Yoshida K, McCormack S, Espana RA et al (2006) Afferents to the orexin neurons of the rat brain. J Comp Neurol 494:845–861

36. Atasoy D, Aponte Y, Su HH, Sternson SM (2008) A FLEX switch targets Channelrhodopsin-2 to multiple cell types for imaging and long-range circuit mapping. J Neurosci 28:7025–7030

37. Matsuki T, Nomiyama M, Takahira H et al (2009) Selective loss of GABA(B) receptors in orexin-producing neurons results in disrupted sleep/wakefulness architecture. Proc Natl Acad Sci U S A 106:4459–4464

38. Adamantidis AR, Zhang F, Aravanis AM et al (2007) Neural substrates of awakening probed with optogenetic control of hypocretin neurons. Nature 450:420–424

39. Carter ME, Adamantidis A, Ohtsu H et al (2009) Sleep homeostasis modulates hypocretin-mediated sleep-to-wake transitions. J Neurosci 29:10939–10949

40. Hondo M, Nagai K, Ohno K et al (2010) Histamine-1 receptor is not required as a downstream effector of orexin-2 receptor in maintenance of basal sleep/wake states. Acta Physiol (Oxf) 198:287–294

41. Scott MM, Krueger KC, Deneris ES (2005) A differentially autoregulated Pet-1 enhancer region is a critical target of the transcriptional cascade that governs serotonin neuron development. J Neurosci 25:2628–2636

42. Hwang DY, Carlezon WA Jr, Isacson O, Kim KS (2001) A high-efficiency synthetic promoter that drives transgene expression selectively in noradrenergic neurons. Hum Gene Ther 12:1731–1740

43. Benedek G, Obal F Jr, Lelkes Z, Obal F (1982) Thermal and chemical stimulations of the hypothalamic heat detectors: the effects of the EEG. Acta Physiol Acad Sci Hung 60:27–35

44. Mendelson WB, Martin JV (1992) Characterization of the hypnotic effects of triazolam microinjections into the medial preoptic area. Life Sci 50:1117–1128

45. Sterman MB, Clemente CD (1962) Forebrain inhibitory mechanisms: cortical synchronization induced by basal forebrain stimulation. Exp Neurol 6:91–102

46. Ticho SR, Radulovacki M (1991) Role of adenosine in sleep and temperature regulation in the preoptic area of rats. Pharmacol Biochem Behav 40:33–40

47. John J, Kumar VM (1998) Effect of NMDA lesion of the medial preoptic neurons on sleep and other functions. Sleep 21:587–598

48. Lu J, Greco MA, Shiromani P, Saper CB (2000) Effect of lesions of the ventrolateral preoptic nucleus on NREM and REM sleep. J Neurosci 20:3830–3842

49. Kaitin KI (1984) Preoptic area unit activity during sleep and wakefulness in the cat. Exp Neurol 83:347–357

50. Koyama Y, Hayaishi O (1994) Firing of neurons in the preoptic/anterior hypothalamic areas in rat: its possible involvement in slow wave sleep and paradoxical sleep. Neurosci Res 19:31–38

51. Gong H, Szymusiak R, King J et al (2000) Sleep-related c-Fos protein expression in the preoptic hypothalamus: effects of ambient warming. Am J Physiol Regul Integr Comp Physiol 279:R2079–R2088

52. Sherin JE, Shiromani PJ, McCarley RW, Saper CB (1996) Activation of ventrolateral preoptic neurons during sleep. Science 271:216–219

53. Sherin JE, Elmquist JK, Torrealba F, Saper CB (1998) Innervation of histaminergic tuberomammillary neurons by GABAergic and galaninergic neurons in the ventrolateral preoptic nucleus of the rat. J Neurosci 18:4705–4721

54. Steininger TL, Gong H, McGinty D, Szymusiak R (2001) Subregional organization of preoptic area/anterior hypothalamic projections to arousal-related monoaminergic cell groups. J Comp Neurol 429:638–653

55. Uschakov A, Gong H, McGinty D, Szymusiak R (2007) Efferent projections from the median preoptic nucleus to sleep- and arousal-regulatory nuclei in the rat brain. Neuroscience 150:104–120

56. Gallopin T, Fort P, Eggermann E et al (2000) Identification of sleep-promoting neurons in vitro. Nature 404:992–995

57. Saper CB, Chou TC, Scammell TE (2001) The sleep switch: hypothalamic control of sleep and wakefulness. Trends Neurosci 24:726–731

58. Ray RS, Corcoran AE, Brust RD et al (2011) Impaired respiratory and body temperature control upon acute serotonergic neuron inhibition. Science 333:637–642

59. Stachniak TJ, Ghosh A, Sternson SM (2014) Chemogenetic synaptic silencing of neural circuits localizes a hypothalamus/midbrain pathway for feeding behavior. Neuron 82:1–12

60. Mahler SV, Vazey EM, Beckley JT et al (2014) Designer receptors show role for ventral pallidum input to ventral tegmental area in cocaine seeking. Nat Neurosci 17:577–585

61. Gao G, Vandenberghe LH, Wilson JM (2005) New recombinant serotypes of AAV vectors. Curr Gene Ther 5:285–297

62. Auricchio A, Hildinger M, O'Connor E et al (2001) Isolation of highly infectious and pure adeno-associated virus type 2 vectors with a single-step gravity-flow column. Hum Gene Ther 12:71–76

63. Zhong L, Li B, Mah CS et al (2008) Next generation of adeno-associated virus 2 vectors: point mutations in tyrosines lead to high-efficiency transduction at lower doses. Proc Natl Acad Sci U S A 105:7827–7832

64. Lazarus M, Shen HY, Cherasse Y et al (2011) Arousal effect of caffeine depends on adenosine A2A receptors in the shell of the nucleus accumbens. J Neurosci 31:10067–10075

65. Klein RL, Dayton RD, Tatom JB et al (2008) AAV8, 9, Rh10, Rh43 vector gene transfer in the rat brain: effects of serotype, promoter and purification method. Mol Ther 16:89–96

66. Tsai HC, Zhang F, Adamantidis A et al (2009) Phasic firing in dopaminergic neurons is sufficient for behavioral conditioning. Science 324:1080–1084

DREADD'ed Addiction: Using Designer Receptors to Delineate Neural Circuits Underlying Drug-Seeking Behaviors

Sunila G. Nair, Denis Smirnov, and John F. Neumaier

Abstract

One of the important problems in the treatment of addiction is the vulnerability of previously addicted individuals to relapse to drug use months or even years after abstinence. Longitudinal, retrospective, and laboratory studies suggest that important factors in drug relapse are exposure to cues previously associated with the reinforcer, exposure to small amounts of the reinforcer itself, or exposure to stressful situations. Thus, studying the neuronal circuitry underlying relapse is critical for the development of effective treatments for addiction. Though studies of relapse to drug seeking using experimental animals, primarily rodents, have provided invaluable information on the neurobiological basis of relapse, the precise neurochemical events that contribute to the various forms of relapse are still not completely understood. Furthermore, treatments available to treat relapse to drug addiction are almost non-existent, suggesting that significant efforts need to be concentrated in delineating the role of distinct neural circuits and cell types within these circuits in the mechanisms underlying drug relapse. In the recent years, much research has been directed at identifying and validating sophisticated new technologies that allow investigators to modulate the activity of specific neurons within a brain region or a neural circuit with unprecedented precision. Here, we describe methods based upon recent advances in molecular biology techniques, using the Designer Receptor Exclusively Activated by Designer Drug (DREADD) technology to identify the role of modulation of neuronal activity within a brain region and in discrete neural circuits during complex behavioral tasks. These techniques will serve as valuable tools not only to parse out the neural circuitry that underlies addictive behaviors, but will also be useful to the neuroscience community in understanding the biological bases of other neuropsychiatric disorders.

Key words Addiction, Designer receptors exclusively activated by designer drugs (DREADDs), Lateral habenula, Viral-mediated gene transfer

1 Background and Introduction

A major problem in the treatment of drug addiction is the high rate of relapse to drugs of abuse following a prolonged abstinence period [1]. Results from studies in humans suggest that in drug-free individuals relapse to drug use during periods of forced or voluntary abstinence can be triggered by acute exposure to the

self-administered drug [2], stimuli previously associated with drug taking [3], or stressors [4]. Acute exposure to the self-administered drug or related drugs, drug-associated cues, or stress also reinstates drug seeking in laboratory rats and monkeys [5]. Because of the similarities between the human condition and the laboratory animal model, the use of the animal model (commonly known as the "reinstatement model") to elucidate the mechanisms underlying relapse to drug seeking has seen a dramatic increase in recent years.

In the drug self-administration version of the reinstatement model, which is based on an operant-conditioning procedure, laboratory animals (rats, mice, monkeys) are initially trained to self-administer drugs by lever pressing (or nose-poking—also commonly used as the operant response) for intravenous drug infusions (or for oral delivery of alcohol). Subsequently, the drug-reinforced behavior is extinguished by substituting the drug solutions with saline or by disconnecting the infusion pumps while providing repeated exposures to the drug cues in the operant chamber. After extinction of the drug-reinforced behavior, the ability of acute non-contingent exposure to drugs (termed "drug priming") [6], drug-associated cues [7], or stress [8] to reinstate lever responding is measured under extinction conditions. The non-reinforced responding on the "active lever"—the lever that previously delivered the drug—is interpreted to reflect reinstatement of drug seeking. The responding on the "inactive lever"—the lever that has not been associated with drug injections—is often interpreted to reflect nonspecific activity, but it may also reflect response generalization [9].

In addition to using the operant self-administration procedure to study relapse, researchers also commonly assess reinstatement of drug seeking in a variation of the reinstatement model that is based on the "conditioned place preference" procedure. In this version of the reinstatement model, animals are trained over several days to associate one environment with injections of a drug and a second distinct environment with vehicle injections. Over the course of training, animals learn to associate the drug-paired environment with drug availability and consequently, when given a choice between the two environments during "test day" (conducted in a drug-free state), animals typically spend significantly more time in the drug-paired environment, indicating a preference for the environment previously associated with drug experience. Similar to the drug self-administration version of the reinstatement model, the preference for the drug-paired environment can be extinguished by pairing this environment with saline over days. Subsequent exposure to drug injections reliably reinstates preference for the drug-paired environment. However, since the total amount of drug intake by experimental animals is relatively low and is non-contingently administered, this model mimics occasional recreational drug use at best. Despite these limitations, the conditioned place preference procedure is relatively more commonly

used to study relapse since it is technically less challenging and less labor intensive than the drug self-administration procedure, which requires intravenous surgical expertise and continuous monitoring of jugular catheters to ensure patency during the course of the experiment.

Despite the availability of these sophisticated models to study relapse, in addition to decades of research that has gone into studying mechanisms that contribute to relapse to drug seeking, the neuronal processes that underlie this phenomenon are not completely understood. Further, there are no effective treatments currently available to treat drug relapse in addicts. This clearly indicates that much research still needs to be done to delineate specific neural circuits and precise cell types within these neural circuits that mediate relapse-related behaviors.

In recent years, several sophisticated technologies using engineered receptors activated by light or by synthetic ligands have been developed. These techniques can be used to modulate the activity of cells of interest with remarkable spatial, temporal, and phenotypic precision. In this chapter, we focus on the use of designer receptors that can be activated by synthetic ligands in examining the neuronal mechanisms that underlie relapse to drug seeking behaviors. For strategies on modulation of neuronal activity using light-activated receptors the reader is referred to detailed reviews that specifically cover this topic [10, 11].

2 DREADDs

2.1 Modulation of Signaling Pathways Using DREADDs

The use of ligand-dependent engineered receptors called *D*esigner *R*eceptors *E*xclusively *A*ctivated by *D*esigner *D*rugs (DREADDs) to selectively modulate neuronal activity is steadily increasing in popularity in recent years. These receptors consist of a family of evolved muscarinic receptors that were engineered by molecular evolution and site-directed mutagenesis in the laboratory of Dr. Bryan Roth at the University of North Carolina [12]. These receptors are the latest addition to the development of ligand–receptor pairs designed to remotely control signaling mediated via different classes of G-protein-coupled receptors (previously called RASSLs for Receptors Activated Solely by Synthetic Ligands). The DREADDs display high affinity for clozapine-N-oxide (CNO), a ligand with negligible binding to known neuroreceptors, while losing affinity for their original cognate endogenous ligand, acetylcholine [12, 13]. Three DREADD receptors have been described to date; the $G_{i/o}$-coupled receptor (also called hM_4D_i) that activates $G\alpha_i$ signaling, the G_s-coupled receptor (also called rM_3Ds) that activates $G\alpha_s$ signaling, and the G_q-coupled receptor (also called hM_3D_q) that activates $G\alpha_q$ signaling. All DREADDs share the same point mutations at $Y^{3.33}C$ and $A^{5.46}G$ that alter the respon-

siveness of these receptors, making them insensitive to acetylcholine and rendering them capable of being selectively activated by CNO. CNO has high CNS penetrance and can be administered by relatively noninvasive methods, such as intraperitoneal injections, addition to drinking water, etc. which enables modulation of G-protein-coupled signaling pathways in desired brain regions with minimal invasiveness. Recently, CNO has also been microinfused into discrete brain regions, allowing investigators to use it as a tool to turn off local neurotransmitter release to modulate neuronal activity with a high degree of spatial precision [14, 15]. Following transduction of DREADDs into neurons in a specific brain region, administration of CNO will stimulate these receptors and initiate downstream signaling pathways that can activate (via $G\alpha_s$ or $G\alpha_q$) or inhibit (via $G\alpha_i$) cells that express the receptors. Mechanistically, activation of hM_4D_i with CNO activates potassium channels, resulting in membrane hyperpolarization and transient inhibition of neuronal activity. Recently, Stachniak et al. [15], in an elegant electrophysiological study, demonstrated that hM_4D_i activation not only leads to hyperpolarization, but also significantly suppresses presynaptic neurotransmitter release that leads to transient inhibition of neuronal activity. In contrast, activation of rM_3D_s or hM_3D_q increases neuronal activity by increasing intracellular signaling cascades or induction of burst firing of neurons, respectively. However, each of these signaling pathways are more complex than simply inducing or inhibiting neuronal firing; rather, activating each of these pathways may also impact gene expression, plasticity, and modulate other signaling pathways. Low levels of DREADD expression can still be highly effective in vivo [16], minimizing the likelihood that unstimulated DREADDs have undesired effects on host cells. DREADDs generally do not demonstrate constitutive activity in vivo (with the exception of rM_3D_s that exhibits constitutive activity in pancreatic beta cells [17], but definitely does not do so in striatal neurons [16]).

A related technique, optogenetics, involves transgenic expression of engineered proteins that can be activated by light to depolarize or hyperpolarize neurons, or activate a G-protein-coupled receptor [10, 11]; this powerful strategy has gained immense popularity in recent years. While optogenetic receptors can be controlled instantaneously with local application of laser light, CNO can be administered systemically and will activate DREADDs on a time scale that is more typical for drug-receptor interactions (i.e., minutes to a few hours). Combined with viral-mediated gene transfer or transgenic expression, DREADDs provide us with a powerful strategy to examine the role of neurons in a specific brain region on behavior because (1) the same methodology can be applied to stimulate as well as inhibit neuronal activity (using different DREADDs, even simultaneously), (2) it exhibits precise anatomical accuracy since CNO will activate only expressed

DREADD receptors without off-target effects, (3) DREADDs can be activated "remotely" by systemically or orally administered CNO, or by local CNO infusion if preferred, (4) activation of DREADDs is ligand-driven, unlike a neurotoxic lesion, and can be timed to coincide with different aspects of behavior, and (5) this technology allows us to localize the site of manipulation precisely by visualizing the expression of DREADD-fluorescent protein fusion proteins directly or by detecting transgenes with immuno-histochemistry. While optogenetics allows subsecond precision in activating neurons or even axon terminals [18, 19], the DREADD approach allows for brief, repeated activation of the engineered receptors at key points during a complex behavioral task over many days [20] without any implantation of fiber-optics, making it less invasive. In addition to neurons, DREADDs have also been targeted at nucleus accumbens shell astrocytes to demonstrate that modulation of glial G-protein-coupled signaling can alter ethanol self-administration [21]. In our laboratory, we have previously used hM_4Di ($G_{i/o}$-coupled DREADD) expressed with viral vectors to selectively target the direct or indirect striatal pathways to show that these pathways play opposing roles in psychostimulant-induced plasticity [22]. It is intriguing that this DREADD affected behavioral plasticity associated with repeated amphetamine exposure without disrupting acute behavioral responses mediated by the striatal circuitry. We have also used both hM_4D_i and hM_3D_q with viral vectors to demonstrate that inhibition and activation of the direct pathway has opposing effects on the plasticity involved in a decision-making task [20]. More recently, we have begun to use DREADDs to examine the role of the lateral habenula (LHb), an understudied epithalamic nucleus, in operant cocaine self-administration and relapse behaviors that will serve as illustrations of how DREADDs can be used to study the precise functional neurocircuitry involved in these behavioral models of addiction.

2.2   Packaging   In addition to transgenic mouse strategies, DREADDs can be packaged into several common viral vectors such as herpes simplex virus 1(HSV), adeno-associated virus (AAV), and lentivirus. The factors that are commonly considered in choosing a vector for virus-mediated gene transfer are (1) the cell types that can be targeted by the virus, (2) the time-course of expression of the transgene (which includes both the onset as well as the duration of expression), (3) the size of the gene/genes that can be packaged, and (4) whether/not the gene is integrated into the host genome. We have used the HSV and AAV vector systems for transducing DREADDs into discrete brain regions successfully; the advantages and disadvantages of these systems are briefly discussed below.

We have used the HSV vector system for more than a decade in our laboratory to express a broad range of receptors and other proteins [23, 24]. The main advantage of this viral vector system is

that it has a very high specificity for neurons and has the largest payload capacity, readily allowing the incorporation of promoters, multiple gene cassettes, etc. In addition, when used with the HSV promoter the onset of transgene expression is fairly rapid (<24 h) with peak expression at 3–4 days. In addition, the vector does not integrate into the host genome. The disadvantages of the HSV system (with the HSV promoter) are that the transgene dissipates after about 6–7 days post-transduction. Further, the number of neurons transduced using HSV-mediated gene transfer is usually lower than the transduction following AAV or lentivirus-mediated gene transfer. However, this limitation of HSV makes it highly suited as a viral vector to transduce genes into small brain regions, such as the lateral habenula (Fig. 1).

In contrast to HSV, expression of transgenes with AAV vectors is relatively slow in onset (1–2 weeks) but long term in duration (months). This makes it possible to perform multiple experiments in the same cohort of animals in a counterbalanced fashion, which is especially useful when performing complex behavioral experiments to study mechanisms of relapse, which are described in Section 3. In addition, AAV vectors have high titres and the inflammatory response generated by infusion of these vectors is minimal. Further, commercial packaging is widely available for these vectors. The limitation of this vector system is the size of the payload that can be incorporated, which is usually less than 3 kb; AAV is thus not the vector of choice for packaging large genes. Furthermore, there are many AAV serotypes in common usage and the field is not in agreement regarding the relative usefulness and cell specificity of even the most commonly used serotypes.

In our experience, the efficiency of transduction with either viral vector depends upon (1) the volume and titre of viral vector infusion, (2) the rate of infusion, (3) the phenotype of neurons in the targeted brain region, and (4) in the case of AAV, the serotype of the viral vector, which is discussed briefly below.

Several serotypes of AAV are commonly available for gene delivery and these include AAV1, 5, 7, 8, 9, etc. While AAV2 is the most extensively used serotype, it has relatively low transduction efficiency. To enhance transduction efficiency, a common strategy is to construct hybrid AAV vectors by packaging recombinant AAV2 genomes into capsids derived from other AAV serotypes. For instance, in AAV 2/5, the genome is based on recombinant AAV2, while the capsid is based on AAV5. There are various studies comparing the efficiency of these various AAV serotypes and hybrids in diverse model systems [25–28]. Taken together, the results from these studies are largely inconclusive. This may be due to a variety of factors such as differences in model systems employed for viral transduction, differences in procedures employed in the generation of the vectors, procedural differences involved in transduction of the model system either in vitro or in vivo, etc. Here, we

A. HSV-hM$_4$D$_i$ transgene amplicon
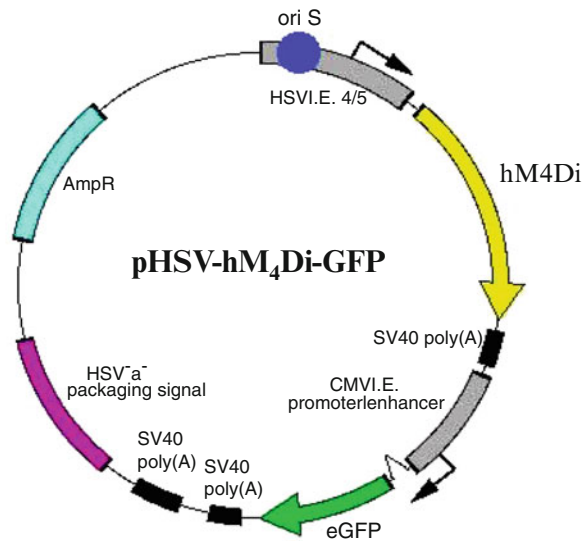
B. Viral vector infusion site
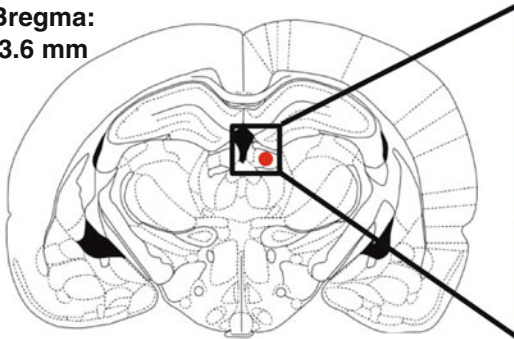
C. Representative image of LHb viral vector injection
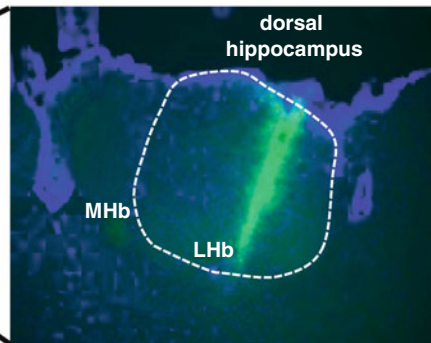
Fig. 1 HSV-mediated gene transfer (**a**) Illustration of the herpes simplex virus-hM$_4$D$_i$ green fluorescent protein transgene amplicon (**b**) Illustration of rat brain coordinates (Paxinos plate 32, −3.6 mm) used for viral vector infusion. The *red* oval depicts the target zone for the viral vector unilaterally. *MHb* Medial habenula, *LHb* Lateral habenula (**c**) Representative histological plate of demonstrating herpes simplex viral vector injection from a coronal section of the LHb 4 days after viral vector infusion

have compared the transduction efficiency of AAV vectors of serotypes 5 and 8 of comparable titres (as measured by dot blot) carrying the DREADD gene (Fig. 3). Under our procedural conditions (described below in detail), we find significantly greater transduction with AAV8 compared to AAV5 in rat lateral habenula neurons, with both Cre-dependent and non Cre-dependent versions of these viral vectors (Fig. 3).

A. Floxed viral vector design

B. Viral vector infusion site

C. Representative image DIO-AAV5- hM$_4$D$_i$ in the LHb and CAV-Cre in the VTA
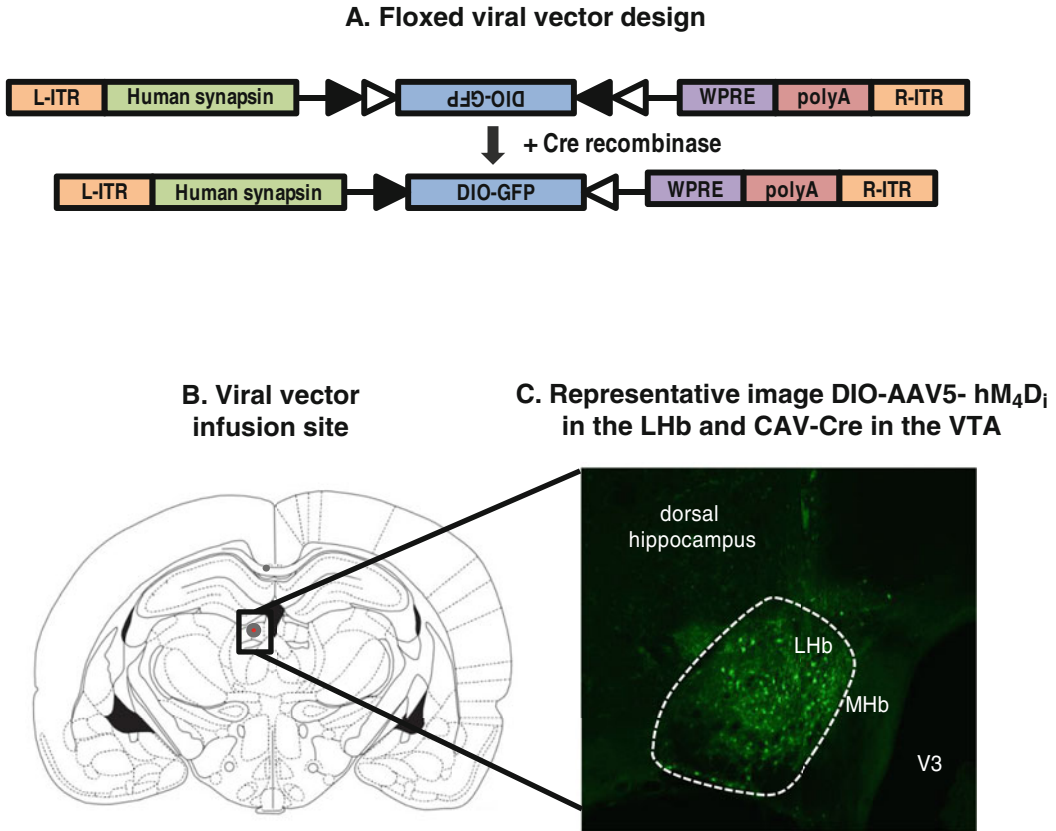
Fig. 2 Dual virus DIO strategy (**a**) Illustration of the DIO Viral vector design. L-ITR: Left inverted terminal repeat, R-ITR: Right inverted terminal repeat, WPRE: Woodchuck hepatitis post-transcriptional regulatory el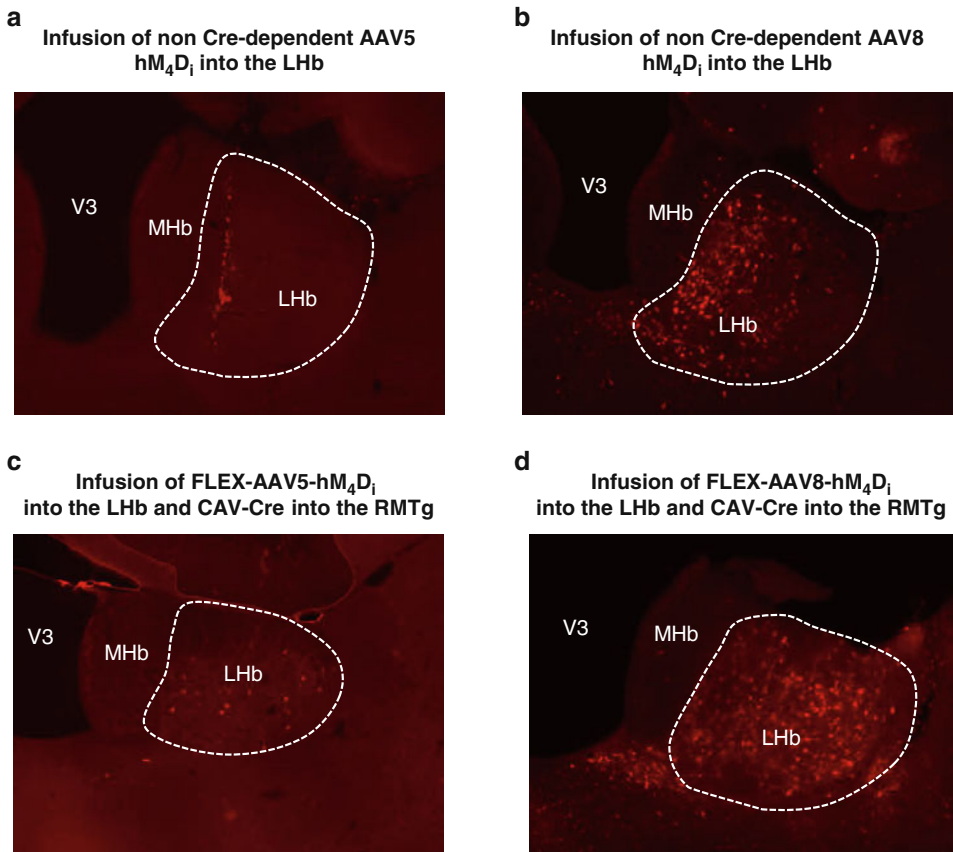ement (**b**) Illustration of LHb rat brain coordinates (Paxinos plate 32, −3.6 mm) used for viral vector infusion. The *red* oval depicts the target zone for the viral vector bilaterally. *MHb* Medial habenula, *LHb* Lateral habenula (**c**) Representative histological plate of demonstrating viral vector injection from a coronal section of the LHb approximately 3 weeks after viral vector infusion (DIO-GFP injected into the LHb and Canine adenovirus expressing Cre injected into the VTA. The GFP signal is enhanced using an anti-GFP antibody)

2.3 Promoter-Driver Expression

Viral vectors that express DREADD transgenes under the control of cell-specific promoters can serve as a powerful tool to manipulate G-protein-coupled signaling in a highly specific group of neurons within a brain region. An important factor that must be taken into consideration while constructing cell-type specific viral vectors is the amount of genetic material that can be packaged which, as stated earlier, depends on the type of viral vector. Nonessential sequences must be removed from the construct to generate the shortest length of the promoter that retains its function. The onset and duration of expression of the viral vector depends largely on the promoter that drives expression of the transgene. For instance,

a
Infusion of non Cre-dependent AAV5 hM$_4$D$_i$ into the LHb

b
Infusion of non Cre-dependent AAV8 hM$_4$D$_i$ into the LHb

c
Infusion of FLEX-AAV5-hM$_4$D$_i$ into the LHb and CAV-Cre into the RMTg

d
Infusion of FLEX-AAV8-hM$_4$D$_i$ into the LHb and CAV-Cre into the RMTg

Fig. 3 Comparison of AAV5 and AAV8 viral vectors (**a**, **b**) Representative histological plate from a coronal section of the LHb approximately 3 weeks after viral vector infusion of AAV5 and AAV8, respectively. The mCherry signal is enhanced using a ds-Red antibody for AAV5 (**c**, **d**) Representative histological plate from a coronal section of the LHb approximately 3 weeks after viral vector infusion of Cre-dependent AAV5 and AAV8 respectively (DIO-hM$_4$D$_i$ injected into the LHb and Canine adenovirus expressing Cre injected into the RMTg. The mCherry signal is enhanced using a ds-Red antibody for AAV5)

in our laboratory we commonly use HSV vectors driven by the HSV1 IE 4/5 promoter that has a rapid onset of expression (less than a day), with peak expression at 3–5 days after which expression rapidly begins to dissipate and is entirely gone by 1 week [29]. In contrast, when a neuropeptide promoter (preprodynorphin or preproenkephalin) is used to drive transgene expression the onset of expression is delayed (detectable at ~7 days), and expression is fairly stable for a couple of months post-injection [22]. Pilot experiments must be performed to determine the onset and duration of transgene expression when working with novel viral vectors. The efficiency of gene expression will vary with each promoter but is likely to be somewhat lower than that observed with the very powerful viral promoters such as the HSV1 IE 4/5 promoter.

2.4   Single and Dual Vector Strategies

2.4.1   Single Virus

For the single-virus approach, we have used both HSV and AAV-mediated gene transfer with DREADDs in our laboratory. While we have observed significant behavioral effects upon modulation of G-protein-coupled signaling with both viral vectors [30, 31], we generally see greater degree of transduction with AAV (Figs. 2 and 3).

2.4.2   Dual Virus DIO Strategy

While a number of brain regions have been identified in mediating relapse to various reinforcers, little is known about the circuitry underlying relapse-related behaviors. In order to study the role of functional neural circuits *during* complex behavioral tasks, we have recently implemented a variation of a recently developed dual virus DIO (double-floxed inverted open reading frame) strategy [32], also referred to as FLEX (FLip and EXcise) switch vectors. This elegant method is a variant of the Cre-lox system that we are currently using in our laboratory to study the functional significance of LHb projections to its major targets—the dopaminergic ventral tegmental area (VTA), the serotonergic dorsal raphe nucleus, the GABAergic rostromedial tegmental nucleus (RMTg), and the cholinergic laterodorsal tegmentum, in drug-reinforced behaviors and relapse. The viruses used for this technique encode a DREADD transgene that is doubly floxed by lox sites, so that Cre recombinase inverts, but does not excise the transgene. The floxed transgene is cloned into the construct in a 3′ to 5′ orientation relative to the promoter, and Cre recombines the DNA such that the transgene is now "flipped" into a 5′ to 3′ orientation to allow transcription. We injected a DIO-$G_{i/o}$-coupled DREADD transgene with adeno-associated virus (Fig. 2) into the LHb of male Long-Evans rats (400–425 g) and then injected canine adenovirus-2 (CAV-2) expressing Cre into neurons that project from LHb to the VTA. CAV-2 efficiently infects axon terminals and is retrogradely transported to the neuronal cell bodies in the LHb where it expresses Cre [30, 33, 34]. The DIO-$G_{i/o}$-coupled DREADD transgene is coupled to a reporter gene (e.g., mCherry) that can be conveniently visualized. Thus, the DIO-DREADD vector can only lead to expression in neurons that are retrogradely infected with Cre, where the DIO-DREADD is flipped into the proper orientation to allow transcription (Fig. 2). We observe no leakage expression with this system whatsoever if Cre is not introduced. This general approach using floxed, inverted DREADDs, where the DREADD is fused to mCherry to monitor receptor expression, has also been applied in mice with genetic/viral Cre expression [35] and more recently in rats [34].

3 Methods

3.1 Equipment, Materials etc

In our laboratory, we typically use Long-Evans rats (350–425 g) for operant self-administration and reinstatement experiments. Rats are initially double-housed and allowed to acclimate to the vivarium for at least 1 week prior to the start of behavioral experiments. Animals are handled 3–4 times prior to the start of behavioral procedures. Food and water are available ad libitum. All experimental procedures must receive approval of local Institutional Animal Care and Use Committees. Additionally, since viral vectors involve recombinant DNA technology and gene transfer, investigators must consult with their local Biosafety Committees that determine the safety and use of all biological materials prior to initiating the use of any viral vector mediated technology. In our experience, the procedures that relate to the use of personal protective equipment required for both preparation as well as use of viruses for in vitro and in vivo work are dependent upon (1) the type of viral vector used and (2) the Institutional Biosafety Committee. In the United States, there are four biosafety levels (Level 1–4), and each biosafety level is associated with a distinct set of personal-safety related rules. The Institutional Biosafety Committee works in collaboration with the Institutional Environmental Health and Use committee to determine the biosafety level of all biological materials. For instance, we are required to use Biosafety Level 2 precautions in our laboratory for packaging Herpes Simplex Viral Vectors that utilizes replication-deficient helper virus. Subsequently, we perform plaque assays to confirm that each batch of virus is indeed replication-deficient, after which that specific batch of virus can be used by investigators with Biosafety Level 1 precautions.

3.2 Stereotaxic Injections

Following the acclimation period, rats are implanted with jugular venous catheters as described [36], following which stereotaxic surgery is performed to deliver viral vectors expressing DREADD transgenes into discrete brain regions. In our laboratory, rats are anesthetized with 3 % isoflurane. Once the animals are in the surgical plane of anesthesia (as evidenced by the absence of the eye blink reflex and withdrawal response to toe pinch) the head of the animal is shaved and prepared with povidine iodine and ethanol. The rat is placed on a heating pad to maintain body temperature and a lubricant eye ointment is applied to the eyes to ensure adequate moisture is provided during surgery. Rats are placed in a Stoelting stereotaxic apparatus, the scalp is incised, skull landmarks are visualized by scraping the periosteum and burr holes are drilled in the skull. A 27 gauge dental needle is directed to the targeted brain region stereotaxically using anatomical co-ordinates from the Paxinos and Watson rat atlas. The 27 gauge needle is connected to polyethylene tubing (PE-20) which is connected to a 10 μl
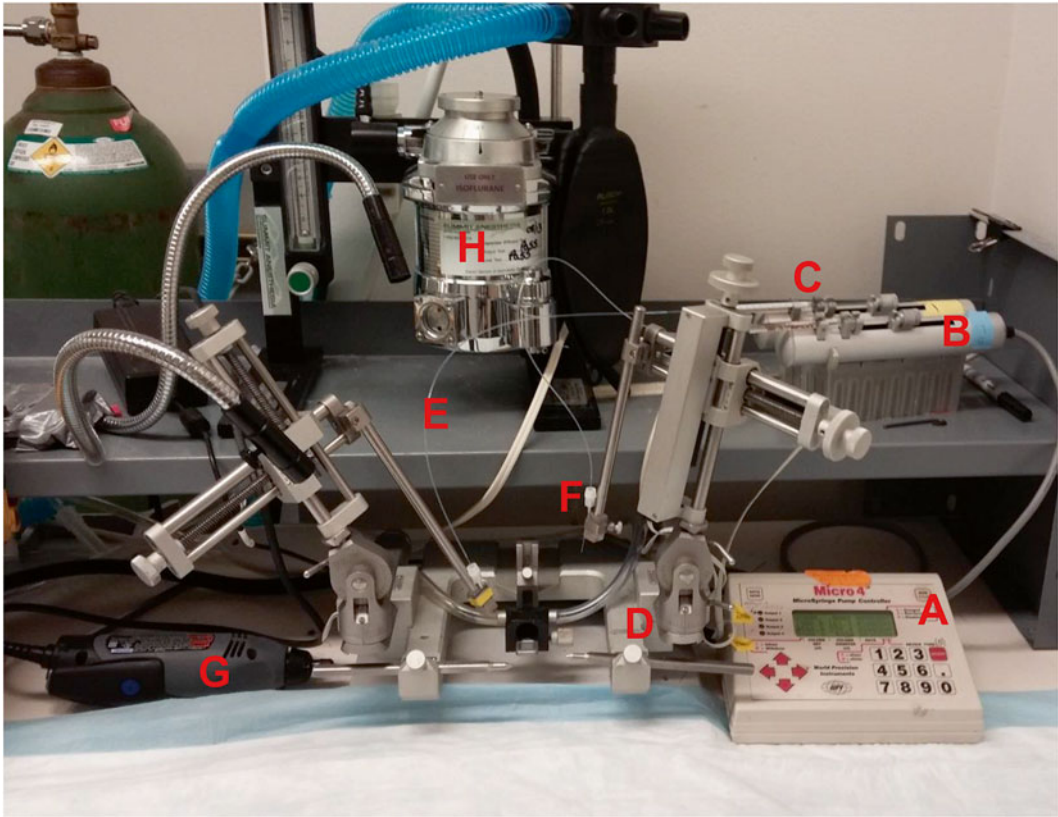
Fig. 4 Stereotaxic set-up for virus-mediated gene transfer (**a**) Microsyringe pump controller (**b**) Microsyringe pump (**c**) Hamilton syringe (**d**) Stoelting stereotaxic apparatus (**e**) PE-20 tubing (**f**) Dental needle (**g**) Drill (**h**) Apparatus for isofluorane anesthesia

Hamilton syringe that is controlled by a microprocessor driven pump. The stereotaxic set-up used for virus-mediated gene transfer used in our laboratory is depicted in Fig. 4. The Hamilton syringe, polyethylene tubing and dental needles are filled with sterile H_2O. Viral vector (that is always stored on ice during the surgery) is backfilled into the dental needle immediately prior to injection. The needle is gradually lowered into the brain and the viral vector is slowly infused into the target brain region at the rate of 0.2–0.4 μl/min. The volume of viral vector injected depends largely on the size of the targeted brain region, the nature of cell types in the targeted brain region, the type of viral vector, and the titer of infectious particles. For instance, herpes simplex viral vector-induced transduction (HSV) is neuron-specific and localized; 1–2 μl of viral vector injection transduces large numbers of neurons because of the high neuronal binding affinity of HSV. In contrast adeno-associated virus (AAV) that transduces both neurons and glia has a greater tendency to spread beyond the site of injection. Infusing viral vector volumes greater than 2 μl can possibly lead to local

toxic effects; multiple lower volume injections can be made to cover large brain regions. Following viral vector injection, the injector is left in place for an additional 5 min to minimize diffusion of the viral vector up the injector tract and withdrawn slowly to minimize withdrawal of the viral vector back into the injector tract. The cranial incision is closed with sterile 3-0 monofilament nylon sutures and may be augmented with sterile *n*-butyl cyanoacrylate glue (VetBond). Buprenorphine (0.1 mg/kg, s.c.), meloxicam (0.2 mg/kg, s.c.) or other analgesics approved by the Institutional Animal Care and Use Committee are administered for post-surgical analgesia. Animals are closely monitored until recovery from anesthesia and during the post-operative recovery period. The onset and duration of transgene expression is largely dependent on the promoter that drives expression and pilot experiments are performed to determine these parameters prior to any behavioral testing. For dual viral vector experiments, prior to injecting rats with viral vectors, we target neuronal projections from one brain region to the other anatomically using a combination of anterograde and retrograde tracers using conventional fluorescent tracing tools (TAMRA-Lys-Dextran and fluorescent FluoSpheres). The methods used for the injection of tracers are identical to the methods used for infusion of viral vectors described above with the exception of injection volumes and dilution, which is in accordance with the manufacturer's instructions.

3.3 Behavior: Self-Administration, Extinction, and Reinstatement

Behavioral testing is performed once transgene expression levels are stabilized. When using viral vectors with rapid onset and short duration of expression, behavioral training may be interrupted to infuse viral vectors. To study operant self-administration behaviors, typically rats are trained to self-administer drugs of abuse (or non-drug reinforcers) for 10–15 days under varying reinforcement schedules. For a description of various reinforcement schedules the reader is directed to the following descriptive behavioral neuroscience articles [37, 38]. Following reinforcement training, rats infused previously with DREADD receptors intracranially are injected with intraperitoneal CNO prior to each test session in a counterbalanced fashion to activate the DREADDs. Since the activity of DREADDs is ligand-dependent, we and others typically utilize a within-subjects experimental design for these complex behavioral experiments [14, 31]. Doses of CNO generally used for rats to modulate G-protein-coupled signaling in vivo range between 1 and 3 mg/kg (injected 20–30 min prior to the test) [20, 22, 31], although doses as high as 20 mg/kg i.p. have been reported in the literature [14]. In our opinion, doses higher than 3–5 mg/kg i.p. are likely to produce off-target effects and should be avoided. For reinstatement tests, following self-administration training, the active lever presses are extinguished over a duration of 10–12 days (duration of extinction varies according to the pharmacological

properties of the reinforcer). Following extinction, the operant response is typically reinstated by exposure to small amounts of the drug itself, exposure to a cue/cues previously associated with the reinforcer or by exposure to various stressors [9]. The commonly used stressors in the reinstatement field are intermittent footshock (0.5–1 mA administered non-contingently for 10–15 min prior to the start of the test session) [8, 39], and yohimbine (an alpha2 adrenoceptor antagonist that produces anxiogenic effects in humans and in experimental animals) [40, 41]. Rats are injected with CNO prior to extinction sessions or reinstatement sessions to determine the effect of modulation of G-protein-coupled signaling (depending of which DREADD is expressed) in discrete brain regions on extinction responding and/or reinstatement of drug seeking. In our experience, as well as from a recently published study [14, 31], repeated injections of CNO do not influence behavioral responding on subsequent tests, as long as testing days are separated by an interval of at least 24 h to allow for complete drug clearance. Experimental timelines for reinstatement experiments using HSV and AAV vectors are depicted in Fig. 5. Results from our behavioral experiments using DREADDs in combination with virus-mediated gene transfer in rats indicate that activation of $G_{i/o}$-coupled signaling in LHb neurons increases operant cocaine self-administration, while activation of G_q-coupled signaling in these neurons decreases cocaine intake. Further, our initial results using the dual vector technology indicate that activation of $G_{i/o}$-coupled signaling in LHb neurons projecting to the VTA does not influence operant cocaine self-administration, but decreases reinstatement of cocaine seeking induced by a priming injection of cocaine [31, 42].

3.4 Perfusion, Immunohistochemistry and Microscopy

For verification of expression of the transgene, all rats are perfused at the end of the behavioral experiment. In our laboratory, rats are deeply anesthetized with a combination of pentobarbital sodium and phenytoin sodium. Once the corneal reflex is absent and the rat is unresponsive to paw pinch we proceed to perfuse the rat. Intracardiac perfusions are performed with 100 ml of phosphate-buffered saline followed by 200 ml of 4 % paraformaldehyde, both at pH 7.4 and stored on ice for the duration of perfusion. The rat brains are dissected and post-fixed in 4 % paraformaldehyde for 24 h, after which they were placed in phosphate-buffered saline. Coronal sections (40 µm) were made on a Leica VT 1000S microtome, mounted and coverslipped with VECTASHIELD mounting medium (VectorLabs, Burlingame, CA). The sections were subsequently examined for immunofluorescence on a Nikon Eclipse E600 microscope. While microscopy can be used to visualize fluorescent proteins such as GFP and mCherry, we and others routinely detect a few-fold increase in the number of cells when the signal for the reporter transcript is enhanced using immunohistochemistry.

A. Experimental design using HSV vectors
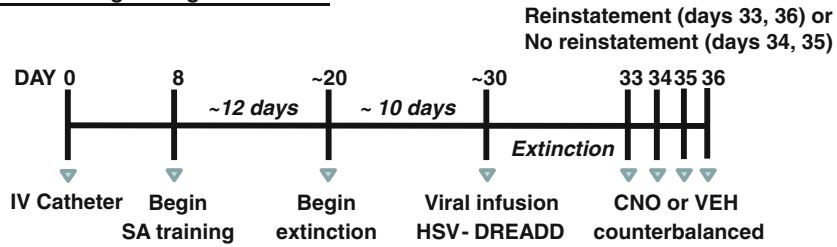
B. Experimental design using AAV vectors
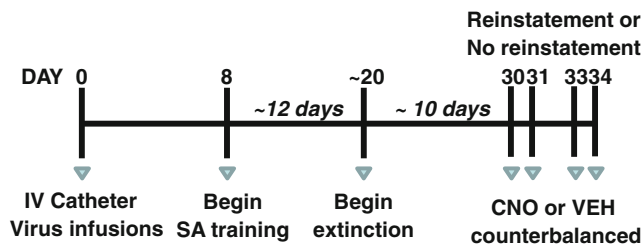
Fig. 5 Recommended experimental designs for reinstatement experiments using HSV and AAV vectors. *IV* intravenous, *SA* self-administration, *CNO* clozapine-N-oxide

Representative images are depicted in Figs. 1 and 2. We typically examine brain sections for immunofluorescence of the reporter gene instead of measuring the number of DREADD receptors since these receptors get translocated away from the site of injection and hence cannot be reliably quantified. If the viral vector is under the control of a specific promoter that restricts the expression of the transgene to a specific cell type, dual immunohistochemistry should be performed to confirm that the transgene markers co-localize with neuronal markers of the specific cell type.

4   Summary

In this chapter, we have highlighted the use of DREADDs as tools to study the role of various brain regions and neural circuits during complex behaviors. DREADDs can be used in conjunction with a variety of viral vectors the choice of which depends largely upon the initiation and duration of transgene expression in accordance with key elements of the behavioral testing procedure. Transgene expression can be easily verified with histological techniques following completion of behavioral testing. Further, expression of the DREADD transgene can be driven by a variety of different promoters to selectively target a specific phenotype of neurons within a brain region or neural circuit. In the future, the use of

promoter-driven DREADDs coupled with viral vector (and transgenic) strategies is likely to yield significantly useful information on the mechanisms underlying addictive behaviors and other complex behavioral questions in neuroscience.

References

1. O'Brien CP (1997) Progress in the science of addiction. Am J Psychiatry 154:1195–1197

2. de Wit H (1998) Individual differences in acute effects of drugs in humans: their relevance to risk for abuse. NIDA Res Monogr 169:176–187

3. O'Brien CP, Childress AR, McLellan AT, Ehrman R (1992) Classical conditioning in drug-dependent humans. Ann N Y Acad Sci 654:400–415

4. Sinha R, Fuse T, Aubin LR, O'Malley SS (2000) Psychological stress, drug-related cues and cocaine craving. Psychopharmacology (Berl) 152:140–148

5. Shaham Y, Shalev U, Lu L, De Wit H, Stewart J (2003) The reinstatement model of drug relapse: history, methodology and major findings. Psychopharmacology (Berl) 168:3–20

6. Stretch R, Gerber GJ (1973) Drug-induced reinstatement of amphetamine self-administration behaviour in monkeys. Can J Psychol 27:168–177

7. Davis WM, Smith SG (1976) Role of conditioned reinforcers in the initiation, maintenance and extinction of drug-seeking behavior. Pavlov J Biol Sci 11:222–236

8. Shaham Y, Stewart J (1995) Stress reinstates heroin-seeking in drug-free animals: an effect mimicking heroin, not withdrawal. Psychopharmacology (Berl) 119:334–341

9. Shalev U, Grimm JW, Shaham Y (2002) Neurobiology of relapse to heroin and cocaine seeking: a review. Pharmacol Rev 54:1–42

10. Zhang F, Gradinaru V, Adamantidis AR, Durand R, Airan RD, de Lecea L, Deisseroth K (2010) Optogenetic interrogation of neural circuits: technology for probing mammalian brain structures. Nat Protoc 5:439–456

11. Fenno L, Yizhar O, Deisseroth K (2011) The development and application of optogenetics. Annu Rev Neurosci 34:389–412

12. Armbruster BN, Li X, Pausch MH, Herlitze S, Roth BL (2007) Evolving the lock to fit the key to create a family of G protein-coupled receptors potently activated by an inert ligand. Proc Natl Acad Sci U S A 104:5163–5168

13. Rogan SC, Roth BL (2011) Remote control of neuronal signaling. Pharmacol Rev 63:291–315

14. Mahler SV, Vazey EM, Beckley JT, Keistler CR, McGlinchey EM, Kaufling J, Wilson SP, Deisseroth K, Woodward JJ, Aston-Jones G (2014) Designer receptors show role for ventral pallidum input to ventral tegmental area in cocaine seeking. Nat Neurosci 17:577–585

15. Stachniak TJ, Ghosh A, Sternson SM (2014) Chemogenetic synaptic silencing of neural circuits localizes a hypothalamus→midbrain pathway for feeding behavior. Neuron 82:797–808

16. Farrell MS, Pei Y, Wan Y, Yadav PN, Daigle TL, Urban DJ, Lee HM, Sciaky N, Simmons A, Nonneman RJ, Huang XP, Hufeisen SJ, Guettier JM, Moy SS, Wess J, Caron MG, Calakos N, Roth BL (2013) A Galphas DREADD mouse for selective modulation of cAMP production in striatopallidal neurons. Neuropsychopharmacology 38:854–862

17. Guettier JM, Gautam D, Scarselli M, Ruiz de Azua I, Li JH, Rosemond E, Ma X, Gonzalez FJ, Armbruster BN, Lu H, Roth BL, Wess J (2009) A chemical-genetic approach to study G protein regulation of beta cell function in vivo. Proc Natl Acad Sci U S A 106:19197–19202

18. Adamantidis AR, Tsai HC, Boutrel B, Zhang F, Stuber GD, Budygin EA, Tourino C, Bonci A, Deisseroth K, de Lecea L (2011) Optogenetic interrogation of dopaminergic modulation of the multiple phases of reward-seeking behavior. J Neurosci 31:10829–10835

19. Stuber GD, Sparta DR, Stamatakis AM, van Leeuwen WA, Hardjoprajitno JE, Cho S, Tye KM, Kempadoo KA, Zhang F, Deisseroth K, Bonci A (2011) Excitatory transmission from the amygdala to nucleus accumbens facilitates reward seeking. Nature 475:377–380

20. Ferguson SM, Phillips PE, Roth BL, Wess J, Neumaier JF (2013) Direct-pathway striatal neurons regulate the retention of decision-making strategies. J Neurosci 33:11668–11676

21. Bull C, Freitas KC, Zou S, Poland RS, Syed WA, Urban DJ, Minter SC, Shelton KL, Hauser KF, Negus SS, Knapp PE, Bowers MS (2014) Rat nucleus accumbens core astrocytes modulate reward and the motivation to self-administer ethanol after abstinence. Neuropsychopharmacology 39:2835–2845

22. Ferguson SM, Eskenazi D, Ishikawa M, Wanat MJ, Phillips PE, Dong Y, Roth BL, Neumaier JF (2011) Transient neuronal inhibition reveals opposing roles of indirect and direct pathways in sensitization. Nat Neurosci 14:22–24

23. Clark MS, Sexton TJ, McClain M, Root D, Kohen R, Neumaier JF (2002) Overexpression of 5-HT1B receptor in dorsal raphe nucleus using Herpes Simplex Virus gene transfer increases anxiety behavior after inescapable stress. J Neurosci 22:4550–4562

24. Neumaier JF, Edwards E, Plotsky PM (2002) 5-HT(1B) mrna regulation in two animal models of altered stress reactivity. Biol Psychiatry 51:902–908

25. Aschauer DF, Kreuz S, Rumpel S (2013) Analysis of transduction efficiency, tropism and axonal transport of AAV serotypes 1, 2, 5, 6, 8 and 9 in the mouse brain. PLoS One 8, e76310

26. Chen C, Akerstrom V, Baus J, Lan MS, Breslin MB (2013) Comparative analysis of the transduction efficiency of five adeno associated virus serotypes and VSV-G pseudotype lentiviral vector in lung cancer cells. Virol J 10:86

27. Holehonnur R, Luong JA, Chaturvedi D, Ho A, Lella SK, Hosek MP, Ploski JE (2014) Adeno-associated viral serotypes produce differing titers and differentially transduce neurons within the rat basal and lateral amygdala. BMC Neurosci 15:28

28. Dirren E, Towne CL, Setola V, Redmond DE Jr, Schneider BL, Aebischer P (2014) Intracerebroventricular injection of adeno-associated virus 6 and 9 vectors for cell type-specific transgene expression in the spinal cord. Hum Gene Ther 25:109–120

29. Barot SK, Ferguson SM, Neumaier JF (2007) 5-HT(1B) receptors in nucleus accumbens efferents enhance both rewarding and aversive effects of cocaine. Eur J Neurosci 25:3125–3131

30. Nair SG, Strand NS, Neumaier JF (2013) DREADDing the lateral habenula: a review of methodological approaches for studying lateral habenula function. Brain Res 1511:93–101

31. Nair SG, Smirov D, Neumaier JF (2014) DREADD'ed addiction: Investigating the effect of DREADD-mediated modulation of G-protein coupled signaling in lateral habenula neurons projecting to the ventral tegmental area on cocaine self-administration and reinstatement. Society for Neuroscience Abstract 233.09/W32

32. Atasoy D, Aponte Y, Su HH, Sternson SM (2008) A FLEX switch targets Channelrhodopsin-2 to multiple cell types for imaging and long-range circuit mapping. J Neurosci 28:7025–7030

33. Kremer EJ, Boutin S, Chillon M, Danos O (2000) Canine adenovirus vectors: an alternative for adenovirus-mediated gene transfer. J Virol 74:505–512

34. Boender AJ, de Jong JW, Boekhoudt L, Luijendijk MC, van der Plasse G, Adan RA (2014) Combined use of the canine adenovirus-2 and DREADD-technology to activate specific neural pathways in vivo. PLoS One 9, e95392

35. Krashes MJ, Koda S, Ye C, Rogan SC, Adams AC, Cusher DS, Maratos-Flier E, Roth BL, Lowell BB (2011) Rapid, reversible activation of AgRP neurons drives feeding behavior in mice. J Clin Invest 121:1424–1428

36. Nair SG, Furay AR, Liu Y, Neumaier JF (2013) Differential effect of viral overexpression of nucleus accumbens shell 5-HT1B receptors on stress- and cocaine priming-induced reinstatement of cocaine seeking. Pharmacol Biochem Behav 112:89–95

37. Roberts DC, Morgan D, Liu Y (2007) How to make a rat addicted to cocaine. Prog Neuropsychopharmacol Biol Psychiatry 31:1614–1624

38. Morgan D, Liu Y, Oleson EB, Roberts DC (2009) Cocaine self-administration on a hold-down schedule of reinforcement in rats. Psychopharmacology (Berl) 201:601–609

39. Shaham Y, Funk D, Erb S, Brown TJ, Walker CD, Stewart J (1997) Corticotropin-releasing factor, but not corticosterone, is involved in stress-induced relapse to heroin-seeking in rats. J Neurosci 17:2605–2614

40. Nair SG, Adams-Deutsch T, Epstein DH, Shaham Y (2009) The neuropharmacology of relapse to food seeking: methodology, main findings, and comparison with relapse to drug seeking. Prog Neurobiol 89:18–45

41. Nair SG, Navarre BM, Cifani C, Pickens CL, Bossert JM, Shaham Y (2011) Role of dorsal medial prefrontal cortex dopamine D1-family receptors in relapse to high-fat food seeking induced by the anxiogenic drug yohimbine. Neuropsychopharmacology 36:497–510

42. Nair SG, Smirnov D, Neumaier JF (2013) Effect of DREADD-mediated modulation of G-protein coupled signaling in the lateral habenula on cocaine reinforced operant responding. Society for Neuroscience Abstract 733.10/FF2

Chapter 9

DREADDs in *Drosophila melanogaster*

Charles D. Nichols and Jaime Becnel

Abstract

The fruit fly, *Drosophila melanogaster*, is a powerful genetic model organism that has been crucial for our current understanding of human biology and behavior. Key features of this system include powerful genetic methods, sophisticated behaviors, and conservation of fundamental aspects of development and physiology with mammals. There have been several methods of conditional control of neuronal activity developed for the fly; however, they are primarily switch-like, and/or require expensive and dedicated equipment. We recently adapted Designer Receptors Exclusively Activated by Designer Receptors (DREADD) technology to the fly to provide convenient and true dose responsive conditional control of neuronal activity and behaviors in *Drosophila*. Significantly, the DREADD system also allows for analysis of signal transduction effectors and second messengers not only in neurons, but conceivably any other tissue in the fly. This chapter is intended to provide practical guidance on the use of in the model organism *Drosophila melanogaster*. A brief introduction on the usefulness of the fly as a model system is provided, followed by sections relevant to the use of DREADDs in flies. These include protocols for synthesizing CNO, performing experiments in adults, experiments in larva, and considerations for use of this system.

Key words *Drosophila*, GPCR, Behavior

---

1 Introduction

The fruit fly, *Drosophila melanogaster*, has been an important model organism for over a century. Unlike simpler organisms like yeast, or even the worm *C. elegans*, the fly is sufficiently complex to model advanced physiological processes and behaviors relevant to human biology. Greater than 75 % of known disease related genes in humans have a functional ortholog in the fly [1]. Significantly, similarity extends beyond gene function and homology to the systems level where these conserved genes direct the development and function of organs in the fly that perform equivalent functions as the gut, brain, kidney, and lung, among other systems. Accordingly, the fly is being used to model not only fundamental developmental and physiological processes but also several diseases including cancer, diabetes, cardiovascular disease, and neurological disorders [2].

An important feature of the fly is its repertoire of sophisticated behaviors that range from social interaction (e.g., aggression, courtship) to flight navigation. The brain of the fruit fly is comprised of about 100,000 neurons (but the brain also contains glia) that form several distinct specialized regions for such processes as vision, learning and memory, olfaction, and motor coordination [3]. Communication between neurons is mediated by conserved neurotransmitters (serotonin, dopamine, glutamate, GABA, etc.) and the fly has been instrumental in elucidating fundamental mechanistic aspects of neuronal and synaptic function [3].

In addition to a high degree of complexity relevant to human biology and behaviors, attractive features of the fly as a model also include a rapid and prolific life cycle (10 days at 25 °C), and an extremely low cost of maintenance compared to rodent or other mammalian models. Perhaps the most valuable aspect of *D. melanogaster* is the extensive genetic toolkit available. Compared to rodent models, it is quite easy and affordable to generate transgenics (~$300 to generate several independent founder strains), mutations, and to manipulate gene expression within discreet tissues or populations of cells. Within this framework of facile genetic manipulation, several methods have been developed for control of neuronal function and behavior. Early technologies included selective expression of toxins to ablate neurons, and a dominant negative temperature sensitive dynamin mutant (*shibirets*) to halt neurotransmitter vesicle recycling [4]. Later technologies included expression of ion channels to either activate or silence neurons (e.g., dTRPA1, NaChBac, Kir) [5–8]. These channels can be expressed throughout development, or induced at any time in development using a Gene Switch approach [9]. Some, like the dTRPA1 channel, are temperature sensitive and modulation of neuronal activity simply requires shifting flies to the appropriate temperature. A significant drawback to these channel-based approaches is that they are all essentially on/off switches. Channelrhodopsins have also been developed to provide control of neuronal activity using light [10] and employed in the fly [11]. These optogenetic approaches have been refined to enable both activation and silencing of neurons through modification of several different forms of microorganism light sensitive channels. Whereas early optogenetic technologies suffered from desensitization issues, and were primarily on/off switches, recent technological advances have address these concerns to some extent. Further, relevant to the fly, the blue light necessary to activate many channelrhodopsins poorly penetrates the cuticle. An additional barrier to the use of optogenetic approaches is the requirement for expensive and sophisticated light and fiber optic equipment. Although optogenetic approaches are used in the *Drosophila* community, it is not widespread and there are very

few publications that report using this method. Most laboratories still rely on the temperature sensitive channel-based "switches" to control neuronal activity. A major disadvantage of the switch approach is that by either fully activating or inactivating a neuron or circuit, more subtle behaviors that a neuron or circuit controls will not be uncovered for study or analysis. Further, these channel methods only modify neuron firing activity and are not useful for probing the function of non-neuronal tissues.

We have translated DREADD technology to the fly to allow for easy, cost effective conditional control of neuronal function [12]. Significantly, this control is truly dose responsive over several orders of magnitude and allows for the study of subtle behaviors mediated by neuronal circuits that are otherwise masked by complete activation or inactivation. Control is achieved by simply feeding the activating ligand, clozapine-N-oxide (CNO), to the fly. No specialized equipment like light sources or dedicated temperature controlled incubators are required. In this chapter we provide information for using DREADDs in *Drosophila*, and considerations for their optimal use based upon our experience. Protocols for performing individual behavioral assays are not provided here, but may be found elsewhere [13]. Here, we focus on clozapine-N-oxide synthesis and preparation, feeding techniques, and logistics of fly culturing leading up to feeding drug.

1.1 Essential Features of the Drosophila DREADD System

The fly DREADD system is based upon the bipartite GAL4/UAS expression system [14]. This system allows for precise spatial control of gene expression in the fly. The yeast transcription factor GAL4 is driven by enhancers for a specific gene in one strain (the driver strain), and in another strain (the responder strain) DREADD receptor cDNA has been cloned downstream of the GAL4 binding sequence (UAS site) and the entire element inserted at random into the fly genome by P-element transposition. When the driver and responder strains are mated, the progeny express functional DREADD protein in the pattern defined by the driver.

There are several methods for generating "GAL4-driver" strains including insertions of the GAL4 element into genes where expression is driven by local enhancers (enhancer trap), and constructing transgenic elements with a known promoter region of genomic DNA upstream of the GAL4 gene (promoter fusion) that are then inserted into the genome. Importantly there are several thousand of these GAL4 driver strains available from public stock centers that demonstrate expression representing the entire repertoire of cells a particular gene is expressed in to more highly restricted discreet sub-populations of cells.

The set of UAS-DREADDs include the UAS-hM1D (Dq), UAS-hM4D (Di), and rM3DBar (Ds) that are coupled to Gαq, Gαi, and Gαs, respectively. They were created in a w^{1118}

background, and the insertion elements moved to our laboratory standard strain of w^{1118}. Each has been tested for inducible expression, and has been validated in cellular, physiological, and behavioral experiments [12]. Dq activation results in calcium mobilization, closing of KCNQ channels, and membrane hypopolarization (facilitation of neuronal activation). Di activation results in inhibition of adenylate cyclase, lower cAMP levels, and opening of GIRK channels through Gβγ leading to membrane hyperpolarization (neuronal silencing). Ds activation results in activation of adenylate and production of cAMP.

2   Materials

UAS-DREADD flies are currently available from Dr. Charles Nichols, LSU Health Sciences Center, New Orleans LA. Clozapine used to synthesize CNO was purchased from Enzo Life Sciences (Farmingdale, NY). All other chemicals were purchased from Sigma-Aldrich (St. Louis, MO). Four-well culture dishes and 5 ml plastic culture tubes were from Thermo Fisher Scientific (Waltham, MA, USA). Glass capillary tubes used to feed individual flies are from Trikinetics (Waltham, MA). Polypropylene fly culture bottles (6 and 8 oz), and mesh for the large 64 oz bottles are from Genesee Scientific (San Diego, CA, USA). Large 64 oz plastic juice bottles are from the local grocery.

3   Methods

3.1   Clozapine-N-Oxide

Some commercial CNO, and the CNO produced by the NIMH chemical synthesis program, is not water soluble. Good water solubility of CNO is necessary because drug is administered in the food, and agents like DMSO or ethanol may interfere with palatability and confound experiments. The CNO available from Tocris has been reported to be water soluble and effective in the *Drosophila* DREADD system (cat# 4936). Our cost-effective solution has been to synthesize and purify our own CNO from clozapine. This CNO is water soluble to at least 50 mM; however, we have found that the aqueous solution is not stable for more than a few hours before precipitating out of solution. Further, storage at 4 °C or –20 °C precipitates the CNO out of solution rapidly and it does not go back into solution. Therefore, only enough stock solution is prepared from powder that is necessary for setting up a given experiment. Typically, a 20 mM solution of CNO in sterile water is prepared and diluted accordingly into the feeding substrate. Our protocol for CNO synthesis is described next and is modified from [15]. Our typical yield of CNO is ~75 % of the starting amount of clozapine.

3.1.1 CNO Synthesis

1. Dissolve clozapine (400 mg, 1.22 mmol) in 5 ml of CH_2Cl_2.

2. Treat dropwise with a solution of *m*-chloroperoxybenzoic acid (273 mg of 77 % mCPBA, 1.22 mmol) at 0 °C.

3. Stir at 0 °C for 90 min, then store reaction at 4 °C overnight.

4. Place the reaction onto a 30 g column of dry neutral alumina (about 2 cm × 26 cm).

5. Elute the column with dichloromethane. The desired CNO will stick to the column, but unreacted clozapine as well as the *m*-chloroperoxybenzoic acid will elute off. *A wet packed column gives a better elution than a dry column.*

6. Several slow brown/orange/pink bands will be evident near the top of the column. Once no more impurities are observed in the eluent by TLC, the product is then eluted from the column with methanol, collecting eluent until it is no longer pink colored.

7. Concentrate the pink solution to dryness under a vacuum to an orange crystalline residue.

3.1.2 Optional: Recrystallization (This Step May Enhance Water Solubility Depending on the Purity of the Initial Product)

1. Dissolve the crystals in a minimal amount of warm ethanol, followed by slowly adding ether until the solution is just on the verge of turning cloudy.

2. Add a seed crystal and let stand at room temperature for several hours, then at 4 °C overnight.

3. Filter and air-dry orange crystals.

4. Store in the dark at –20 °C. Allow storage vial to warm to room temperature before opening and weighing out powder.

   MW clozapine = 326.82.

   MW clozapine-N-oxide = 342.82.

   MW MCPBA = 172.57.

   TLC (silica, 8:2 CH_2Cl_2–MeOH).

3.1.3 Preparing Working Solutions of CNO

- Weigh out an appropriate amount of CNO for a concentrated stock solution and mix in an appropriate volume of sterile water (usually for a 20 mM CNO solution). Do not greatly exceed the amount necessary for the assay, as the concentrated stock does not store well (*see* general **notes** below). This should readily go into solution with brief vortexing.

- 3.42 mg CNO in 500 μl H_2O = 20 μM CNO stock.

- Dilute stock solution to a working solution of drug in the feeding substrate and mix (usually 1–3 mM).

- 50 μl CNO stock (20 mM) + 950 μl warm molten food = 1 mM CNO in food.

- 50 μl CNO stock (20 mM)+500 μl 20 % sucrose/2 % aga-rose+450 μl H$_2$O = 10 % sucrose, 1 % agarose, 1 mM CNO.

- Mix 4.0 g sucrose with 20 ml of water, add 0.4 g agarose in a 125 ml Erlenmeyer flask. Microwave on low until agarose is melted, avoiding boil-over (e.g., 2 min on power level 2), and swirl to mix and repeat until the agarose is dissolved. After the solution has cooled to ~55 °C, add 500 μl to a 1 ml microfuge tube containing 50 μl CNO stock and 450 μl H$_2$O. Vortex briefly to mix and allow to solidify for about 1 h.

3.2   Setting Up Crosses to Express DREADD Receptors

Most experiments will involve testing the F1 progeny of the GAL4-driver strain crossed with the UAS-DREADD responder strain, either as larva or adults.

3.2.1   Adult Collection

- Start fresh bottles (6 oz) of each parental strain needed (10 female+6 male young adults) and incubate at 25 °C.

- Allow the adults a few days (up to a week) to mate and lay eggs before removing the adults.

- As the newly eclosed adults emerge about 10 days after setting up the bottle, collect and separate the virgin females and sexually naïve males (adults less than 6 h eclosed).

- For the cross, start a new bottle (6 or 8 oz) with 10–15 virgin females of one parental line and 6–10 males of the other paren-tal line. It does not matter which strain is the male, and which the female unless an insertion element is on the X chromo-some. In that case, only the female F1 will contain both the GAL4 driver and UAS-DREADD.

- Allow these flies a few days (up to a week) to mate and lay eggs at 25 °C. Remove the adults from the bottles before the pupa begin to eclose.

- As the F1 generation emerges, collect the adult flies as needed depending on the assay being performed.

3.2.2   Larva Collection and Feeding

- Set up 8 oz round bottles with 15 virgin females of one parental strain and ten males of the other parental line and incubate at 25 °C (*see* **step 1** in Adult Collection for setting up these parental bottles).

- Allow flies to mate and lay eggs for 24 h at 25 °C before removing adult flies from the bottle.

- When the majority of the larva in the bottle have reached the third instar stage (~day 6), flood with 50 ml of a 20 % sucrose solution in water (w/v). The larva will float to the surface within 2–3 min.

- Collect floating larva with a large bore serological pipette (e.g., 25 ml) and transfer them to a small mesh basket, and wash twice with deionized water before further use.

- To expose the larva to CNO, transfer approximately fifty larvae to a small 10 ml glass beaker containing 1.2 ml of 5 % sucrose in sterile H_2O (either alone or with the appropriate concentration of CNO) for 15 min to allow time for larvae to ingest drug.

- Transfer the larva back to the mesh basket, rinse quickly with deionized water to remove the excess sucrose and CNO, and transfer them to the appropriate assay chamber (e.g., a petri dish with 1 % hardened agar).

See [13] for further information on larva collection.

3.2.3 Adult CNO Feeding
Some experiments may require an acute feeding of CNO, whereas others will require continuous feeding of the drug (e.g., monitoring circadian activity or mating assays). Acute feeding assesses the immediate effects of CNO on a naïve fly; however, this method is low throughput and the amount of drug ingested is highly variable. Chronic feeding is predicted to achieve steady state levels of drug, and be more reliable in reducing individual variability of ingested drug levels. Further, chronic feeding is easier than acute and amenable to feeding large numbers of flies (e.g., several hundred) simultaneously. The first chronic feeding protocol described is for collecting large numbers of adult flies for use *en masse* in assays like olfactory learning and memory. The second chronic feeding protocol is for feeding small numbers of flies. The third chronic feeding protocol is for administering drug to individual flies for use in assays like locomotor activity monitoring or aggression.

Acute

- For acute administration, collect adult flies approximately 24 h post-eclosure, and starve overnight (~18 h) by placing them in an empty standard vial without food or water (no more than ~50 flies per vial).

- Dilute CNO stock solution in a 10 % sucrose solution for the appropriate working concentration of CNO.

- Cut a small disk of filter paper to fit into the bottom of a 4-well culture plate, and place in a well.

- Apply 50 ml of the CNO/sucrose solution to the filter paper, and place one fly into the chamber and cover (removing the wings of the flies under light anesthetization prior to overnight starvation helps prevent them from flying away during the loading procedure).

- Allow the fly to feed for 5 min immediately prior to the assay. Flies should be observed using a stereo dissection microscope for the proboscis extending to the filter paper to confirm ingestion. If a fly does not begin eating within 1 min, discard and transfer a fresh fly to the well.

- After 15 min the CNO should have full effect, and should remain effective for ~30–45 min, and the appropriate assay should be performed.

- Optional: To determine the amount of drug ingested, spike the feeding solution with a small amount of ^{3}H-glucose. Immediately after the fly has been assayed (or within 60 min of feeding) homogenize individual flies in scintillation fluid and measure radioactivity in a scintillation counter. Compare overall counts to the activity of the feeding solution and calculate volume ingested, and amount of drug ingested based on the concentration of CNO.

3.2.4 Chronic (Several Hundred Adults)

- Set up four to six 8 oz bottles as described above for adult collection (parentals and F1 progeny). Once adults begin to emerge, clear culture bottles and after 48 h collect the recently emerged adult flies and transfer to large 64 oz bottles. Transfer flies without anesthetization.

- Prepare 2 ml of CNO+ food by mixing with either standard fly food or instant food (e.g., Jazz mix) or 1 % agarose + 10 % sucrose to the appropriate concentration of CNO.

- While the CNO + food mixture is still liquid, transfer into a food cup, which is then attached to the interior of the cap of the large 64 oz bottle with Velcro.

- Place the bottle on its side in a well ventilated area and allow the flies to feed 24–72 h depending on the assay. Remove old food and add fresh food + drug every 24 h to prevent the food from drying out.

Notes

- A large 64 oz commercial "juice" bottle is used. A large hole for ventilation is cut out of the bottom, and a fine mesh is glued in place with epoxy to cover the hole and retain flies in the bottle. A small piece of Velcro is attached to the inside of the cap to attach the food cup to. The food cup is the cap of a standard 15 ml conical tube with a small piece of Velcro attached to the top exterior.

- The larger environment prevents over exposure to the food source (flies being covered in food) and allows for proper grooming and feeding, which results in clean, dry flies for the assays.

3.2.5 Chronic (2–15 Adults)

- Dilute the CNO stock solution to an appropriate working solution with standard fly food, instant food (e.g., Jazz mix), or agarose + sucrose to the appropriate concentrations. Add CNO when the mixture is ~55 °C.

- Pipette 1 ml of the mixture into 5 ml polystyrene culture test tubes.

- Cover the test tubes with cheese cloth and allow food to dry overnight in a cool dark place.
- Once flies are collected and placed in the test tubes, the tubes should be plugged with a small piece of cotton and placed on a slight angle and not completely upright.
- Maintain tubes with flies at the appropriate temperature and lighting conditions for the assay to be performed.
- If performing an experiment that requires lengthy periods of feeding, flies will need to be transferred to a fresh tube + food/CNO after 3 days.

Notes

- Some condensation may develop on the side of the tubes. To prevent this, several small holes can be made in the side of the test tube once the food is solidified using a small, heated needle. Moisture can also develop from respiration of the flies after a few days. To combat this, place no more than 15 flies into a test tube and transfer to fresh food/CNO at least every 3 days.

3.2.6 Chronic (1 Adult)

- Prepare a mixture of 1 % agarose, 10 % sucrose, and the desired working concentration of the CNO as described above.
- Glass tubes should be clean, dry, and fitted with a cotton plug on one end.
- Collect adult flies from healthy productive bottles not more than 3 days post eclosure (depending on assay) into an empty fly vial without the use of CO_2.
- Place the vial of flies on ice until they are sedated, but no longer than 10 min.
- While flies are being chilled on ice, place a glass dissection dish onto ice in a small container (e.g., pipette tip box lid) to cool.
- Transfer the appropriate number of cold-anesthetized flies from the vial onto the chilled glass dish for sorting.
- Transfer one fly into one glass tube using fine forceps (we typically only use males). Using a small spatula, fill the free end of the glass tube with a small plug of the agarose mixture (~50–60 µl) and cap with a plastic cap.
- Verify that all flies are awake and freely moving before incubating the tubes at the appropriate temperature and lighting conditions for the assay to be performed.

4 Notes

- Glass capillary tubes are from Trikinetics (Waltham, MA, USA). 1 ml of agarose solution is normally enough for setting up 16 capillary tubes.

- We typically follow this protocol for activity monitoring in the Trikinetics *Drosophila* activity monitoring system (DAMS) to assess the effects of DREADD receptor activation on locomotor activity under both light/light and light/dark environmental conditions. For experiments measuring activity in light/dark conditions, rear flies under light/dark conditions for several days prior to collection to ensure that they are entrained.

- We also use this feeding method to treat individual flies for assays where isolation is necessary (e.g., courtship).

- It is important to not use CO_2 for anesthetization prior to activity assays because it interferes with overt activity for up to 24 h.

5 General Notes

- All of our experiments have been performed with flies containing only one copy of the expression GAL4 driver and one copy of the responder UAS-DREADD. Having two copies of each may increase expression levels of the DREADD and improve assay sensitivity. Another method to increase expression is to rear the flies at 29 °C for 48 h prior to performing the assay to maximally activate the GAL4 transcription factor.

- Although we have found this system to be very effective for many assays, in some instances we have been unable to manipulate behaviors or physiological processes. This may be due to gene dosage (*see* **note** above), or to inherent aspects of the system being probed. If activation of DREADD receptors is not observed to elicit a physiological or behavioral change with up to 10 mM CNO in the feeding substrate, increasing gene dosage of either/or the GAL4 driver or UAS-DREADD can be attempted.

- It is critical to have the GAL4 driver and UAS-DREADD transgenic elements in the same genetic background to properly interpret results, especially with regard to behavioral experiments. A *w^1118* is not a *w^1118* is not a *w^1118* from laboratory to laboratory due to the accumulation of random mutations in isolated laboratory stocks over several hundred generations that can alter behaviors. By having the transgenic elements within identical genetic backgrounds, one can be assured that behavioral differences observed in experiments are due to the presence of and activation of DREADD receptors, and not merely due to general genetic differences between the driver, responder, and F1 flies. Our laboratory standard strain is a *w^1118* originally obtained from Dr. Bih-Hwa Shieh at Vanderbilt University and subsequently isogenized in our laboratory. Each of our UAS-DREADD elements, as well as GAL4 driver elements we use,

has been moved into this background through six successive generations of back crossing prior to behavioral testing.

- We have found that CNO precipitates out of solution when stored overnight, even at –20 °C. Therefore, the stock and working solutions should be used as soon as possible. For final food preparations of either standard or instant or agarose/sucrose, the final solidified product can be stored in darkness at 4 °C, but storage in this manner is not recommended to exceed more than 48 h. When mixing CNO with food substrate that must be melted prior to mixing, the temperature of the food should not rise above 55 °C in order to prevent degradation of the CNO.

- When we use agarose + sucrose to provide drug in we have found that 10 % sucrose works the best. Using 5 % sucrose, the flies do not get enough nutrients and die within a couple days. Using 20 % sucrose, flies appear to not eat as much drug. We believe that 10 % sucrose in 1 % agarose achieves maximum balance between drug intake and viability over several days.

- There have been several attempts at generating light-sensitive GPCRs with mixed success [16–19]. In theory, this technology would mimic DREADD effector control of cellular transduction pathways, only using light as the receptor stimulus. However, these methods still require expensive light sources, and it is unclear how dose responsive these systems are. Further, many suffer from rapid bleaching issues [20]. Regardless, there are not yet any published reports using light activated GPCRs in *Drosophila*.

References

1. Reiter LT, Potocki L, Chien S, Gribskov M, Bier E (2001) A systematic analysis of human disease-associated gene sequences in Drosophila melanogaster. Genome Res 11:1114–1125

2. Pandey UB, Nichols CD (2011) Human disease models in Drosophila melanogaster and the role of the fly in therapeutic drug discovery. Pharmacol Rev 63:411–436

3. Nichols CD (2006) Drosophila melanogaster neurobiology, neuropharmacology, and how the fly can inform central nervous system drug discovery. Pharmacol Ther 112:677–700

4. Kitamoto T (2001) Conditional modification of behavior in Drosophila by targeted expression of a temperature-sensitive shibire allele in defined neurons. J Neurobiol 47:81–92

5. Nitabach M, Blau J, Holmes T (2002) Electrical silencing of Drosophila pacemaker neurons stops the free-running circadian clock. Cell 109:485–495

6. Nitabach MN (2006) Electrical hyperexcitation of lateral ventral pacemaker neurons desynchronizes downstream circadian oscillators in the fly circadian circuit and induces multiple behavioral periods. J Neurosci 26:479–489

7. Hamada FN, Rosenzweig M, Kang K, Pulver SR, Ghezzi A, Jegla TJ, Garrity PA (2008) An internal thermal sensor controlling temperature preference in Drosophila. Nature 454: 217–220

8. Parisky KM, Agosto J, Pulver SR, Shang Y, Kuklin E, Hodge JJL, Kang K, Kang K, Liu X, Garrity PA et al (2008) PDF cells are a GABA-responsive wake-promoting component of the Drosophila sleep circuit. Neuron 60:672–682

9. Roman G, Endo K, Zong L, Davis RL (2001) P[Switch], a system for spatial and temporal control of gene expression in Drosophila melanogaster. Proc Natl Acad Sci U S A 98: 12602–12607

10. Boyden ES, Zhang F, Bamberg E, Nagel G, Deisseroth K (2005) Millisecond-timescale, genetically targeted optical control of neural activity. Nat Neurosci 8:1263–1268

11. Schroll C, Riemensperger T, Bucher D, Ehmer J, Voller T, Erbguth K, Gerber B, Hendel T, Nagel G, Buchner E et al (2006) Light-induced activation of distinct modulatory neurons triggers appetitive or aversive learning in Drosophila larvae. Curr Biol 16:1741–1747

12. Becnel J, Johnson O, Majeed ZR, Tran V, Yu B, Roth BL, Cooper RL, Kerut EK, Nichols CD (2013) DREADDs in Drosophila: a pharmacogenetic approach for controlling behavior, neuronal signaling, and physiology in the fly. Cell Rep 4:1049–1059

13. Nichols CD, Becnel J, Pandey UB (2012) Methods to assay Drosophila behavior. J Vis Exp 61:e3795

14. Brand A, Perrimon N (1993) Targeted gene expression as a means of altering cell fates and generating dominant phenotypes. Development 118:401–415

15. Bender D, Holschbach M, Stöcklin G (1994) Synthesis of nca carbon-11 labelled clozapine and its major metabolite clozapine- N-oxide and comparison of their biodistribution in mice. Nucl Med Biol 21:921–925

16. Airan R, Thompson K, Fenno L, Bernstein H, Deisseroth K (2009) Temporally precise in vivo control of intracellular signalling. Nature 458:1025–1029

17. Masseck OA, Rubelowski JM, Spoida K, Herlitze S (2011) Light- and drug-activated G-protein-coupled receptors to control intracellular signalling. Exp Physiol 96: 51–56

18. Koizumi A, Tanaka KF, Yamanaka A (2013) The manipulation of neural and cellular activities by ectopic expression of melanopsin. Neurosci Res 75:3–5

19. Karunarathne WKA, Giri L, Kalyanaraman V, Gautam N (2013) Optically triggering spatiotemporally confined GPCR activity in a cell and programming neurite initiation and extension. PNAS 110:E1565–1574

20. Bailes HJ, Zhuang L-Y, Lucas RJ (2012) Reproducible and sustained regulation of Gαs signalling using a metazoan opsin as an optogenetic tool. PLoS One 7, e30774

INDEX

A

Adeno-associated virus (AAV) 63, 67, 69, 84, 86, 87, 92, 98, 99, 101, 102, 105, 111, 114, 116–119, 122–124, 133–135, 138, 140, 143
    concentration 122
    dialysis 122
    packaging 98, 119–120, 133–136
    purification 118–119
Adenylate cyclase 150
Agouti-related peptide AGRP neurons 63
AP-1 .... 50, 51, 54, 57
Appetite 62, 63, 65, 79
Arcuate nucleus (ARC) 62, 63, 65, 71, 72, 78

B

Behavior 4, 7, 14, 62, 65–67, 73, 77, 78, 83, 84, 99, 130, 141–142, 148
Behavioral assays 89, 96, 104, 105, 149
Behavior models 95–106, 133
Beta2(β$_2$)-adrenoceptor 2, 3
Beta(β)-arrestin 13, 15–19, 22
Bioluminescence Resonance Energy Transfer (BRET) 15, 16, 18, 24, 31, 39–47

C

Calcium 6, 7, 18–20, 24, 30, 31, 37–39, 54, 150
Calcium measurement 19
CaMKIIa promoter 98
cAMP 51, 150
c-Fos 50, 51, 57
c-Jun 49, 50, 57
Clozapine-N-oxide (CNO) 2, 3, 5–7, 11–15, 17–20, 30–32, 35–39, 42, 44, 46, 57–59, 65, 68–70, 73–78, 84, 89–92, 97–100, 109–112, 114–118, 131–133, 141–143, 149–157
    delivery method 100
    synthesis 150, 151
Confocal microscopy 89
COS-7 cells 31–39, 42, 46
CREB 50–52, 54, 57, 58
Cre-dependent viral vector 63, 67, 69, 70
Cre driver mouse line 64
Cre-recombinase 63, 65, 67, 72, 75, 78, 86, 95, 98, 111, 116, 117, 138

D

Double-floxed inverted orientation (DIO) 64, 67, 86, 98, 99, 136, 138
Drosophila 64, 147–157
Drug relapse 131
Drug-seeking behavior 129–144

E

Egr-1 .... 50, 51, 54, 55, 57
Extracellular signal-regulated protein kinase (ERK) 19, 49

F

Feeding circuits 61–79
Flip-excision (FLEX) switch 111, 114, 116, 117, 119, 123
Fluorescence resonance energy transfer (FRET) 9–13, 17, 18, 23
Fluorescent tracing 141
Fluorometric Imaging Plate Reader (FLIPR) assay 19, 37–39
Food intake measurements 73–74, 76
Fura-2 acetoxymethyl ester (Fura-2AM) 19

G

GABAergic neurons 85–87, 110, 116–117, 138
GAL4 fusion protein 51, 52, 54
GAL4/UAS expression system 149
Gamma amino butyric acid (GABA) 65, 66, 85, 148
Gene switch approach 148
Green Fluorescent Protein (GFP) 10, 40, 59, 85, 101, 135, 136, 142

H

Habituation/dishabituation paradigm 87, 90
HEK293 cells 6, 118, 119
Herpes simplex virus (HSV) vector 133–135, 137–140, 142, 143
hM$_4$D$_i$ 6, 21, 22, 74, 84, 90, 91, 109, 111, 117, 118, 131–133, 137
hM3Dq 21, 22, 74, 78, 84, 109, 111, 112, 114–118, 131–133
Hyperpolarization 6, 84, 96, 97, 109, 132, 150
Hypothalamus 62, 63, 65, 95, 110, 113, 116